



Organic-solvent-free Fabrication of Ultrafiltration Membranes using Polymer Foaming and Extrusion

Dissertation

Aniket Atul Raje

Hamburg, 2023

University of Hamburg

Faculty of Mathematics, Informatics, and Natural Sciences

Department of Chemistry

Dissertation submitted to the University of Hamburg in conformity with the requirements for the degree of *Doctor rerum naturalium* (Dr. rer. nat.)

Supervisor:	Prof. Dr. Volker Abetz
Co-supervisor:	Dr. Prokopios Georgopoulos
1 st Referee:	Prof. Dr. Volker Abetz
2 nd Referee:	Prof. Dr. Gerrit A. Luinstra
Date of oral examination:	January 12, 2024

Preamble

This dissertation, submitted as a cumulative thesis, was prepared under the guidance of Prof. Dr. Volker Abetz at the Institute of Membrane Research, Helmholtz-Zentrum Hereon (Geesthacht, Germany) and the Institute of Physical Chemistry, University of Hamburg (Department of Chemistry, Faculty of Mathematics, Informatics, and Natural Sciences). The work began on January 05, 2020, and was submitted on August 11, 2023. It includes reprints of three first-author publications, with summaries provided for each and acknowledgement of the contributions of co-authors and collaborators.



(Pronounced as *Shree*)

“While addressing the *Guru* (term for a "mentor, guide, expert, or master"), *Sashtra* (word that means "precept, rules, manual, compendium, book or treatise"), *Pujyasthana* (meaning holy places, places of knowledge or worship), the word ***Shree*** should be added at the beginning. Prostrating before them in devotion.”

– Lord Shiva (KulArnava Tantram, Chapter 11, Verse 43.) (Pandit, Vidyāratna and Woodroffe, 1999)

Publications

Publication of the following articles in their respective peer-reviewed journals enabled this cumulative dissertation.

1. Raje, A.; Buhr, K.; Koll, J.; Lillepärq, J.; Abetz, V.; Handge, U.A. Open-Celled Foams of Polyethersulfone/Poly(N-vinylpyrrolidone) Blends for Ultrafiltration Applications. *Polymers* 2022, 14, 1177. <https://doi.org/10.3390/polym14061177>
2. Raje, A.; Georgopanos, P.; Koll, J.; Lillepärq, J.; Handge, U.A.; Abetz, V. Open-Celled Foams from Polyethersulfone/Poly(Ethylene Glycol) Blends Using Foam Extrusion. *Polymers* 2023, 15, 118. <https://doi.org/10.3390/polym15010118>
3. Raje, A.; Koll, J.; Schneider, E. S.; Georgopanos, P. A novel organic solvent-free method for manufacturing polyethersulfone hollow fiber membranes using melt extrusion. *Journal of Membrane Science* 2023, Vol. 683, 121837. <https://doi.org/10.1016/j.memsci.2023.121837>

Patent Applications

The following patent application was submitted to the European Patent Office (EPO) and is pending decision (as of 08/2023)

- Raje, A.; Handge, U. A.; Koll, J.; Gronwald, O.; Weber, M.; Georgopoulos, P. Method for production of open-celled polymer foams for ultrafiltration applications. EP22155113.8. Filing date 04-02-2022.

Table of Contents

Preamble	V
Publications	IX
Patent Applications	XI
Table of Contents	XIII
Figures	XVII
Tables XX	
Abbreviations	XXII
Constants and variables	XXV
1. Abstract	1
2. Zusammenfassung	5
3. Introduction	11
3.1. Polymer Membranes	12
3.1.1. Ultrafiltration	14
3.1.2. Types of Polymer Membranes	15
3.1.3. Polymer Membrane Manufacturing Processes	18
3.1.4. Organic Solvents	21
3.2. Polymer Foams	24
3.2.1. Manufacturing Polymer Foams	29
3.2.2. Polymer Foams as Membranes	36
3.2.3. Other Melt Extrusion Techniques for Manufacturing Membranes	36
3.3. Polymers	37
3.3.1. Polyethersulfone	38
3.3.2. Poly(<i>N</i> -vinylpyrrolidone) and Poly(ethylene glycol)	40
4. Methods	45
4.1. Material Characterization Methods	46
4.1.1. Differential Scanning Calorimetry	46
4.1.2. High Pressure DSC	51
4.1.3. Thermogravimetric Analysis	52
4.1.4. Rheology	55
4.1.5. Sorption and Diffusion Measurements	62
4.1.6. Gel Permeation Chromatography	65
4.1.7. Infrared Spectroscopy	67
4.2. Processing Methods	68

4.2.1.	Blend Formulation	68
4.2.2.	Batch Foaming.....	72
4.2.3.	Extrusion and Foam Extrusion	73
4.2.4.	Post-treatment.....	74
4.3.	Foam & Membrane Characterization Methods.....	75
4.3.1.	Scanning Electron Microscopy.....	75
4.3.2.	Permeability.....	77
4.3.3.	Retention Test.....	78
4.3.4.	Tensile Test	78
5.	Objective of This Work.....	83
6.	Cumulative Part	87
6.1.	Article 1: Open-Celled Foams of Polyethersulfone/Poly(<i>N</i> -vinylpyrrolidone) Blends for Ultrafiltration Applications	89
6.1.1.	Author Contributions	91
6.1.2.	Funding and Acknowledgements	91
6.1.3.	Publication.....	93
6.2.	Article 2: Open-Celled Foams from Polyethersulfone/Poly(Ethylene Glycol) Blends using Foam Extrusion	118
6.2.1.	Author Contributions	121
6.2.2.	Funding and Acknowledgements	121
6.2.3.	Publication.....	123
6.3.	Article 3: A Novel Organic Solvent-Free Method for Manufacturing Polyethersulfone Hollow Fiber Membranes using Melt Extrusion	150
6.3.1.	Author Contributions	153
6.3.2.	Funding and Acknowledgements	153
6.3.3.	Publication.....	155
7.	Discussions	171
7.1.	Summary of Findings of This Work.....	172
7.2.	Future Scope	177
8.	Bibliography	179
9.	Appendix	205
9.1.	Article 1: Open-Celled Foams of Polyethersulfone/Poly(<i>N</i> -vinylpyrrolidone) Blends for Ultrafiltration Applications	206
9.1.1.	Graphical Abstract.....	206
9.1.2.	Miscellaneous Information.....	206
9.1.3.	Supporting Information.....	207

9.2. Article 2: Open-Celled Foams from Polyethersulfone/Poly(Ethylene Glycol) Blends using Foam Extrusion	217
9.2.1. Graphical Abstract	217
9.2.2. Miscellaneous Information.....	217
9.2.3. Supporting Information.....	218
9.3. Article 3: A Novel Organic Solvent-Free Method of Manufacturing Polyethersulfone Hollow Fiber Membranes using Melt Extrusion	222
9.3.1. Graphical Abstract	222
9.3.2. Miscellaneous Information.....	222
9.3.3. Supporting Information.....	223
9.4. Software/Websites Used.....	227
9.5. Safety Hazards	229
9.6. Copyright Permissions.....	232
9.6.1. Figure 4	232
9.6.2. Figure 13	233
9.6.3. Figure 17	239
10. Acknowledgements.....	247
11. Declaration of Oath.....	253

Figures

Figure 1: Basic illustration of a membrane system. Feed solution containing small (green) and large (red) particles in a liquid (blue) being separated by a membrane (orange) resulting in a permeate solution containing only small particles while a solution concentrated with red particles is rejected as a retentate.	13
Figure 2: A flat sheet membrane roll.	16
Figure 3: Hollow fiber membrane.	17
Figure 4: An illustration of a continuous process of flat sheet membrane production (left) and hollow fiber membrane production (right) employing the non-solvent induced phase separation. <i>Reprinted (adapted) with permission from Tree et al., 2018. Copyright 2023 American Chemical Society. (Tree et al., 2018)</i>	21
Figure 5: (a) Closed-cell foam structure; (b) Open-cell foam structure.	25
Figure 6: Bubble nucleation and nucleus growth as function of free energy change and its dependence on critical radius. (Okolieocha <i>et al.</i> , 2015)	28
Figure 7: Illustration showing batch foaming also known as solid-state foaming process.	31
Figure 8: Illustration indicating variation of the microstructure across the thickness in cross-sectioned polymer foam, foamed using batch foaming.	32
Figure 9: A basic foam extrusion schematic. A single screw extruder with four heating zones having an inlet for foaming agent at the compression zone of the screw, connected to static mixers, a melt pump and a nozzle, working in a serial configuration to deliver a foamed extrudate.	33
Figure 10: Molecular structure of PESU.	39
Figure 11: Molecular structure of PVP (left) and PEG (right).	41
Figure 12: Differential scanning calorimeter measurement cell's schematic representation. ..	47
Figure 13: Interpretation guide of a sample DSC thermogram. <i>Reprinted (adapted) with permission from Kalogeras et. al, 2016. Copyright 2023 John Wiley and Sons.</i>	48
Figure 14: Illustration of a TGA instrumentation.	53
Figure 15: Illustration of a plate-plate geometry configuration operating in oscillatory motion in a rheometer.	56
Figure 16: Illustration showing principle of GPC. Detection of molecules of different molecular weights is visualized on a chromatogram versus elution time; Molecular weight is derived from elution time according to the calibration.	66
Figure 17: Evolution of polymer along a twin-screw compounding extruder's axis. <i>Reprinted (adapted) with permission from Lee and Han, 2000. Copyright 2023 Elsevier.</i>	70
Figure 18: Twin-screw compounding extruder used in this work.	70
Figure 19: Material penetration of PEG liquid into PESU flakes by rotating flasks containing their mixture.	71
Figure 20: High pressure vessel (left) and hot plate hydraulic press (right) used for batch foaming in this work.	72
Figure 21: Single screw extruder coupled with static mixer, melt pump and nozzle, used for foam extrusion.	73
Figure 22: Illustration of a scanning electron microscope. (Michler, 2016)	76
Figure 23: A stress-strain curve of different types of polymers denoting various information such as stress at break (σ_B), strain at break (ϵ_B) and yield stress (σ_Y) obtained from	

tensile testing. The Young’s modulus (E) of the brittle polymer can be calculated by measuring the slope of the red dashed line i.e. the elastic region. The area under the curve denoted by blue color is measured to calculate the deformation energy of the respective polymer.80

Figure 24: Universal tensile testing machine used in this work.....81

Figure 25: A Venn diagram visualizing the state-of-the-art of polymer foams.83

Figure 26: A Venn diagram visualizing the scope of each published article of this cumulative work.....87

Figure 27: Water flux through the extrusion foamed hollow fibers of blend PESU/PEG 80/20 produced at various nozzle temperatures. Hollow fibers produced at $T_{Nozzle} = 145\text{ }^{\circ}\text{C}$ and $150\text{ }^{\circ}\text{C}$, due to low tensile strength, could not bear any water pressure above ATP and thus could not be tested for water flux. 151

Figure 28: Illustration showing mutual miscibility of polymers based on the findings of this work..... 174

Figure 29: Graphical abstract of article 1.206

Figure 30: Graphical abstract of article 2.217

Figure 31: Graphical abstract of article 3.222

Tables

Table 1: List of abbreviations.	XXIII
Table 2: Constants and variables table.	XXVI
Table 3: Parameters of Differential Scanning Calorimetry (DSC).	49
Table 4: Common experiments in shear-rheometry.	58
Table 5: Mathematical models used to describe viscoelastic behaviour in polymers. (Osswald and Rudolph, 2015; NETZSCH, 2023a)	59
Table 6: Steps with respective goals, scale, the selected process and forms.	85
Table 7: Author contributions for article 1.	91
Table 8: Author contributions for article 2.	121
Table 9: Author contributions for article 3.	153
Table 10: Software/websites used for this work	228
Table 11: Safety instructions and hazardousness of used substances.	231

Abbreviations

ATP	Atmospheric Pressure at Sea Level
BASF	Badische Anilin und Soda Fabrik
CDC	Center For Disease Control
DMAC	Dimethylacetamide
DMF	Dimethylformamide
DMSO	Dimethyl sulfoxide
DNA	Deoxyribonucleic Acid
DSC	Differential Scanning Calorimetry
FEM	Finite Element Method
FTIR	Fourier Transform Infrared Spectroscopy
GPC	Gel Permeation Chromatography
GVL	γ -Valerolactone
HF	Hollow Fiber
HP-DSC	High Pressure DSC
MWCO	Molecular Weight Cut-off
MWD	Molecular Weight Distribution
NIPS	Non-Solvent Induced Phase Separation
NMP	<i>N</i> -Methyl-2-Pyrrolidone
PA	Polyamide
PAN	Polyacrylonitrile
PC	Polycarbonate
PE	Polyethylene
PEG	Poly(ethylene glycol)
PEI	Polyetherimide
PEO	Poly(ethylene oxide)
PESU	Polysulfone
PLA	Poly(lactic acid)
PP	Polypropylene
PPSU	Polyphenylsulfone
PS	Polystyrene
PSU	Polysulfone
PTO	Please Turn Over
PU	Polyurethane

PVDF	Poly(vinylidene fluoride)
PVP	Poly(<i>N</i> -vinylpyrrolidone)
RI	Refractive Index
RNA	Ribonucleic Acid
RPM	Rotations Per Minute
SE	Society Europa
SEC	Size Exclusion Chromatography
SEM	Scanning Election Microscopy
TEP	Triethylphosphate
TGA	Thermogravimetric Analysis
THF	Tetrahydrofuran
TIPS	Thermally Induced Phase Separation
UF	Ultrafiltration
URL	Uniform Resource Locator
UV	Ultraviolet
WHO	World Health Organization
WLF	William-Landel-Ferry

Table 1: List of abbreviations.

Constants and variables

Constant / Variable	Symbol
Gibbs Free energy change when foaming	ΔG_E
Radius of nucleus of foaming site	R_n
Critical radius of foam-bubble	r^*
Free volume	$\Delta V_{free\ vol}$
Pressure difference between inside and outside the foam-bubble	ΔP
Interfacial energy	$\gamma_{\alpha\beta}$
Gibb's free energy barrier for homogenous nucleation	$\Delta G_{E,Hom}^*$
Shape factor	$S(\theta)$
Contact angle between foam-bubble and surface of nucleating particle	θ
Gibb's free energy barrier for heterogenous nucleation	$\Delta G_{E,Het}^*$
Glass transition temperature	T_g
Mass fraction of polymer	w
Heat capacity of polymer	Δc_p
Saturation time for gas to absorb into polymer	t_{sat}
Diffusion coefficient of polymer	D
Radius of polymer particle	R_p
Shear strain	γ
Shear modulus	G
Complex modulus	G^*
Storage modulus	G'
Loss modulus	G''
Complex viscosity	η^*
Angular frequency	ω
Loss factor	$\tan\delta$
Time	t
Relaxation time	τ
Viscosity	η
Instantaneous strain	$\varepsilon(t)$
Young's modulus	E
Strain rate	$\varepsilon'(t)$
Shear stress	σ
Shear rate	$\dot{\gamma}$

Power law index	n
Yield stress	σ_Y
Bingham viscosity	η_B
Zero shear viscosity	η_0
Infinite viscosity	η_∞
Shift factor	a_T
Activation energy	E_a
Universal gas constant	R
Characteristic time	k
Parameter denoting the transition between Newtonian and power law	a
Change in the mass of sorption balance	Δm
Experimental force	F_{EXP}
Gravitational constant	g
Mass of sample container	m^{sc}
Mass of sample in vacuum	m^s
Mass of adsorbent	m^A
Volume of sample container	V^{sc}
Volume of sample	V^s
Volume of adsorbent	V^A
Density of fluid	ρ
Diffusion coefficient at temperature T	D_T
Mass of gas absorbed by sample at time t	M_t
Mass of gas absorbed by sample at time $t \rightarrow \infty$; i.e., equilibrium	M_∞
Thickness of the cylindrical sample	l
Water-flux	L
Volume of water passed through membrane	V
Membrane surface area	A
Overpressure	P
Retention coefficient	R_C
Mass of solute in permeate	m_P
Mass of solute in feed	m_F

Table 2: Constants and variables table.

1. Abstract

Polymer based microfiltration and ultrafiltration membranes are commonly manufactured using methods that take advantage of the phase-inversion phenomenon essential in creating porous structures. To facilitate phase-inversion, organic solvents are fundamental ingredients in manufacturing porous polymer membranes. Commonly used organic solvents such as *N*-methyl-2-pyrrolidone (NMP), Dimethylacetamide (DMAc), Dimethylformamide (DMF), Dimethyl sulfoxide (DMSO), Tetrahydrofuran (THF), etc. are classified as hazardous materials by most health and environmental agencies. Exposure to organic solvents is associated with liver and lung diseases in humans and animals. Their improper disposal can pose a significant threat to the environment. The development of alternative membrane manufacturing methods that do not use organic solvents is a need of the hour since an eventual prohibition of some of them is foreseen.

Like porous polymer membranes, another class of materials called polymer foams are defined by their porous nature. However, most polymer foams' production methods do not involve any organic solvents. Therefore, the implementation polymer foams as polymer membranes offers the potential to eliminate organic solvents, making the membrane manufacturing process more sustainable, safe, and environmentally friendlier than the current state-of-the-art membrane manufacturing methods. Although polymer foams are used in some filtration applications such as air filters that restrict macroscopic particle sizes, they cannot be implemented as membranes for microscopic separation applications such as ultrafiltration due to the unavailability of open-celled nanocellular foams.

Therefore, based on the abundant state of the art available in the field of polymer membranes and polymer foams, this work aims to develop open-celled nanocellular polymer foams capable of ultrafiltration. Development of methods that deliver such

foams is pursued, and the creation of foam-based ultrafiltration membranes is aimed, thus eliminating organic solvent usage.

Polyethersulfone (PESU) was selected as the base material to produce polymer foams owing to its prominent use in ultrafiltration (UF) membranes. A blend of PESU and poly(*N*-vinylpyrrolidone) (PVP) was developed and characterized for batch foaming. This method was found to yield nanocellular foams. However, these foams were not directly usable for UF applications due to the presence of a non-foamed skin layer. The non-foamed skin layer was eliminated using an innovative sandwich sample method and aqueous sodium hypochlorite (NaOCl) solution treatment. The resultant foam was found to exhibit retention performance that was comparable to state-of-the-art UF membranes, while the water flux required significant improvements.

In order to investigate the potential of a similar blend combination i.e. PESU along with a water-soluble polymer for large-scale production of foams, foam extrusion was pursued, and PESU/poly(ethylene glycol) (PEG) blends were investigated. Unlike the PESU/PVP blend, manufactured through melt-state compounding, the PESU/PEG blend was developed material absorption i.e. by allowing liquid PEG to absorb within PESU taking advantage of the porous structure of PESU flakes and was directly used in foam extrusion. The blend composition was optimized to produce continuous microcellular open-celled foams when CO₂ and H₂O were utilized as foaming agents at specific process settings. Additionally, adding PEG resulted in a processing temperature 120 – 150 °C lower than that of PESU (320 °C – 350 °C). Using an annular slit nozzle, extruded hollow fibers with open-celled foam structure with an average cell size of 5 μm were produced.

The same PESU/PEG blend, when extruded without any foaming agents, resulted in the formation of uniformly distributed closed cell pores with an average pore size of 500 nm throughout the extrudate. However, the extrudate did not maintain the hollow fiber shape

due to low melt elasticity at the nozzle. Also, the absence of open porosity posed a significant challenge in any utilization for permeation.

In order to address these limitations, a ternary blend PESU/PEG/PVP was developed using the same material absorption method as PESU/PEG. The extrusion of this blend without using any foaming agents resulted in an increased melt elasticity, thus retaining the nozzle's hollow fiber geometry. Also, the ternary blend's extruded hollow fiber showed a higher porosity than the PESU/PEG blend. Subsequently, through optimization of the processing parameters, the porosity was increased. After post-treatment of the hollow fibers with aqueous NaOCl, large portions of PEG and PVP were dissolved, further increasing porosity and making the fibers partially open cellular and permeable. This enabled the functionalization of these hollow fibers as membranes.

The different miscibilities of PVP and PEG with PESU resulted in different dissolution mechanisms, combined with the surface evaporation of PEG from the extruded fibers synergistically, resulting in different surface and internal porosities. As a result, the separation layer on the outer surface of these extruded hollow fiber membranes was found to have a pore size of approximately 100 nm and an internal open pore size of $< 1 \mu\text{m}$. In addition, filtration performance and water flux comparable to state-of-the-art ultrafiltration (UF) membranes were observed.

This study found polymer foaming as a viable alternative to traditional polymer membrane production methods that rely on organic solvents. Flat sheet and hollow fiber foam-based membranes were produced using binary and ternary blends of PESU, PVP, and PEG. The characteristics and performance were found to be comparable to those produced using production methods that involve the use of organic solvents. However, further optimization and improvements are needed to fully realize this method's potential. Nevertheless, this research opens up new horizons and fields of research in developing foam-based ultrafiltration membranes that are more sustainable and safe.

2. Zusammenfassung

Bei der Herstellung polymerbasierter Mikrofiltrations- und Ultrafiltrationsmembranen werden in der Regel Verfahren eingesetzt, die sich für die Schaffung poröser Strukturen das Phänomen der Phaseninversion zunutze machen. Zur Erleichterung der Phaseninversion sind organische Lösungsmittel ein wesentlicher Bestandteil der Herstellung poröser Polymermembranen. Häufig verwendete organische Lösungsmittel wie *N*-Methyl-2-pyrrolidon (NMP), *N,N*-Dimethylacetamid (DMAc), *N,N*-Dimethylformamid (DMF), Dimethylsulfoxid (DMSO), Tetrahydrofuran (THF) usw. werden von den meisten Gesundheits- und Umweltbehörden als Gefahrstoffe eingestuft. Die Exposition gegenüber organischen Lösungsmitteln wird unter anderem mit Leber- und Lungenkrankheiten bei Menschen und Tieren in Verbindung gebracht. Ihre unsachgemäße Entsorgung kann eine erhebliche Gefahr für die Umwelt darstellen. Die Entwicklung alternativer Membranherstellungsmethoden, die ohne organische Lösungsmittel auskommen, ist ein Gebot der Stunde, da ein Verbot einiger dieser Stoffe absehbar ist.

Wie poröse Polymermembranen zeichnen sich auch die Polymerschäume durch ihre poröse Struktur aus. Die meisten Verfahren zur Herstellung von Polymerschäumen kommen jedoch ohne organische Lösungsmittel aus. Daher bietet die Verwendung von Polymerschäumen als Membranen das Potenzial, organische Lösungsmittel zu eliminieren, was den Herstellungsprozess von Membranen nachhaltiger, sicherer und umweltfreundlicher macht als die derzeitigen modernen Membranherstellungsverfahren. Obwohl Polymerschäume in einigen Filtrationsanwendungen wie z.B. Luftfiltern verwendet werden, die makroskopische Partikelgrößen begrenzen, können sie nicht als Membranen für mikroskopische Trennanwendungen wie z.B. Ultrafiltration eingesetzt werden, da offenzellige nanozelluläre Strukturen nicht verfügbar sind.

Daher zielt diese Arbeit auf die Entwicklung offenzelliger nanozellulärer Polymerschäume ab, die zur Ultrafiltration fähig sind, auf der Grundlage des umfangreichen Stands der Technik auf dem Gebiet der Polymermembranen und Polymerschäume. Es werden Methoden entwickelt, die solche Schäume liefern, und es wird die Herstellung von Ultrafiltrationsmembranen auf Schaumbasis angestrebt, wodurch die Verwendung organischer Lösungsmittel vermieden wird.

Polyethersulfon (PESU) wurde als Ausgangsmaterial für die Herstellung von Polymerschäumen ausgewählt, da es häufig in Ultrafiltrationsmembranen (UF) verwendet wird. Eine Mischung aus PESU und Poly(*N*-vinylpyrrolidon) (PVP) wurde entwickelt und für das Batch-Schäumen charakterisiert. Es wurde festgestellt, dass diese Methode offenzellige nanozelluläre Schäume ergibt. Diese Schäume waren jedoch nicht direkt für UF-Anwendungen verwendbar, da sie eine nicht geschäumte Hautschicht aufwiesen. Die Bildung dieser nicht geschäumten Hautschicht wurde durch eine innovative Sandwich-Probenmethode und eine Behandlung mit wässriger Natriumhypochloritlösung (NaOCl) umgangen. Es wurde festgestellt, dass der daraus resultierende Schaum eine Rückhalteleistung aufwies, die mit den modernsten UF-Membranen vergleichbar war, während der Wasserdurchfluss erheblich verbessert werden musste.

Um das Potenzial einer ähnlichen Mischungskombination, d.h. PESU zusammen mit einem wasserlöslichen Polymer, für die großtechnische Herstellung von Schaumstoffen zu untersuchen, wurde die Schaumextrusion weiterverfolgt und PESU/Polyethylenglykol (PEG)-Mischungen wurden untersucht. Im Gegensatz zur PESU/PVP-Mischung, die durch Schmelzcompoundierung hergestellt wurde, wurde die PESU/PEG-Mischung durch Materialabsorption entwickelt. Flüssiges PEG wurde unter Ausnutzung der porösen Struktur von PESU-Flocken absorbiert und die Mischung wurde direkt in der Schaumextrusion verwendet. Die Mischungszusammensetzung wurde optimiert, um kontinuierliche mikrozelluläre offenzellige Schäume zu erzeugen, wenn CO₂ und H₂O als Schaumbildner bei bestimmten Prozesseinstellungen verwendet wurden. Darüber hinaus

fürte die Zugabe von PEG zu einer Verarbeitungstemperatur, die 120 - 150 °C niedriger war als die von PESU (320 °C - 350 °C). Unter Verwendung einer ringförmigen Schlitzdüse wurden extrudierte Hohlfasern mit offenzelliger Schaumstruktur und einer durchschnittlichen Zellgröße von 5 µm hergestellt.

Wurde dieselbe PESU/PEG-Mischung ohne Schaumbildner extrudiert, so bildeten sich im gesamten Extrudat gleichmäßig verteilte geschlossene Zellporen mit einer durchschnittlichen Porengröße von 500 nm. Allerdings behielt das Extrudat aufgrund der geringen Schmelzelastizität an der Düse nicht die Hohlfaserform bei. Außerdem stellte das Fehlen offener Poren eine große Herausforderung bei der Anwendung für die Permeation dar.

Um diese Einschränkungen überwinden zu können, wurde eine ternäre Mischung aus PESU/PEG/PVP entwickelt, die die gleiche Materialabsorptionmethode wie PESU/PEG verwendet. Die Extrusion dieser Mischung ohne Verwendung von Schaumbildnern führte zu einer erhöhten Schmelzeelastizität, wodurch die Hohlfasergeometrie der Düse erhalten blieb. Außerdem wiesen die extrudierten Hohlfasern der ternären Mischung eine höhere Porosität auf als die der PESU/PEG-Mischung. Durch die Optimierung der Verarbeitungsparameter konnte die Porosität anschließend erhöht werden. Durch eine Nachbehandlung der Hohlfasern mit wässriger NaOCl-Lösung wurden große Teile von PEG und PVP aufgelöst, was die Porosität weiter erhöhte und die Fasern teilweise offenzellig und durchlässig machte. Dies ermöglichte die Anwendung dieser Hohlfasern als Membranen.

Die unterschiedlichen Mischbarkeiten von PVP und PEG mit PESU führten zu unterschiedlichen Auflösungsmechanismen, die in Kombination mit der Oberflächenverdampfung von PEG aus den extrudierten Fasern synergistisch zu unterschiedlichen Oberflächen- und Innenporositäten führten. Infolgedessen wurde festgestellt, dass die Trennschicht auf der äußeren Oberfläche dieser extrudierten

Hohlfasermembranen eine Porengröße von etwa 100 nm und eine innere offene Porengröße von $< 1 \mu\text{m}$ aufwies. Darüber hinaus wurden Filtrationsleistung und Wasserdurchfluss vergleichbar mit modernen Ultrafiltrationsmembranen (UF) festgestellt.

In dieser Studie wurde festgestellt, dass das Schäumen von Polymeren eine praktikable Alternative zu den herkömmlichen Verfahren zur Herstellung von Polymermembranen darstellt, die auf organische Lösungsmittel angewiesen sind. Unter Verwendung von binären und ternären Mischungen aus PESU, PVP und PEG wurden flache Platten und Hohlfasermembranen auf Schaumbasis hergestellt. Es wurde festgestellt, dass die Eigenschaften und die Leistung vergleichbar sind mit denen von Membranen, die unter Einsatz organischer Lösungsmittel hergestellt werden. Es sind jedoch weitere Optimierungen und Verbesserungen erforderlich, um das Potenzial dieser Methode voll auszuschöpfen. Nichtsdestotrotz eröffnet diese Forschung neue Horizonte und Forschungsfelder für die Entwicklung von Ultrafiltrationsmembranen auf Schaumbasis, die nachhaltiger und sicherer sind.

3. Introduction

Membrane science and technology is a highly researched and rapidly growing field that focuses on permeable barriers for substance separation, filtration, adsorption, and purification. Together, principles from material science, chemistry, physics, and engineering play a role in delivering its numerous applications in industries such as water treatment, biomedical, chemical processing, gas separation, etc. Over the past few decades, new and improved materials and processes have led to greater efficiency and sustainability in membrane science, offering innovative solutions to a broad spectrum of new challenges such as distillation, selective ion separation, hemodialysis, CO₂, CH₄, H₂ separation and capture, etc. (Halder *et al.*, 2017; Pulyalina *et al.*, 2018; Abdul Latif *et al.*, 2021; Norddahl *et al.*, 2021; Rahman, 2021)

To design, optimize, and implement membrane-based processes, it is essential to have a deep understanding of the materials, from molecular structure to physical properties, high customization of manufacturing processes, and a complete overview of the operating conditions of these membranes. The field of membrane science continues to progress, with the development of new materials and fabrication techniques that cater to the needs and demands of the new world. Depending on the requirement, different materials, including polymers, composites, ceramics, and metals, are used to develop membranes, each offering unique properties and limitations. In the past few decades, polymer membranes have gained widespread popularity for their versatility, affordability, adaptability, and exceptional performance. (Baker, 2012; Singh, 2015; Drioli, Giorno and Fontananova, 2017; Liguori *et al.*, 2020; Nunes *et al.*, 2020; Abetz, Brinkmann and Sözbilir, 2021; Arumugham *et al.*, 2021)

3.1. Polymer Membranes

Polymer membranes are versatile and widely used in various industries. They are porous objects made of polymers used for separating, filtering, and absorbing various particles, fluids, and molecules (Abetz, Brinkmann and Sözbilir, 2021). The type of polymer membrane utilized depends on the target application and the size of the particles to be separated. The polymers and the processes involved can be tailored to achieve desired pore sizes and porosities that facilitate separation and exclusion of required scale and level. In addition to filtration, polymer membranes can be used for absorption processes (Ahmad *et al.*, 2010; Klingberg *et al.*, 2019). They are ideal for gas and liquid separations, with their selective permeability allowing for the effective separation of different components, including specific ions. By customizing the polymer materials and processes, polymer membranes can be tailored specifically to attract or repel particles or molecules based on their size, charge, or polarity. (Ulbricht, 2006; Abetz, Brinkmann and Sözbilir, 2021; Glass *et al.*, 2021)

In the field of filtration membranes, polymer membranes can be divided into subtypes based on the level of separation, including microporous, ultrafiltration, nanofiltration, and reverse osmosis membranes (Abetz, Brinkmann and Sözbilir, 2021). Microporous membranes have pore sizes ranging from 0.1 to 10 micrometers and are used for removing microorganisms, protein aggregates, and suspended matter from liquids. Ultrafiltration membranes have pore sizes ranging from 10 to 100 nanometers and are used for removing colloidal matter, viruses, and macromolecules from liquids. Nanofiltration membranes have pore sizes ranging from 1 to 10 nanometers and are used for removing ions, oligomers, and small organic molecules from liquids. Reverse osmosis membranes have pore sizes of less than 1 nanometer and are used for desalination and removing dissolved inorganic salts from liquids. (Ferry, 1936; Spivakov and Shkinev, 2005; Al Aani, Mustafa and Hilal, 2020)

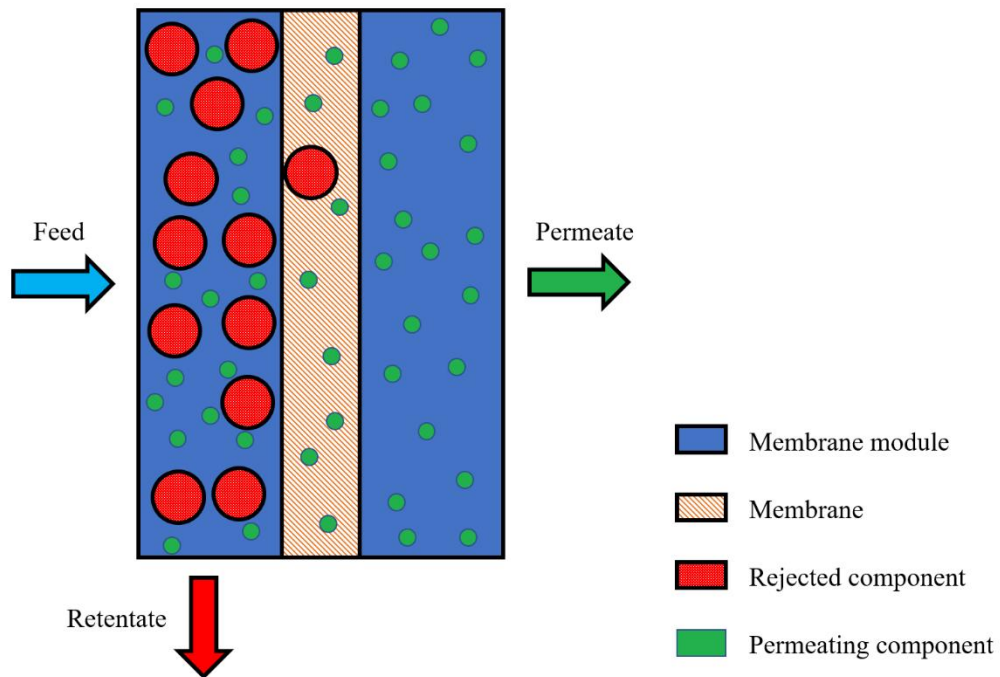


Figure 1: Basic illustration of a membrane system. Feed solution containing small (green) and large (red) particles in a liquid (blue) being separated by a membrane (orange) resulting in a permeate solution containing only small particles while a solution concentrated with red particles is rejected as a retentate.

Figure 1 shows a basic illustration of a membrane system. As the solution passes through the porous membrane, the solutes larger than the membrane's pore size are retained on the membrane surface, while the solvent and smaller solutes pass through the membrane and are collected. This passed solution is known as 'permeate'. The solutes retained on the membrane surface are called the 'retentate'. (Xu and Alsahy Qusay, 2004; Pezeshk *et al.*, 2012; Grünig *et al.*, 2020; Abetz, Brinkmann and Sözbilir, 2021)

The performance of an ultrafiltration membrane is characterized by its permeability and selectivity. The permeability of a membrane is defined as the intrinsic membrane's ability to allow the solution to pass through the membrane independent on the membrane

thickness, whereas selectivity is a measure of its ability to retain solutes of a particular molecular weight or size from the passed solution. The membrane's material, surface area, thickness, pore size, pore types, etc., are a few of the critical factors that influence the permeance and selectivity of the membrane. In addition, operating conditions such as incoming pressure, operational temperature, and type of membrane module also influence the performance of these membranes. (Siddiqui, Arif and Bashmal, 2016)

The pores in polymer membranes can also be classified based on their geometry and connectivity. These include round, cylindrical, slit-shaped, cone-shaped, inkbottle, blind, and interconnecting pores. Round pores are spherical, while cylindrical pores are circular in cross-section and elongated along the membrane axis. Slit-shaped pores are narrow channels that run parallel to the membrane surface and extend perpendicular towards the depth, whereas interconnecting pores are interconnected channels that allow for the transport of larger molecules. Apart from open and closed pores, there are pores open at only one end. The shape and connectivity of the pores in a membrane can significantly impact its separation performance, and the fabrication of polymer membranes plays a vital role in determining the porous properties. (Rouquerol *et al.*, 1994; Zdravkov *et al.*, 2007; Siddiqui, Arif and Bashmal, 2016; Gu *et al.*, 2020)

3.1.1. Ultrafiltration

As mentioned before, ultrafiltration is used to separate solutes of high molecular weight and size from a solution. The typical pore sizes in ultrafiltration membranes between 10 and 100 nanometres allow the separation of solutes with molecular weights ranging from 1000 to 1 million Daltons (Ferry, 1936; Spivakov and Shkinev, 2005; Youcai, 2018). As these sizes find high use in various industries, including food and beverage, pharmaceuticals, biotechnology, wastewater treatment, chemical, etc., development of highly efficient and affordable ultrafiltration membranes deems high value and importance.

Ultrafiltration membranes are made of various polymers such as polyethersulfone, poly(vinylidene fluoride), cellulose acetate, etc., as well as modern composite materials involving carbon nanotubes, activated carbon and also the class of polymers, called block copolymers that have the ability to microphase separate which is responsible for exceptional isoporous structures (Radjabian *et al.*, 2014; Abetz, 2015; Schulze *et al.*, 2015; Georgopoulos *et al.*, 2016; Rahman, 2021). Ultrafiltration is driven mainly through the transmembrane pressure applied by the solution on the membrane surface to perform size exclusion. (Xu and Alsahy Qusay, 2004; Pezeshk *et al.*, 2012; Grünig *et al.*, 2020; Abetz, Brinkmann and Sözbilir, 2021)

Besides water filtration, the primary application of ultrafiltration membranes where suspended solids, colloids, bacteria, etc., are removed from the water, ultrafiltration has several other applications in other industries. For example, ultrafiltration membranes have many uses in the food industry, such as concentrating milk, separating whey proteins, clarifying fruit juices, filtering alcohol, etc. In biomedicine, ultrafiltration membranes are used to purify proteins and peptides, dialysis, isolate viruses & bacteria, concentrate drug formulations, and separate and purify DNA and RNA. (Tang *et al.*, 2009; Chamberland *et al.*, 2019; Al Aani, Mustafa and Hilal, 2020; Castro-Muñoz *et al.*, 2020; Vu, LeBlanc and Chou, 2020; Bazrafshan *et al.*, 2021; Murugan *et al.*, 2021; Alavijeh and Baltus, 2022)

3.1.2. Types of Polymer Membranes

Polymer membranes have different shapes and sizes, including flat-sheet membranes and hollow fiber membranes. For generalized and industrially scaled applications, membrane modules are constructed as assemblies of multiple membranes, providing in this way the necessary membrane area which is necessary for a certain separation application. Both flat-sheet and hollow fiber membranes are used in their respective modules that are available in various sizes and shapes. Depending upon the application requirements,

multiple membrane modules can be designed for parallel or continuous setups in a more extensive filtration/separation system.

Flat-sheet membranes comprise a thin, porous polymer layer cast or constructed on a thick flat porous substrate for support. The pore sizes of the thin layer are generally much smaller than the substrate. Flat-sheet membranes, as shown in Figure 2, are used in gas separation and liquid filtration applications where high flux and low pressure are required, such as in water treatment, CO₂ capture, and reverse osmosis. These membranes can be cut into different shapes and sizes, stacked on top of one another, or spiraled onto a cylindrical core to fit different process requirements. (Pezeshk *et al.*, 2012; Yin, Zhu and Deng, 2013; Zhou *et al.*, 2020; Abdul Latif *et al.*, 2021; Mantel *et al.*, 2022)



Figure 2: A flat sheet membrane roll.

Hollow fiber membranes, as shown in Figure 3, are cylindrical tubes with a hollow core and a thin wall. They are used for applications requiring a large surface area to dissipate the incoming pressure and yield a high flux. Multiple hollow fiber membranes are stacked together into a module such that the permeate enters all fibers from the hollow cross-

section and exits through their walls simultaneously. This leads to a large surface area in a compact module. Both liquid and gas separation applications are carried out using hollow fiber membranes.



Figure 3: Hollow fiber membrane.

The most commonly used materials for polymer membranes are polyacrylonitrile (PAN), polyethylene (PE), polyamide (PA), polypropylene (PP), poly(vinylidene fluoride) (PVDF), and polyarylsulfones such as polysulfone (PSU), Polyethersulfone (PESU) and polyphynelinesulfone (PPSU). Properties, such as mechanical strength, thermal stability, chemical resistance, fouling performance, philicity, etc. are assessed when selecting the polymer for any required application. For example, PE and PP are economical polymers frequently utilized for water treatment due to their excellent chemical resistance and decent mechanical strength (Razzaz, Mohebbi and Rodrigue, 2018; Luo, Xie and Qin, 2021). Meanwhile, PVDF is a costlier material for high-temperature and high-pressure applications because of its exceptional thermal stability and chemical resistance (Wang, Li and Teo, 1999). Polyarylsulfones offer enhanced thermal and mechanical stability, chemical resistance, and high-performance filtration properties, making them ideal for demanding applications in various industries, including medical, chemical processing, and water treatment. However, most membrane applications use polymers that contain

additives or are polymer blends or copolymers that influence specific membrane properties such as the material's attraction or repulsion towards certain compounds, surface roughness, porosity, etc. (Liu *et al.*, 2011; Al Malek *et al.*, 2012; Yin, Zhu and Deng, 2013; Wang *et al.*, 2014; Fang *et al.*, 2015; Guo, Nicolae and Kumar, 2016; Tsehaye, Velizarov and Van der Bruggen, 2018; Grünig *et al.*, 2020; Zhou *et al.*, 2020; Mantel *et al.*, 2022)

3.1.3. Polymer Membrane Manufacturing Processes

The most common method to manufacture polymer membranes is phase separation/inversion. Phase inversion involves a change in the state of a polymer solution from a homogeneous solution to a heterogeneous one, forming a porous solid polymeric membrane. Various phase separation techniques involving varied mechanisms depend on the polymer used, the application aimed, and expected performance.

Solution casting or evaporation-induced phase separation is a simple process for manufacturing flat-sheet polymer membranes. A polymer is dissolved in a compatible organic solvent to form a homogeneous polymer solution. The solution is then cast onto a flat surface, and the solvent evaporates until a solid polymeric membrane remains. The choice of solvent, its concentration and rate of evaporation strongly influence the final membrane's properties, such as morphology and mechanical strength. This process is inexpensive, given its simplicity and upscalability. However, it lacks the customizability of other techniques and is typically used for producing low-performance membranes used in simple filtration applications. (Lalia *et al.*, 2013; Galiano, 2015)

Thermally Induced Phase Separation (TIPS) is another process that removes thermal energy to induce phase separation of a polymer solvent system with an upper critical solution temperature (miscible only at higher temperature). The process has various

advantages, including simplicity and high reproducibility. The polymer is generally dissolved in a low molecular weight solvent at high temperatures, generally above the polymer's melting point/glass transition temperature. This solution is then cast, similar to the solution casting process. However, as the solution is cooled down in a controlled manner, phase separation occurs due to immiscibility of the components. Phase separation can also be driven by crystallization and in fact most TIPS polymers are semicrystalline. (Fu *et al.*, 2006; Kim *et al.*, 2016; Liu *et al.*, 2016)

The Non-Solvent Induced Phase Separation (NIPS) method is a versatile and cost-effective approach that produces high-performance polymer membranes with well-controlled morphologies and mechanical and separation properties. A non-solvent is a substance that does not dissolve a particular solute (in this case, a polymer) in a given solvent (in this case, an organic solvent), resulting in the solute separating from the solution. The polymer is first dissolved in the solvent to form a polymer solution, which is then added to a non-solvent. The controlled interaction between the polymer-solvent solution and the non-solvent causes phase separation, forming a porous polymer membrane. The properties of the final membrane, such as the pore size and its distribution, mechanical strength, and selectivity, can be tailored by adjusting the polymer, solvent, and non-solvent type, and processing conditions. Other additives to tailor specific properties or membrane performance can be added during this process. Temperature, evaporation time and humidity play a crucial role in the NIPS process. The NIPS process can be used to manufacture both hollow fiber and flat sheet membranes. (Xu and Alsahy Qusay, 2004; Sankhala *et al.*, 2017; Noor *et al.*, 2018; Liu *et al.*, 2019; Wang *et al.*, 2019; Grünig *et al.*, 2020)

For flat sheet membrane manufacturing through the NIPS process, the polymer solution is cast onto a substrate and immersed into a coagulation bath where the non-solvent solvent exchange occurs, causing the polymer to phase separate and form a porous structure. The solvent is then allowed to evaporate, yielding a thin film of the polymer. Similarly, for manufacturing hollow fiber membranes, a process known as spinning is

used. First, the polymer-solvent solution is forced through a small orifice with a needle called a spinneret. Next, it is mixed with a non-solvent when exiting the spinneret, which causes the solution to precipitate out of the polymer and form a porous fiber. The fiber is then collected onto a spool or winding drum, resulting in a hollow fiber membrane. This process can be performed using either a dry-spinning or a wet-spinning process. In the dry-spinning process, as the fiber is extruded through a spinneret, the solvent is evaporated by air-drying or bypassing the jet through a heated chamber, leaving behind a solid polymer fiber. The fiber is then collected on a rotating drum, forming a continuous, porous fiber. In the wet-spinning process, the fiber is extruded through a spinneret, passed through a spinning bath, mainly consisting of the non-solvent, and helps stabilize the fiber. The fiber is then collected directly from the spinning bath or further dried to remove any remaining solvent from the fiber. Figure 4 shows an illustration of continuous process of membrane production employing NIPS. (Lalia *et al.*, 2013; Tree *et al.*, 2018)

Spinning is an efficient and scalable process, allowing for a high degree of control over the fiber diameter, pore size, and membrane structure. The properties of the final membrane can be tuned by adjusting the spinning conditions, such as the bore fluid flow rate, spinning speed, temperature, solution concentration, additives, etc. Spinning can also produce hollow fiber membranes with high mechanical strength and permeability, making them suitable for various separation applications, such as water treatment and gas separation. However, spinning leads to challenges, such as high-volume reproducibility, that must be addressed. In addition, slight variations in the process can result in defects in the membrane structure, such as cracks or voids, which can affect its performance and durability. (Ahmad, Otitoju and Ooi, 2019)

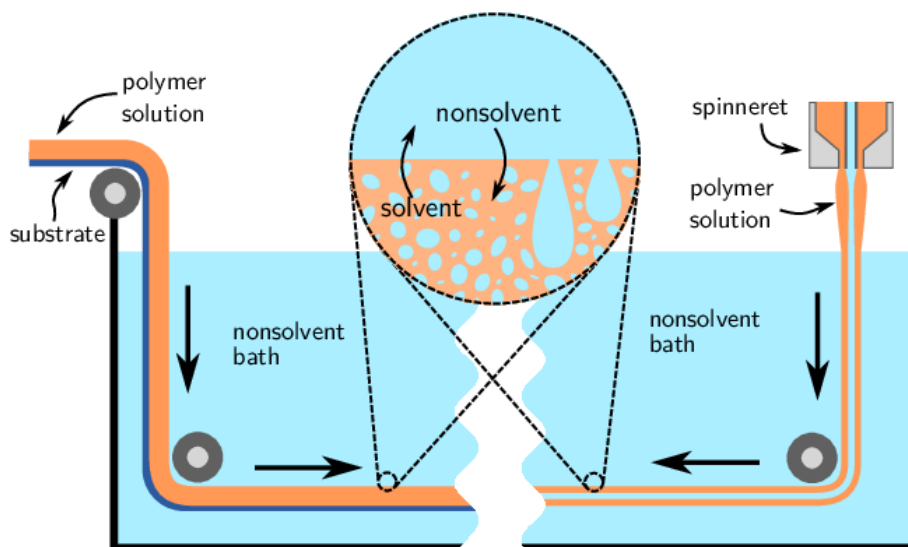


Figure 4: An illustration of a continuous process of flat sheet membrane production (left) and hollow fiber membrane production (right) employing the non-solvent induced phase separation. Reprinted (adapted) with permission from Tree et al., 2018. Copyright 2023 American Chemical Society. (Tree et al., 2018)

3.1.4. Organic Solvents

Organic solvents play a crucial role in the discussed membrane fabrication methods as they serve as the medium for dissolving the polymer and facilitating the formation of pores in the membrane. The pore formation mechanism depends upon solvent evaporation, causing voids as the polymer condenses into a porous membrane. The solvent is chosen based on the polymer and the process involved. Therefore, the choice of solvent and its concentration strongly influence the membrane's morphology and pore size. (Wienk et al., 1996; Ahmad, Otitoju and Ooi, 2019)

The most commonly used organic solvents in the manufacture of polymer membranes are *N*-methyl-2-pyrrolidone (NMP), dimethylformamide (DMF), dimethyl sulfoxide (DMSO), dimethylacetamide (DMAc), and tetrahydrofuran (THF). The choice of

solvents depends mainly on the polymer used, but every solvent has its unique characteristics. For example, DMF and NMP share similar solubility, but NMP has a higher boiling point than DMF. On the other hand, DMSO is a polar solvent with a good swelling capability towards most polymers. (Monge, Darcos and Haddleton, 2004; Guan *et al.*, 2006; Dong *et al.*, 2021; Shi, Xu and Qiu, 2022)

Outside of the membrane fabrication world, organic solvents have significant disadvantages. Organic solvents are flammable, toxic, and have a negative impact on human health and the environment. NMP having a low flash point makes it a fire hazard. It also causes skin, eyes, and respiratory tract irritation on short exposures and may lead to long-term health disorders (Åkesson, 2001; ILO and WHO, 2021). DMF is linked to several human disorders including liver damage and has a high vapor pressure causing it to evaporate rapidly (Redlich, Beckett and Cullen, 1987; Redlich *et al.*, 1987, 1988; CDC, 1990). DMSO is hygroscopic and can cause equipment corrosion during storage, transport, and operation (Ellson *et al.*, 2005). Some organic solvents are planned to be banned by certain governments due to the risks associated with their use (European Union, 2023).

Many researchers have devised alternatives to organic solvents to address these disadvantages, namely *green solvents*. These green solvents include PolarClean, ionic liquids, triethylphosphate (TEP), methyl lactate, γ -valerolactone (GVL), etc. Some researchers have also explored processes that do not use organic solvents but are based on other ways of phase inversion, such as salt dilution-induced phase separation, which takes advantage of polyanionic and polycationic interaction (Emonds *et al.*, 2021). However, although providing promising results, such processes, and green solvents bear disadvantages. For example, the process of salt dilution-induced phase separation makes use of expensive materials making the process uneconomical. Ionic liquids' manufacturing process is neither clean nor energy efficient, and they exhibit insufficient biodegradability (Kamp *et al.*, 2021). If exposed to the environment, TEP can cause eutrophication in water bodies, stimulating algae growth and devastating natural

ecosystems. Methyl lactate is unable to dissolve most polymers. (Figoli *et al.*, 2014; Dong *et al.*, 2021; Emonds *et al.*, 2021; Kamp *et al.*, 2021)

In the industry, the disposal or reuse of organic solvents involved in manufacturing polymer membranes is typically done through distillation and recycling. Distillation involves separating the solvent from the polymer solution, allowing the solvent to be reused or safely disposed of (Schuldt, Brinkmann and Georgopoulos, 2021). Recycling involves the reuse of the solvent in subsequent batches of the polymer solution (Razali *et al.*, 2015). However, distillation requires a significant investment in equipment. In addition, it can be energy intensive, and recycled organic solvents suffer from a loss of quality over time, leading to unacceptable product quality and contamination. (Seader J. D., 1997; Gadalla *et al.*, 2005)

3.2. Polymer Foams

One of the key aspects that provides polymer membranes with their intrinsic ability of filtration and separation is their inherent porosity. The pores' interconnection, sizes, and porosity determine the filtration and separation performance. Similarly, polymer foams are a class of materials that are characterized by their low density and pores. Foams, however, generally do not require organic solvents in their production processes up to large scale.

Polymer foams are mainly classified as closed-cell foams or open-cell foams. Closed-cell polymer foams have a cellular structure in which the cells are entirely enclosed within a continuous macromolecular phase, creating a low-density, soft, and impermeable material. Some applications of closed-cell foams are thermal insulation, floatation devices, protective packaging, structural insulation panels, sports equipment, etc. Open-cell polymer foams have a cellular structure in which the cells are interconnected, creating a network of open pores throughout the solid macromolecular phase. These interconnections allow air and liquids to flow through these foams, making open-cell foam soft and flexible. These foams generally have a lower bulk density and porosity than closed-cell foams. Open cell foams are commercially used for furniture & automotive cushioning, bedding materials, sponges, air filters, sound insulation, etc. Figure 5 provides a cross sectional schematic of closed and open cell foam. (Khemani, 1997; Okolieocha *et al.*, 2015; Gama, Ferreira and Barros-Timmons, 2018)

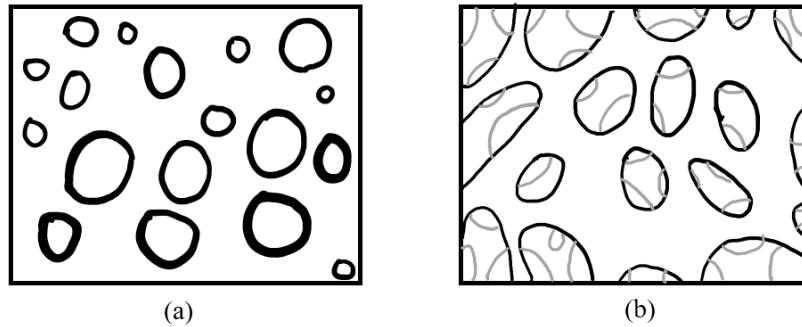


Figure 5: (a) Closed-cell foam structure; (b) Open-cell foam structure.

To manufacture foams, the first general step is that a foaming agent impregnates the polymer matrix under significant pressure. Foaming takes advantage of the plasticizing effect of the foaming agent on the polymer chains, allowing foaming to occur at temperatures well below the polymer's processing temperatures. The degree of reduction of the polymer's glass transition temperature by a foaming agent is influenced by the amount of it that can enter the polymer matrix at a specific temperature and pressure, i.e., the sorption capacity. The sorption of a foaming agent can be measured in any solid polymer by performing a sorption measurement using a balance. Similarly, the diffusion of the foaming agent through the polymer influences the foaming characteristics, which can also be calculated based on the sorption balance measurements. Sorption and diffusion measurements are discussed in section 4.1.5 in detail.

After the foaming agent diffuses within the polymer matrix at a particular pressure and temperature, the polymer-foaming agent exists in a homogenous phase. Change or fluctuations in the boundary conditions leads to nucleation. In polymers, nucleation is the initial formation of a new phase (generally called the daughter phase) that has the potential to grow and become a larger nucleus within the parent phase. This new phase has lower free energy than the original parent phase. In polymer foaming, the parent phase is the polymer melt, and the daughter phase is the bubble or foam cell. The difference in

the Gibbs free energy between the two systems drives the transformation from the parent phase to the daughter phase. The classical nucleation theory is the most commonly used empirical theory to explain the mechanisms of cell nucleation and growth in polymeric foams. The theory assumes that the nucleus (bubble) is a spherical droplet with a sharp boundary and that all nuclei have the same physical properties as the bulk. It also considers the effect of pressure drop on cell nucleation but disregards the effect of pressure drop rates. The cell nucleation theory assumes that instantaneous pressure drop is followed by instantaneous nucleation, although the pressure drop occurs over a span of time. The theory also describes the bubble interface as an infinite flat plane surface. Although these assumptions have limitations, the cell nucleation theory provides a basic conceptual understanding of the nucleation process. It is therefore used to explain the mechanism of bubble nucleation and growth in polymer foams. (Oxtoby, 1998; Kim *et al.*, 2011; Xu *et al.*, 2013; Jung, 2014; Okolieocha *et al.*, 2015)

There are two types of nucleation, homogenous nucleation and heterogeneous nucleation. As the names convey, the formation of cells occurring solely as a response to changes in temperature, pressure, or movement is defined as homogenous nucleation. Heterogenous nucleation, on the other hand, involves triggering through the presence of foreign particles, additives, or pre-existing defects, such as cavities that act as the centers for nucleation. (Costeux *et al.*, 2015; Okolieocha *et al.*, 2015; Mokhtari Motameni Shirvan, Famili and Golbang, 2016)

A form of Gibbs free energy equation (equation (1)) is used to define the nucleation process. The Gibbs free energy change ΔG_E is at its maximum when the radius of nucleus R_n is equal to the critical radius r^* . The critical radius can be defined as the minimum radius a nucleus must have to become a stable cell in the polymer matrix. Below this radius, the nucleus is reabsorbed into the polymer as the energy is insufficient for a nucleus growth. The free volume $\Delta V_{free\ vol}$ due to the presence of additives can be ignored for pristine polymers. The critical radius depends on the pressure difference ΔP and interfacial energy $\gamma_{\alpha\beta}$ as given in equation (2) providing equation (3) for determining

the Gibb's free energy barrier for homogenous nucleation $\Delta G_{E,Hom}^*$. As heterogenous nucleation is triggered by and around the additives or defects, the particle type and topography of its surface play an additional role in influencing the nucleation. The shape factor $S(\theta)$ as given in equation (4) is dependent on the contact angle θ between the bubble and the surface of the particle. This results into equation (5) denoting the Gibb's free energy barrier for heterogenous nucleation $\Delta G_{E,Het}^*$ as a product of the Gibb's free energy barrier for homogenous nucleation and surface factor. This lowers the activation energy needed for bubble formation as shown in Figure 6.

$$\Delta G_E(R_n) = -\frac{4}{3}\pi R_n^3 \Delta P + \pi R_n^3 \gamma_{\alpha\beta} - \Delta V_{free\ vol} \quad \dots(1)$$

$$r^* = \frac{2\gamma_{\alpha\beta}}{\Delta P} \quad \dots(2)$$

$$\Delta G_{E,Hom}^* = \frac{16\pi\gamma_{\alpha\beta}^3}{3\Delta P^2} \quad \dots(3)$$

$$S(\theta) = \frac{1}{4}(2 + 3 \cos(\theta) - \cos^3(\theta)) \quad \dots(4)$$

$$\Delta G_{E,Het}^* = \Delta G_{E,Hom}^* S(\theta)$$

...(5)

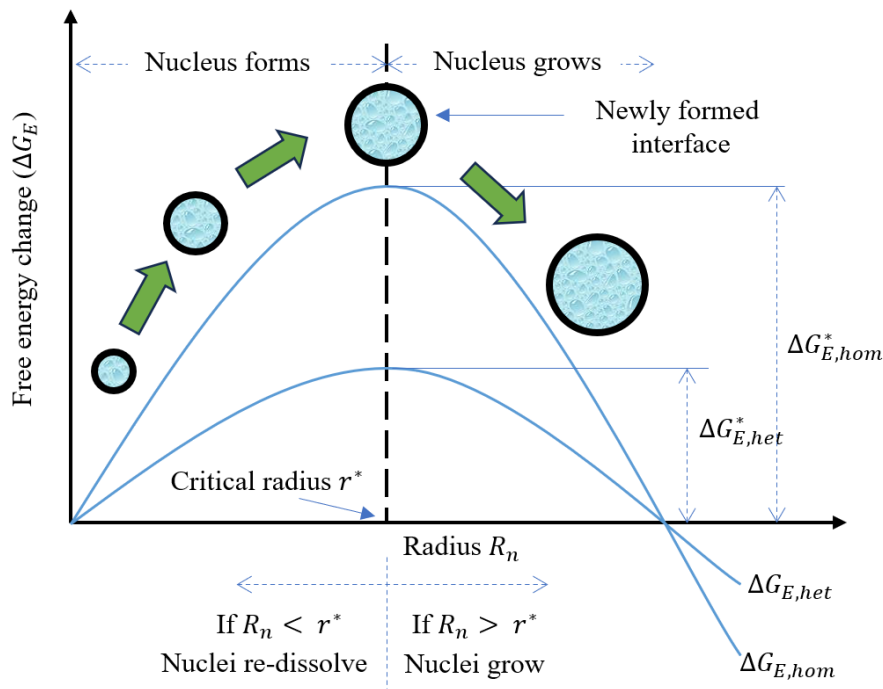


Figure 6: Bubble nucleation and nucleus growth as function of free energy change and its dependence on critical radius. (Okolieocha *et al.*, 2015)

Due to imperfections of the cell nucleation theory, researchers have developed various modifications that take various factors into consideration. Some of these factors are different contact angles based on the variety of shapes and sizes of nucleating agents/defects, the polymer-filler interaction, the interaction between the foaming agents and the polymers, etc. (Okolieocha *et al.*, 2015; Mokhtari Motameni Shirvan, Famili and Golbang, 2016)

In the processing of thermoplastic foams, the most commonly used physical foaming agent is carbon dioxide (CO₂). It has been widely established to provide highly porous foams in most foaming processes. Along with high permeability in polymers, it offers plasticization effect which reduces the polymer's viscosity. This reduced viscosity causes an increased amount of diffusion, which enables higher expansion and foamability. Especially, CO₂ in the supercritical state produces highly porous foams with high cell nucleation. (Han *et al.*, 2002; Sauceau *et al.*, 2011; Okolieocha *et al.*, 2015; Chauvet, Sauceau and Fages, 2017; Owusu-Nkwantabisah, Staudt and Lesser, 2018; Jin *et al.*, 2019)

Other foaming agents include nitrogen, water, air, Freon, hexane, dichloroethane and certain other organic liquids. Chemical blowing agents are mainly used in manufacturing elastomeric foams. They include sodium bicarbonate, hydrogen peroxide, etc. (Han, Kim and Malhotra, 1976; Gutmann *et al.*, 2010; Jin *et al.*, 2019)

3.2.1. Manufacturing Polymer Foams

There are several methods for manufacturing polymer foams, including batch foaming, foam extrusion, injection molding, compression molding, and chemical foaming. Unlike the processes used to manufacture polymer membranes, the following methods do not involve organic solvents.

3.2.1.1. Batch Foaming

Batch foaming, also known as solid-state foaming, is a technique commonly practiced by researchers to examine the foaming performance of various polymers at various processing conditions. Additionally, it offers high control of process parameters allowing high reproducibility of the foaming results. The method takes advantage of the sorption of the foaming agent into the polymer at temperatures well below the polymer's glass

transition temperature by exerting high pressure. The two-stage process in batch foaming involves diffusion of gas into the polymer followed by controlled expansion of foam cells at higher temperatures. As shown in Figure 7, in the first stage, a polymer sample is placed within a pressure vessel at a given temperature, and a foaming agent is introduced at high pressure. The pressure vessel is allowed to stay in this state for a given amount of time until equilibrium is reached. The equilibrium is generally determined by the time taken for the sample to be thoroughly saturated with the foaming agent. For the second stage, the pressure vessel is depressurized, and the sample is exposed to a higher temperature for a limited time, generally ranging between a few seconds to a few minutes. This high-temperature exposure could include immersing the sample in an oil bath, inserting it in a preheated oven, or placing it between hot plates. This higher temperature, also known as foaming temperature, softens the polymer and simultaneously causes the expansion and release of the diffused foaming agent. This expansion of the foaming agent within the polymer matrix in the presence of heat leads to the formation of foam cells. The foaming temperature can be below the glass transition temperature of the pristine polymer as the diffused gas within the polymer chains enables their mobility, thus resulting in glass transition occurring at a lower temperature. However, the foaming temperature may also be higher depending on the resultant foam properties. Complex shapes of polymers pre-formed using techniques such as compression molding, injection molding, or additive manufacturing can be foamed using this batch foaming. As it is a discontinuous process, the boundary conditions can be set with high customization and accuracy. The polymer, foaming agent, as well as the process parameters such as loading temperature, pressure, time, and foaming temperature, time, influence the final properties of the foam such as pore size, porosity, density, open/close cells, pore density, mechanical strength, etc. Batch foaming being a discontinuous, lengthy, and non-scalable process, limits its execution on a large scale. However, the customizability and accuracy offered at small scale by batch foaming, makes it attractive for studying the foaming performance of new polymers or polymeric materials. (Miller, Chatchaisucha and Kumar, 2009; Guo and Kumar, 2015; Guo, Nicolae and Kumar, 2015; Okolieocha *et al.*, 2015)

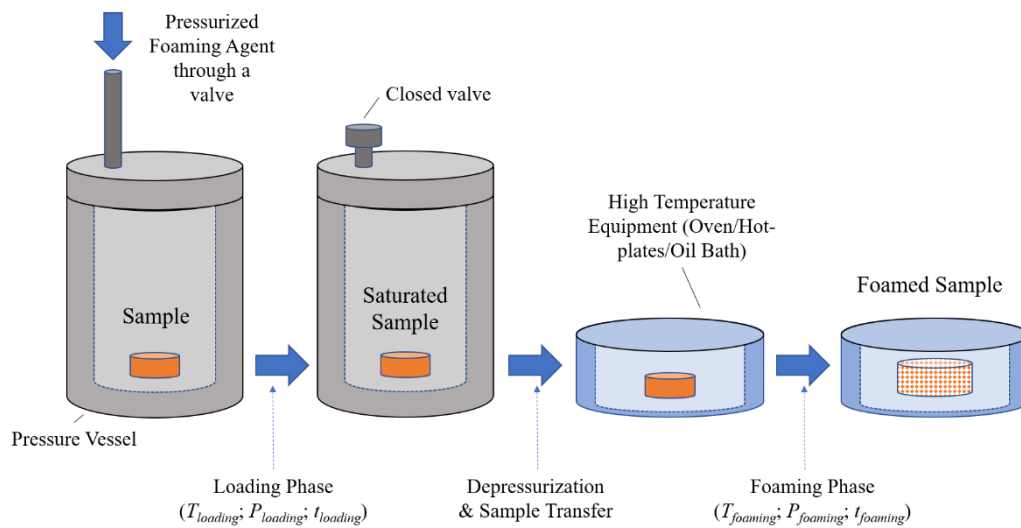


Figure 7: Illustration showing batch foaming also known as solid-state foaming process.

A significant drawback of the batch foaming process is the non-foamed 'skin layer' lurking on the surface of the batch foamed sample. As the whole sample is covered with this non-foamed layer, no cell structures are seen unless the sample is cross-sectioned or through any cracks occurring in the sample during foaming due to expansion. Between the loading and the foaming stage of batch foaming, there is a time gap when the samples are depressurized and subjected to foaming temperatures. During this time, desorption of the foaming agent occurs from the sample. This desorption begins at the surface and progresses inwards until the sample is subjected to foaming temperatures, where the remaining foaming agent causes foaming. Due to the absence of a foaming agent on the surface of the samples, the surface layer does not foam, leading to the formation of the skin layer. Figure 8 shows a schematic of a cross-sectional scanning electron micrograph of a batch foamed polymer sample showing the progression of foam structure through sample thickness. Thus, although an open-celled foam structure is achieved in a polymer sample during batch foaming, the skin layer does not allow the usage of this foam for

permeation. A solution to this is proposed and successfully implemented in this work. (Kumar and Weller, 1994; Guo, Nicolae and Kumar, 2015)

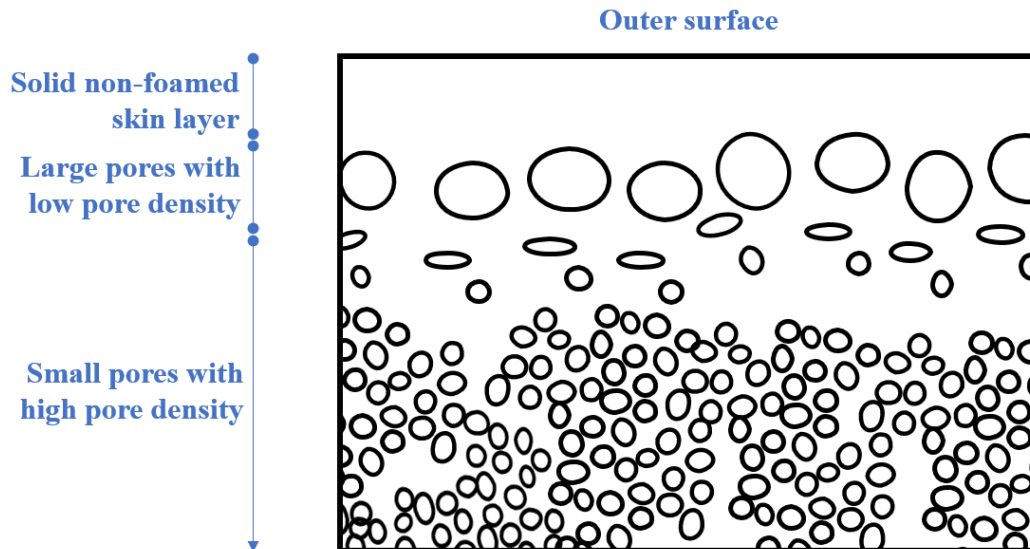


Figure 8: Illustration indicating variation of the microstructure across the thickness in cross-sectioned polymer foam, foamed using batch foaming.

3.2.1.2. Foam Extrusion

Foam extrusion is a well-established technology for producing foamed polymer extrudates, and it can be easily scaled up for industrial production. Unlike batch foaming, foam extrusion is a continuous process that utilizes the physical mixing of the polymer melt with the foaming agent at elevated temperatures and pressures. Foam extrusion is based on ‘melt extrusion’, the more widely used polymer processing technique only second to injection molding. Melt extrusion is a process of melting polymer pellets in an extruder at elevated temperatures, allowing the required mixing and releasing the melt in a two-dimensional form through a nozzle. The two-dimensional form allows a continuous production of extrudate that takes its shape as the melt cools down. Additional to the

extruder, foam extrusion typically consists of an inlet for the foaming agent in case of physical foaming agents, with optional additions of mixing elements such as twin-screw, static or rotary mixers, melt pumps, etc. (Huang, 2000; Sauceau *et al.*, 2011; Lee and Park, 2014)

As shown in Figure 9, the polymer is fed through the hopper and is allowed to melt in the initial heating zones of the extruder whose rotating screw transports the polymer melt towards the nozzle due to the screw's helical profile. The foaming agent is then introduced into the extruder and thoroughly mixed with the polymer melt under elevated pressures and temperatures. The high pressures facilitate the diffusion of the foaming agent within the polymer matrix. In addition, the high temperatures help to reduce the viscosity of the melt. In certain polymers, the high temperatures further accelerate the diffusion into the polymer matrix up to a certain temperature limit. As the material exits the extruder through a nozzle towards ambient conditions, the foaming agent nucleates due to the change in temperature and pressure and expands into cells, forming a foam structure. (Lee *et al.*, 2000; Lee and Park, 2014)

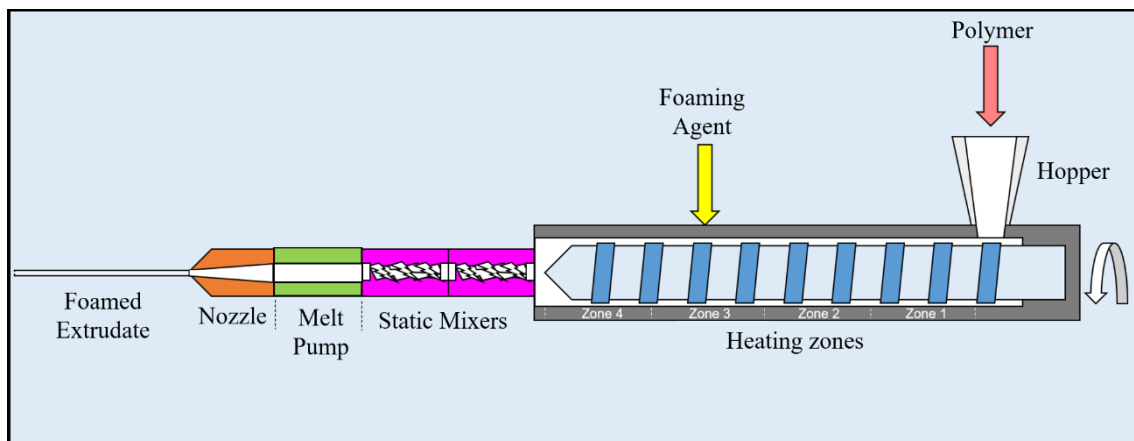


Figure 9: A basic foam extrusion schematic. A single screw extruder with four heating zones having an inlet for foaming agent at the compression zone of the screw,

connected to static mixers, a melt pump and a nozzle, working in a serial configuration to deliver a foamed extrudate.

Like batch foaming, various factors influence the formation of cells or pores, such as the polymer, foaming agent, feed rate, extruder temperature, extruder type (amount of mixing taking place), nozzle size, nozzle temperature, pressures, etc. Most thermoplastics polymers can be foam extruded. However, the quality and properties of the foam depend on the factors discussed before. Many researchers have studied the influence of various processing conditions on the foaming behavior of various polymers using foam extrusion. Besides the polymer and the foaming agent, the most influential process parameter determined by these studies is the nozzle temperature, as the pressure & temperature drop that facilitates the cell/pore formation occurs at the nozzle. (Park, Behravesch and Venter, 1998; Lee and Park, 2014; Standau, Zhao, *et al.*, 2019; Yeh *et al.*, 2019; Shabani *et al.*, 2021; Doyle, 2022; Kalia *et al.*, 2022)

In foam extrusion, the extruder temperatures are generally set slightly below the processing temperatures of the respective polymers due to the plasticization effect occurring due to the introduction of a foaming agent, thus decreasing the viscosity. Generally, the nozzle temperature is set lower than the extruder temperatures. A lower nozzle temperature increases viscosity, leading to high pressures that facilitate better nucleation. However, the hindrance towards bubble expansion caused by the increased viscosity may lead to smaller pore sizes and low porosity. On the other hand, a high nozzle temperature leads to a lower viscosity allowing low resistance to bubble growth, causing fewer cells to be nucleated in the first place due to lower pressures. Therefore, it is essential that optimum nozzle temperatures are identified and set to obtain the desired foam quality. Similarly, other processing conditions need to be optimized individually and in combinations. (Verreck *et al.*, 2006; Standau, Castellón, *et al.*, 2019; Shabani *et al.*, 2021; Kalia *et al.*, 2022)

Although not as accurate and controllable due to its large scale, foam extrusion provides a simple and flexible method for producing polymer foams. Due to its continuous production, foam extrusion is a cost-effective and scalable technology for producing foamed polymer extrudates of various shapes and sizes, with applications in the construction, packaging, and automotive industries. (Lee and Park, 2014)

3.2.1.3. Other Foaming Techniques

Chemical foaming is a method in which two chemical components react to expand and produce a polymer foam. Polyurethane (PU) foams are mainly manufactured using this process. PU foam is created by mixing two components, a polyol, and an isocyanate prepolymer, in the presence of a foaming agent and a catalyst such as an amine, which then react exothermically and expand to form a foam structure while simultaneously solidifying over time. For producing PU foam products, the mixture is poured into a mold immediately after mixing the two components, where expansion and solidification are allowed to occur, producing the final PU foam product. PU foams can be manufactured as both closed-cell and open-cell foams. (Sambasivam, White and Cutting, 2016; Gama, Ferreira and Barros-Timmons, 2018; Skleničková *et al.*, 2021)

Foam injection molding, also known as microcellular injection molding, is a process that combines injection molding and foaming. Similar to foam extrusion, inlets on the screw barrel allow the influx of the foaming agent into the polymer melt. Using the lateral movement of the screw, this mixture is injected into the mold, where it foams into the mold's shape. After cooling, the foamed product is ejected and ready for further use. The process is commonly known as the MuCell[®] process due to the first patented microcellular injection molding machine. Like injection molding, this process is widely used in the industry to manufacture foamed articles and products on a large scale. (Wang *et al.*, 2018; Jiang *et al.*, 2021)

3.2.2. Polymer Foams as Membranes

Although filtration is a widely used application of open-cell foams, the application of polymer foams as separation membranes has yet to be widely pursued. Of those attempted, there have never been any foams capable of ultrafiltration. Producing a foam with cell sizes in the nanometer range and maintaining open cellularity would allow the implementation of this foam as an ultrafiltration membrane is produced in the form of thin films (to resemble flat sheet membranes) and hollow fibers (as hollow fiber membranes). Interestingly there have been many studies and successful attempts by researchers to manufacture foams with cell sizes in the nanometer range. However, they were closed cellular foams lacking permeation. (Huang, 2000; Krause, van der Vegt and Wessling, 2002; Sorrentino, Aurilia and Iannace, 2011; Gong, Taniguchi and Ohshima, 2014; Guo and Kumar, 2015; Guo, Nicolae and Kumar, 2015, 2016; Brincat *et al.*, 2016)

3.2.3. Other Melt Extrusion Techniques for Manufacturing Membranes

Using melt extrusion, some researchers have attempted to develop permeable membranes with separation performance via cold stretching. As the polymer melt exits the extruder, it is stretched by rollers or conveyors with a drawing speed higher than the extruder throughput. The stresses caused due to these tensile forces exerted while drawing the extrudate cause formation of microcracks throughout the extrudate, which act as pores. Apart from polymer and extruder parameters, another significant factor influencing the porous morphology is the degree of stretching. The porosity results from *crazing*, a pore/cavity formation phenomenon occurring due to the induction of external stresses combined with crystalline structures in the polymer matrix. Thus, this method is limited to semi-crystalline polymers and unsuitable for amorphous polymers. (Kim *et al.*, 1994; Xanthos *et al.*, 2002; Chandavasu *et al.*, 2003; Feng *et al.*, 2018; Luo, Xie and Qin, 2021)

3.3. Polymers

One of the initial decisions in choosing a polymer for foaming is based on the presence of crystallinity. Although high crystallinity improves the mechanical properties of polymers, semi-crystalline polymers with high crystalline content are not preferred for producing highly porous foams due to their low foamability. The presence of crystalline structures hinders the diffusion of the foaming agent into the amorphous parts of the polymer leading to foam with low porosity. However, due to low costs, certain commercial semi-crystalline polymers, polyethylene (PE), and polypropylene (PP), are used to manufacture foamed products. For foaming such polymers, the process settings are optimized such that a low amount of crystallinity exists. Further, these crystallites act as nucleation sites during foaming, thus allowing uniform foaming. (Tabatabaei Naeini, 2012; Okolieocha *et al.*, 2015)

In amorphous polymers, the molecular weight of the polymer also plays a vital role in the foaming results. A high molecular weight due to presence of high free volume delivers high porosity and smaller cell sizes. However, high molecular weight also increases the processing temperatures by increasing the viscosity of the polymers. In addition, high molecular weight polymers are generally expensive and difficult to produce. (Zhang, Rodrigue and Ait-Kadi, 2003; Yeh *et al.*, 2020)

Many researchers have used polymer blends taking advantage of the synergetic performance of more than one polymer to deliver highly porous foams with small cell sizes. Preparation of a blend comprising miscible as well as non-miscible polymers can uniquely enhance the foaming characteristics. For example, miscible polymers form homogenous blends where homogenous nucleation occurs throughout the polymer delivering a uniformly distributed foam structure. Non-miscible polymers, on the other hand, form heterogeneous blends in which the minor component acts as nucleation locations for bubble formation. A uniform distribution of the various blend components

is desired in this case. (Ruckdäschel *et al.*, 2010; Bärwinkel *et al.*, 2016; Kong *et al.*, 2016; Pinto, Dumon and Rodriguez-Perez, 2017; Haurat and Dumon, 2020)

Polymer blends are generally manufactured using a twin-screw compounding extruder. First, the polymers are pre-mixed and inserted in the extruder, where they are melted and allowed to mix as the melt travels through a series of mixing elements on the extruder screw. Finally, the blend emerges from the extruder nozzle and is generally cut into pellets using a granulator. Another method of manufacturing polymer blends uses a common organic solvent in which both polymers are dissolved. After mixing, the solvent is allowed to precipitate, leaving behind a polymer blend.

3.3.1. Polyethersulfone

Polyarylsulfones such as polysulfone (PSU), polyethersulfone (PESU), and polyphenylsulfone (PPSU) are a class of high-performance thermoplastic polymers. Polyethersulfone (PESU) is a well established polymer for manufacturing ultrafiltration membranes. PESU's molecular structure, as shown in Figure 10 contains aromatic rings, ether linkages, and sulfonyl groups that provide thermal, chemical, and structural stability, making PESU ideal for applications requiring high strength, high temperature, and chemical resistance. The glass transition temperature of PESU lies between 220 °C – 240 °C, depending on the molecular weight. This high thermal stability enables processing temperatures ranging from 320°C to 400°C for melt processes such as extrusion and injection molding. The use of high temperatures in its processing accounts for its high costs compared to economic polymers such as PS, PP, PE, etc. The presence of sulfonyl groups and ether linkages in PESU provides high resistance to various chemical solvents and aggressive environments, making it ideal for anti-fouling membrane applications. The presence of two aromatic groups provides high mechanical strength providing structural resistance to high pressures. (Qi and Huang, 1998; Giesa and Schmidt, 2001; Lutz, 2010; Biernat, 2018; Tsehaye, Velizarov and Van der Bruggen, 2018; BASF SE, 2022)

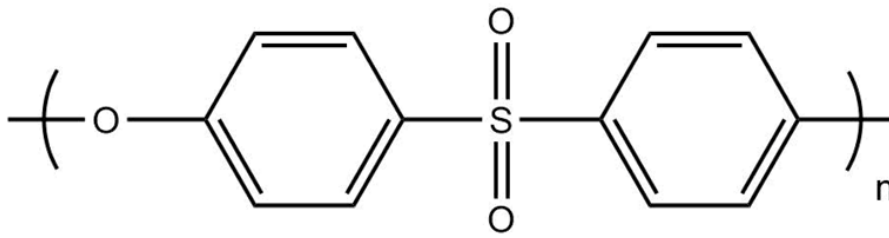


Figure 10: Molecular structure of PESU.

Using batch foaming, Krause et al. manufactured PSU uniform open-celled foams with cell sizes averaging 1 μm . The thin-film application of these foams was aimed at manufacturing membranes. However, this manufacturing process involved using the organic solvent THF whereas, without its use, open cellularity could not be achieved. They reported open-cell structures on the walls of the microcells ranging between 10 and 100 nm in one study and between 50 and 200 nm in another. In addition, the influence of critical carbon dioxide on the foaming performance was studied. Similar results were reported when PESU was used. However, this manufacturing process involved using the organic solvent THF whereas, without its use, open cellularity could not be achieved. (Krause *et al.*, 2001; Krause, van der Vegt and Wessling, 2002)

Sorrentino et al. used two similar methods of solid-state foaming on PESU, PPSU, and other polymers, one where the foaming temperature was reached in the pressure vessel before depressurization and one where the vessel was depressurized before subjecting the samples to the foaming temperature using an oil bath. To differentiate between the processes in their study, they named the former batch foaming process and the latter solid-state foaming process. The processes delivered closed cell foams with average cell sizes of approximately 1 μm for PESU and PPSU. They also reported the presence of nanopores on the cell walls of the microcells. In addition, a dense skin layer on the foamed samples hindered any permeability for these foams. (Sorrentino, Aurilia and Iannace, 2011)

Guo et al. reported PSU and PPSU foams with microcellular cell sizes that contained open porous cell walls with cells ranging between 20 and 40 nm. Although thorough permeability was not achieved, the interconnection between the nanocellular 'bi-continuous' pores was established. The formation of nanopores on the cell walls was evaluated, and stress-induced nucleation and spinodal decomposition were proposed as the likely reasons. Gong et al. studied the same phenomenon using polycarbonate (PC) foams. They justified the formation of such structures due to the biaxial tensile deformation caused by the stretching of fibrils in the polymer matrix due to nucleation and bubble growth. (Gong, Taniguchi and Ohshima, 2014; Guo, Nicolae and Kumar, 2015, 2016)

Owusu-Nkwantabisah et al. created open-cell PESU foams using supercritical CO₂ and superheated water as co-blowing agents in solid-state foaming. As a result, microcellular open-celled foam with cell sizes between 4 and 10 μm was achieved. (Owusu-Nkwantabisah, Staudt and Lesser, 2018)

Using foam extrusion, Huang manufactured PESU closed cell foams with cell sizes averaging 10 μm. An annular slit nozzle was used to extrude the said foam in hollow-fiber geometry. The high-temperature characteristics of PESU leading towards high viscosity required the extruder temperatures of 350 °C, and a nozzle temperature of 280 °C was the lowest possible. (Huang, 2000)

3.3.2. Poly(*N*-vinylpyrrolidone) and Poly(ethylene glycol)

In polymer membranes, along with the primary matrix polymer, two commonly used polymers are Poly(*N*-vinylpyrrolidone) (PVP) and Poly(ethylene glycol) (PEG). Their pore-opening characteristic and water-solubility make them attractive for manufacturing polyarylsulfone membranes. In addition, such membranes have been reported in the

literature to bear high hydrophilicity and state-of-the-art ultrafiltration performance. (Al Malek *et al.*, 2012; Hao *et al.*, 2012; Raviv and Klein, 2012; Ibrahim, El-Wassefy and Farahat, 2017; Dai *et al.*, 2019; Aili *et al.*, 2020; Dibrov *et al.*, 2020; Gronwald and Weber, 2020; Gronwald *et al.*, 2020; Grünig *et al.*, 2020; Jaleh *et al.*, 2020; Zhang *et al.*, 2021; Choi, Ingole and Park, 2022)

Poly(*N*-vinylpyrrolidone) (PVP) is a water-soluble polymer made of repeating *N*-vinylpyrrolidone monomers, available in a wide range of molecular weights ranging from 2500 to 1000000 Da. It has good film-forming properties due to less frictional properties. PVP finds intensive use in the pharmaceutical, food, and cosmetic industries due to its non-toxicity and affinity to polar molecules. Along with its role as a pore-opener in fabricating polymer membranes, PVP also improves properties such as accelerating phase separation in processes involving organic solvents and increasing water flux. PVP can be incorporated into the polymer matrix or applied as a membrane surface coating. Similar to PESU, PVP is soluble in NMP. (Haaf, Sanner and Straub, 1985; Bühler, 2005; Göthlich, Koltzenburg and Schornick, 2005; Ashland, 2013; Tiron, Vlad and Baltă, 2018; BASF SE, 2023)

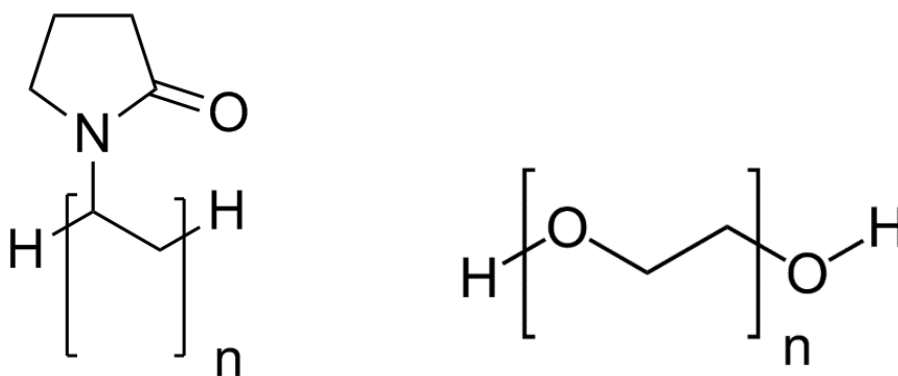


Figure 11: Molecular structure of PVP (left) and PEG (right).

Poly(ethylene glycol) (PEG) is a versatile, water-soluble polymer known for its biocompatibility and low toxicity. PEG is synthesized by the polymerization of ethylene oxide. However, molecular weights above 20,000 Da are generally referred to as poly(ethylene oxide) (PEO). With molecular weights ranging from 200 to a few million Daltons, PEG finds its applications widely in the pharmaceutical and cosmetic industry, as well as in adhesives and paints. Along with water, PEG is soluble in ethanol, benzene, and various other solvents. PEG has a high affinity towards CO₂ and is therefore used in gas separation membranes for CO₂ absorption. (Lillepärq, Georgopoulos and Shishatskiy, 2014; Rahman *et al.*, 2015; Halder *et al.*, 2018)

In water filtration membranes, the hydrophilic nature of PEG allows for high water flux and low fouling. However, the mechanical properties are weakened with high amounts of PEG. In melt processing of polymers resistant to high temperatures, adding PEG reduces the processing temperature, thus acting as a plasticizer. (Car *et al.*, 2008; Porter, Sackett and Liu, 2009; Ma *et al.*, 2011; Dimitrov and Tsvetanov, 2012; Hutanu, 2014; Francolini, Hall-Stoodley and Stoodley, 2020; Zarrintaj *et al.*, 2020; Shah *et al.*, 2021)

4. Methods

The principles behind the methods used in this work are mentioned in this section. The exact steps and conditions for the carried-out measurements and experiments are already published in the articles of this cumulative work. However, for specific methods mentioned here, more details are provided.

4.1. Material Characterization Methods

4.1.1. Differential Scanning Calorimetry

In polymer characterization, differential scanning calorimetry (DSC) is a widely used thermal analysis method. This technique measures the difference in heat flow between a sample and a reference material as a function of temperature or time under controlled heating and cooling conditions. The amount of heat absorbed or released by the sample is measured, which helps determine and study the thermal events occurring in the sample at that specific background conditions. Thermal events associated with changes in the material, such as glass transitions, melting, crystallization, decomposition, etc., and reactions occurring within the sample can be observed. The polymer's structure and properties can be inferred from this information. This allows a better understanding of the polymer and can assist vastly in its identification and applications.

DSC is carried on a calorimeter which consists of two compartments, one for the sample and another for reference material. The reference material is generally inert, or the compartment is kept empty. During the measurement of the sample, both compartments are subjected to inert gas and are maintained at a constant temperature difference by being subjected to the same temperature program. As the sample and reference are heated or cooled, they may undergo phase transitions (e.g., melting, crystallization, glass transition) that absorb or release heat. These thermal events cause a change in the heat flow to the sample and reference pans, which are then detected by a differential thermocouple. The differential thermocouple records the difference in heat flow between the sample and reference as a function of temperature. The heat flow is determined by measuring the temperature difference between the sample and reference pans and converting it to a voltage signal. This voltage is then converted to a digital signal that can be displayed and analyzed on a computer. The resulting data are then plotted as a function of temperature, with the heat flow on the y-axis and temperature on the x-axis, into so-called thermograms. The thermograms are analyzed to identify the thermal events associated

with changes in the polymer and to determine their characteristic parameters, such as the glass transition temperature, melting point, crystallization, etc. Multiple heating/cooling cycles are carried out with precise control over the temperature. The heating/cooling rate can also be controlled as certain thermal events may or may not occur at specific rates, whereas the effect of this rate on the intensity of these events may also be studied. Figure 12 provides a basic illustration of a calorimeter. (Kong and Hay, 2002; Schick, 2009; Kalogeras, 2016; Drzeżdżon *et al.*, 2019; NETZSCH, 2023b)

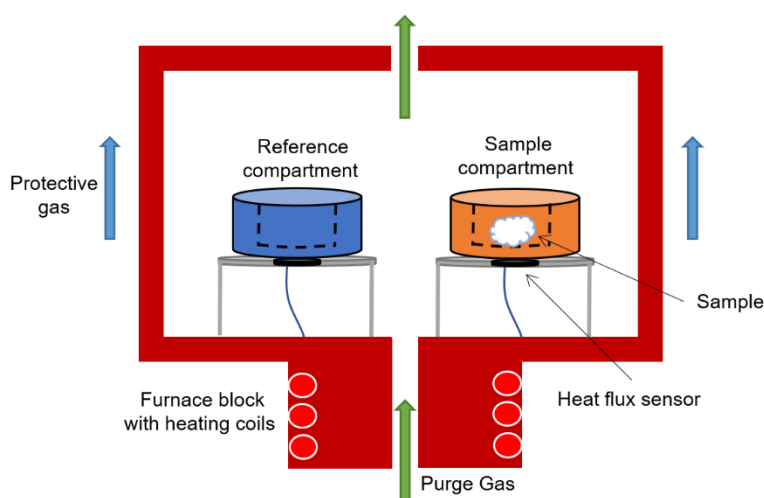


Figure 12: Differential scanning calorimeter measurement cell's schematic representation.

The glass transition temperature (T_g) is an essential parameter for polymers. It is usually determined from the DSC data as the onset of a step change in the heat flow signal during heating. This step change is associated with the relaxation of the amorphous regions of the polymer from a rigid to a rubbery state, indicative of the mobility of the polymer chains. The melting point (T_m) is determined from the endothermic peak in the heat flow signal during heating and is associated with the melting of the crystalline regions of the polymer. The enthalpy of fusion is calculated from the area under the melting peak and

is related to the energy required to melt the crystalline regions of the polymer. Figure 13 provides an overview of a DSC thermogram. (Kong and Hay, 2002; Schick, 2009; Kalogeras, 2016; Drzeżdżon *et al.*, 2019)

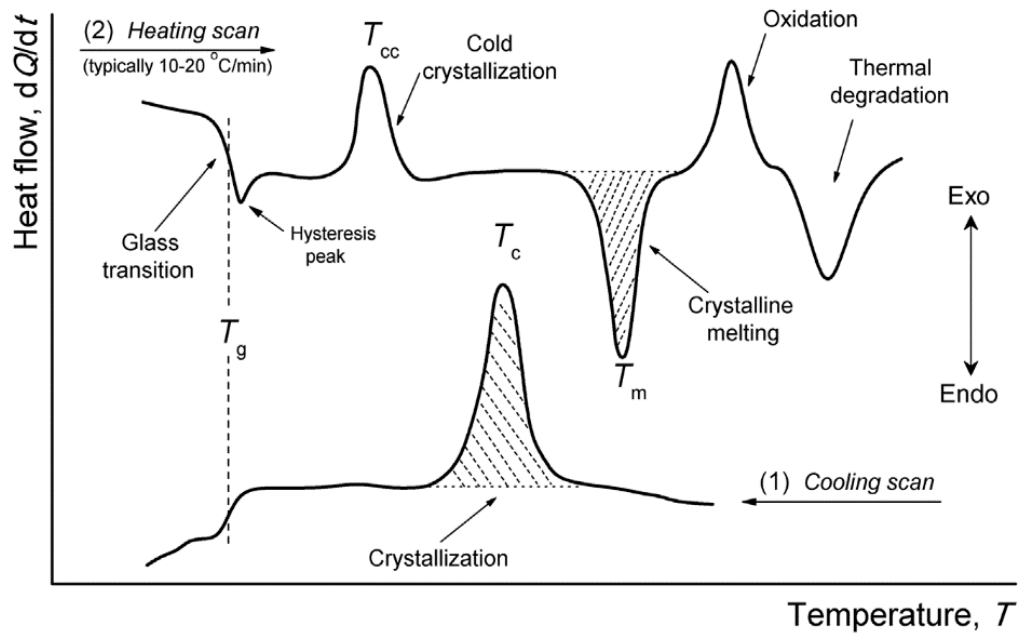


Figure 13: Interpretation guide of a sample DSC thermogram. Reprinted (adapted) with permission from Kalogeras *et al.*, 2016. Copyright 2023 John Wiley and Sons.

For the characterization of the thermal properties of the polymers and polymer blends used in this work, DSC was carried out. Although denoted specifically in each published article, due to its wide use in this work, Table 3 shows the parameters used in DSC for respective polymers.

Polymer / Polymer Blend	Temperature Intervals for First Two Cycles [°C]	Heating Rate for First Two Cycles [K min ⁻¹]	Temperature Interval for Third Cycle [°C]	Heating Rate for Third Cycle [K min ⁻¹]	T _g Determination
PEG	-130 to 100	10	-130 to 260	30	Third heating interval
PESU	25 to 260		-	-	Second heating interval
PESU/PVP	25 to 260		-	-	Second heating interval
PESU/PEG	-130 to 180		-130 to 260	30	Third heating interval
PESU/PEG/PVP	-130 to 260		-130 to 260	20	Second heating interval

Table 3: Parameters of Differential Scanning Calorimetry (DSC).

The T_g of a polymer blend comprising of miscible polymers can be determined by following the Couchman equation (equation (5)) and Fox equation (equation (6)). Similarity or dissimilarity between a polymer blend's calculated T_g and the measured T_g can be used to determine the homogeneity or heterogeneity of the said blend. The information such as the polymers' T_g and the change in heat capacities is obtained using DSC.

$$\ln(T_g/T_{g,1}) = \frac{w_2\Delta c_{p,2}\ln(T_{g,2}/T_{g,1})}{w_1\Delta c_{p,1}+w_2\Delta c_{p,2}} \quad \dots(6)$$

$$\frac{1}{T_g} = \frac{w_I}{T_{g,I}} + \frac{w_{II}}{T_{g,II}} \quad \dots(7)$$

where,

w_1 = Mass fraction of polymer I

$c_{p,1}$ = Heat capacity of polymer I

$T_{g,1}$ = Glass transition temperature of polymer I

w_2 = Mass fraction of polymer II

$c_{p,2}$ = Heat capacity of polymer II

$T_{g,2}$ = Glass transition temperature of polymer II

4.1.2. High Pressure DSC

High-pressure differential scanning calorimetry (HP-DSC) is an expanded form of DSC where the sample and reference compartments are kept in a pressure vessel. This pressure vessel can then be pressurized with gas while carrying out a measurement. The used gas's effect and pressure on the thermal characteristics and events are analyzed. Carbon dioxide (CO₂) is commonly used for HP-DSC. (Höhne, 1999; Roß and Frerich, 2021; Mettler-Toledo, 2022)

As CO₂ is a plasticizing agent, its presence decreases the T_g and the T_m of polymers while increasing the crystallization rate. As discussed earlier, CO₂ molecules can diffuse into the polymer chains and increase the free volume, reducing the intermolecular forces and making the polymer chains more flexible. This displacement of T_g and T_m of the polymer due to CO₂ varies for different polymers as well as can be dependent on CO₂ pressure. As the diffusion of CO₂ into the polymer matrix and the following plasticization effect is highly important in polymer foaming, performing HP-DSC on polymers gives a comprehensive understanding of the same. For example, a polymer sample, showing high displacement in T_g when applied with certain CO₂ pressure may be predicted to foam better, whereas a small or no displacement in T_g may indicate a disappointing foaming performance. (Höhne, 1999; Huang *et al.*, 2016)

In this work, HP-DSC was employed to investigate the influence of CO₂ pressure on the thermal properties of PESU and PESU/PVP blends such that their foaming performances could be predicted and compared. To determine the saturation time, a diffusion coefficient D and the sample particle radius R_p of the polymer powder were used. Saturation time was calculated using $t_{sat} = \frac{R_p^2}{D}$ which allowed running the measurement only after allowing the sample to saturate with CO₂ in this time.

4.1.3. Thermogravimetric Analysis

Thermogravimetric analysis (TGA) is used to determine the thermal stability and composition of polymers by measuring the change in mass as a function of temperature and time. This method is widely used to characterize polymers to determine their decomposition behavior. TGA can also support in the identification of the composition of polymer mixtures.

The basic principle of TGA is to measure the weight loss of a sample as it is heated under controlled conditions. The TGA instrument consists of a balance, a furnace, a temperature controller, and a computer. The balance measures the mass of the sample, and the furnace can provide a controlled heating rate or a constant temperature, and depending on the type of experiment, (mass loss of the sample as a function of temperature or time). The analysis of TGA data involves the interpretation of the thermograms. The different stages of the thermal degradation process are identified by looking for changes in the amount and the mass loss rate, which correspond to different thermal events.

As shown in Figure 14, TGA works by heating the crucible holding the sample in a controlled environment, typically under an 'inert' non-reactive and non-flammable gas such as Argon or Nitrogen, which is used to prevent reactions such as oxidation occurring in polymers primarily due to exposure to high temperatures in the presence of air. The gas is introduced into the sample chamber to displace air, thus creating a controlled atmosphere at ATM. There are multiple ways of using TGA, such as adiabatic and isothermal heating. In adiabatic heating, the sample is heated at a constant rate, and the change in mass is recorded as the temperature increases, whereas, in isothermal heating, the sample is heated to a certain temperature, and this temperature is maintained for a certain amount of time where the mass change is recorded as a function of time.

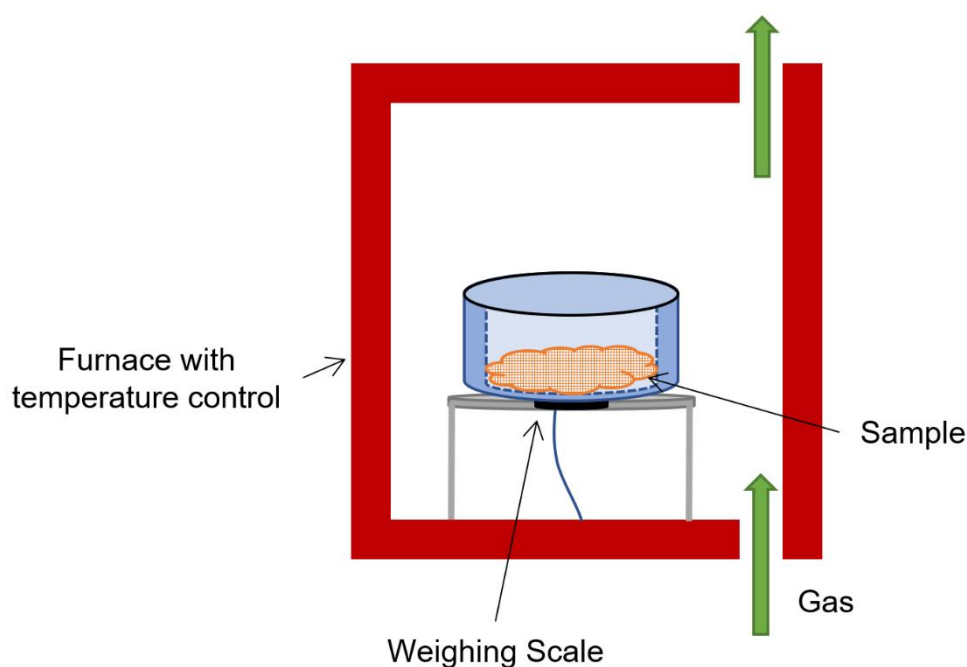


Figure 14: Illustration of a TGA instrumentation.

In polymers, the mass change when exposed to high temperatures may occur due to various thermal events, such as decomposition, oxidation, dehydration, sublimation, vaporization, and desorption. The temperature at which a significant weight loss occurs is an indicator of the thermal stability of the polymer sample. TGA also provides indications that help determine the drying temperatures, processing temperature ranges, and presence of any unfamiliar component in the polymer sample. The determination of drying temperatures is carried out by observing the mass loss below and above 100 °C. For example, a non-pre-dried polymer having a slight mass loss between 50 – 60 °C may need drying temperatures of no more than 60 °C, whereas another one experiencing mass loss only after 120 °C may require a higher drying temperature. This also indicates that the former polymer would be softer than the latter, i.e., it has a lower glass transition temperature, which allows the polymer chains to move enough, allowing water to escape the polymer matrix and evaporate.

Determining at what temperature the decomposition of a polymer occurs is of high importance as it allows for setting appropriate processing temperatures for polymers. In the case of blending polymers, if one polymer has a glass transition temperature near the decomposition temperature of the other, blending using melt-compounding is not feasible. The composition of a particular polymer blend may also be determined if the decomposition of the individual components occurs at different temperatures. The percent mass loss at the respective temperature indicates the amount of the polymer component in the sample. The purity of a sample can also be determined by noticing mass losses occurring at unexpected temperatures. A polymer's thermal stability over time can also be analyzed using isothermal TGA.

(Coats and Redfern, 1963; Gabbott, 2008; Ng *et al.*, 2018; Rigoli *et al.*, 2019)

As in this work melt-processing of polymers is important, TGA was used to determine their thermal stability.

4.1.4. Rheology

Rheology is defined as the science of flow. It studies the relationship between the force and deformation of matter and is mainly used in materials that display flow-like properties. In the field of polymers, rheology is a vital tool used to study how the polymer deforms at various temperatures, frequencies, and loads. This allows a detailed outlook of the viscoelastic properties often found for polymers. (Giles, Wagner and Mount, 2005; Ebnesajjad, 2015; Widyatmoko, 2016)

Viscoelastic properties are a combination of two properties: viscosity and elasticity. Viscosity is the measure of a material's resistance to flow, where higher values mean high resistance, i.e., less flow, and lower values mean low resistance. When constant stress is applied to a viscous material, it deforms constantly and maintains the final form upon stress release. Elasticity is the measure of a material's ability to recover its original shape after deformation. The more elastic a material is, the more it can be deformed until the original shape is unrecoverable. Viscoelastic materials such as polymers exhibit both these characteristics. In polymers, various properties, including molecular weight, chemical composition, additives, temperature, processing conditions, etc., significantly affect their viscoelastic behavior. Therefore, measurement of the viscoelastic behavior is crucial in polymer characterization. (Papanicolaou and Zaoutsos, 2011)

Rheological properties of polymers, such as viscosity, storage and loss moduli, strain-softening, etc., are most commonly studied using a shear rheometer. However, other devices, such as viscometers, extensional rheometers, etc., are also used to provide certain viscoelastic characteristics of the polymers. When analyzing using a shear-rheometer, a controlled deformation is applied to a sample, and the resulting stress and strain are measured. There are various configurations a rheometer may be configured with, which can be classified into two types, one used on samples that are solid at room temperature and another that are used to measure liquids and solutions. The former configuration may be a plate-plate, plate-cone, cone-cone, or double cone-plate geometry where the sample

is placed between plates/cones, and one of them applies deformation to the sample relative to the other. In the latter configuration, the liquid sample in a cylinder and another cylinder/spindle rotates or oscillates. In both configurations, the rheometer measures the force resulting from the deformation and computes it to provide the associated stress and strain. This allows for further calculations that provide the sample's viscoelastic properties, such as complex moduli, viscosity, etc. Figure 15 illustrates a plate-plate geometry configuration operating in oscillatory motion in a rheometer. (Ramli *et al.*, 2022)

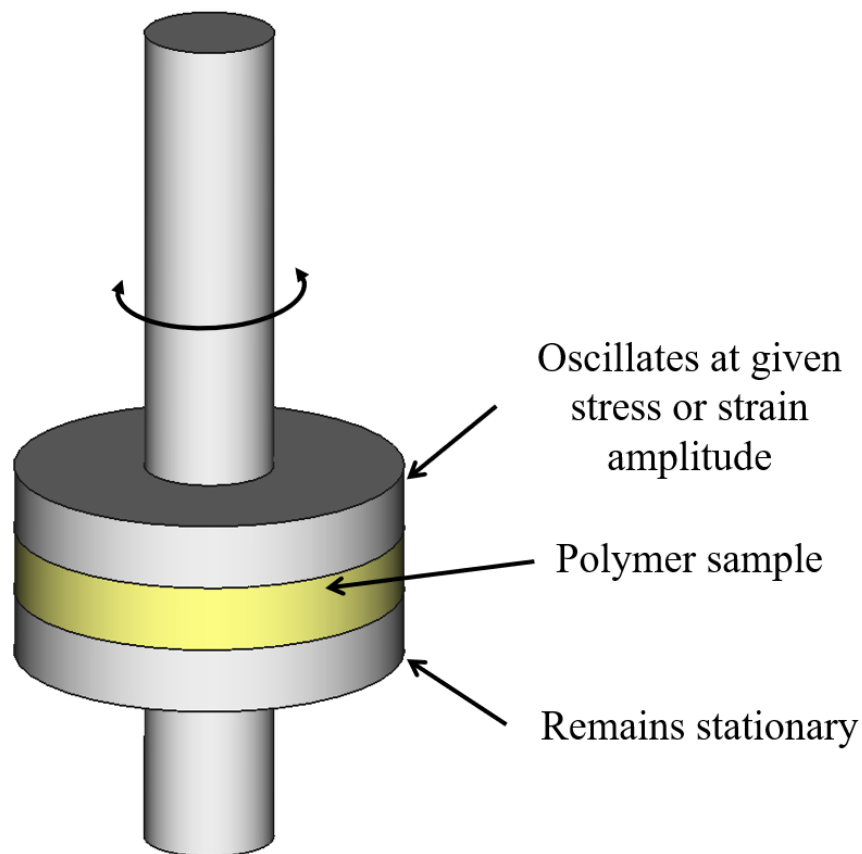


Figure 15: Illustration of a plate-plate geometry configuration operating in oscillatory motion in a rheometer.

The material stiffness or its resistance of deformation is measured by the complex modulus (G^*),

$$G^* = \frac{\sigma_{max}}{\gamma_{max}} \quad \dots(8)$$

where, σ_{max} is the applied stress and γ_{max} is the measured strain in a controlled strain measurement, whereas in a controlled stress measurement σ_{max} is the measured stress and γ_{max} is the applied strain.

In a viscoelastic material, the storage modulus (G') represents the elastic component to the complex modulus, whereas the loss modulus (G'') represents the viscous component. Their relationship can be determined using the following equations,

$$G^* = G' + iG'' \quad \dots(9)$$

$$\tan\delta = \frac{G''}{G'} \quad \dots(10)$$

The complex viscosity (η^*), providing the total resistance to flow, can be found using the following equation,

$$\eta^* = \frac{G^*}{\omega} \quad \dots(11)$$

where, ω is the applied angular frequency.

Rheological measurements can be performed in various ways, depending on the desired properties of the polymer. The following table shows common types of experiments used to study the viscoelastic behavior of polymers.

Sweep Type	Constant Parameter	Information Provided
Frequency	Shear amplitude, Temperature	Complex modulus (G^*) i.e. the elastic (G') and viscous (G'') components of a material's response, loss tangent ($\tan \delta$), crossover frequency (where G' and G'' intersect)
Amplitude	Frequency, Temperature	Linear viscoelastic range, nonlinear viscoelastic properties, yield stress and strain, amplitude region where the relationship between applied stress and resulting strain is linear
Time	Frequency, Temperature	Time-dependent viscoelastic properties such as relaxation time, creep compliance, etc., thermal stability, crosslinking in polymers
Temperature	Frequency, Strain amplitude	Temperature-dependent viscoelastic properties, glass transition temperature (T_g), melting point (T_m),

Table 4: Common experiments in shear-rheometry.

The rheological behavior of polymers can be described using various mathematical models, which attempt to describe the relationship between the deformation of the material and the applied stress or strain. Some of the commonly used mathematical models in rheology of polymers are:

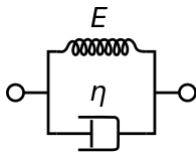
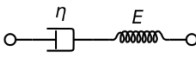
Model	Description	Illustration	Equation	Uses
Maxwell Model	A simple viscoelastic model consisting of a spring and a dashpot in series		$\gamma = \tau \left(\frac{t}{\eta} + \frac{1}{G} \right) \dots(12)$ <p>where, γ = stain, G: shear modulus, τ = time of relaxation, η = Viscosity, t = time</p>	Characterization of viscoelastic properties of polymer melts and solutions
Kelvin-Voigt Model	A simple viscoelastic model consisting of a spring and a dashpot in parallel		$\sigma(t) = \eta \varepsilon(t) + E \varepsilon'(t) \dots(13)$ <p>where, η = viscosity, E = Young's modulus, $\varepsilon(t)$ = instantaneous strain, $\varepsilon'(t)$ = strain rate</p>	Characterization of elastomeric materials
Power Law Model	A model describing non-Newtonian flow of materials with a power-law dependence	$\sigma = \eta \dot{\gamma}^n \dots(14)$ <p>where, σ = shear stress, $\dot{\gamma}$ = shear rate, n = power law index</p>	Characterization of viscoelastic properties of polymer melts and solutions	
Bingham Model	A model describing the behaviour of materials that exhibit a yield stress before flow occurs	$\sigma = \sigma_y + \eta_B \dot{\gamma} \dots(15)$ <p>where, σ_y = yield stress, η_B = Bingham viscosity</p>	Characterization of polymer melts and solutions under processing conditions	
Carreau-Yasuda Model	A model describing shear thinning behaviour using a shear rate dependent parameter	$\frac{\eta - \eta_\infty}{\eta_0 - \eta_\infty} = [1 + (k\dot{\gamma})^a]^{-\frac{n-1}{a}} \dots(16)$ <p>Where, η_0 = zero shear viscosity, η_∞ = infinite viscosity, k = characteristic time, a = parameter denoting the transition between Newtonian and power law</p>	Characterization of polymer solutions and melts ($\eta_\infty = 0$) under processing conditions	
Cross Model	A model describing pseudoplastic flow with asymptotic viscosities.	$\frac{\eta - \eta_\infty}{\eta_0 - \eta_\infty} = \frac{1}{1 + (k\dot{\gamma})^n} \dots(17)$	Characterization of viscoelastic properties of polymer melts, solutions and dispersions	

Table 5: Mathematical models used to describe viscoelastic behaviour in polymers. (Osswald and Rudolph, 2015; NETZSCH, 2023a)

These models are used to describe the complex viscoelastic behavior of polymeric materials. By fitting experimental data to these models, one can extract useful information about the polymers' molecular architecture, relaxation behavior, and flow properties.

Rheological data can also be used to study the miscibility of polymeric blends. A polymer blend exhibiting viscoelastic behavior similar to a homopolymer can be classified as a homogenous blend. To study the miscibility of blends that showed single glass transition in DSC, the time temperatures superposition principle was used to investigate the viscoelastic behavior of the blends. The William-Landel-Ferry (WLF) equation was used to describe the dependence of the horizontal shift factor a_T on temperature T in constructing master curves for amorphous polymers. The shift factor a_T provides the degree of temperature dependence of dynamic moduli for the polymer (Haenelt *et al.*, 2014; Schulze *et al.*, 2015). The shift factor for polymer melts can be determined using the following equation.

$$a_T = \frac{\eta_T}{\eta_{T_{ref}}} \quad \dots(18)$$

Where, η_T is the viscosity at temperature T and $\eta_{T_{ref}}$ is the viscosity at reference temperature T_{ref} . For temperatures higher than 100 K than the glass transition temperature, the shift factor can also be described in terms of activation energy by using the Arrhenius equation as follows.

$$\log(a_T) = -\frac{E_a}{2.303R} \left(\frac{1}{T} - \frac{1}{T_{ref}} \right) \quad \dots(19)$$

Where, E_a is the activation energy and R is the universal gas constant. (Naya *et al.*, 2013)

When studying blends that exhibit multiple glass transitions in DSC measurements, the time-temperature superposition principle does not apply, and the construction of a WLF curve is not possible. This is due to the presence of two glass transition temperatures, which indicates a considerable degree of heterogeneity. To investigate the rheological properties of such blends, a "Han plot" was constructed by plotting the frequency-dependent storage versus the loss modulus at various temperatures for both PESU and the selected blends. The resulting data points were consolidated into a linear curve by fitting the lower values of the loss modulus, from which the slope values were determined. A value of 2 in the low-frequency range indicates a completely homogeneous polymeric system, while lower values indicate a non-homogeneous mixture. (Kalogeras, 2016)

4.1.5. Sorption and Diffusion Measurements

Polymer-gas interactions are understood by analyzing the sorption and diffusion of the gas with the polymer. These are important in analyzing the performance of gas separation membranes. In addition, the foaming performance of a polymer can be predicted by analyzing the diffusion of the foaming agent within the polymer at various pressures and temperatures. Sorption is the process by which a gas molecule is adsorbed onto the surface of a polymer, whereas the movement of gas molecules through the polymer matrix is defined by diffusion. (Lillepär, Georgopoulos and Shishatskiy, 2014)

A sorption balance is used for sorption and diffusion measurements. To measure the sorption of a gas in a polymer, gravimetric method is used. In this method, the gas is injected into an evacuated chamber holding the polymer sample at a certain pressure. The sample's thickness to diameter ratio is maintained as low as possible to minimize sorption occurring from the cylindrical side, thus providing accurate analysis of the diffusion occurring over the thickness of the sample. The change in the weight Δm of the polymer is measured over time, thus providing information on the sorption of the gas adsorbing onto the polymer.

$$\Delta m = \frac{F_{EXP}}{g} = m^{sc} + m^s + m^A - (V^{sc} + V^s + V^A) \cdot \rho \quad \dots(20)$$

Where,

F_{EXP} = experimental force

g = gravitational constant

m^{sc} = mass of sample container

m^s = mass of sample in vacuum

m^A = mass of adsorbent

V^{sc} = volume of sample container

V^s = volume of sample

V^A = volume of adsorbent (For excessive adsorption only, else = 0)

ρ = density of gas

The change in m^A is observed over time or increasing pressure as per the carried-out experiment. However, excessive adsorption occurring in the case of a rough surface of the sample needs to be corrected accordingly. Various parameters such as the pressure, pressure rate, temperature, heating/cooling, and concentration of a specific gas in a gas mixture, can be experimented with to study the sorption behavior at various working conditions.

The diffusion coefficient D_T is a measure of the amount of gas passing through the polymer under the given conditions. It is calculated using the following relationship,

$$\frac{M_t}{M_\infty} = 4 \sqrt{\frac{D_T t}{\pi l^2}} \quad \dots(21)$$

where:

M_t = mass of gas absorbed by sample at time t

M_∞ = mass of gas absorbed by sample at time $t \rightarrow \infty$; i.e., equilibrium

l = thickness of the cylindrical sample

Values used for $\frac{M_t}{M_\infty}$ were lower than 0.6.

Understanding a polymer's sorption and diffusion properties can give a good overview of the foaming behavior of the same polymer. Diffusion is significantly increased by the plasticization phenomena in glassy polymers as well as the existence of rubber phases in a polymer matrix. Therefore, a polymer with a high diffusion coefficient undergoes better nucleation and expansion during the foaming process. (Barrer and Rideal, 1939; Frisch, 1980; Barrer, 1984; Wang and Kamiya, 1995; Gendron, 2004; Gutmann *et al.*, 2010; Lee and Park, 2014; Lillepärq, Georgopoulos and Shishatskiy, 2014; Schulze *et al.*, 2015; Halder *et al.*, 2017)

4.1.6. Gel Permeation Chromatography

Gel Permeation Chromatography (GPC), also known as Size Exclusion Chromatography (SEC), is a technique used to determine a polymer sample's molecular weight and molecular weight distribution. GPC operates on the principle of separating polymeric species based on their hydrodynamic size. The technique is based on the concept that smaller polymer chains penetrate more deeply into the pores of the gel, whereas larger chains do not penetrate as deeply and are eluted more quickly. (Moore, 1964; Toray, 2022)

The GPC system consists of three main components: a pump, a column, and a detector. The pump forces the sample through the column packed with porous beads, usually made of styrene-divinylbenzene copolymers or silica gels. The sample is dissolved in a suitable solvent and injected onto the column. As the sample passes through the column, the different polymer chains elute at different times, depending on their molecular weight. A differential refractive index (RI) or UV-visible detector is generally used. The detector measures the difference in refractive index between the column's mobile phase and the stationary phase. The difference in refractive index measures the polymer concentration in the column. This data is analyzed by generating a chromatogram. Figure 16 provides an overview of GPC principle. (Agilent Technologies, 2015)

In order to determine the molecular weight of the polymer, the GPC system needs to be calibrated using a set of standard samples with known molecular weights. One common calibration method is polystyrene calibration, which involves using a series of polystyrene standards of known molecular weights. The samples are run through the column using the same solvent and conditions as the unknown sample, and the retention time of each standard is determined. A calibration curve is then generated by plotting the logarithm of the molecular weight of the standards versus their retention time. The molecular weight of the unknown sample is then determined by comparing its retention time to the calibration curve. (Gaborieau and Castignolles, 2011; Waters, 2023)

In addition to determining molecular weight, the polymer's molecular weight distribution (MWD) can also be calculated using data obtained from GPC. The MWD can be calculated from the chromatogram using mathematical models, such as the Schulz-Zimm, the Log-Normal, or the Polydispersity Index model. The MWD of a polymer can influence its properties, such as mechanical properties, glass transition temperature, processing behavior, etc. (Miyake, 1960)

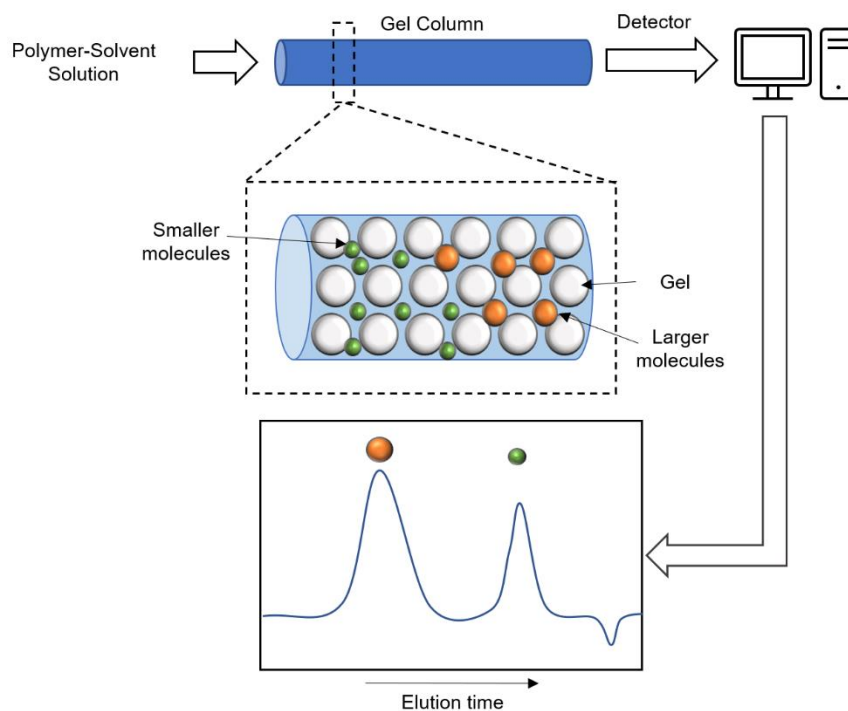


Figure 16: Illustration showing principle of GPC. Detection of molecules of different molecular weights is visualized on a chromatogram versus elution time; Molecular weight is derived from elution time according to the calibration.

This work used GPC for determining molecular weight and MWD of certain polymers, and to analyze the same in the samples of retention test discussed further in section 4.3.3.

4.1.7. Infrared Spectroscopy

Fourier-transform infrared (FTIR) spectroscopy is used to study the chemical composition and molecular structure of chemical compounds such as polymers. FTIR is based on the absorption/transmittance of infrared radiation by a polymer sample, which is used to identify the polymer's molecular structure. The different functional groups present in polymers absorb/transmit different wavelengths of radiation. Infrared radiation interacts with the polymer by stretching and bending molecular bonds. This absorbance or transmittance is used to identify the specific functional groups in the polymer.

First, the sample is prepared as a thin film, pellet, or solution and then placed onto the spectrometer. An infrared beam enters the interferometer within the spectrometer and passes through a beam splitter where it is split to be travel onto a fixed mirror and a moving mirror. The light then travels back onto the splitter and is recombined causing interference and is directed onto the sample followed by the detector. This allows measurement of the spectral information of wavelengths at once. The information of the light intensity versus the movable mirror's position is Fourier transformed and plotted into a plot of light intensity versus wavenumber. The reference spectra containing the background IR absorbance/transmittance is the subtracted mathematically from the sample's plot, thus providing the IR spectrograph of the material. (Bruker, 2023)

FTIR data analysis involves identifying the functional groups and molecular vibrations present in the sample. This is done by comparing the spectrum of the sample to a library of spectra of known compounds and identifying the peaks that correspond to specific functional groups. In addition, quantitative information on the sample composition can be obtained by analyzing the intensity of corresponding peaks versus a sample with known composition. This can be useful when comparing samples of similar components. (Smith, 2021)

4.2. Processing Methods

4.2.1. Blend Formulation

Polymer blends are mixtures of two or more macromolecular compounds that form a material with different properties. They are divided into three categories, such as immiscible, compatible, and miscible blends. The constituent polymers of immiscible blends, , co-exist in separate phases, and their respective T_g are observed. They are also known as heterogenous blends. A compatible blend is an immiscible blend that exhibits uniform physical properties macroscopically due to strong interactions between constituent polymers. Miscible blends, also known as homogenous polymer blends, form a single-phase structure and exhibit a single T_g . Some polymer blends are also partially miscible, i.e., they exhibit multiple glass transitions but are shifted towards one another compared to their constituent polymers. (Kalogeras, 2016; Qin, 2016)

Polymer blends can be formed using chemical techniques, such as dissolution in organic solvents as well as physical techniques such as melt-state compounding,, material penetration, etc. Below are the two methods used mainly in this work. The technical details of the equipment and process settings are provided in their published articles about this cumulative work and are not repeated in this section.

4.2.1.1. Compounding

Compounding is a widely used technique to blend two or more polymers, especially in the plastics industry. The polymers are inserted into a compounding extruder, most commonly a twin-screw extruder, where they are melted at temperatures above their T_g or T_m and allowed to physically mix by the screw action while being transported towards the nozzle, where they are extruded into the desired form and granulated/cut to be stored. Various factors influence the mixing and the blend morphologies during compounding, such as processing parameters like the temperature profile, residence time,

screw speed, screw profile, mixing elements, degassing, etc., as well as material properties such as the blend composition, viscosity ratio, elasticity ratio, interfacial tension, etc. Figure 17 shows the evolution of polymer along a twin-screw compounding extruder's axis. (Lee and Han, 2000)

As having both constituent polymers in a melt state is an essential requirement for compounding, polymers having T_g closer to each other are preferred. However, polymers with significant differences in T_g can be blended using a compounding extruder. However, the processing temperature required for every component should be well below the lowest decomposition temperature among all components. (Cassagnau *et al.*, 2005)

In this work, PESU, as flakes and PVP as powder, were physically mixed at room temperature after vacuum drying. Following another drying cycle, this mixture was inserted in a twin-screw extruder as shown in Figure 18 that extruded a PESU/PVP blend into a cylindrical extrudate that was continuously cut into pellets using a granulator.

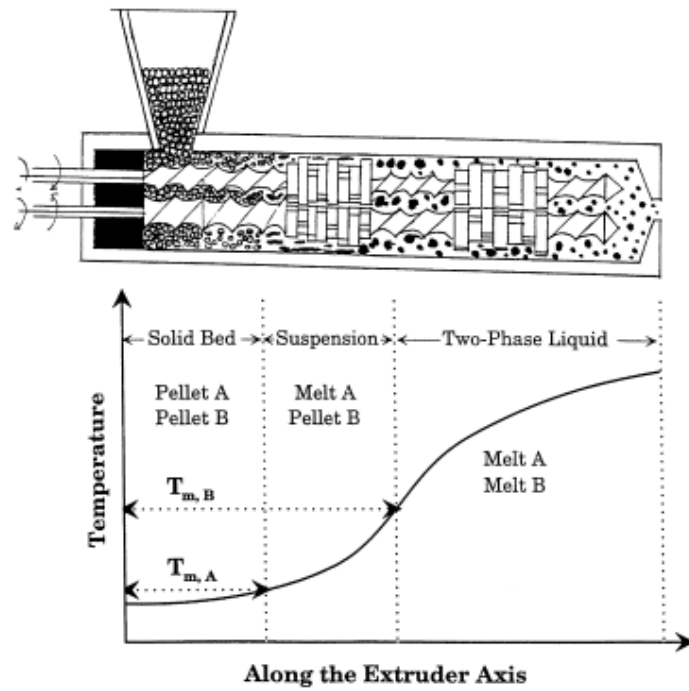


Figure 17: Evolution of polymer along a twin-screw compounding extruder's axis.
Reprinted (adapted) with permission from Lee and Han, 2000. Copyright 2023 Elsevier.



Figure 18: Twin-screw compounding extruder used in this work.

4.2.1.2. Material Penetration

Less commonly used than compounding, material penetration is another method that allows the formation of polymer blends. Similar to the dissolution of polymer granulate in organic solvent, where the solvent first penetrates into the polymer and mobilizes the polymer chains, a liquid polymer can be absorbed within a solid polymer. However, after mobilizing the polymer chains, an organic solvent causes the polymer chains to fall apart, but a liquid polymer stays within the solid polymer's chain thus forming a blend.

In this work, a novel method involving material penetration was attempted. The capillary forces induced by the porous structure of PESU flakes were taken advantage of to absorb polymer and polymer mixtures that were in liquid state. By physically mixing vacuum-dried PESU flakes with liquid PEG or liquid PEG/PVP mixture, the liquid was allowed to soak into the flakes and absorbed into the polymer matrix while continuous movement was provided as shown in Figure 19.



Figure 19: Material penetration of PEG liquid into PESU flakes by rotating flasks containing their mixture.

4.2.2. Batch Foaming

The principles of batch foaming are already discussed in section 3.2.1.1. In this work, as shown in Figure 20, a high-pressure vessel was used for the loading phase, whereas hot plates of a hydraulic press were used for the foaming phase. The temperature of the high-pressure vessel was controlled, while the pressure of the foaming agent was determined by a high-pressure syringe pump connected to a dip-tube bottle. After the completion of the loading phase, the pressure was released, and the samples were placed onto the hot plates for foaming. The foaming time and temperature were controlled whereas it was carried out at ATP.



Figure 20: High pressure vessel (left) and hot plate hydraulic press (right) used for batch foaming in this work.

4.2.3. Extrusion and Foam Extrusion

The principles of extrusion and foam extrusion are already discussed in section 3.2.1.2.

As shown in Figure 21, a Brabender single screw extruder coupled with static mixers and a melt pump was used for foam extrusion in this work. Granules, pellets, and flakes of the polymers were inserted. The extruder was equipped with two inlets to inject two blowing agents simultaneously. An annular slit nozzle was used to extrude hollow fiber geometry. Temperature and pressure control were established at every element of the extruder.

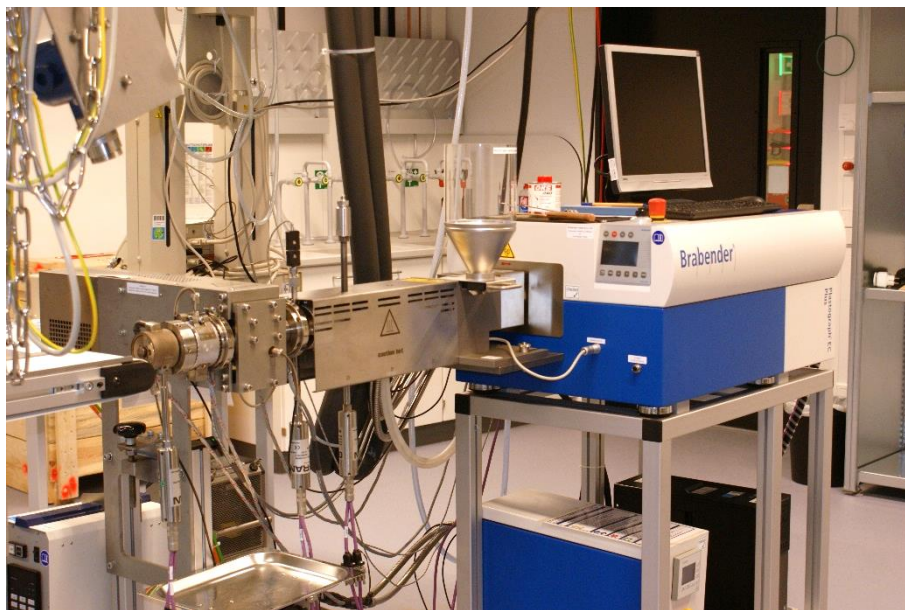


Figure 21: Single screw extruder coupled with static mixer, melt pump and nozzle, used for foam extrusion.

4.2.4. Post-treatment

Treatment of polymer membranes using inorganic aqueous solutions of sodium hypochlorite (NaOCl) and hydrogen peroxide (H₂O₂) is a common practice to remove the soluble components from the membranes, thus increasing the porosity of the membranes. In this work, aqueous NaOCl was used to dissolve water-soluble polymers such as PVP and PEG from the foamed membranes. Removal of these components termed the foams permeable for water and allowed ultrafiltration. (Grünig *et al.*, 2020)

4.3. Foam & Membrane Characterization Methods

4.3.1. Scanning Electron Microscopy

Scanning electron microscopy (SEM) is a commonly used microscopic method in research and industry. The micrograph generated using this technique resembles a photograph and can be easily interpreted. The main advantage of using this type of microscopy is the resolution and magnification at scales up to a few nanometers. As visible light's wavelength lies between 400 and 650 nm, it is difficult for optical microscopes to visualize samples around or below this range. Electrons, however, are 'dimensionless' sub-atomic particles that co-exhibit particles, and wave-like properties can be used to visualize these lengths. Their scattering off a surface can be recorded and amplified to determine the topography of the surface at a few nanometers. (ThermoFischer Scientific, 2023)

SEM focuses a beam of electrons on a surface and records and amplifies the reciprocating signals to visualize the topography of the surface. To avoid any interaction of electrons with anything other than the sample, the sample is placed in an column. Two types of columbs can be used, viz. environmental column and ultra-high vacuum sealed column. Figure 22 illustrates the principles of a scanning electron microscope.

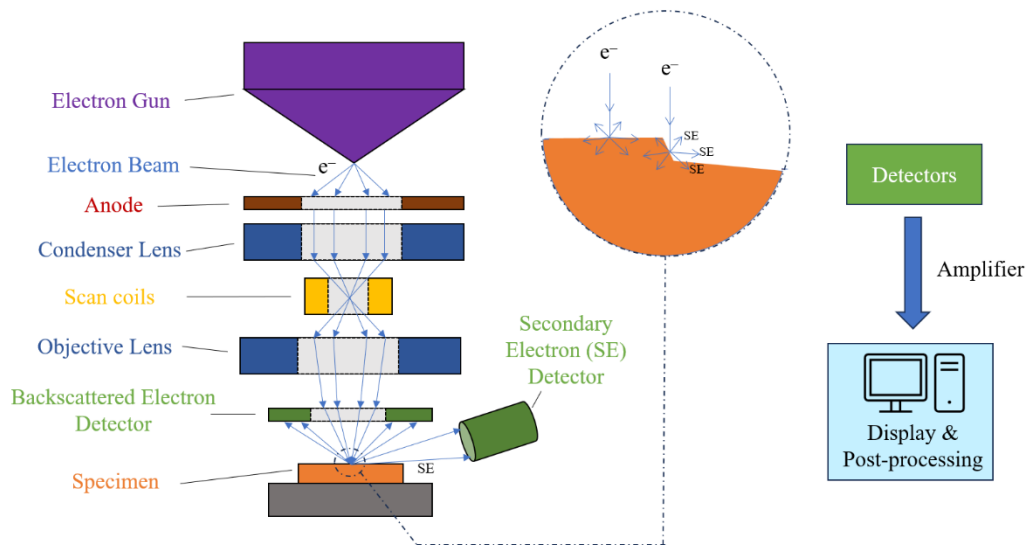


Figure 22: Illustration of a scanning electron microscope. (Michler, 2016)

As illustrated in Figure 22, the electron gun shoots electrons that are lensed onto the sample. To obtain a sharp image of the surface, the sample is coated with an electrically conducting material. As the electrons bounce back from the sample surface, they are detected using a backscattering (BSE) detector as well as a secondary (SE) detector. BSE detectors detect the electrons scattered back from areas below the sample's top surface, thus providing depth contrast. These electrons have higher energy than the SEs and originate deeper within the sample. SE detectors, on the other hand, detect the low-energy electrons emitted from the sample's surface due to the electron beam interactions. SEs originate from the top few nanometers of the sample's surface and are sensitive to the sample's topography and texture. SE imaging can reveal fine details of the sample's surface, such as surface morphology, surface roughness, and surface features. These signals are visualized as a grayscale image containing a length scale based on the magnification. (Michler, 2016)

SEM is an essential tool to visualize the cells and pores of polymer foams and membranes in high resolution and determine their sizes and morphological features. As this work

engages in microcellular and nanocellular cell sizes, as well as determination of the open/closed cellularity of these foams, in the further application as membranes, the accurate determination of pore sizes, porosity, and pore type was pursued using SEM.

4.3.2. Permeability

In the characterization of polymer membranes, the measurement of permeability of the substances it is designed to separate from, is one of the most important methods. For membranes involving water or liquid filtration applications, the water-flux through these membranes is measured.

The amount of pure water passing through a unit square surface area of the membrane per unit time at unit pressure is called the water flux. Water flux is calculated using equation (8).

$$L = \frac{V}{t.A.P} \quad \dots(22)$$

Where L = water-flux, V = volume of water passed through the membrane, t = time, A = membrane surface area, P = transmembranic pressure.

Apart from these parameters, water flux depends on other factors such as the membrane material, type, morphology, porosity, tortuosity, ambient temperature, etc.

4.3.3. Retention Test

The performance of membranes designed for separation applications is characterized by their ability to separate specific sizes of particles/molecules. A retention test is performed to test the separation performance of such membranes. A 'feed' solution of pure water and a solute is passed through the membrane. The solution passed through the membrane is called the permeate, and the retained solution is called the retentate. The amount of solute in the feed, permeate, and retentate is measured, and its ratio is calculated using equation (9). Figure 1 provides an overview of their flow through a membrane.

$$R_C = 1 - \frac{m_P}{m_F} \quad \dots(23)$$

Where R_C = retention coefficient, m_P = amount of solute in permeate, m_F = amount of solute in feed.

In the measurement of retention of ultrafiltration membranes, water-soluble molecules such as PEO, Dextran, etc. of desired and standardized molecular weight are used. Their concentrations in the feed, permeate, and retentate are determined using GPC as discussed in section 4.1.6.

4.3.4. Tensile Test

Tensile testing is a mechanical testing method widely used to analyze the mechanical properties of materials. It involves applying tension to a material sample by pulling it until deformation or breakage is observed. It is usually used as a destructive test process providing information about a material's tensile strength, yield strength, toughness, and ductility. However, non-destructive tests can also be performed such as to evaluate the elasticity of rubbers.

Tensile testing machines typically consist of a loading frame, a crosshead that moves vertically, and grips that hold the specimen in place. The specimen is secured between the grips and by moving the crosshead upwards, which exerts tensile force onto the sample by pulling one end against the one held stationary. The amount of force applied is measured by a load cell, and a displacement transducer measures the displacement of the crosshead. These measurements allow for the calculation of stress and strain values, which are used to determine the material's mechanical properties (Davis, 2004). Mechanical properties, such as tensile strength, yield strength, elongation, and modulus of elasticity, are obtained using tensile tests on polymers. By plotting a stress-strain curve as shown in Figure 23 a tensile test can be evaluated. This information is used to select appropriate materials for specific applications, design products, and optimize processing conditions. (Worgull, 2009; Yang, 2019)

The tensile testing of polymer foams takes place similarly to that of polymers. However, the mechanical properties of foams are influenced by the foam morphology and density. Foams exhibit rate-dependent behavior, and prediction can be complicated due to various structural responses arising from trapped gases within the foam cells. Generally, foams exhibit low tensile strength than the parent polymer, but the possession of high ductility makes polymer foams significantly attractive for various applications. In this work, tensile testing was performed on polymer foams and membranes to measure their mechanical strength using a universal tensile testing machine as shown in Figure 24. The effects of different materials, process settings and morphologies on the tensile strength of foams and membranes are studied. As membranes operate under high pressure in their modules, testing their mechanical strength is essential. In addition, the quantification of foam and membrane characteristics such as brittleness and ductility are possible using tensile testing. (Fu *et al.*, 2006; Kabir, Saha and Jeelani, 2006; Zhang, Lu and Zhao, 2014; Liu *et al.*, 2019)

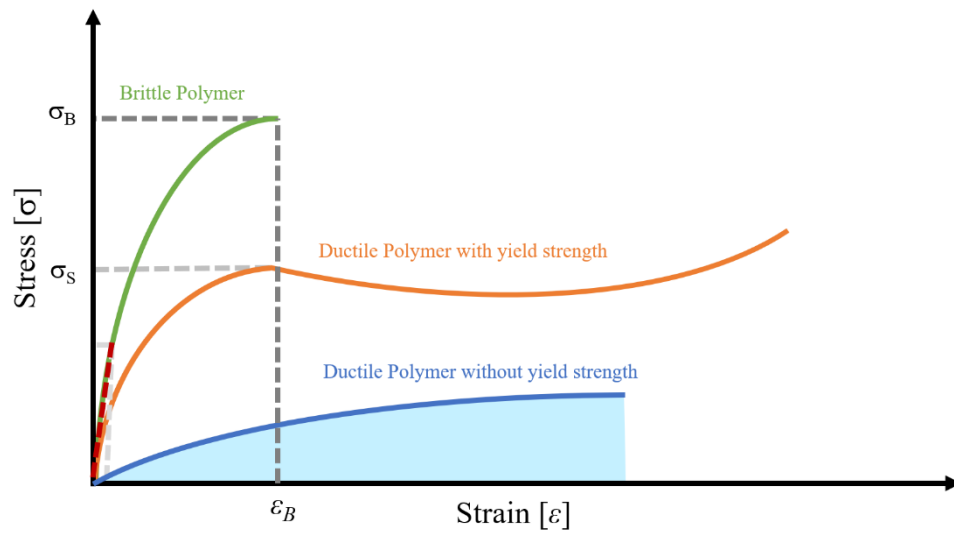


Figure 23: A stress-strain curve of different types of polymers denoting various information such as stress at break (σ_B), strain at break (ϵ_B) and yield stress (σ_s) obtained from tensile testing. The Young's modulus (E) of the brittle polymer can be calculated by measuring the slope of the red dashed line i.e. the elastic region. The area under the curve denoted by blue color is measured to calculate the deformation energy of the respective polymer.

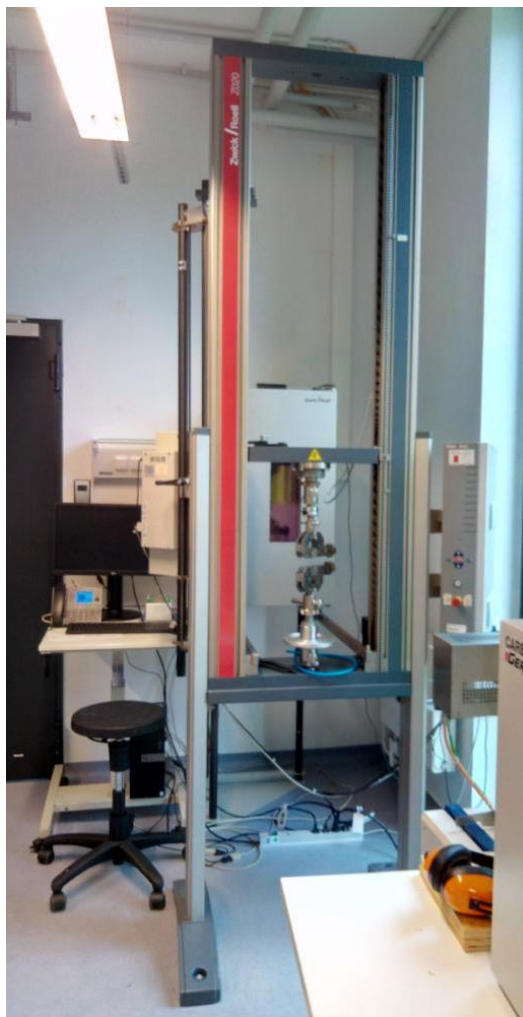


Figure 24: Universal tensile testing machine used in this work.

5. Objective of This Work

The current state-of-the-art techniques and processes for manufacturing polymer membranes capable of ultrafiltration use organic solvents. Due to their disadvantages, a vital requirement for alternative methods arises. This need is recognized by a few researchers, which led to the development of alternative methods involving *green organic solvents* and techniques using uneconomic polymeric systems. Melt-extrusion followed by bi-axial stretching, an organic-solvent-free process, is limited to semi-crystalline polymers. Polymer foaming, a method widely used industrially and in polymer research for obtaining porous polymers, is only sparsely investigated for the fabrication of membranes. The significant barrier to using foams as ultrafiltration membranes is the lack of open-celled morphologies that contain pore sizes smaller than 1 μm . Therefore, ultrafiltration-level separation cannot be achieved using these foams. The following Venn diagram in Figure 25 visualizes the state-of-the-art research in foams. Some researchers have been able to produce polymer foams with nanocellular cell sizes, while some have been able to produce open cellular polymer foams. However, no nanocellular open-celled permeable foams were not available at the beginning of this work.

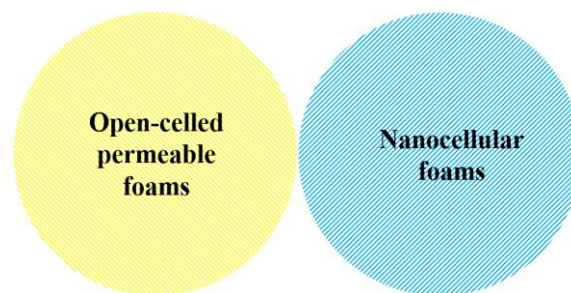


Figure 25: A Venn diagram visualizing the state-of-the-art of polymer foams.

Therefore, this work aims to manufacture ultrafiltration membranes, both as flat sheet membranes and hollow fiber membranes, using foams. Commercial amorphous polymers already used in ultrafiltration membranes are selected to develop open-celled permeable nanocellular polymer foams. A high permeability of these foams, a consequence of open cellularity, would be achieved by aiming for high porosity. At the same time, the cell size should be restricted to a few nanometers to cause a 90% MWCO for molecules of PEO with a molecular weight of 1 million Da, a criterion used to classify ultrafiltration membranes.

PESU, a high-performance polymer preferred commonly in manufacturing ultrafiltration membranes is selected. By forming binary and ternary blends of PESU with water-soluble polymers such as PEG and PVP, these works take advantage of the extensive research available in polymer blends, characterization, processing, foams, and ultrafiltration membranes. Material development using intensive polymer characterization techniques, as discussed in section 4.1 was pursued.

To realize the main goal 'nanocellular open-celled foam capable of ultrafiltration' in continuous large-scale production, following steps were followed.

- Step 1: Complete realization of the goal as a prototype on a small scale.

- Step 2: Setting up a continuous large-scale production with only partial realization of the goal.

- Step 3: Complete realization of goal at a continuous large scale.

Table 6 shows the steps along with their respective processes and pursued forms.

Step	Goal	Scale	Process	Form
1	Nanocellular open-celled foam	Small, prototype	Batch foaming	Flat sheet
2	Open-celled microcellular foam	Large, continuous	Foam extrusion	Hollow fiber
3	Nanocellular open-celled foam	Large, continuous	Foam extrusion	Hollow fiber

Table 6: Steps with respective goals, scale, the selected process and forms.

The characterization of the manufactured foams and membranes thereof is pursued mainly using scanning electron microscopy, water-flux measurements, and retention tests as explained in section 4.3.

6. Cumulative Part

Upon successful completion, each step described in the objective was manifested into a scientific article published in academic journals. As illustrated in Figure 26, the three first-authored publications, together encompass this work into a cumulative doctoral dissertation.

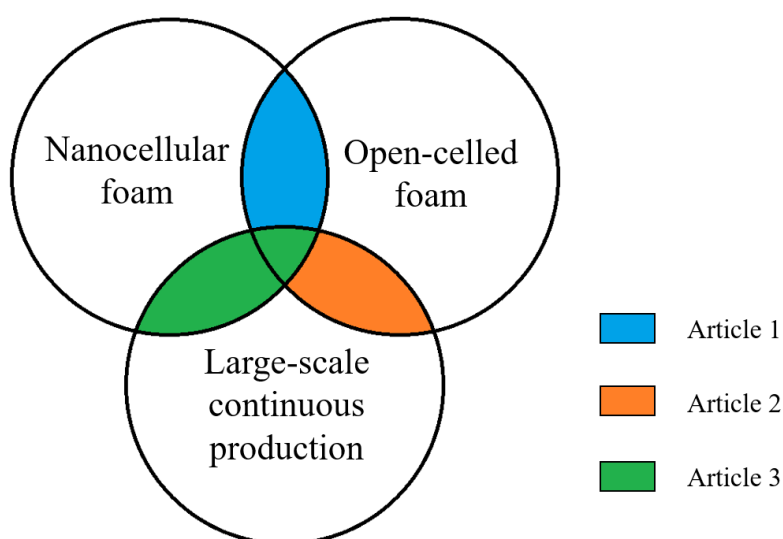


Figure 26: A Venn diagram visualizing the scope of each published article of this cumulative work.

Every article contains a smooth flow of information, i.e., aim, current state-of-the-art, research necessity, methodology, results realization, discussion of observations and inferences, and conclusion. However, gaining insight into how one article's inferences helped the next one's inception is important. Therefore, along with every article's reprint, brief information is provided, which assists the reader in understanding the journey the author(s) went through, the scientific and engineering challenges faced, and the

circumstances that led to the realization of successful results. Therefore, certain unpublished information is provided.

6.1. Article 1: Open-Celled Foams of Polyethersulfone/Poly(*N*-vinylpyrrolidone) Blends for Ultrafiltration Applications

Authors: Aniket Raje, Kristian Buhr, Joachim Koll, Volker Abetz, Ulrich A. Handge

Given its prototype nature, the first step was based on batch foaming to control the characteristics precisely. For this, polyethersulfone was selected as it was already a desired ultrafiltration membrane material, with literature supporting its decent foaming characteristics. Blends with poly(*N*-vinylpyrrolidone) were developed and extensively characterized to determine their miscibility and thermal and rheological properties. This allowed confirming their suitability in processing and foaming.

In batch foaming, water, along with CO₂ as foaming agents, delivered highly porous foams that contained closed-cell morphology around a few micrometers whose cell walls had open nanocellular pores connecting the microcells. However, a non-foamed skin layer on the outer surface of these foamed samples hindered the implementation of these foams as membranes.

To find a solution, various shapes and sizes of samples were tried, along with machining foamed samples. However, the foaming results did not improve. During trials with thin rectangular samples, due to some irregularities in laying the PESU/PVP blends' samples correctly in the sample holder of the batch foaming reactor, some samples were found stuck on the inner wall of the reactor when the reactor was depressurized after the loading phase. The stuck areas of these samples appeared strangely different than those that were not stuck. Instead of discarding them, they were immediately foamed in the foaming stage as per protocol. After foaming, the samples were studied using scanning electron microscopy (SEM). It was revealed that the stuck regions of the samples foamed vastly different than the non-stuck regions as the non-stuck regions foamed as the earlier samples. The stuck regions did not possess a non-foamed skin layer, and the foam was open-celled with cell sizes less than 1 μm. As discussed in this article, studying the reason behind this phenomenon led to the development of two sample manufacturing techniques, one of which led to a permeable open-celled foam with an average pore size of ~ 100 μm and ultrafiltration capabilities.

This study validated the idea of using polymer foams as ultrafiltration membranes and motivated the upscaling of this process utilizing foam extrusion, as attempted in Article 2.

6.1.1. Author Contributions

Aniket Rajee (A.R.), Kristian Buhr (K.B.), Joachim Koll (J.K.), Jelena Lillepärög (J.L.), Volker Abetz (V.A.), Ulrich A. Handge (U.A.H.)

Contributions	Authors					
	A.R.	K.B.	J.K.	J.L.	V.A.	U.A.H.
First Author (1) and Corresponding Author (*)	1					*
Conceptualization, methodology and material characterization	✓					✓
Batch foaming experiments	✓	✓				
Water-flux and retention			✓			
Writing-original draft preparation	✓					
Writing-review and editing		✓	✓	✓	✓	✓
Visualization	✓					✓
Scientific consultation				✓	✓	
Scientific supervision					✓	✓
Project administration and funding acquisition						✓

Table 7: Author contributions for article 1.

6.1.2. Funding and Acknowledgements

This work was partially funded by BASF SE (Ludwigshafen, Germany) as a part of a co-operation project.

The authors express their gratitude towards the individuals and institutions who have contributed to this research project. Ivonne Ternes played an instrumental role in conducting rheology, thermal analysis, and batch foaming experiments. Petra Merten, Maren Brinkmann contributed their expertise in gel permeation chromatography, while Martin Held, Anke-Lisa Höhme, and Erik Schneider provided invaluable support in the field of microscopy. The authors also extend their appreciation to Prokopios Georgopoulos and Mahboubeh Kargar for their insightful scientific discussions. Additionally, the authors acknowledge that apart from the partial funding, the donation of materials, as well as the valuable discussions held with Oliver Gronwald and Martin Weber from BASF SE are appreciated. These contributions have been integral to the success of this work and are greatly appreciated.

6.1.3. Publication



Article



Open-Celled Foams of Polyethersulfone/Poly(*N*-vinylpyrrolidone) Blends for Ultrafiltration Applications

Aniket Raje, Kristian Buhr, Joachim Koll, Jelena Lillepärq, Volker Abetz and Ulrich A. Handge



Article

Open-Celled Foams of Polyethersulfone/ Poly(*N*-vinylpyrrolidone) Blends for Ultrafiltration Applications

Aniket Rajе¹, Kristian Buhr¹, Joachim Koll¹, Jelena Lillepärğ¹, Volker Abetz^{1,2}
and Ulrich A. Handge^{1,3,*}

- ¹ Institute of Membrane Research, Helmholtz-Zentrum Hereon, Max-Planck-Strasse 1, 21502 Geesthacht, Germany; aniket.raje@hereon.de (A.R.); kristian.buhr@hereon.de (K.B.); joachim.koll@hereon.de (J.K.); jelena.lillepaerg@hereon.de (J.L.); volker.abetz@hereon.de (V.A.)
² Institute of Physical Chemistry, Universität Hamburg, Grindelallee 117, 20146 Hamburg, Germany
³ Chair of Plastics Technology, Faculty of Mechanical Engineering, TU Dortmund University, Leonhard-Euler-Straße 5, 44227 Dortmund, Germany
* Correspondence: ulrich.handge@tu-dortmund.de; Tel.: +49-231-755-8628

Abstract: Since membranes made of open porous polymer foams can eliminate the use of organic solvents during their manufacturing, a series of previous studies have explored the foaming process of various polymers including polyethersulfone (PESU) using physical blowing agents but failed to produce ultrafiltration membranes. In this study, blends containing different ratios of PESU and poly(*N*-vinylpyrrolidone) (PVP) were used for preparation of open-celled polymer foams. In batch foaming experiments involving a combination of supercritical CO₂ and superheated water as blowing agents, blends with low concentration of PVP delivered uniform open-celled foams that consisted of cells with average cell size less than 20 μm and cell walls containing open pores with average pore size less than 100 nm. A novel sample preparation method was developed to eliminate the non-foamed skin layer and to achieve a high porosity. Flat sheet membranes with an average cell size of 50 nm in the selective layer and average internal pore size of 200 nm were manufactured by batch foaming a PESU blend with higher concentration of PVP and post-treatment with an aqueous solution of sodium hypochlorite. These foams are associated with a water-flux up to 45 L/(h m² bar). Retention tests confirmed their applicability as ultrafiltration membranes.

Keywords: polymer membranes; open-celled foams; solvent-free membrane fabrication; polyethersulfone; ultrafiltration



Citation: Rajе, A.; Buhr, K.; Koll, J.; Lillepärğ, J.; Abetz, V.; Handge, U.A. Open-Celled Foams of Polyethersulfone/Poly(*N*-vinylpyrrolidone) Blends for Ultrafiltration Applications. *Polymers* **2022**, *14*, 1177. <https://doi.org/10.3390/polym14061177>

Academic Editor: Johannes Carolus (John) Jansen

Received: 14 February 2022

Accepted: 12 March 2022

Published: 15 March 2022

Publisher's Note: MDPI stays neutral with regard to jurisdictional claims in published maps and institutional affiliations.



Copyright: © 2022 by the authors. Licensee MDPI, Basel, Switzerland. This article is an open access article distributed under the terms and conditions of the Creative Commons Attribution (CC BY) license (<https://creativecommons.org/licenses/by/4.0/>).

1. Introduction

Ultrafiltration is an established membrane separation technique that is implemented to filter out nanoparticles by means of size exclusion or particle capture [1]. Ultrafiltration is used to purify liquids, e.g., water, whey, poly(vinyl alcohol) [2]. Porous polymeric membranes for ultrafiltration are typically manufactured using processes such as the non-solvent induced and thermally induced phase separation process (NIPS and TIPS, respectively) [3–7]. These processes involve organic solvents such as *N,N*-dimethylacetamide (DMAc), *N*-methyl-2-pyrrolidone (NMP), formic acid and *N,N*-dimethylformamide (DMF) and are classified as harmful chemicals [8–11]. Some of them are associated with liver disease in human beings [12]. The contamination of environmental water supply due to the disposal of organic solvents poses a serious risk. On-site incinerations are a common practice due to economic reasons [13]. To avoid wastage of organic solvents, in membrane industry it is a general practice to recirculate organic solvents using distillation, which consumes high amounts of energy leading to increased carbon emissions [14,15].

Over the past decades, polymer foaming is seen as a possible alternative to these organic solvent-based processes for fabrication of membranes. Various studies use the discontinuous process of batch foaming or solid state foaming [16]. Batch foaming involves

a two-stage process where a physical gaseous blowing agent such as carbon dioxide (CO₂) diffuses into a polymer at elevated temperature and pressure for a limited period. The temperature is generally below the glass transition temperature of the gas-loaded polymer causing it to remain in a so-called “solid state”. After completion of this stage, this polymer is exposed to a higher temperature for a short time, which causes nucleation and expansion of foam cells by taking advantage of the softened polymer. This creates a closed-celled or open-celled foam structure depending on the polymer properties and processing conditions. Open-celled polymer foams, when customized to desirable cell size, deliver a permeance that enables them to be implemented as separation membranes. As the aim of this work is to produce prototype ultrafiltration membranes without the use of organic solvents, we develop a manufacturing process using the batch foaming technique.

Krause et al. [17] produced closed-cellular polymer foams with an average pore diameter in the micrometer range (~100 µm) from PSU. After preparation of the said foam, they used the organic solvent tetrahydrofuran (THF) to form open pores in the nanometer range within the walls of the micro-sized cells. Krause et al. [18] used discontinuous solid state foaming of PSU/polyimide blends with CO₂ as physical blowing agent to develop nanocellular foams. Microcellular open-cellular foams (diameter in the range of 1–10 µm) were achieved by the use of organic solvents. Nanocellular foams (range of pore diameter 2–50 nm) were achieved by increasing the CO₂ saturation levels such that CO₂ stays in a continuous phase, which leads to an open-celled structure. Although these foams find potential application as ultrafiltration membranes, their production involved the use of an organic solvent to achieve open pores smaller than 1 µm. Similarly, Gong et al. [19] produced porous cell walls in microcellular polycarbonate foams by using acetone with CO₂ during foaming. The use of acetone induced crazing within the polymer thus resulting in a porous structure on the microcell walls. Without the use of organic solvents, Sorrentino et al. [20] and Guo et al. [21–23] developed foams with a similar structure. They investigated the foaming of high performance polymers including PESU and found that PESU exhibited nanocellular foams whereas the other investigated polymers exhibited pores with a diameter only in the micrometer range. They reported the formation of a nano-structure on the cell walls of microcellular foam of PESU and polyetherimide (PEI) without the use of organic solvents. This nano-structure appeared to have a tendency towards making the cell walls of the microcellular foams partially porous with pores less than 1 µm in diameter. Guo et al. [21,22] applied a solid state CO₂ foaming process on PSU and PPSU where they used low temperatures between –10 °C to 60 °C for loading the samples with CO₂ without using organic solvents. They reported a similar nanoscale structure on the cell walls of the closed microcellular foams. They describe this structure as a ‘network of stretched struts’ that are nanoscale fibers formed due to stress-induced nucleation or spinodal decomposition, i.e., a biaxial tensile deformation caused by the expansion of cells. Although this structure appears uniformly distributed on the cells, it does not appear to be open-celled foam. To obtain open pores within these foams, a higher porosity would be desirable such that pores would be created within such a nanoscale structure due to high degree of stretching.

Li et al. [24] used assisted mold foaming to manufacture polysulfone foams with high expansion ratios. They applied mechanical pressure on CO₂-loaded polysulfone samples while subjecting them to foaming temperatures. By using this method, high expansion ratios were obtained in the resulting foams. However, the cell size was above 15 µm and only a closed-cellular structure was achieved.

CO₂ has been established as an ideal blowing agent for delivering high porosity polymer foams [16,25,26]. In addition, CO₂ in supercritical state provides better foaming results than gaseous CO₂ in subcritical phase [16,27]. Hu et al. [28] studied the use of ethanol as a co-blowing agent during the foaming of polysulfone (PSU) and poly(phenylene sulfone) (PPSU). The expansion ratio and the foaming temperature window of the foams were significantly increased due to the use of co-blowing agent. Owusu-Nkwantabisah et al. [29] used a combination of supercritical CO₂ and superheated H₂O to produce PESU foams and

found a significantly increased level of porosity and interconnectivity between pores as compared to a PESU foam that was foamed by using only supercritical CO₂. Schulze et al. [30] also achieved open-celled foams using block copolymers and CO₂ as foaming agent in the presence of water during the loading process. Water in superheated state has a significantly reduced polarity such that it shows solvent properties [31]. Therefore, the usage of superheated water with supercritical CO₂ (shH₂O + scCO₂) for foaming emerges to be promising.

Polyarylsulfones such as polyethersulfone (PESU), polysulfone (PSU) and polyphenylsulfone (PPSU) have been widely studied for obtaining permeable foams [17,18,20–22,29]. PESU is widely used for membranes as it provides high thermal stability due to its high glass transition temperature, good chemical stability due to the presence of sulfonyl groups and ether linkages, and favorable structural stability due to the presence of two aromatic groups in the repeating unit [32]. PESU membranes are also preferred for ultrafiltration applications due to their capability to deliver reliable retention values and high porosity [33]. Some researchers used poly(*N*-vinylpyrrolidone) (PVP) as a water-soluble ‘pore-opener’ along with poly(arylsulfones) to produce ultrafiltration membranes from solutions in organic solvent [33–40]. Therefore, due to the proven application of PESU and PVP in ultrafiltration membranes, we use blends of PESU and PVP in this work. Shi et al. [41] used PMMA/PVDF blends to achieve highly porous nanocellular foams. The use of PVDF to form a miscible blend with PMMA was determined to increase the porosity and decrease cell size in both macro and micro cells. Therefore, we plan studies to confirm the miscibility of PESU and PVP, and observe the effect of polymer content on various material characteristics and foaming results.

Ultrafiltration requires an average pore diameter between 10 nm and 100 nm in the selective layer. Thus, open-cellular foams with cell size of approximately 100 nm are targeted. As PVP is soluble in a variety of commonly available compounds such as water and aqueous solutions of sodium hypochlorite (NaOCl), a permeable selective layer could be created through the dissolution of PVP. NaOCl is selected due to its proven suitability for post-processing of PESU/PVP membranes [33,35,39]. The outer surface in batch foams commonly contains cracks that occur due to the expansion of the sample during foaming. If the cell size of the foam cells were in the range of micrometers, these cracks would lead to functional failure as ultrafiltration membrane and deem the selective layer useless. Therefore, the cell size is also desired to be similar to the cell size of the selective layer such that flaws occurring on the surface during foaming can be easily compensated by the internal structure. We focus on manufacturing completely open nanocellular foams, which the previous studies [17–30,41–43] did not fully realize. In recent years, the research on polymer foams has shifted towards composites involving graphene and other nanoparticles to deliver highly porous microcellular and nanocellular foams [44–49]. However, this is out of the scope of this work, as we focus on obtaining the said foam from the pristine polymers.

Batch foaming often yields a non-foamed outer layer after foaming due to fast diffusion of the blowing agent [21]. In order to employ these foams as membranes, an intuitive method is developed to avoid this non-foamed layer and at the same time improve the foam quality. We aim to achieve a complete open-cellular foam structure with a nanometer cell size by combination of batch foaming and post-treatment in inorganic solvents. The membranes prepared using this organic solvent-free method would be permeable to water and have retention values that are near to those of ultrafiltration membranes based on methods using organic solvent in their manufacture.

2. Materials

In this study, commercial grades of polyethersulfone and poly(*N*-vinylpyrrolidone) BASF Luvitec® K 30 (PVP K 30) were used for blend preparation. The blends were obtained from BASF SE (Ludwigshafen, Germany). Two variants of PESU that varied in molecular weight were used viz., BASF Ultrason® E 2010 (PESU E 2010) and BASF Ultrason® E 3020

P (PESU E 3020 P). Although high molecular weight PVP such as PVP K 90 is used in the fabrication of ultrafiltration membranes, PVP K 30 (BASF Luvitec® K 30 molecular weight around 40,000 Da [50]) is used here because CO₂ shows a higher miscibility with low molecular weight PVP than with high molecular weight PVP [51]. The blend formulations and nomenclature are given in Table 1.

Table 1. Nomenclature of blends with respect to their composition.

Blend Name	PESU		PVP K 30
	Type	Content [wt%]	Content [wt%]
L-8	PESU E 2010	92	8
L-16	PESU E 2010	84	16
L-24	PESU E 2010	76	24
L-32	PESU E 2010	68	32
H-8	PESU E 3020 P	92	8
H-16	PESU E 3020 P	84	16
H-24	PESU E 3020 P	76	24
H-32	PESU E 3020 P	68	32

BASF Luvitec® K 90 (PVP K 90) and Kapton® foil (Polyimide (PI) foil) was chosen for preparing sandwich-type samples. All materials were dried in a vacuum chamber at 130 °C for 24 h before further use.

For post-treatment, sodium hypochlorite (Roth GmbH & Co. KG, Karlsruhe, Germany) and sodium bisulfate (Roth GmbH & Co. KG) were used.

3. Experimental and Methodology

3.1. Material Characterization

Differential scanning calorimetry (DSC) measurements were carried out using a calorimeter DSC 1 (Mettler Toledo, Gießen, Germany), and analyzed using STARE SW 16.20 software (Mettler Toledo). 40 µL aluminum pan with a mono-perforated lid was filled with approximately 10 mg of polymer. A heating rate of 10 K min⁻¹ in the temperature interval from 25 °C to 260 °C in a nitrogen atmosphere was chosen. Heating-cooling-heating cycles were executed. Then the glass transition temperature was determined by analyzing the second heating interval.

The glass transition temperatures and the heat capacities when changing from the glassy to the rubbery state of the homopolymers were used in the Equation (1) as derived by Couchman [52] and the glass transition temperatures were used in Equation (2) as derived by Fox [53] to find the expected glass transition temperature of miscible blends at various polymer mass fractions.

$$\ln(T_g/T_{g,I}) = \frac{w_{II}\Delta c_{p,II} \ln(T_{g,II}/T_{g,I})}{w_I\Delta c_{p,I} + w_{II}\Delta c_{p,II}} \quad (1)$$

$$\frac{1}{T_g} = \frac{w_I}{T_{g,I}} + \frac{w_{II}}{T_{g,II}} \quad (2)$$

In Equations (1) and (2), T_g is the glass transition temperature of the blend, w_I and w_{II} are mass fractions, $\Delta c_{p,I}$ and $\Delta c_{p,II}$ are the differences of the heat capacity when changing from the glassy to the rubbery state measured using DSC, and $T_{g,I}$ and $T_{g,II}$ are the glass transition temperatures of polymers I and II respectively.

High pressure differential scanning calorimetry (HP-DSC) measurements were carried out using a calorimeter HP-DSC 1 (Mettler Toledo), and analyzed using STARE SW 16.20 software (Mettler Toledo). The aluminum pan with a multi-perforated lid was filled with approximately 7 mg of powdered polymer. The sample was rinsed with CO₂ for 5 min in the equipment. First, a heating rate of 10 K min⁻¹ was applied from 25 °C to 260 °C in a CO₂ atmosphere at 1 bar. Then, the sample was allowed to cool down to 150 °C and then

held at this temperature for 3 h at the desired CO₂ pressure (1 bar, 10 bar, 20 bar or 30 bar). The sample was then heated up to 260 °C at a heating rate of 10 K/min while maintaining the CO₂ pressure. Considering the diffusion coefficient of $D = 3 \times 10^{-8}$ cm²/s for PESU at room temperature [54,55] and the sample particles having radius of $R = 100\text{--}150$ μm, the saturation time can be calculated using $t_{sat} = R^2/D$, i.e., approximately between 55 and 130 min. Since, saturation time decreases with increasing temperature due to softening of the polymer, the selected time of 3 h is sufficient for saturation for PESU and the blends at 150 °C. The T_g was determined by analysing the final heating interval when the sample was assumed to be saturated with CO₂.

For rheological measurements, cylindrical samples measuring 8 mm in diameter and 2 mm in thickness were prepared using compression molding at 270 °C for a total time of 10 min. For compression molding of PESU and blend samples, a hot press (Paul-Otto Weber, Remshalden, Germany) was used. As PVP K 30 was available in powder form, cylindrical samples measuring 8 mm in diameter and 2 mm in thickness were prepared using Vacuum MR Hei-End (MeltPrep GmbH, Graz, Austria) at 240 °C. It was ensured that the samples had no air bubbles, cracks, weld lines or rough surfaces through visual inspection. Rheological measurements were carried out on an Anton Paar MCR 502 rheometer with a plate-plate geometry. Frequency sweeps in the frequency range between 0.01 and 100 rad/s were carried out at temperatures 190, 200, 220, 240 and 260 °C for PVP K 30, and at 260, 280, 300 and 320 °C for the other materials. The frequency sweeps started with the highest frequency. The master curves were constructed using the software LSSHIFT developed by Honerkamp and Weese in 1993 [56]. For amorphous polymers, the dependence of the horizontal shift factor a_T on temperature T in the construction of master curves can be described using the William-Landel-Ferry (WLF) equation [57],

$$\log(a_T) = -\frac{c_1(T - T_{ref})}{c_2 + (T - T_{ref})} \quad (3)$$

The WLF parameters c_1 and c_2 were obtained by applying a least-squares fit of Equation (2) to the master curves at reference temperature T_{ref} using LSSHIFT.

3.2. Batch Foaming

The batch foaming process was carried out on samples similar to those used for rheological measurements. Batch foaming can be divided into two stages. In stage one, i.e., the loading phase, samples were placed in a high pressure vessel (highpreactor BHM-500, Berghof, Enningen, Germany). CO₂ gas was used as a foaming agent and was inserted into the vessel through an inlet from a dip-tube bottle (99.995% purity, Linde PLC, Dublin, Ireland) using a high pressure syringe pump (Teledyne ISCO, Lincoln, NE, USA) at room temperature up to a pressure value that was calculated based on the combined gas law using the desired temperature and CO₂ pressure. The vessel was then heated to the desired loading temperature ranging from 125 to 175 °C. This temperature was maintained for a loading time of 24 or 48 h, depending on the experiment. In some trials, water was used as a co-foaming agent along with CO₂. In these trials, the vessel was filled with 40 mL ultrapure water. Immediately after completion of the loading interval, the pressure was released in a controlled manner for 7 s ensuring a pressure drop to ambient pressure and to initiate foaming (stage 2). Immediately, the samples were placed for 100 s between two hot plates of a hot-press at the desired foaming temperature that ranged between 210 to 270 °C.

3.3. Membrane Manufacturing

Blends H-8 and H-32 (with weight fractions 92/08 wt% and 68/32 wt%, respectively) were the main materials of interest for manufacture of membranes and were additionally produced by blending PESU E 3020 P with PVP K 30 in a twin screw extruder (Brabender, Duisburg, Germany). Blend samples for preparing sandwich-type layers were prepared by

compression molding. These sandwich-type samples contained a separate PVP layer where BASF Luvitec® K 90 (PVP K 90) was used due to higher ductility and mechanical stability compared to PVP K 30. Each layer was manufactured separately with the dimensions shown in Figure 1. Two manufacturing methods were used, method I (Figure 1a) where PVP layers were made from an aqueous PVP solution (ratio 50/50 wt%), and method II (Figure 1b) where compression molded PVP layers were used. For both methods, the blend films were manufactured using compression molding at 270 °C. In the first method, the blend sample was adhered to the polyimide foil using the aqueous PVP solution as PVP has adhesive properties [58]. The samples were allowed to dry for up to 24 h. In the second method, the temperature used for compression molding was 240 °C for PVP K 90. The layers, as shown in Figure 1b were placed on top of one another and pressed for 3 min together at 205 °C under 20 kN loading using a hot press (Paul-Otto Weber). Polyimide foil was used at the top and the bottom layer as a protection during handling. In both methods, the polymer blend film would thus be completely covered by another polymer, i.e., PVP K 90, and would be implemented as a membrane later. Batch foaming was carried out on these samples using the same process explored previously. The first method of sandwich-type samples was initially implemented on both blends and the second method was only used with the better performing blend.

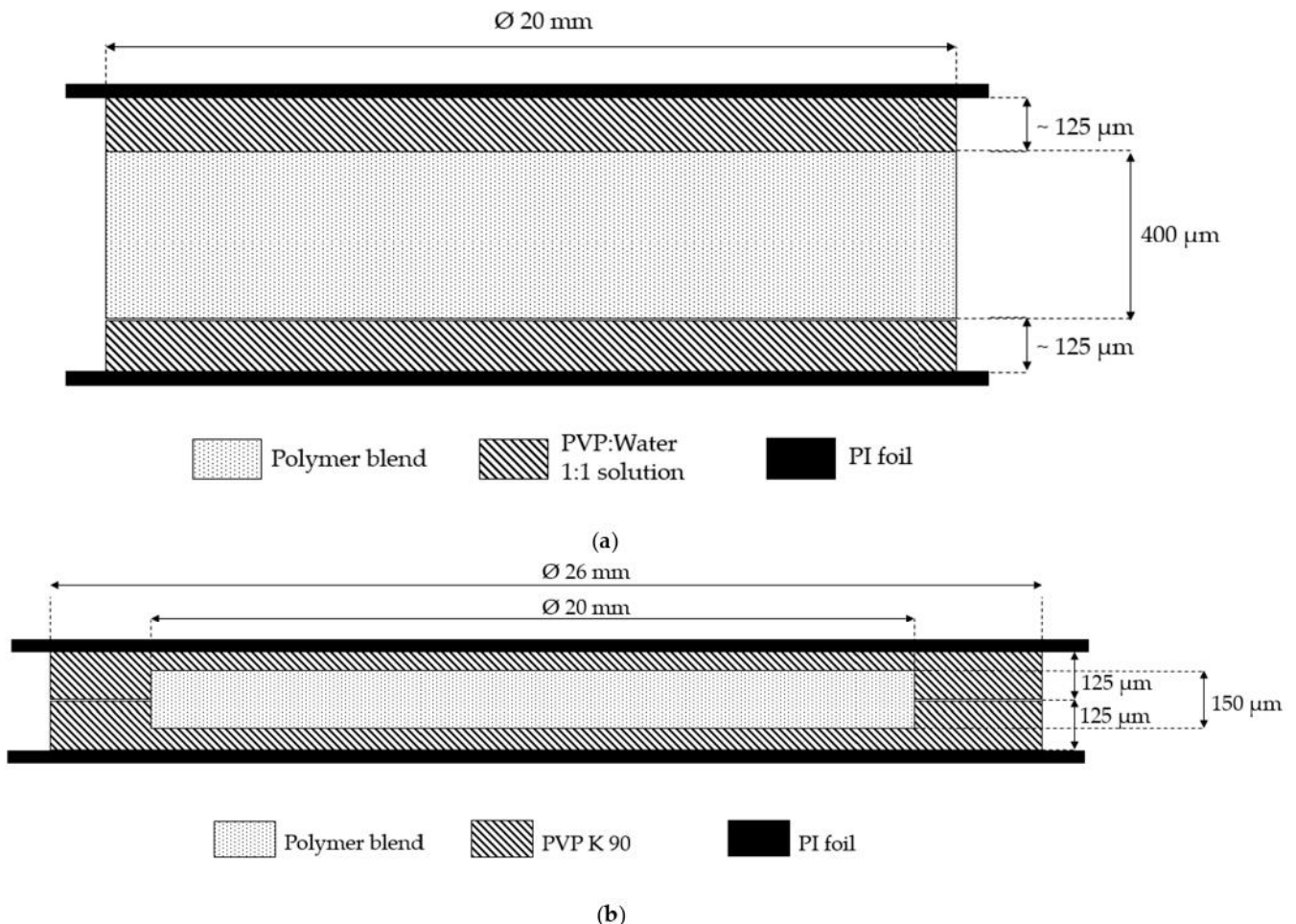


Figure 1. Scheme of a sandwich-type sample: (a) Method I; (b) Method II.

The foamed samples were subjected to post-treatment using an aqueous solution of 0.1 wt% sodium hypochlorite (pH = 11.5). Samples were initially inserted as a solution in a closed glass bottle at a maintained temperature of 80 °C for 24 h. During this time the solution became saturated with PVP K 90 and the PI foils detached themselves. The polymer of interest with some remnants of PVP K 90 on its surface was carefully transferred in a

new solution of NaOCl in a new bottle and subjected to a temperature of 80 °C for 48 h. The choice of this temperature was based on the results of solubility tests of non-foamed polymer films (cf. Supporting Information). To wash out the residual NaOCl and active chlorine, the samples were rinsed in decalcified water at 35 °C for 10 min, aqueous solution of 0.5 wt% sodium bisulfite at 20 °C for 10 min and finally with decalcified water at 80 °C for 10 min [33].

3.4. Foam Characterization and Membrane Properties

Scanning electron microscopy (SEM) was used to characterize the foams. For large samples, foams were broken using liquid nitrogen to retain their nanostructure. For smaller samples, foams were cut using a sanitized sharp razor blade which caused smearing of the nanoscale structures present in the cutting plane. The average cell size was measured for selected foams using the scanning electron micrographs and the measurement tool in Photoshop CS6 (Adobe, San Jose, CA, USA). The porosity was measured for selected foams from the micrographs by measuring the number of pixels taken by visible cells and calculating the percentage versus the total number of pixels in the micrographs.

Density measurement was carried out using the buoyancy method on a density measurement device (Mettler Toledo, Gießen, Germany). Water-flux measurements were carried out on samples after completion of post-treatment using a membrane-holding cell with a diameter of 20 mm and an in-house constructed testing facility. The measurements were carried out with decalcified water at 7 bar pressure.

Retention tests were carried out using a Millipore cell that held a solution of 0.01 wt% poly(ethylene oxide) (PEO) in water of average molecular weight 400,000 Da. The broad molecular weight distribution of the chosen PEO allowed filterability of various length molecules to be observed. The solution was allowed to mix thoroughly using constant magnetic stirring in a closed flask for 24 h before using in retention tests. The feed solution and the permeate solutions were collected and further analysed using gel permeation chromatography (GPC). The retention coefficient R was calculated using the Equation (4) where, w_P and w_F are the mass fractions of PEO in permeate and feed solutions respectively.

$$R = 1 - \frac{w_P}{w_F} \quad (4)$$

4. Results and Discussion

4.1. Material Characterization

In our DSC measurements, all homopolymers and blends showed a single glass transition. As an example, Figure 2 shows the DSC graph of blend L-32.

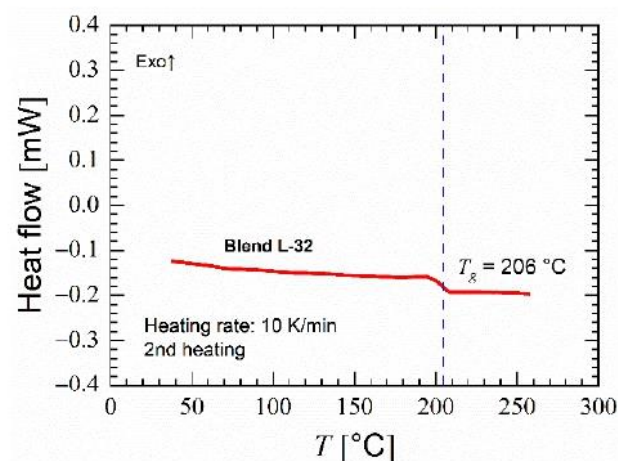


Figure 2. Heat flow versus temperature in second heating of blend L-32 showing single glass transition.

This provides an indication that the homopolymer chains are mixed on a segmental level in a single phase within these blends. As seen in Figure 3a,b, the blends with high molecular weight PESU undergo a higher reduction of glass transition temperature with increase in PVP content than low molecular weight PESU. This suggests a higher reduction of free volume caused by PVP K 30 in the blends with higher molecular weight PESU than in the blends with lower molecular weight PESU. Figure 3a,b also show the change in glass transition temperature due to change in polymer content as prediction of Equations (1) and (2) based on the glass transition temperatures of polyethersulfone as polymer I and poly(*N*-vinyl pyrrolidone) as polymer II. Blends with PESU E 2010 exhibited glass transition temperatures near the predicted values of both equations, whereas in blends with PESU E 3020 P the observed glass transition temperatures are more close to the values predicted by Equation (1). The predictions of Equation (1) correspond closely with both L-x and H-x blend combinations as the change in heat capacities at glass transition are dissimilar for both blend components and the ratio between their glass transition temperatures is unequal to unity. As stated by Couchman [52], when a polymer blend fulfils the premise of Equation (1), it provides an indication that the blend is composed of miscible polymers.

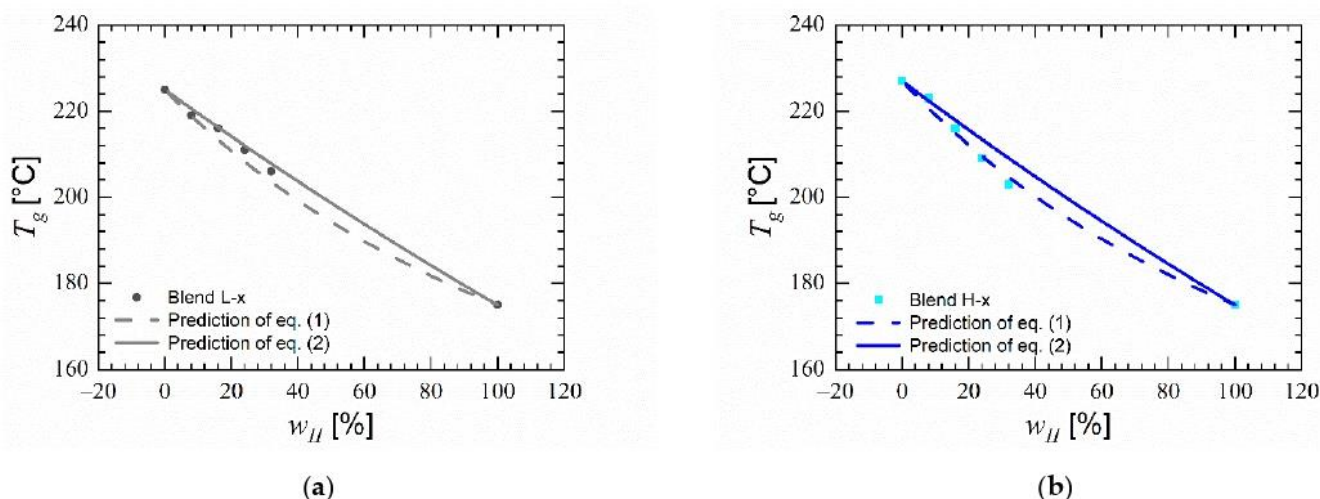


Figure 3. Glass transition temperature versus weight concentration of PVP in blends and predictions of Equations (1) and (2) based on glass transition temperatures of homopolymers; (a) Blends with PESU E 2010 (L-x) (b) Blends with PESU E 3020 P (H-x).

The influence of CO_2 on the thermal properties of the materials was studied by using HP-DSC. Compared to the sharp glass transition occurring observed by DSC under nitrogen, the glass transition occurs gradually spreading over a larger range of temperature. This spread increases with increasing CO_2 pressure as seen in Figure 4a for blend L-8. In some blends and materials, the glass transition occurred gradually without a distinct inflection point. Figure 4b shows a linear decrease of glass transition temperature with increasing CO_2 pressure for both grades of PESU. However, for PVP K 30 the glass transition temperature stayed constant above 10 bar CO_2 pressure. These influences on PESU and PVP act proportionally in the blends according to their weight contents. With increasing CO_2 pressure blends with 8% PVP content undergo a larger decrease in T_g than blends with 32% PVP. A larger free volume in a polymer leads to a lower glass transition temperature. Therefore, the HP-DSC measurements show that CO_2 has a larger effect on the free volume in PESU than PVP K 30 [59,60]. Foaming was observed in some of the samples after removal from the device.

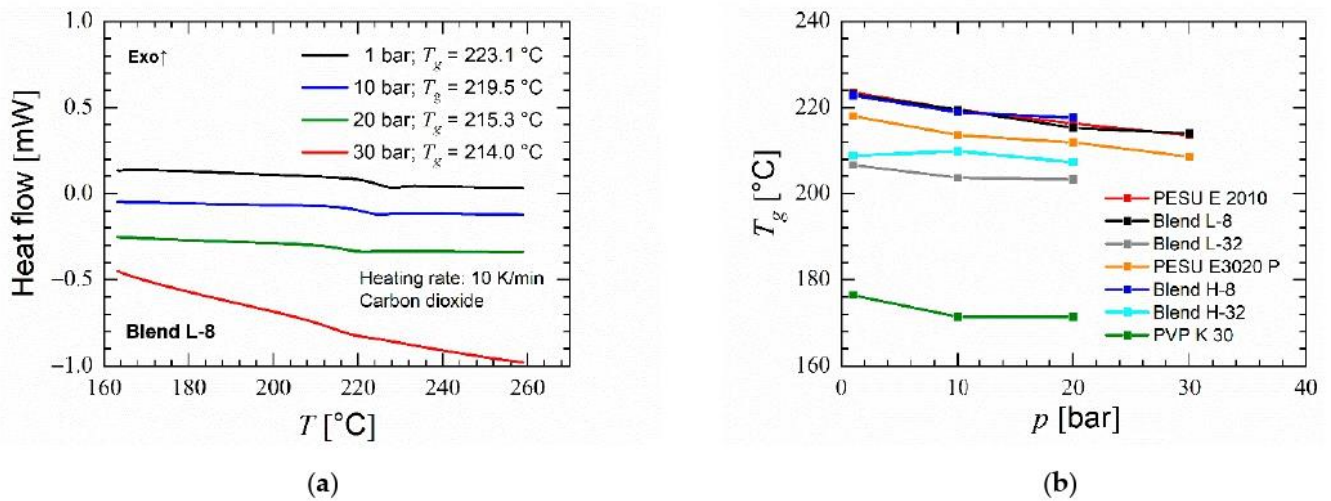


Figure 4. HP-DSC results for selected blends: (a) Effect of CO₂ pressure on glass transition temperature of blend L-8 (b) T_g at various CO₂ pressures (Some materials did not show an identifiable glass transition at 30 bar).

The effects of composition and type of the polymer blends on the dynamic moduli of the blends were determined by rheological analysis. In PESU, the storage modulus G' remains lower than the loss modulus G'' at frequencies lower than the crossover point. With decreasing angular frequency, in double logarithmic presentation, the storage modulus decreases with a slope nearly equal to 2 and the loss modulus with a slope nearly equal to 1. PVP K 30 does not adhere to the slopes equal to one and two of storage and loss modulus, respectively, and shows an increasing storage modulus with decreasing angular frequency because of thermally induced crosslinking. Since crosslinking increases the elasticity of the polymer, it could lead to a limited foam expansion and collapse during foaming of pure PVP or blends with high content of PVP. The data for pristine PESU and PVP are provided in the Supporting Information. The master curves of the moduli vs. angular frequency measurements shown in Figure 5a,b show that the blends translate the behaviors of PESU and PVP K 30 with their polymer contents correspondingly. Since both PESU and PVP are amorphous polymers [61,62], the temperature dependence of the horizontal shift factor in the construction of master curves for their blends can be described using the Equation (3) where reference temperature of 320 °C was chosen. As seen in Figure 5c,d, both blends obey the WLF equation which provides another evidence that PESU and PVP are miscible at both high and low concentrations of PVP [63,64].

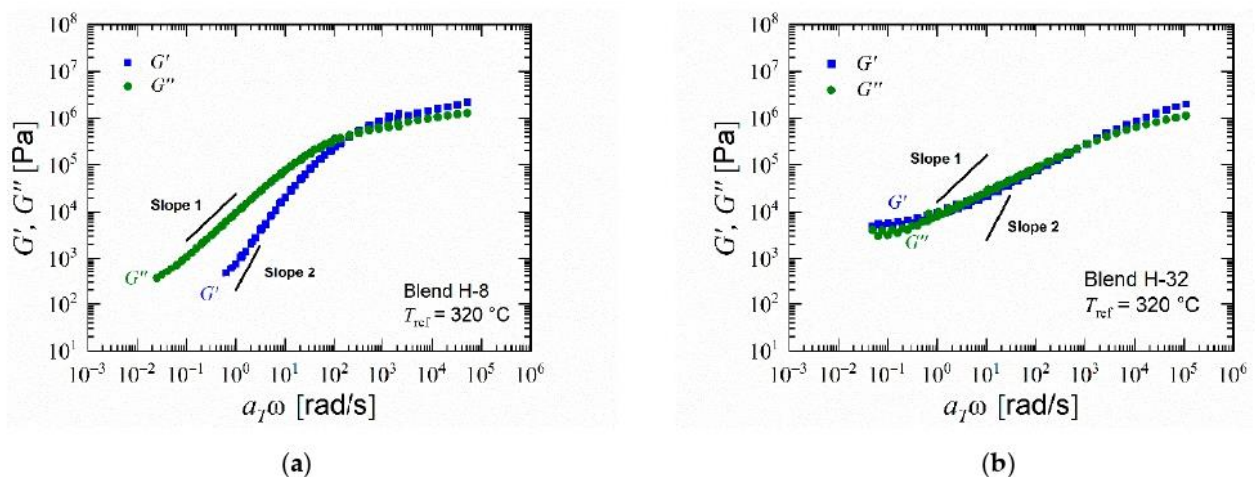


Figure 5. Cont.

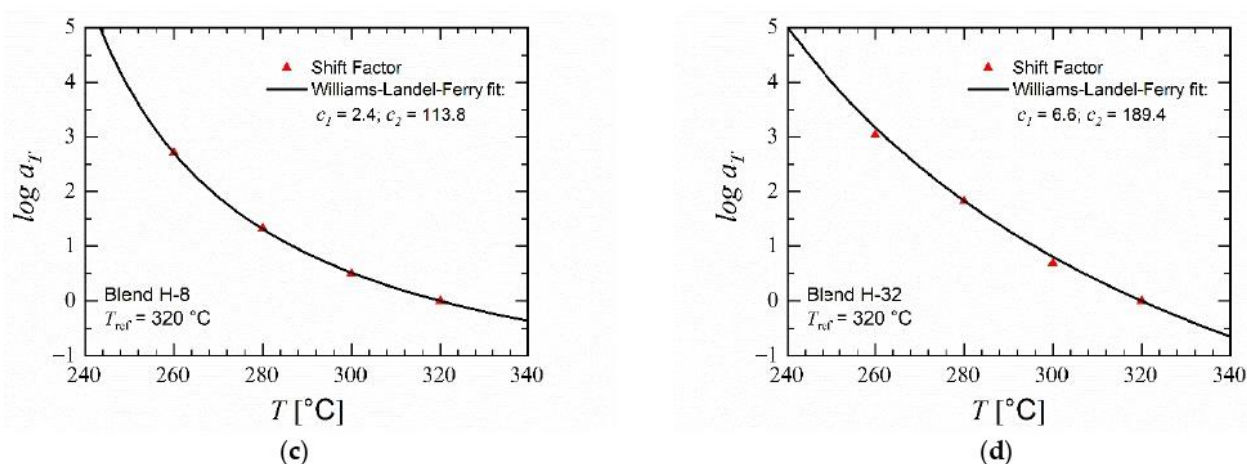


Figure 5. Rheological analysis of selected materials: (a,b) Master curve of blends H-8 and H-32; (c,d) Shift factor and WLF fit of blends H-8 and H-32.

4.2. Batch Foaming

In the experiments where CO₂ was used as a foaming agent, all selected materials yielded mostly closed-cellular foams. PVP K 30 delivered the lowest density foams among all materials in most trials. However, in some trials, during the foaming stage, the PVP samples initially grew into 3–4 times the original size as observed visually, and collapsed instantaneously after 45 to 60 s of exposure to the foaming temperature. This foam collapse occurred only when the loading pressure was set to 50 bar but did not occur in the trials conducted at 100 bar. As PVP is a highly elastic material in the melt state, the expansion caused by bubble growth is easily reversed, thus attaining the original size. Figure S10 in the Supporting Information show that this collapse has resulted into a crushed foam structure. Foams of blends with 32% PVP had the highest porosity among the blends. This increase in porosity due to increase of PVP content supports the findings by Shi et al. [41] where the increase in the polymer content of the minor component in the single-phase polymer blend yielded in higher porosity.

Although majorly closed microcellular foams, the blends L-8 and H-8 exhibit a certain nanoscale structure on the cell-walls of the microcellular foams as shown in Figure 6. As discussed in the Introduction, many researchers have found this structure in foams of various polymers at certain processing conditions. Fukasawa et al. [65] and Gong et al. [19] found a similar structure in polycarbonate foams under certain processing conditions. Their structure consisted of partially open pores formed within this structure. Fukasawa et al. [65] linked the formation of these pores to the crystallization of polycarbonate resulting in a fibrillary structure that was stretched as a result of bubble growth in the amorphous region during foaming. This explanation was based on various studies that focused on the crystallization of polycarbonate where such fibrillary structure was also reported. However, this explanation remains a speculation as evidence of CO₂ induced crystallization cannot be identified in their samples. Gong et al. [19] and Guo et al. [21–23] provide explanations that seem more plausible towards the cause of this structure. Gong et al. [19] explained that the formation of the fibril structure on the cell walls is due to the phenomenon called crazing. The nucleation and bubble growth induced due to foaming in the polymer results in biaxial tensile deformation. Thus, the fibrils are stretched and result in the formation of voids. They also found a direct relation of the strain energy around the pores during nucleation and bubble growth towards the formation of the nanostructure. Guo et al. [21–23] found a similar structure in polysulfone, polyphenylsulfone and a cyclic olefin copolymer. They named the structure as bicontinuous structure and suggest that an open or closed nanoscale structure may be a result of stress induced nucleation. Although the reasoning given by Gong et al. [19] and Guo et al. [21–23] differ, they agree in that the structure is caused by stretching induced by the growth of micro cells.

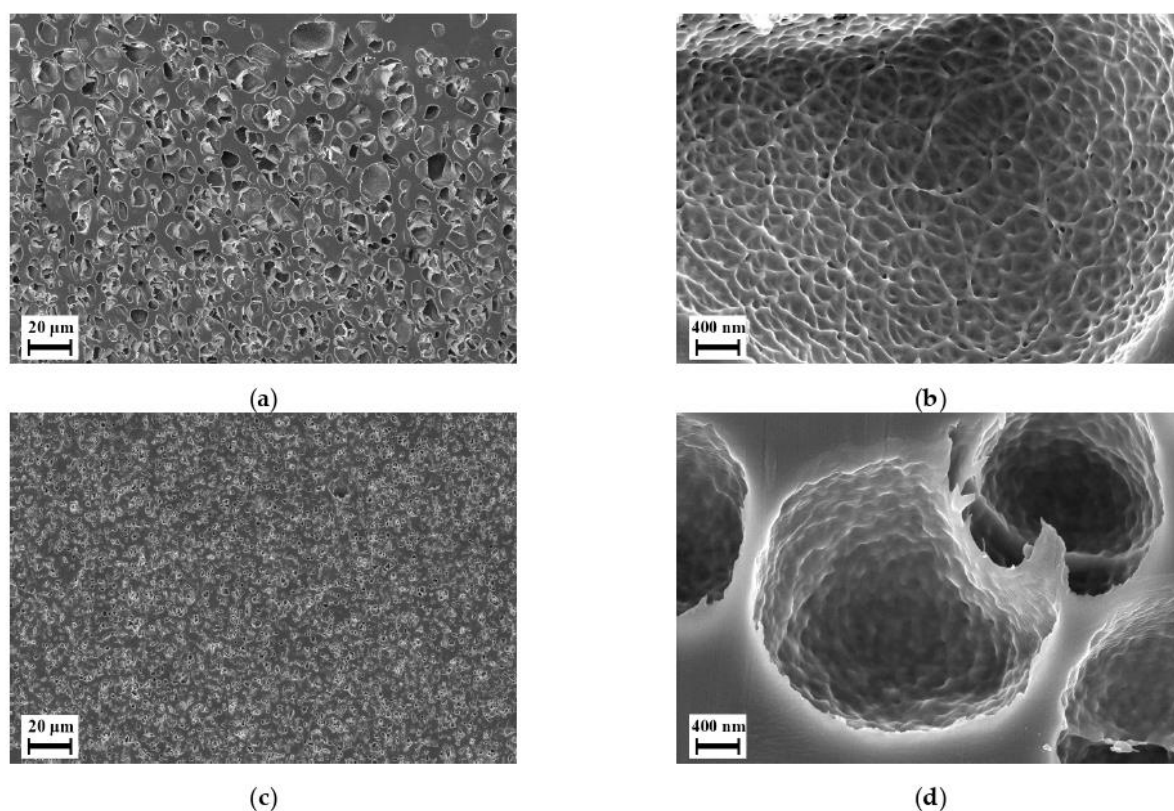


Figure 6. Scanning electron micrographs of selected foams manufactured using foaming agent CO₂: (a,b) Blend L-8; (c,d) Blend H-8.

In our case, the blends L-8 and H-8 delivered similar structure on the cell-walls of the microcells, which however is not open porous. This can be explained by the lack of sufficient deformation provided during the growth of microcells since a higher expansion during foaming is required for fabrication of open-celled foams [22,23]. A higher expansion would lead towards stretching the nanostructure enough such that open nanocellular foams are obtained.

Initially in the trials with CO₂ and water, the effect of foaming temperature was analyzed. The parameters loading temperature (150 °C), loading time (48 h), pressure (100 bar) and foaming time (100 s) were kept constant.

As expected, when using CO₂ and water as foaming agent an increased porosity was found in foams of blends H-8 and H-32 in the microcells as seen in Figures 7 and 8. Blend H-32 showed a higher porosity and partially open-cellular foam, but failed in providing any nanoscale structure. Foams of blends L-8 (cf. Supporting Information Figure S7) and H-8 contained high uniformity and similar cell size. The walls of these cells were made of a mesh of open pores smaller than 200 nm. The increased porosity enabled formation of pores within the nanoscale structure. This structure was seen at samples foamed at temperatures of 210, 230 and 250 °C for both materials. At 270 °C, this structure was not found. Comparing the porosity and the cell size distribution, the foaming temperature 230 °C provides an average cell size below 100 nm and the highest porosity of this type of pores was larger than 20%. At this foaming temperature, among the two blends, H-8 blend provides the lowest average cell size while maintaining a high porosity in both microcells and the smaller open pores. To maintain connectivity between the microcells through the smaller open pores, an overall high porosity is also desired. Therefore, blend H-8 is taken as an optimum candidate for the further tests by selecting the foaming temperature as 230 °C. As shown in Figure 9, the average size of the pores on the microcell walls in the foams obtained using loading temperature as 150 °C is below 100 nm and has a porosity larger than 25%. The loading temperature 175 °C delivers higher porosity and larger cell size than the loading temperature 150 °C in both microcells and the pores on their cell-walls. Scanning electron micrographs of the effect of

loading temperature is available in the Supporting Information as Figure S9. A higher loading temperature softens the polymer more and aids in faster diffusion of the foaming agents. This results in higher porosity and larger microcells during the foaming stage. An increased growth of microcells causes higher stretching of the cell walls wherein the nodal structures aid in creation of larger pores. Similarly, a lower loading temperature causes a lower solubility of foaming agents in the polymer and results in low porosity and smaller cell sizes. Therefore, the originally selected loading temperature of 150 °C appears ideal in this case for the blend H-8 such that an interconnectivity is achieved.

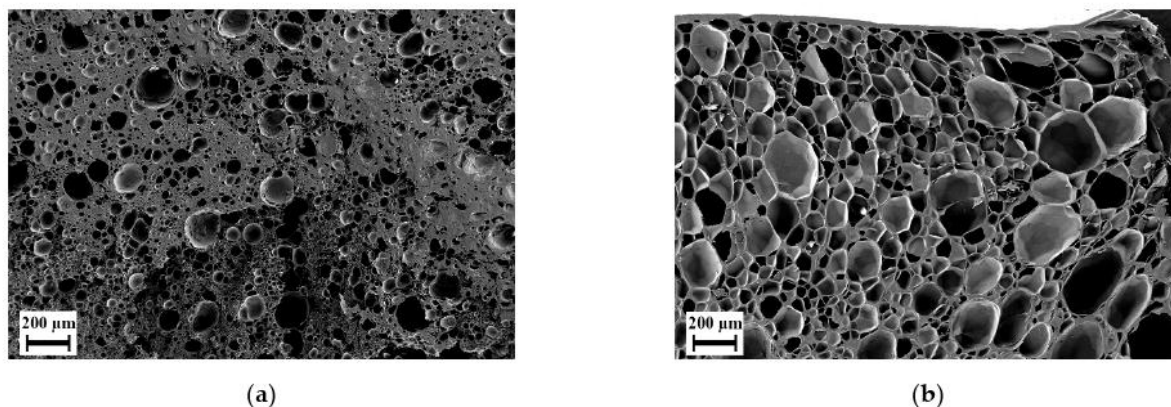


Figure 7. Scanning electron micrographs of foams of blend H-32 manufactured at loading time 48 h, pressure 100 bar, loading temperature 150 °C, foaming time 100 s and foaming temperature 230 °C: (a) Using only CO₂ as foaming agent; (b) Using CO₂ and H₂O as foaming agents.

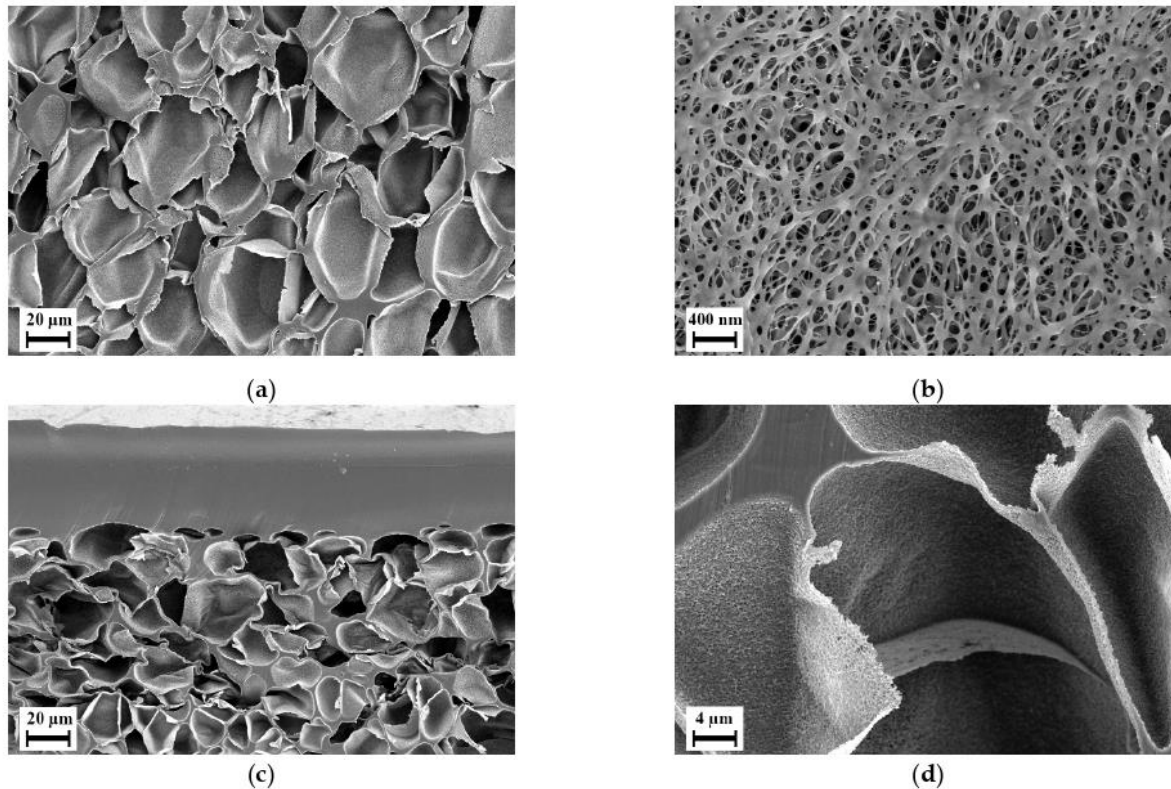


Figure 8. Scanning electron micrographs of foams manufactured using blowing agent CO₂ and H₂O at loading time 48 h, pressure 100 bar, loading temperature 150 °C, foaming time 100 s and foaming temperature 230 °C for Blend H-8: (a) internal structure at 500× magnification; (b) internal structure at 20,000× magnification; (c) structure near the surface at 500× magnification; (d) internal structure at 2500× magnification.

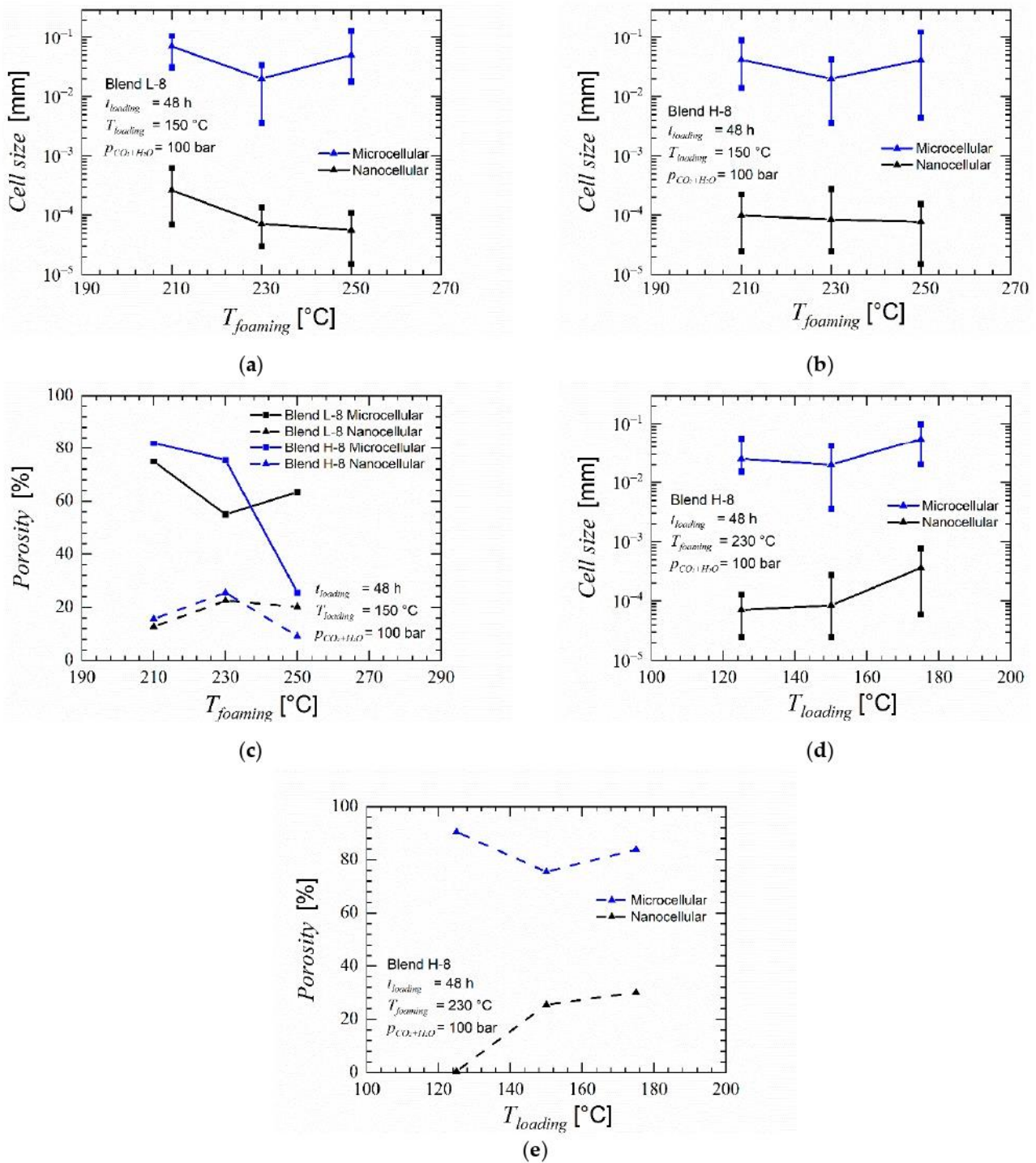


Figure 9. Average cell size and porosity: (a) Average cell size vs. foaming temperature in foams of blend L-8; (b) Average cell size vs. foaming temperature in foams of blend H-8; (c) Porosity vs. foaming temperature in foams of blends L-8 and H-8; (d) Average cell size vs. loading temperature in foams of blend H-8; (e) Porosity vs. loading temperature in foams of blend H-8.

Owusu-Nkwantabisah et al. [29] analysed the effects of using H₂O along with CO₂ as a foaming agent for foaming of polyethersulfone and found that using scCO₂ + shH₂O as foaming agent delivered an increased porosity and in some cases, open pores. As the structure found in foams H-8 and L-8 previously could develop open pores if the overall porosity is increased, scCO₂ + shH₂O was used as foaming agent.

4.3. Membranes

All foams discussed in Section 3.2, exhibit a solid non-foamed skin layer of approximately 20–50 μm thickness similar to as shown in Figure 9c. To use these foams for their permeation properties, this outer layer is necessary to be eliminated and thus sandwich-type samples were used. The sandwich-type samples have an additional layer of another polymer, PVP K 90 in this case, such that it behaves as a faux outer layer where the escape of diffused foaming agent would take place during depressurization thus limiting the non-foamed surface layer towards the PVP K 90. This allows the polymer of interest to stay completely foamed. During post-treatment, the PVP layers dissolve into the NaOCl solution and the thoroughly foamed polymer of interest is obtained.

During the batch foaming of sandwich-type samples that were prepared using aqueous solution of PVP, blend H-8 showed a similar internal foam structure as it was seen in the previous batch foaming experiments. However, the surface layer was foamed with a separate foaming pattern, i.e., with smaller closed-cells with an average diameter of 100 nm and blind open pores on the surface. Figure 10a,b show the microstructure of foam of blend H-8 manufactured using sandwich method. The influence of using the sandwich-type samples can be seen but applicable results were not delivered. Blend H-32 however, yielded a completely permeable open nanocellular foam with slit type open pores as shown in Figure 10d on the surface with average width 50 nm as shown in Figure 10f. This foam structure was available only in the regions indicated in green in Figure 10c. The region highlighted in red were non-foamed as seen in Figure 10e. This indicated that the blend layer was too thick. The sample could therefore not be used for testing permeation. Also, in some samples, the blend layer was not fully covered by the PVP due to the adhesive solution not flowing in certain areas between the PI foil and the blend. This caused certain samples to have non-foamed skin layers in the regions where the blend film was not covered by PVP K 90.

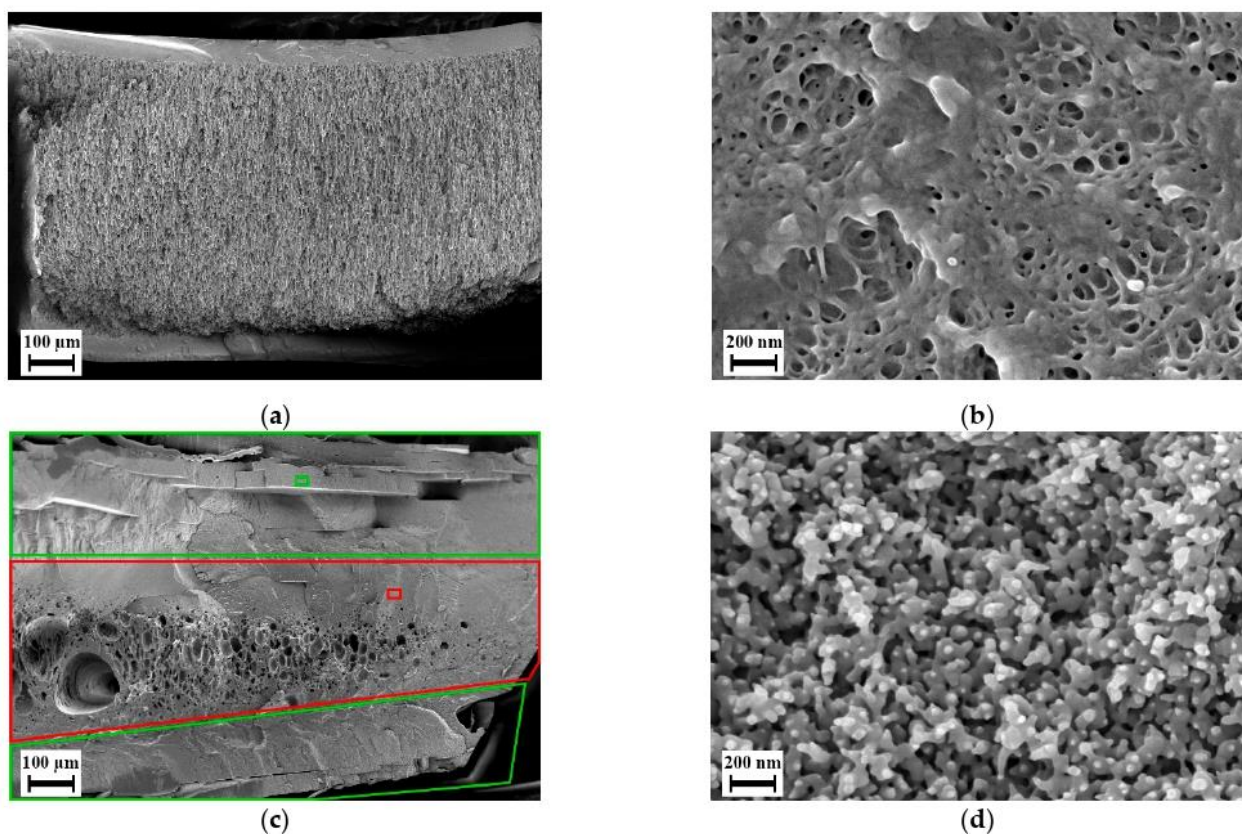


Figure 10. Cont.

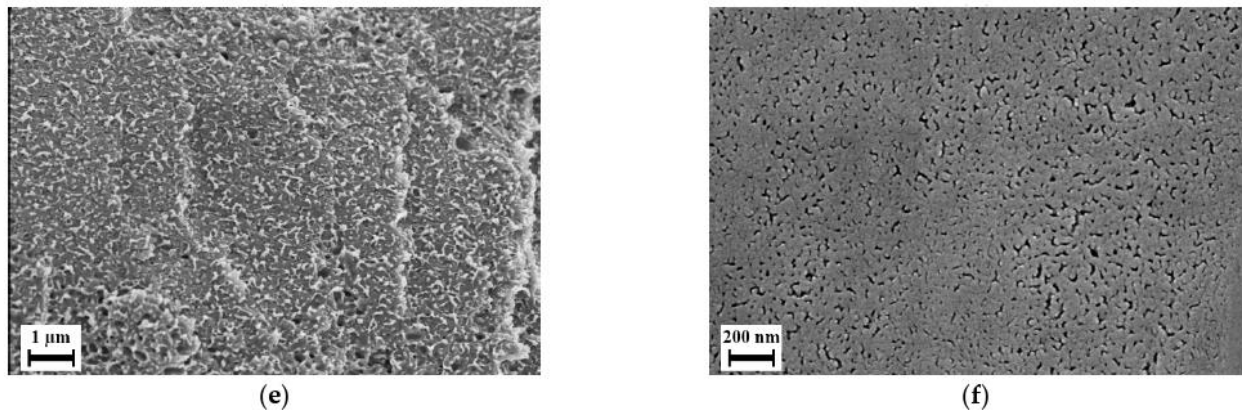


Figure 10. Scanning electron micrographs of sandwich-type samples manufactured using method I, batch foamed and post-treated: (a) Cross section of blend H-8; (b) Microstructure observed in the skin layer from figure (a); (c) Cross section of blend H-32; (d) microstructure observed in smaller green box and commonly found across the area enclosed by larger green boxes in figure (c); (e) Observed solid structure in the smaller red box and commonly found across the area enclosed by the larger red box in figure (c); (f) Outer surface of blend H-32.

To overcome these issues, thinner blend samples were used in method II of preparing sandwich-type samples, and to ensure completely sealed covering of the blend layer, the PVP layer was compression molded instead. Since only blend H-32 delivered promising results, only blend H-32 was subjected to further experiments using the second method of preparing sandwich-type samples. After batch foaming, along with the blend layer, the outer PVP K 90 layer foamed. This PVP foam could be dissolved during post-treatment. Figure 11 show that the blend layer yields a completely permeable open-cellular foam with cell sizes less than 300 nm. The membranes after post-treatment as shown in Figure 12 had a thickness in the range of 300 to 350 μm , approximately two times thicker than the polymer layer in the sandwich-type samples. This open-cellular structure was not observed in the foams of blend H-32 that were manufactured during the batch foaming trials using cylindrical samples as seen in Figure 7. Comparison of the morphologies after the loading phase of batch foaming, after foaming and after post-treatment, shows that the internal open-cellular structure is obtained only after foaming and the post-treatment aids in the removal of the outer PVP layer and provides an open porous surface. This open porous surface has an average cell size around 50 nm and is slightly larger than the internal porous structure of the foam which is around 200 nm. Therefore, due to this pore size, this porous surface is capable of functioning as a selective layer for ultrafiltration [2].

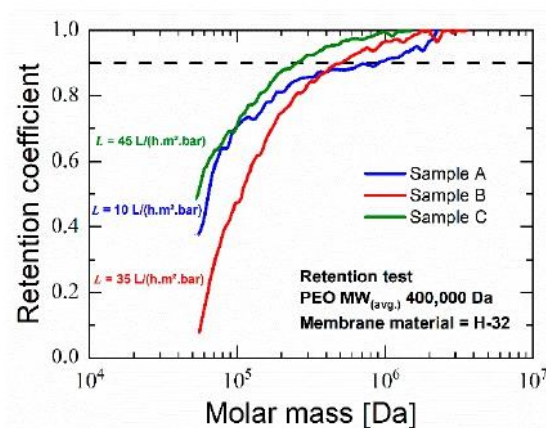


Figure 11. Retention coefficient of membrane manufactured using sandwich-type samples vs. molar mass.

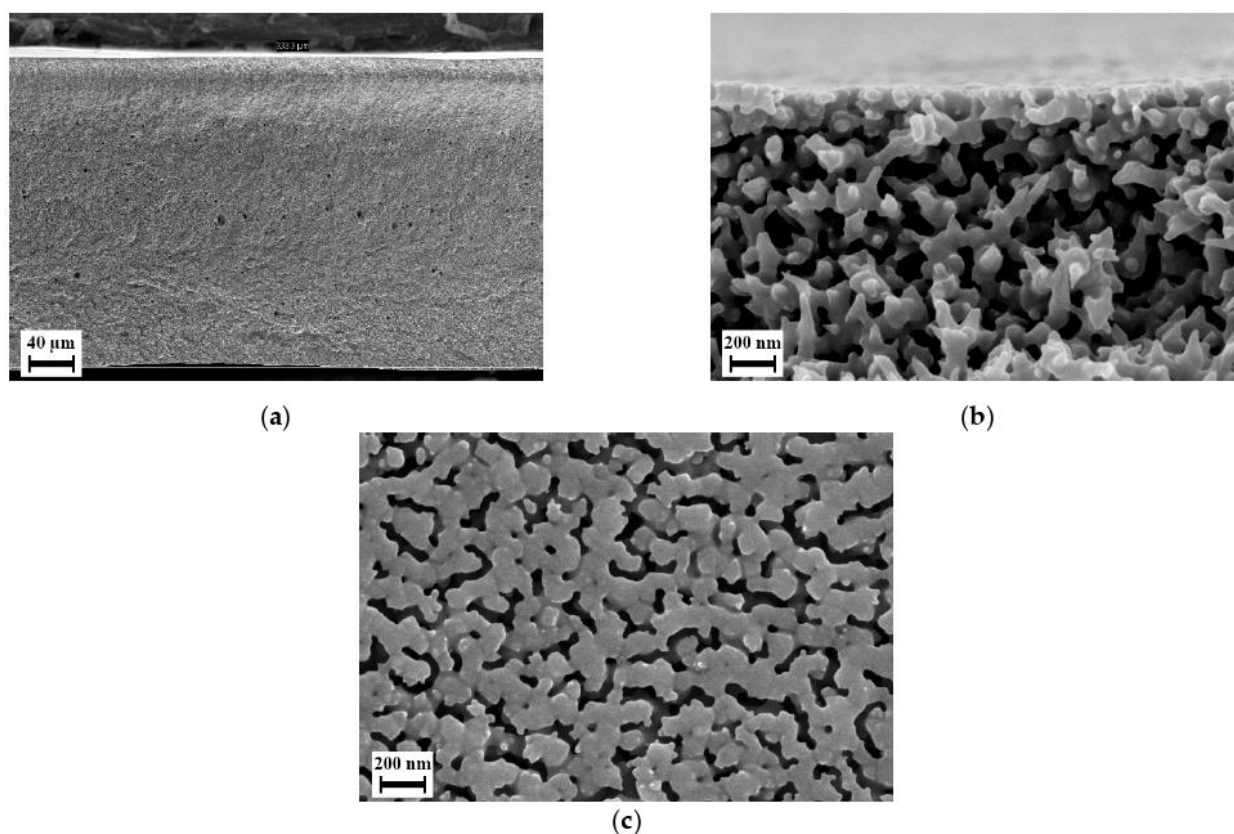


Figure 12. Scanning electron micrographs of sandwich-type sample manufactured using method II with blend H-32, after batch foaming and post-treatment: (a) cross section; (b) internal structure; (c) surface.

The mechanism behind the realization of such a structure using sandwich-type samples is depicted in Figure 13. In a standard sample, during the loading phase, the foaming agent dissolves within the sample over time t_x and attains near-saturated state. During depressurization of the batch foaming reactor, the dissolved foaming agent begins to escape from the polymer matrix. The rate of escaping is highest at the surface and lowest in the middle of the sample. This occurs as long as the depressurization time along with the time taken to transfer the samples from the reactor to the foaming temperatures, is larger than zero. Therefore, the samples are no more in their fully saturated state. This yields low level of nucleation and causes closed-cellular foams with non-foamed outer surface layer. Therefore, blend H-32 when foamed as a standard sample, yielded closed microcellular foam as seen in Figure 7b. In sandwich-type samples, when one polymer is covered by another polymer, under similar conditions the amount of time taken for the foaming agent to dissolve within both polymers until saturation, t_y is larger than time t_x due to larger thickness and different diffusion coefficients. During depressurization, similar to standard samples, the foaming agent begins escaping from the sample, but this occurs mainly in the outer polymer. As the internal polymer layer is tightly enclosed by the outer polymer layer, any escape of foaming agent from internal polymer would need permeation of the foaming agent through the outer polymer layer. As the outer polymer is different from the inner polymer, they have different permeation and solubility properties. The internal polymer remains near to its completely saturated state and delivers highly porous nanocellular foam whereas, the non-foamed outer surface layer is restricted to the outer polymer. Therefore, based on this principle, an open-celled foam with cell size in nanometers was realized in blend H-32 using this method as seen in Figure 14. Removal of the outer polymer was required to use the inner polymer for any applications. Thus, selection of the outer polymer as a water-soluble or inorganic solvent soluble polymer is essential such that the

post-treatment of the sandwich-type sample would lead to dissolution of the outer layer and the internal layer stays unaffected.

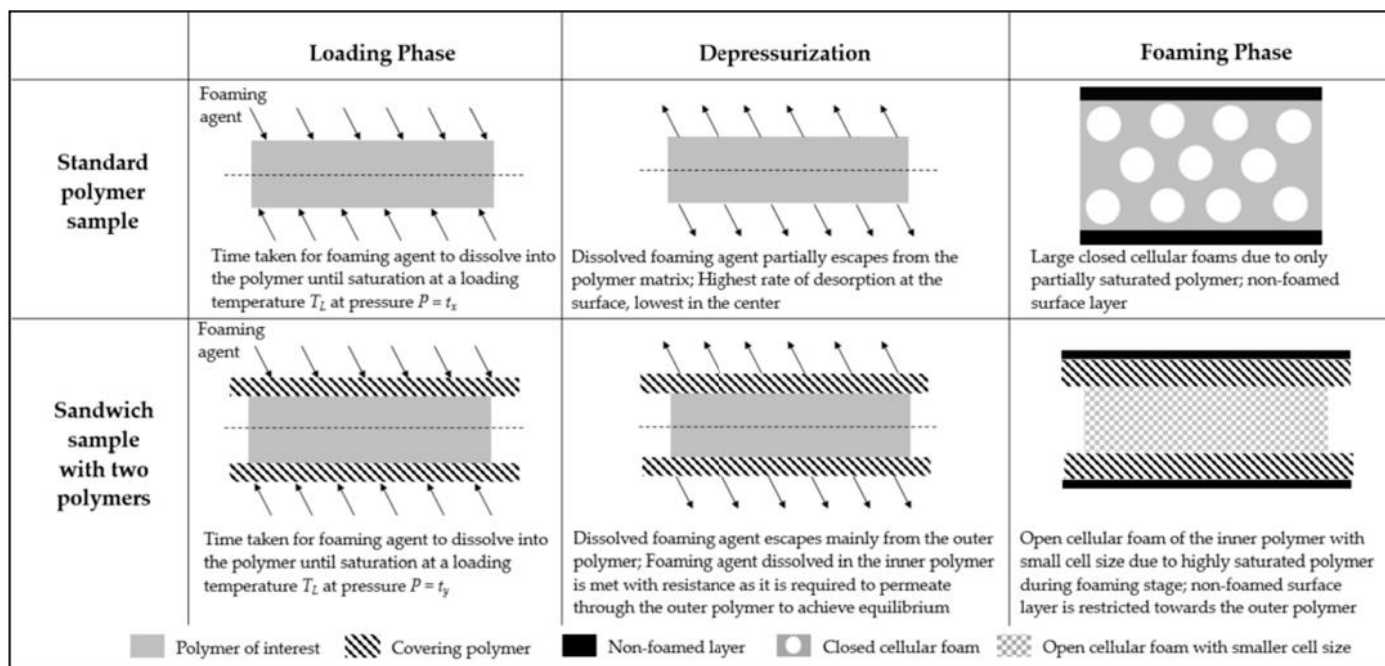


Figure 13. Functioning of sandwich-type sample during batch foaming versus a standard sample.

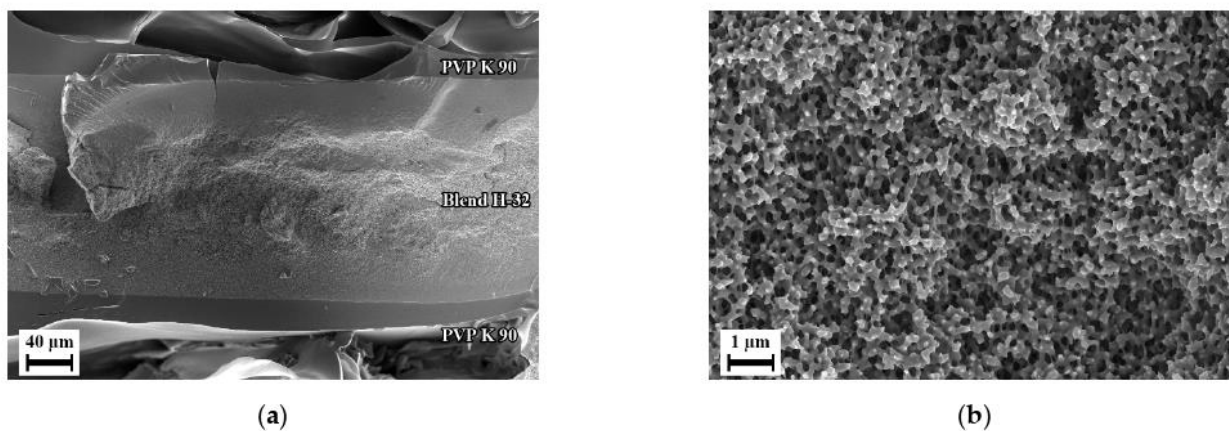


Figure 14. Scanning electron micrographs of sandwich-type sample manufactured using method II with blend H-32 after batch foaming before post-treatment: (a) at 200× magnification; (b) at 10,000× magnification on layer with Blend H-32.

Three membrane samples from blend H-32, viz. A, B and C were tested for water flux and yielded a flux of 10, 35 and 45 L/(h m² bar), respectively. These values of water flux are similar to those seen with polyethersulfone ultrafiltration membranes manufactured using methods involving organic solvent [66,67]. Since larger membrane thickness adds further resistance to water flow, future studies could employ thinner samples so as to increase the water flux. As seen in Figure 11, retention tests reveal a retention coefficient above 0.9 for PEO with molecular weight higher than ~260,000 Da for sample C and an average of ~480,000 Da for all measured samples. Since retention of molecules between 10³–10⁶ Da is classified under ultrafiltration [1,68,69], these values although near the upper limit, provide evidence that these membranes have potential for ultrafiltration. Although the performance of this developed membrane is lower than modern ultrafiltration membranes manufactured using organic solvents [39,70–73], these membranes provide

a genesis towards large-scale development of ultrafiltration membranes using foaming. Future studies focus on optimizations and improvements of the membranes to match the ultrafiltration standards of membranes manufactured using other methods and also on developing ways to manufacture them efficiently and on a large scale.

5. Conclusions

Batch foaming experiments on PESU/PVP blends using CO₂ as blowing agent show a clear influence of PVP content on the foaming behavior. Foams of PESU blends with 32% PVP exhibited the highest density and foams of blends with 8% PVP show a tendency towards formation of a fibril structure on the cell walls of the closed-cells. Using superheated H₂O with CO₂ as foaming agents the porosity of the foams was significantly increased. This lead towards increased expansion of the fibril structures on the walls of foam cells thus creating a smaller porous structure connecting the larger cells. Optimal processing conditions and blend compositions for obtaining high porosity and lowest cell size were found. The samples, however, contain a solid non-foamed surface layer which hinders the direct application of the open-celled foam as membranes. Sample preparation methods developed by us eliminated the formation of the non-foamed surface layer, and at the same time allowed the sample to be in near-saturated state. Using this method, blend with 8% PVP foams completely including the outer surface but cannot deliver a complete open-cellular foam. A blend with 32% PVP however, due to high saturation of foaming agent, exhibits complete open-cellular foam containing porous surface with average surface cell size of 50 nm and average internal cell size of 200 nm. These open nanocellular foams provide an average water flux of 30 L/(h m² bar) and an average retention coefficient above 0.9 for PEO with molecular weights above 480,000 Da confirming the proof of concept for proposed application of these foams as ultrafiltration membranes.

Supplementary Materials: The following are available online at <https://www.mdpi.com/article/10.3390/polym14061177/s1>, Figure S1: Time taken to dissolve PVP K 30 samples in water at various temperatures. Figure S2: Scanning electron micrographs of post-treated blends in NaOCl at various temperatures: (a) Surface of film of blend H-8 at 80 °C (b) Surface of film of blend H-32 at RT; (c) Surface of film of blend H-32 at 80 °C; (d) Cross-section of film of blend H-32 at 80 °C. Figure S3: IR spectra of blend, non-foamed blend H-8 and after foaming with various foaming agents. Figure S4: DSC 2nd heating curves of non-foamed blend H-8 and after foaming with various foaming agents. Figure S5. Master curves of selected materials from rheological analysis: (a) PESU E 2010; (b) PESU E 3020 P; (c) PVP K 30; (d) Blend L-8; (e) Blend L-32. Figure S6. Results of thermogravimetric analysis for selected materials. Figure S7. Scanning electron micrographs of blend L-8 foams manufactured using blowing agents CO₂ and H₂O at loading time 48 h, pressure 100 bar, loading temperature 150 °C, foaming time 100 s and various foaming temperatures: (a,b) 210 °C; (c,d) 230 °C; (e,f) 250 °C; (g,h) 270 °C. Figure S8. Scanning electron micrographs of blend H-8 foams manufactured using blowing agents CO₂ and H₂O at loading time 48 h, pressure 100 bar, loading temperature 150 °C, foaming time 100 s and various foaming temperatures: (a,b) 210 °C; (c,d) 250 °C; (e,f) 270 °C. Figure S9. Scanning electron micrographs of foams of blend H-8 at the loading time 48 h, pressure 100 bar, foaming temperature 230 °C, foaming time 100 s, the blowing agent CO₂ and H₂O and various loading temperatures: (a,b): 125 °C; (c,d): 175 °C. Figure S10. Scanning electron micrograph of collapsed PVP foam manufactured using blowing agent CO₂ at loading time 48 h, pressure 50 bar, loading temperature 150 °C, foaming time 100 s and foaming temperature 250 °C. Figure S11. Scanning electron micrographs of sandwich-type sample manufactured using method II with blend H-32: (a,b) after loading phase without subjecting to foaming temperatures (Similar settings and method used as Figure 12).

Author Contributions: Conceptualization, methodology and material characterization A.R. and U.A.H.; batch foaming experiments, A.R. and K.B.; water-flux and retention, J.K.; writing—original draft preparation, A.R.; writing—review and editing, U.A.H., J.L., K.B., J.K., V.A.; visualization, A.R. and U.A.H.; scientific consultation, J.L. and V.A.; scientific supervision, U.A.H. and V.A.; project administration and funding acquisition, U.A.H. All authors have read and agreed to the published version of the manuscript.

Funding: This research was partially funded by BASF SE.

Institutional Review Board Statement: Not applicable.

Informed Consent Statement: Not applicable.

Data Availability Statement: The characterization data are available upon request from the authors.

Acknowledgments: The authors thank Ivonne Ternes (rheology, thermal analysis, batch foaming), Petra Merten, Maren Brinkmann (gel permeation chromatography), Martin Held, Anke-Lisa Höhme, Erik Schneider (microscopy), and Prokopios Georgopoulos, Mahboubeh Kargar (scientific discussions). The partial funding, donation of materials and the discussions with Oliver Gronwald and Martin Weber (BASF SE) are gratefully acknowledged.

Conflicts of Interest: The authors declare no conflict of interest. The funders had no role in the design of the study; in the collection, analyses, or interpretation of data; in the writing of the manuscript, or in the decision to publish the results.

Abbreviation

Symbols used in Equations (1)–(3).

Symbol	Parameter	Unit
T_g	Glass transition temperature of the blend	K
w_I	Mass fraction of polymer I	-
$c_{p,I}$	Heat capacity of polymer I	mW
$T_{g,I}$	Glass transition temperature of polymer I	K
w_{II}	Mass fraction of polymer II	-
$c_{p,II}$	Heat capacity of polymer II	mW
$T_{g,II}$	Glass transition temperature of polymer II	K
a_T	Horizontal shift factor	-
c_1, c_2	WLF parameters	K
T	Temperature	°C
T_{ref}	Reference temperature	°C
R	Retention coefficient	-
w_p	Mass fraction of PEO in permeate	-
w_F	Mass fraction of PEO in feed	-

References

- Zhao, Y. Chapter 2—Physical and chemical treatment processes for leachate. In *Pollution Control Technology for Leachate from Municipal Solid Waste*; Youcai, Z., Ed.; Butterworth-Heinemann: Oxford, UK, 2018; pp. 31–183. [CrossRef]
- Singh, R. Chapter 1—Introduction to Membrane Technology. In *Membrane Technology and Engineering for Water Purification*, 2nd ed.; Butterworth-Heinemann: Oxford, UK, 2015; pp. 1–80. [CrossRef]
- Zhang, F. Preparation of cation exchange resin filled EVAL hollow fiber membrane adsorbent. *Int. J. Chem.* **2009**, *1*, 87–90. [CrossRef]
- Verissimo, S.; Peinemann, K.V.; Bordado, J. Thin-film composite hollow fiber membranes: An optimized manufacturing method. *J. Membr. Sci.* **2005**, *264*, 48–55. [CrossRef]
- Wang, D.L.; Teo, W.K.; Li, K. Preparation and characterization of high-flux polysulfone hollow fibre gas separation membranes. *J. Membr. Sci.* **2002**, *204*, 247–256. [CrossRef]
- Bulte, A.M.W.; Mulder, M.H.V.; Smolders, C.A.; Strathmann, H. Diffusion induced phase separation with crystallizable nylons. 1. Mass transfer processes for nylon 4,6. *J. Membr. Sci.* **1996**, *121*, 37–49. [CrossRef]
- Bulte, A.M.W.; Mulder, M.H.V.; Smolders, C.A.; Strathmann, H. Diffusion induced phase separation with crystallizable nylons. 2. Relation to final membrane morphology. *J. Membr. Sci.* **1996**, *121*, 51–58. [CrossRef]
- Preventing Adverse Health Effects from Exposure to: Dimethylformamide (DMF). Available online: <https://www.cdc.gov/niosh/docs/90-105/default.html> (accessed on 13 February 2022).
- Åkesson, D.B. N-Methyl-2-pyrrolidone. Available online: <https://www.who.int/ipcs/publications/cicad/en/cicad35.pdf> (accessed on 13 February 2022).
- Dimethyl Acetamide. Available online: <https://nj.gov/health/eoh/rtkweb/documents/fs/0736.pdf> (accessed on 13 February 2022).
- ECHA, E.C.A. Formic Acid. Available online: <https://echa.europa.eu/de/substance-information/-/substanceinfo/100.000.527> (accessed on 13 February 2022).

12. Redlich, C.A.; Beckett, W.S.; Sparer, J.; Barwick, K.W.; Riely, C.A.; Miller, H.; Sigal, S.L.; Shalat, S.L.; Cullen, M.R. Liver-disease associated with occupational exposure to the solvent dimethylformamide. *Ann. Intern. Med.* **1988**, *108*, 680–686. [[CrossRef](#)] [[PubMed](#)]
13. Rundquist, E.M.; Pink, C.J.; Livingston, A.G. Organic solvent nanofiltration: A potential alternative to distillation for solvent recovery from crystallisation mother liquors. *Green Chem.* **2012**, *14*, 2197–2205. [[CrossRef](#)]
14. Perry, R.H.; Green, D.W.; Maloney, J.O. Distillation. In *Perry's Chemical Engineers' Handbook*, 7th ed.; McGraw-Hill: New York, NY, USA, 1997.
15. Gadalla, M.A.; Olujic, Z.; Jansens, P.J.; Jobson, M.; Smith, R. Reducing CO₂ emissions and energy consumption of heat-integrated distillation systems. *Environ. Sci. Technol.* **2005**, *39*, 6860–6870. [[CrossRef](#)]
16. Okolieocha, C.; Raps, D.; Subramaniam, K.; Altstädt, V. Microcellular to nanocellular polymer foams: Progress (2004–2015) and future directions—A review. *Eur. Polym. J.* **2015**, *73*, 500–519. [[CrossRef](#)]
17. Krause, B.; Boerrigter, M.E.; van der Vegt, N.F.A.; Strathmann, H.; Wessling, M. Novel open-cellular polysulfone morphologies produced with trace concentrations of solvents as pore opener. *J. Membr. Sci.* **2001**, *187*, 181–192. [[CrossRef](#)]
18. Krause, B.; van der Vegt, N.F.A.; Wessling, M. New ways to produce porous polymeric membranes by carbon dioxide foaming. *Desalination* **2002**, *144*, 5–7. [[CrossRef](#)]
19. Gong, P.J.; Taniguchi, T.; Ohshima, M. Nanoporous structure of the cell walls of polycarbonate foams. *J. Mater. Sci.* **2014**, *49*, 2605–2617. [[CrossRef](#)]
20. Sorrentino, L.; Aurilia, M.; Iannace, S. Polymeric Foams from High-Performance Thermoplastics. *Adv. Polym. Technol.* **2011**, *30*, 234–243. [[CrossRef](#)]
21. Guo, H.M.; Nicolae, A.; Kumar, V. Solid-state microcellular and nanocellular polysulfone foams. *J. Polym. Sci. Pol. Phys.* **2015**, *53*, 975–985. [[CrossRef](#)]
22. Guo, H.M.; Nicolae, A.; Kumar, V. Fabrication of high temperature polyphenylsulfone nanofoams using high pressure liquid carbon dioxide. *Cell Polym.* **2016**, *35*, 119–142. [[CrossRef](#)]
23. Guo, H.M.; Kumar, V. Effect of glass transition temperature and saturation temperature on the solid-state microcellular foaming of cyclic olefin copolymer. *J. Appl. Polym. Sci.* **2015**, *132*, 42226. [[CrossRef](#)]
24. Li, Z.K.; Jia, Y.B.; Bai, S.B. Polysulfone foam with high expansion ratio prepared by supercritical carbon dioxide assisted molding foaming method. *RSC Adv.* **2018**, *8*, 2880–2886. [[CrossRef](#)]
25. Hwang, Y.D.; Cha, S.W. The relationship between gas absorption and the glass transition temperature in a batch microcellular foaming process. *Polym. Test.* **2002**, *21*, 269–275. [[CrossRef](#)]
26. Sauceau, M.; Fages, J.; Common, A.; Nikitine, C.; Rodier, E. New challenges in polymer foaming: A review of extrusion processes assisted by supercritical carbon dioxide. *Prog. Polym. Sci.* **2011**, *36*, 749–766. [[CrossRef](#)]
27. Jacobs, L.J.M. Carbon Dioxide as a Sustainable Means to Control Polymer Foam Morphology. Ph.D. Thesis, Technische Universiteit Eindhoven, Eindhoven, The Netherlands, 2008.
28. Hu, D.D.; Gu, Y.; Liu, T.; Zhao, L. Microcellular foaming of polysulfones in supercritical CO₂ and the effect of co-blowing agent. *J. Supercrit. Fluid* **2018**, *140*, 21–31. [[CrossRef](#)]
29. Owusu-Nkwantabisah, S.; Staudt, C.; Lesser, A.J. Synergy of supercritical CO₂ and superheated H₂O for enhanced processability of polyethersulfone towards open cell foams. *Polym. Eng. Sci.* **2018**, *58*, 1108–1114. [[CrossRef](#)]
30. Schulze, M.; Handge, U.A.; Abetz, V. Preparation and characterisation of open-celled foams using polystyrene-*b*-poly(4-vinylpyridine) and poly(4-methylstyrene)-*b*-poly(4-vinylpyridine) diblock copolymers. *Polymer* **2017**, *108*, 400–412. [[CrossRef](#)]
31. Smith, R.M. Extractions with superheated water. *J. Chromatogr. A* **2002**, *975*, 31–46. [[CrossRef](#)]
32. Tsehaye, M.T.; Velizarov, S.; Van der Bruggen, B. Stability of polyethersulfone membranes to oxidative agents: A review. *Polym. Degrad. Stabil.* **2018**, *157*, 15–33. [[CrossRef](#)]
33. Grunig, L.; Handge, U.A.; Koll, J.; Gronwald, O.; Weber, M.; Hankiewicz, B.; Scharnagl, N.; Abetz, V. Hydrophilic dual layer hollow fiber membranes for ultrafiltration. *Membranes* **2020**, *10*, 143. [[CrossRef](#)]
34. Jaleh, B.; Zare, E.; Azizian, S.; Qanati, O.; Nasrollahzadeh, M.; Varma, R.S. Preparation and Characterization of Polyvinylpyrrolidone/Polysulfone Ultrafiltration Membrane Modified by Graphene Oxide and Titanium Dioxide for Enhancing Hydrophilicity and Antifouling Properties. *J. Inorg. Organomet. Polym. Mater.* **2020**, *30*, 2213–2223. [[CrossRef](#)]
35. Dibrov, G.; Kagramanov, G.; Sudin, V.; Grushevenko, E.; Yushkin, A.; Volkov, A. Influence of sodium hypochlorite treatment on pore size distribution of polysulfone/polyvinylpyrrolidone membranes. *Membranes* **2020**, *10*, 356. [[CrossRef](#)]
36. Al Malek, S.A.; Abu Seman, M.N.; Johnson, D.; Hilal, N. Formation and characterization of polyethersulfone membranes using different concentrations of polyvinylpyrrolidone. *Desalination* **2012**, *288*, 31–39. [[CrossRef](#)]
37. Zhang, J.; Chen, S.; Bai, H.J.; Lu, S.F.; Xiang, Y.; Jiang, S.P. Effects of phosphotungstic acid on performance of phosphoric acid doped polyethersulfone-polyvinylpyrrolidone membranes for high temperature fuel cells. *Int. J. Hydrogen Energy* **2021**, *46*, 11104–11114. [[CrossRef](#)]
38. Dai, Y.; Wang, J.; Tao, P.P.; He, R.H. Various hydrophilic carbon dots doped high temperature proton exchange composite membranes based on polyvinylpyrrolidone and polyethersulfone. *J. Colloid Interf. Sci.* **2019**, *553*, 503–511. [[CrossRef](#)]
39. Gronwald, O.; Weber, M. AGNIQUE AMD 3L as green solvent for polyethersulfone ultrafiltration membrane preparation. *J. Appl. Polym. Sci.* **2020**, *137*, 48419. [[CrossRef](#)]

40. Aili, D.; Kraglund, M.R.; Tavacoli, J.; Chatzichristodoulou, C.; Jensen, J.O. Polysulfone-polyvinylpyrrolidone blend membranes as electrolytes in alkaline water electrolysis. *J. Membr. Sci.* **2020**, *598*, 117674. [[CrossRef](#)]
41. Shi, Z.L.; Ma, X.W.; Zhao, G.Q.; Wang, G.L.; Zhang, L.; Li, B. Fabrication of high porosity Nanocellular polymer foams based on PMMA/PVDF blends. *Mater. Des.* **2020**, *195*, 109002. [[CrossRef](#)]
42. Costeux, S.; Khan, I.; Bunker, S.P.; Jeon, H.K. Experimental study and modeling of nanofoams formation from single phase acrylic copolymers. *J. Cell. Plast.* **2015**, *51*, 197–221. [[CrossRef](#)]
43. Sun, H.L.; Sur, G.S.; Mark, J.E. Microcellular foams from polyethersulfone and polyphenylsulfone—Preparation and mechanical properties. *Eur. Polym. J.* **2002**, *38*, 2373–2381. [[CrossRef](#)]
44. Xie, Y.P.; Ye, F.; Chen, W.H.; Tang, J.H.; Liu, P.J. Preparation of high-strength and lightweight microcellular polysulfone foam with a segregated CNT network for excellent electromagnetic shielding. *RSC Adv.* **2020**, *10*, 11994–12003. [[CrossRef](#)]
45. Abbasi, H.; Antunes, M.; Velasco, J.I. Effects of graphene nanoplatelets and cellular structure on the thermal conductivity of polysulfone nanocomposite foams. *Polymers* **2020**, *12*, 25. [[CrossRef](#)]
46. Antunes, M.; Abbasi, H.; Velasco, J.I. The effect of microcellular structure on the dynamic mechanical thermal properties of high-performance nanocomposite foams made of graphene nanoplatelets-filled polysulfone. *Polymers* **2021**, *13*, 437. [[CrossRef](#)]
47. Abbasi, H.; Antunes, M.; Velasco, J.I. Electrical conduction behavior of high-performance microcellular nanocomposites made of graphene nanoplatelet-filled polysulfone. *Nanomaterials* **2020**, *10*, 2425. [[CrossRef](#)]
48. Lu, Y.Q.; Li, S.Y.; Chen, F.Y.; Ma, H.; Gao, C.J.; Xue, L.X. Development of coin-shaped ZIF-7 functionalized superhydrophobic polysulfone composite foams for continuous removal of oily contaminants from water. *J. Hazard. Mater.* **2022**, *421*, 126788. [[CrossRef](#)]
49. Liu, S.Q.; Yin, S.; Duvigneau, J.; Vancso, G.J. Bubble seeding nanocavities: Multiple polymer foam cell nucleation by polydimethylsiloxane-grafted designer silica nanoparticles. *ACS Nano* **2020**, *14*, 1623–1634. [[CrossRef](#)]
50. Ismail, A.F.; Mustaffar, M.I.; Illias, R.M.; Abdullah, M.S. Effect of dope extrusion rate on morphology and performance of hollow fibers membrane for ultrafiltration. *Sep. Purif. Technol.* **2006**, *49*, 10–19. [[CrossRef](#)]
51. Jim, J.S.; Chang, C.W.; Zhu, J.; Wu, H.; Zhang, Z.T. Solubility of poly(vinylpyrrolidone) with different molecular weights in supercritical carbon dioxide. *J. Chem. Eng. Data* **2015**, *60*, 3397–3403. [[CrossRef](#)]
52. Couchman, P.R. Compositional variation of glass-transition temperatures. 2. Application of thermodynamic theory to compatible polymer blends. *Macromolecules* **1978**, *11*, 1156–1161. [[CrossRef](#)]
53. Fox, T.G. Influence of diluent and of copolymer composition on the glass temperature of a polymer system. *Bull. Am. Phys. Soc.* **1956**, *1*, 123.
54. Kargar, M.; Handge, U.A. Numerical simulations of gas sorption experiments in polymers: Influence of aspect ratio and pressure increase rate on the determination of diffusion coefficient. *Macromol. Theory Simul.* **2021**, *30*, 2100016. [[CrossRef](#)]
55. Sun, H.L.; Mark, E.J. Preparation, characterization, and mechanical properties of some microcellular polysulfone foams. *J. Appl. Polym. Sci.* **2002**, *86*, 1692–1701. [[CrossRef](#)]
56. Honerkamp, J.; Weese, J. A note on estimating mastercurves. *Rheol. Acta* **1993**, *32*, 57–64. [[CrossRef](#)]
57. Ferry, J.D. *Viscoelastic Properties of Polymers*, 3rd ed.; Wiley: New York, NY, USA, 1980.
58. Lee, J. Intrinsic adhesion properties of poly(vinyl pyrrolidone) to pharmaceutical materials: Humidity effect. *Macromol. Biosci.* **2005**, *5*, 1085–1093. [[CrossRef](#)]
59. Maeda, Y.; Paul, D.R. Effect of antiplasticization on gas sorption and transport. 1. polysulfone. *J. Polym. Sci. Pol. Phys.* **1987**, *25*, 957–980. [[CrossRef](#)]
60. Maeda, Y.; Paul, D.R. Effect of antiplasticization on gas sorption and transport. 3. free-volume interpretation. *J. Polym. Sci. Pol. Phys.* **1987**, *25*, 1005–1016. [[CrossRef](#)]
61. Hiremath, P.; Nuguru, K.; Agrahari, V. Chapter 8—Material attributes and their impact on wet granulation process performance. In *Handbook of Pharmaceutical Wet Granulation*; Narang, A.S., Badawy, S.I.F., Eds.; Academic Press: Cambridge, MA, USA, 2019; pp. 263–315. [[CrossRef](#)]
62. McKeen, L.W. 4-Binders. In *Fluorinated Coatings and Finishes Handbook*; McKeen, L.W., Ed.; William Andrew Publishing: Norwich, NY, USA, 2006; pp. 45–58. [[CrossRef](#)]
63. Haenelt, T.G.; Georgopoulos, P.; Abetz, C.; Rangou, S.; Alisch, D.; Meyer, A.; Handge, U.A.; Abetz, V. Morphology and elasticity of polystyrene-block-polyisoprene diblock copolymers in the melt. *Korea-Aust. Rheol. J.* **2014**, *26*, 263–275. [[CrossRef](#)]
64. Georgopoulos, P.; Rangou, S.; Haenelt, T.G.; Abetz, C.; Meyer, A.; Filiz, V.; Handge, U.A.; Abetz, V. Analysis of glass transition and relaxation processes of low molecular weight polystyrene-b-polyisoprene diblock copolymers. *Colloid Polym. Sci.* **2014**, *292*, 1877–1891. [[CrossRef](#)]
65. Fukasawa, Y.; Chen, J.; Saito, H. A novel nanoporous structure on the surface of bubbles in polycarbonate foams. *J. Polym. Sci. Pol. Phys.* **2008**, *46*, 843–846. [[CrossRef](#)]
66. Hliavitskaya, T.; Plisko, T.; Bilydukevich, A.; Lipnizki, F.; Rodrigues, G.; Sjolín, M. Modification of PES ultrafiltration membranes by cationic polyelectrolyte Praestol 859: Characterization, performance and application for purification of hemicellulose. *Chem. Eng. Res. Des.* **2020**, *162*, 187–199. [[CrossRef](#)]
67. Kim, D.; Vovusha, H.; Schwingenschlogl, U.; Nunes, S.P. Polyethersulfone flat sheet and hollow fiber membranes from solutions in ionic liquids. *J. Membr. Sci.* **2017**, *539*, 161–171. [[CrossRef](#)]

68. Fang, X.F.; Li, J.S.; Li, X.; Pan, S.L.; Zhang, X.; Sun, X.Y.; Shen, J.Y.; Han, W.Q.; Wang, L.J. Internal pore decoration with polydopamine nanoparticle on polymeric ultrafiltration membrane for enhanced heavy metal removal. *Chem. Eng. J.* **2017**, *314*, 38–49. [[CrossRef](#)]
69. Lee, E.K.; Koros, W.J. Membranes, Synthetic, Applications. In *Encyclopedia of Physical Science and Technology*, 3rd ed.; Meyers, R.A., Ed.; Academic Press: New York, NY, USA, 2003; pp. 279–344.
70. Adamczak, M.; Kaminska, G.; Bohdziewicz, J. Relationship between the addition of carbon nanotubes and cut-off of ultrafiltration membranes and their effect on retention of microcontaminants. *Desalination Water Treat.* **2021**, *214*, 263–272. [[CrossRef](#)]
71. Mantel, T.; Benne, P.; Parsin, S.; Ernst, M. Electro-conductive composite gold-polyethersulfone-ultrafiltration-membrane: Characterization of membrane and natural organic matter (NOM) filtration performance at different in-situ applied surface potentials. *Membranes* **2018**, *8*, 64. [[CrossRef](#)]
72. Fang, X.F.; Li, J.S.; Li, X.; Sun, X.Y.; Shen, J.Y.; Han, W.Q.; Wang, L.J. Polyethyleneimine, an effective additive for polyethersulfone ultrafiltration membrane with enhanced permeability and selectivity. *J. Membr. Sci.* **2015**, *476*, 216–223. [[CrossRef](#)]
73. Gronwald, O.; Frost, I.; Ulbricht, M.; Shalmani, A.K.; Panglisch, S.; Grunig, L.; Handge, U.A.; Abetz, V.; Heijnen, M.; Weber, M. Hydrophilic poly(phenylene sulfone) membranes for ultrafiltration. *Sep. Purif. Technol.* **2020**, *250*, 117107. [[CrossRef](#)]

6.2. Article 2: Open-Celled Foams from Polyethersulfone/Poly(Ethylene Glycol) Blends using Foam Extrusion

Authors: Aniket Raje, Prokopios Georgopoulos, Joachim Koll, Jelena Lillepärq,
Ulrich A. Handge, Volker Abetz.

In Article 1, as PESU/PVP blends successfully manufactured nanocellular open-celled permeable foams capable of ultrafiltration, the upscaling of this process utilizing foam extrusion was explored.

PESU/PVP blends were manufactured by compounding using a twin-screw extruder (Brabender). For compounding, temperatures between 320 °C to 370 °C were used to combine PESU and PVP as polymer melts. The resulting blend's extrudates were transported to a granulator using a conveyer belt and obtained as blend pellets. An average rate of 100 g per hour was achieved while producing the blend. Screw speeds ranging from 10 to 60 RPM were applied. For batch foaming, small quantities (~ 50 – 100 g) of PESU/PVP blends were compounded in this extruder using these configurations. However, larger quantities of around 1 – 2 kg per trial were needed for foam extrusion, and the longer production times to produce these amounts of PESU/PVP blends caused a series of failures. First, the blend's yellow and transparent color gradually darkened and ended up as straight-up black. Subsequently, the extruder experienced blockage and caused damage to the twin-screw elements.

The processing temperatures suitable for PESU to melt were too high for PVP, which caused gradual degradation, whereas the thermal crosslinking phenomenon in PVP caused the blockage. Initially, the residence time was too less for this to occur. However, over time, the accumulation of PVP in certain dead zones in the extruder caused the thermally overexposed PVP to come out of the extruder along with the blend. As a result, it was concluded that PESU/PVP blend is not producible in large quantities and therefore was unsuitable for large-scale production to be used in a foam extruder.

Therefore, based on the same principles used in selecting PVP led to selecting PEG. As explained in detail in this article, the PESU/PEG blends were produced using neither compounding nor organic solvents but using material penetration by taking advantage of the porous morphology of the PESU flakes.

In line with Article 1, extensive material characterization was also used for this study. Due to the discovery of two glass transition temperatures in DSC measurements, rheological measurements were used to plot Han plots which determined the miscibility of the blends. The partially miscible blends also showed an indication of a gel state present in these blends. In addition, sorption experiments were performed to study the sorption and diffusion behavior of CO₂ in the PESU/PEG blends. The material characterization allowed for going ahead with foam extrusion by suggesting processing temperatures and foamability of the blends.

Due to the plasticization effect of PEG, the processing temperature required for this blend was 200-235 °C, around 120-150 °C lower than those required by PESU. These blends were extruded using the foam extruder through an annular slit nozzle, thus obtaining a continuous hollow fiber geometry. Using CO₂ and water as co-blowing agents were attempted for the first time in foam extrusion and yielded higher porosity and cell uniformity than using CO₂. The optimum PESU/PEG blend composition yielded open-celled continuous foam with the smallest cell size in literature for extruded foams.

This study paved the way to produce open-celled foam continuously using foam extrusion in continuous hollow fiber geometry.

6.2.1. Author Contributions

Aniket Rajee (A.R.), Prokopios Georgopoulos (P.G.), Joachim Koll (J.K.), Jelena Lillepärög (J.L.), Ulrich A. Handge (U.A.H.), Volker Abetz (V.A.).

Contributions	Authors					
	A.R.	P.G.	J.K.	J.L.	U.A.H.	V.A.
First Author (1) and Corresponding Author (*)	1	*				
Conceptualization and methodology	✓	✓			✓	
Material characterization	✓			✓		
Foam extrusion trials	✓		✓			
Writing—original draft preparation	✓					
Writing—review and editing	✓	✓	✓	✓	✓	✓
Analysis of data and visualization	✓			✓		
Scientific supervision		✓				✓

Table 8: Author contributions for article 2.

6.2.2. Funding and Acknowledgements

No external funding was received for this work.

The authors of this article would like to express their gratitude to the individuals who provided valuable support for this research. First and foremost, the authors extend their thanks to Ivonne Ternes for her skilled contribution in the area of thermal analysis. They would also like to thank Kristian Buhr for his assistance in rheology, Maren Brinkmann for her expertise in GPC, and Martin Held, Anke-Lisa Höhme, Erik Schneider and Evgeni Sperling for their microscopy assistance. The authors are also grateful to Sarah Glaß for her insightful scientific discussions.

In addition, the authors would like to acknowledge the generous donations of PESU by Oliver Gronwald and Erik Gubbels from BASF SE. The discussions with Oliver Gronwald and Martin Weber from BASF SE during the initial stage of this work are also greatly appreciated. The authors recognize the significant contributions of these individuals and organizations to their research, and they extend their sincere appreciation for their support.

6.2.3. Publication



Article

Open-Celled Foams from Polyethersulfone/Poly(Ethylene Glycol) Blends Using Foam Extrusion

Aniket Rajee, Prokopios Georgopoulos, Joachim Koll, Jelena Lillepärq, Ulrich A. Handge and Volker Abetz

Special Issue

Polymer Microcellular Foaming and Its Functionalization







Edited by

Dr. Xiaoli Zhang and Prof. Dr. Xia Liao



Article

Open-Celled Foams from Polyethersulfone/Poly(Ethylene Glycol) Blends Using Foam Extrusion

Aniket Raje ¹, Prokopios Georgopoulos ^{1,*}, Joachim Koll ¹, Jelena Lillepärög ¹, Ulrich A. Handge ^{1,2}
and Volker Abetz ^{1,3}

¹ Helmholtz-Zentrum Hereon, Institute of Membrane Research, Max-Planck-Strasse 1, 21502 Geesthacht, Germany

² Chair of Plastics Technology, Faculty of Mechanical Engineering, TU Dortmund University, Leonhard-Euler-Straße 5, 44227 Dortmund, Germany

³ Institute of Physical Chemistry, Universität Hamburg, Grindelallee 117, 20146 Hamburg, Germany

* Correspondence: prokopios.georgopoulos@hereon.de; Tel.: +49-4152-87-2420

Abstract: Polyethersulfone (PESU), as both a pristine polymer and a component of a blend, can be used to obtain highly porous foams through batch foaming. However, batch foaming is limited to a small scale and is a slow process. In our study, we used foam extrusion due to its capacity for large-scale continuous production and deployed carbon dioxide (CO₂) and water as physical foaming agents. PESU is a high-temperature thermoplastic polymer that requires processing temperatures of at least 320 °C. To lower the processing temperature and obtain foams with higher porosity, we produced PESU/poly(ethylene glycol) (PEG) blends using material penetration. In this way, without the use of organic solvents or a compounding extruder, a partially miscible PESU/PEG blend was prepared. The thermal and rheological properties of homopolymers and blends were characterized and the CO₂ sorption performance of selected blends was evaluated. By using these blends, we were able to significantly reduce the processing temperature required for the extrusion foaming process by approximately 100 °C without changing the duration of processing. This is a significant advancement that makes this process more energy-efficient and sustainable. Additionally, the effects of blend composition, nozzle temperature and foaming agent type were investigated, and we found that higher concentrations of PEG, lower nozzle temperatures, and a combination of CO₂ and water as the foaming agent delivered high porosity. The optimum blend process settings provided foams with a porosity of approximately 51% and an average foam cell diameter of 5 µm, which is the lowest yet reported for extruded polymer foams according to the literature.

Keywords: polyethersulfone; poly(ethylene glycol); foam extrusion; polymer blends; open-cell foam



Citation: Raje, A.; Georgopoulos, P.; Koll, J.; Lillepärög, J.; Handge, U.A.; Abetz, V. Open-Celled Foams from Polyethersulfone/Poly(Ethylene Glycol) Blends Using Foam Extrusion. *Polymers* **2023**, *15*, 118. <https://doi.org/10.3390/polym15010118>

Academic Editors: Xia Liao, Xiaoli Zhang and Luigi Sorrentino

Received: 4 November 2022

Revised: 16 December 2022

Accepted: 22 December 2022

Published: 27 December 2022



Copyright: © 2022 by the authors. Licensee MDPI, Basel, Switzerland. This article is an open access article distributed under the terms and conditions of the Creative Commons Attribution (CC BY) license (<https://creativecommons.org/licenses/by/4.0/>).

1. Introduction

Polyarylsulfones, such as polysulfone (PSU), polyethersulfone (PESU) and polyphenylene-sulfone (PPSU), are high-performance thermoplastic polymers that are used for many applications where high strength, high temperature and chemical resistance are required [1–4]. PESU has thermal, structural and chemical stability due to the combination of sulfonyl groups and aromatic rings in its molecular structure [5]. The high-thermal stability of PESU, a desirable property, enables the use of processing temperatures between 320 °C and 400 °C for extrusion and injection molding [4,6]. This high-temperature processing partially accounts for the high material and production costs. Polyarylsulfone foams have been studied for the last couple of decades for use in various applications. Using the method of batch foaming, highly porous microcellular foams, as well as nanocellular foams, have been produced with PESU, PSU, PPSU and their blends [7–14].

Foam extrusion is a continuous process used to obtain foamed polymer extrudate. It is possible to scale-up the method to an industrial level easily. Unlike batch foaming, which relies on the absorption of the foaming agent into the polymer in the semi-solid

state over a longer period to ensure cell nucleation, foam extrusion uses physical mixing at temperatures where the polymer softens or is in the melt state.

The main component of foam extrusion is an extruder with an inlet for the foaming agent. Temperature profiles and screw speed are set on the extruder and a feed rate for the physical foaming agent is specified. The foaming agent mixes with the polymer melt within the extruder at significantly higher pressures than ambient pressure. The foaming agent is dispersed and dissolved due to this high-temperature and high-pressure mixing, reducing the viscosity of the melt [15]. The foaming agent nucleates and expands into pores as the material exits the extruder through a nozzle. This expansion is dependent on various parameters, such as the polymer type, foaming agent, nozzle temperature, pressure, etc. The foamed extrudate takes the shape of the nozzle in two dimensions, as the extrusion process is a continuous process [16].

Huang [17] investigated the foaming of PESU using CO₂ at various melt temperatures and obtained closed-cell foams with an average cell size of 10 μm at the lowest possible processing temperature of 280 °C. Extrusion below this temperature was not possible due to excessive extruder pressures (high viscosity of the melt).

In previous studies, researchers used polymer blends that delivered higher porosity and smaller cell sizes than their respective homopolymers [14,18–21]. As the processing temperatures for PESU lie near or above the degradation temperatures of most polymers, it is essential to lower the processing temperature. Poly(*N*-vinylpyrrolidone) (PVP), a water-soluble polymer, results in improved porosity and pore size in foams of blends with PESU manufactured using batch foaming [14,22]. PVP, however, is susceptible to crosslinking at higher temperatures and is not directly processable in an extruder with PESU [23]. Poly(ethylene glycol) (PEG), another water-soluble polymer [24,25], is also a plasticizer [26,27]; i.e., blending a high-temperature resistant polymer with it would lead to lowered processing temperatures. PEG is used in various applications ranging from medicine to industry [28,29]. Similar to PVP, in the manufacturing of membranes using the non-solvent-induced phase separation process, PEG is used as a pore opener [30,31]. The fabrication of open porous foams is of great importance for the fabrication of polymer membranes [14] and for the creation of sorption foams [32]. These technological applications led us to investigate the possibility of obtaining such structures. Thus, a blend of PESU/PEG was selected in this work, as it could potentially produce highly porous foams using foam extrusion.

Our aim was to produce PESU/PEG blends with PESU as the matrix component that can be processed at significantly lower processing temperatures than pristine PESU. The formation of blends using organic solvents and compounding is well-known, as well as being a common industrial practice. Organic solvents are classified as auxiliary substances—i.e., substances to be reduced or eliminated wherever possible—and are harmful to human health [33–35]. Compounding requires the use of high temperatures to melt all polymer components and consumes energy in similar amounts as a foam extruder. Furthermore, this removes the significance of using a plasticizer as a blend component. Material penetration of organic liquids into polymers has been successfully proven by Gutmann et al. [36] and, as low-molecular-weight PEG is a liquid at room temperature, absorption of PEG into the PESU matrix was pursued. In this way, we prepared blends of PESU with low-molecular-weight PEG without using melt-state compounding or organic solvents.

Out of three low-molecular-weight PEGs, the one in which no crystalline formation was detected and which had the lowest viscosity at near-room temperature was selected and blended with PESU in various proportions. The processibility of these blends in foam extrusion was determined using polymer characterization techniques, such as thermal analysis and rheology. Using foam extrusion, foams were manufactured from the selected blends with various process settings and the effects of blend composition, foaming agent type and nozzle temperature were studied. An annular slit nozzle was selected for extrusion in order to create hollow-fiber-geometry extrudates. This would enable the use of these foams as hollow-fiber membranes in separation applications in the future.

The use of CO₂ as a foaming agent, especially in the supercritical state, to achieve porous foams in both batch foaming and foam extrusion is widely accepted and studied by researchers [17,37–46]. Sorption measurements have been conducted to understand the influence of blend composition on CO₂ diffusion [44,47]. The use of water along with CO₂ as co-foaming agents increases the porosity of foams and provides smaller cell sizes than the foams obtained when only using CO₂ as a foaming agent [13,14,48]. Evans et al. observed a twentyfold decrease in the viscosity of polyamide in extrusion when superheated water was used [49]. We used CO₂ and water together as foaming agents and confirmed their better performance in processing and foam formation in comparison to foams manufactured using only CO₂. Using CO₂ and water together as foaming agents delivered more uniform foams than only CO₂. Evaluation parameters that provide open-celled foams, such as average cell size and porosity, the optimum blend composition and process settings, were identified.

2. Experiment

2.1. Materials and Methods

In this study, all polymers used were commercial grade. The type of PESU was selected based on previous foaming studies [10,14,17]. PESU homopolymers, BASF Ultrason[®] E 3010 (PESU E 3010) in the form of granules and BASF Ultrason[®] E 3020 P (PESU E 3020 P) in the form of flakes were kindly provided by BASF SE (Ludwigshafen, Germany). As PEG in liquid form was desired, low-molecular-weight PEG 200, 400 and 600 were obtained from Sigma-Aldrich (St. Louis, MO, USA) in liquid form.

PESU/PEG blends were produced by adding liquid PEG to PESU flakes in a 5 L cylindrical glass container. The required proportions of PESU and PEG were added in small portions at a time such that the net mass of the mixture added at once was 50 g. Specifically, to prepare the PESU/PEG 80/20 blend, 10 g of PEG was added to 40 g of PESU, summing up to a total of 50 g in the 5 L container. This addition was repeated 32 times, resulting in a total of 1.6 kg of polymer, and the container was filled approximately up to 4 L, leaving 1 L of air in the container after closing. Not filling the container completely allowed free movement of the mixture during rotation. Following that, the glass container was closed and placed on mechanical rollers at 20 rpm for 24 h. This facilitated the uniform distribution of the PEG around the PESU flakes and the thorough mixing of the components. This method can be graphically interpreted from Figure 1.

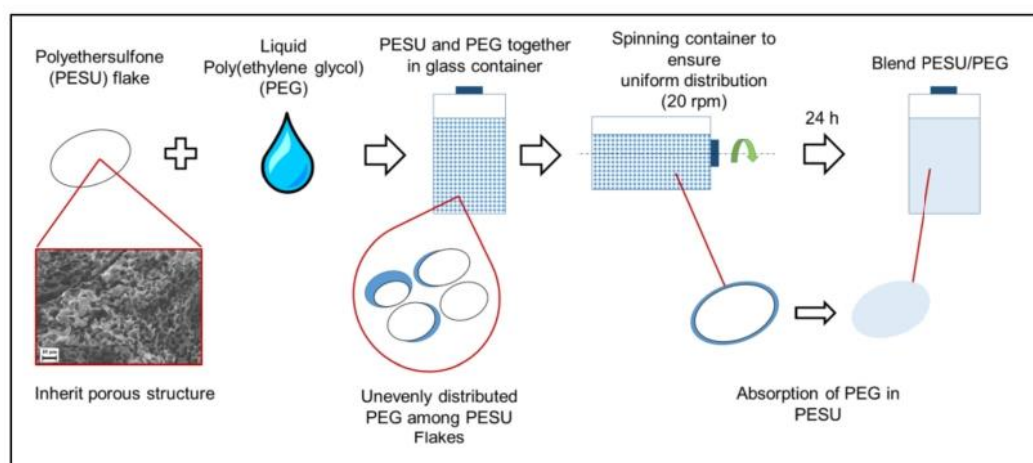


Figure 1. Schematic representation of the method followed for the blending of PEG with PESU.

The mixture was dried for a minimum of 24 h at 50 °C under vacuum before use. For foam extrusion, the blended flakes were used directly after drying, whereas for material characterization, the blended flakes were ground into powder using a grinder and particles < 350 µm were filtered using an industrial sieve.

The blend formulations, along with the nomenclature, can be found in Table 1. Here, only blends with PEG 200 are shown due to the selection of this molecular weight based on the material characterization, as discussed later.

Table 1. Nomenclature for PESU/PEG blends.

Blend Name	PESU E 3020 P	PEG 200
	Content (wt%)	Content (wt%)
E3_PEG200_08	92	8
E3_PEG200_14	86	14
E3_PEG200_20	80	20
E3_PEG200_26	74	26

2.2. Material Characterization

Gel permeation chromatography (GPC) was performed in dimethylacetamide using 5 μ PSS SDV gel columns (PSS GmbH, Mainz, Germany) at a flow rate of 1 mL min⁻¹ (VWR-Hitachi 2130 pump) and 50 °C. For the detection of the concentration, a Waters UV photometer (typically operated at λ = 254 nm) and a Waters 2410 refractive index (RI) detector (λ = 930 nm) were used. A Waters 717 autosampler with an injection volume of 60 μ L was used for the injection of samples. The raw data were analyzed using the PSS WinGPC Unity software package (PSS GmbH, Mainz, Germany). To calculate the apparent average molecular weight and distribution, polystyrene standards (PSS GmbH, Mainz, Germany) calibration was used.

Differential scanning calorimetry (DSC) was undertaken using a DSC 1 calorimeter (Mettler Toledo, Gießen, Germany) and analyzed with the software STARe SW 16.20 (Mettler Toledo, Gießen, Germany). An aluminum pan with a capacity of 40 μ L was filled with approximately 10 mg of polymer and closed with a mono-perforated lid. Heating–cooling–heating cycles were implemented at a heating rate of 10 K min⁻¹ in a nitrogen atmosphere. The first two temperature intervals for PEG, PESU and PESU/PEG blends were –130 to 100 °C, 25 °C to 260 °C and –130 to 180 °C, respectively. For PESU, the glass transition temperature was determined by evaluating the second heating interval. For PEG and PESU/PEG blends, a third heating–cooling cycle was used from –130 to 260 °C. The heating rate for this cycle was set to 30 K min⁻¹ to obtain a pronounced glass transition signal [50].

For rheological measurements of PEG, 0.67 mL of the liquid polymer was measured in a cone-plate geometry with an Anton Paar MCR 502 rheometer (Anton Paar, Graz, Austria). A shear amplitude of 5% was applied and viscosities were measured in the angular frequency range from 0.01 to 100 rad/s.

For rheological measurements of polymers in a glassy state at room temperature, cylindrical samples (8 mm diameter, 2 mm thickness) were prepared using compression molding. A hot press (Paul-Otto Weber, Remshalden, Germany) was used. The temperatures chosen for PESU and PESU/PEG blends were 270 °C and 200 °C, respectively. Samples that were free from defects, such as dents, weldlines, air-bubbles, scratches, etc., resulting from compression molding were used. Rheological measurements were carried out on an Anton Paar MCR 502 rheometer (Anton Paar, Graz, Austria) with a plate–plate geometry. Frequency sweeps in the frequency range between 0.01 and 100 rad/s were carried out at 260, 280, 300 and 320 °C for PESU and 160, 180, 200, 220 and 240 °C for the blends. The frequency sweeps started at the highest frequency.

Absorption of PEG 200 into PESU was observed by immersing samples of PESU into PEG 200 in an evacuated nitrogen environment at room temperature for 24 h. Then, 1 mm thick compression-molded samples with a diameter of 24 mm were used after drying under a vacuum for 24 h. The mass of the samples was measured before immersion into PEG 200 and after 24 h in PEG 200 using a weighing scale. Before measurement, the samples

were dried clean using Kimtech® Science Precision Wipes (Irving, TX, USA) and blow-dried using pressurized nitrogen gas [36].

Sorption experiments were carried out with a IsoSORP® Static gravimetric sorption analyzer from Rubotherm (Bochum, Germany). Flat sheet samples (diameter: 14 mm, thickness: 0.5 mm) were prepared using compression molding. For compression molding, the blend flakes were added to a mold with four voids of the required dimensions and the mold was inserted into a hot press (Paul-Otto Weber, Remshalden, Germany) to be subjected to 200 °C for 10 min. A vacuum was applied from the fourth minute and a force of 60 kN from the sixth minute. The mold was then removed and allowed to cool down towards room temperature when the samples were removed. The thicknesses of the isotropic flat sheet samples were measured with a DELTASCOPE® FMP10 digital micrometer (Fischer, Sindelfingen, Germany). The densities of the flat sheet samples were estimated with the buoyancy method using an Excellence XP105DR analytical balance (Mettler Toledo, Gießen, Germany) and auxiliary liquid FC-770 (3M, Saint Paul, MN, USA), as described elsewhere [51]. The measurement protocol for the sorption experiments and the interpretation of the results were undertaken following previous studies [51–53]. All samples were dried in a vacuum for 48 h. A CO₂ pressure of 50 bar was applied and samples of selected polymers were measured at 35 °C, 50 °C and 75 °C. The weight concentration of CO₂ per gram of polymer was measured and the data points were smoothed using an adjacent averaging method in Origin (OriginLab, Northampton, MA, USA). The diffusion coefficient D_T at temperature T was calculated by fitting the kinetic sorption curve using the theory of Fickian diffusion following the equation below [54,55]:

$$\frac{M_t}{M_\infty} = 4\sqrt{\frac{D_T t}{\pi l^2}} \quad (1)$$

where:

M_t = mass of gas absorbed by sample at time t ;

M_∞ = mass of gas absorbed by sample at time $t \rightarrow \infty$; i.e., equilibrium;

l = thickness of the cylindrical sample.

Values used for $\frac{M_t}{M_\infty}$ were lower than 0.6.

The apparent density ρ_b of the polymer granules and flakes was measured by filling a graduated cylinder (Hirschmann EM Techcolor, Erberstadt, Germany) up to 10 mL with the respective polymers without compression. The mass of the polymer M was measured and the apparent density was calculated.

2.3. Foam Extrusion

An Extrusiograph 19/25D single-screw extruder (Brabender GmbH & Co. KG, Duisburg, Germany) was used for foam extrusion. This extruder was coupled with two static mixers with diameters of 2 cm each and a combined length of 16 cm. A melt pump maintained a speed of 10 rpm for all experiments. An annular slit nozzle with a 2 mm outer diameter and 1 mm inner diameter was used with the aim of preparing hollow fiber specimens. The extruder configuration is shown in Figure 2. The temperatures and pressures in the extruder and components were constantly monitored using WINExt software (Brabender Technologies GmbH, Duisburg, Germany). Pressure sensors were present in zone 3, zone 4 and before the nozzle.

Foaming agents, CO₂ and water were pressurized using two separate high-pressure syringe pumps (Teledyne ISCO, Thousand Oaks, CA, USA). Water and CO₂ were injected at zone 3 of the extruder through different inlets on the same longitudinal point of the extruder's axis, separated by 90° on the extruder barrel. The source of CO₂ was a dip-tube bottle (99.995% purity, Linde PLC, Dublin, Ireland) and ultrapure water was used.

Extruder temperatures approximately 100–130 °C higher than the observed glass transition temperatures for the respective blends were set to obtain better mixing due to lower viscosity. Table 2 shows the extruder temperatures for the materials that could be processed in the extruder.

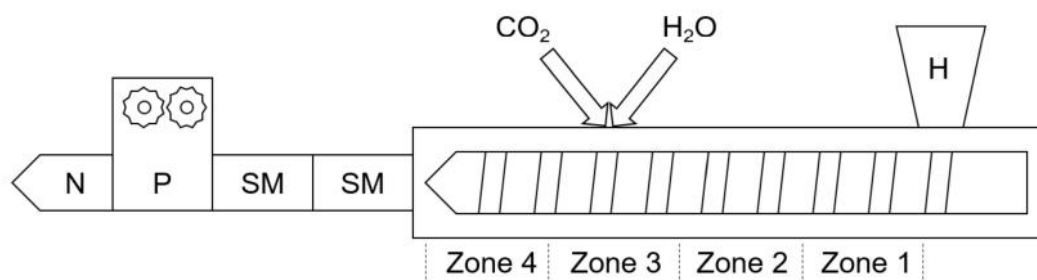


Figure 2. Illustration of the foam extruder setup; H = hopper, SM = static mixer, P = melt pump, N = nozzle.

Table 2. Temperatures set on extruders for selected materials.

Material	T_{ext}
	(°C)
E3_PEG_14	230
E3_PEG_20	200

For the trials conducted to study the effect of nozzle temperature on the foaming behavior, the screw speed was set to 10 rpm, and the feed rates of CO₂ and water were both 0.5 mL/min.

At the beginning of each trial, the nozzle temperatures were equal to the extruder temperatures and CO₂ and water were injected after ensuring that a constant extrudate was obtained from the nozzle at 10 rpm without any unstable extruder pressures. To observe the effects of the changed extruder setting, the extruder was allowed to run for 20 min before collecting samples. This ensured that the collected sample corresponded to the given settings. To observe the effect of nozzle temperature on the foam, the samples were collected for nozzle temperatures moving from the highest to the lowest possible nozzle temperature.

2.4. Foam Characterization

The morphologies of the polymer, polymer blend and their foams were examined using scanning electron microscopy (SEM) on a Merlin microscope (Carl Zeiss AG, Oberkochen, Germany) at an acceleration voltage of 3 kV. Extrudates were cross-sectioned using liquid nitrogen and sputter-coated with approximately 2 nm of platinum [56]. The average cell size was measured for selected foams using the measurement tool in Photoshop CS6 (Adobe, San Jose, CA, USA) from the scanning electron micrographs. The porosity was measured for selected foams from the SEM micrographs by measuring the number of pixels occupied by visible cells and calculating the percentage versus the total number of pixels in the micrographs. Three micrographs were measured per sample.

Tensile tests were performed at room temperature using a Zwick Roell Z020 (Zwick Roell, Ulm, Germany) and a load cell of 1 kN. Extrudates with a length of 110 mm were used. The tests were operated and evaluated using the program TestXpert III (Zwick Roell, Ulm, Germany), and data on the true stress and the nominal strain were obtained. Three samples with each process setting were measured and an average curve was calculated until breakpoint. FTIR spectroscopy was performed with the blend and its extruded foams using a Bruker Alpha-P platinum attenuated total reflector equipped with a diamond head (Bruker, Billerica, MA, USA). The measurements were performed by recording 32 scans with a resolution of 4 cm⁻¹ within a spectral range of 400–4000 cm⁻¹ [57].

The dye uptake test was performed by dipping a 20 mm long extrudate into a 0.1 mg solution of 1-1 methylene in ethanol. The change in the color of the extrudate to blue indicated the uptake of the solution into the extrudate.

3. Results and Discussions

Although PESU E 3010 was directly usable in the extruder, we selected PESU E 3020 P for blending with PEG due to its porous structure, as seen in Figure 3.

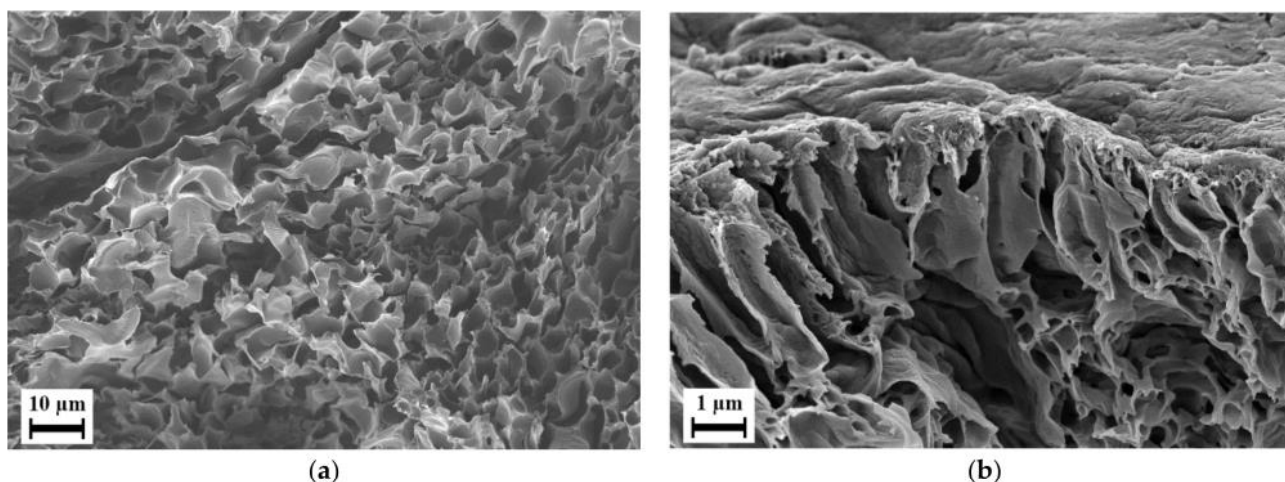


Figure 3. Scanning electron micrograph of PESU E 3020 P flake: (a) cross-section, (b) surface morphologies.

The average molecular weights and the molecular weight distributions of PESU E 3010 and E 3020 P were examined using GPC and determined to be similar (see the Supplementary Materials). According to the material manufacturer, the third numbers in the material names (1 and 2) indicate granules and flakes, respectively, while the suffix P in PESU E 3020 P denotes the material's intended use for solution preparation [4].

Although low-viscosity polymers can be mixed with a high T_g polymer in a single phase using a compounding extruder [58], since we used porous PESU flakes, we could obtain the absorption of the liquid PEG in an easier way. Therefore, low-molecular-weight PEG 200, PEG 400 and PEG 600 were selected as possible candidates for blending with PESU due to their liquid state at room temperature. The capillary action of this porous structure allowed for liquid PEG to enter the flakes and facilitated the absorption of PEG into the PESU matrix. The phenomenon of absorption was confirmed with an absorption test on compression-molded samples, where, for a surface area of 452.38 mm² (sample mass 0.72 g), the mass uptake after one day of immersion in liquid PEG was 0.17%. Due to the porous structure, the active area for material penetration increased enormously, as the pore sizes were in the range of a few micrometers. This significantly increased the ratio of the surface area of contact between PEG and PESU to the volume of PEG. Therefore, PESU/PEG blends were formed.

The viscosities of PEG 200, PEG 400 and PEG 600 at 25 °C were measured as 55, 98, and 190 mPa s, respectively. As we made use of the porous structure of PESU flakes to assist with the absorption of liquid PEG, the lowest viscosity was favored. As seen in Figure 4, PEG 400 and PEG 600 demonstrated melting peaks during the third heating cycle of the DSC. These melting peaks indicated the presence of crystallinity in PEG 400 and PEG 600. As crystallinity is not desired in polymer foaming [59], PEG 400 and PEG 600 were not selected for further investigation. PEG 200 had the lowest viscosity, a low glass transition temperature and did not indicate signs of crystallinity; therefore, it was chosen for blending with PESU. Compression-molded samples of PESU/PEG200 blends were opaque and white in color. This provided our first impression that complete miscibility would not occur for this blend comprising transparent amorphous polymers [60].

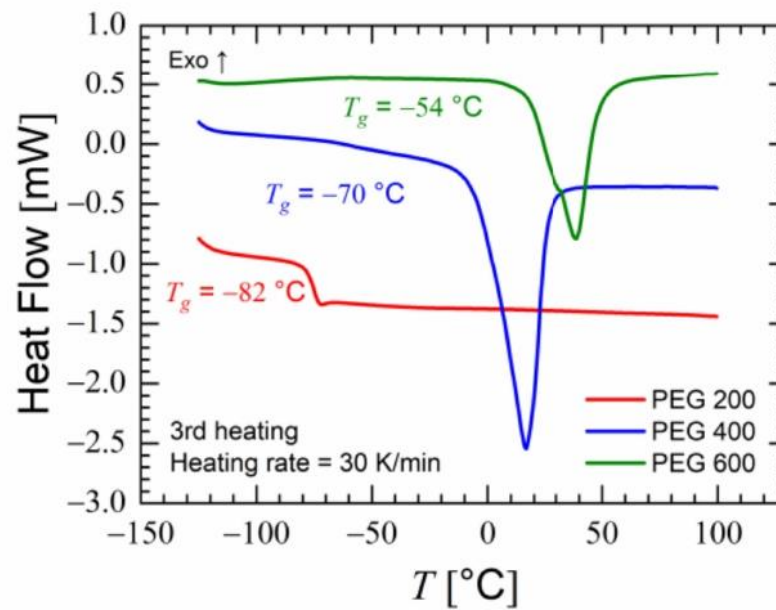


Figure 4. Heat flow measured using differential scanning calorimetry (DSC) during the third heating cycle of PEG 200, 400 and 600.

Figure 5a shows the third heating cycle of the DSC for the blend E3_PEG200_20. The glass transition of PEG 200 was visible in the blend at $-82\text{ }^{\circ}\text{C}$ and a second glass transition was seen at $97\text{ }^{\circ}\text{C}$. This appearance of a new glass transition temperature that did not belong to any of the polymer components suggested the formation of a miscible polymer blend. This supported the hypothesis that PEG would be absorbed into the PESU matrix after being absorbed on a macro scale by the capillary effect of the porous PESU flakes. Above $160\text{ }^{\circ}\text{C}$, the heat flow measurement exhibited noise, which hindered the observation of the thermal behavior of the blend around the glass transition temperature of PESU; i.e., $227\text{ }^{\circ}\text{C}$. This noise occurred during the DSC measurements, likely because the boiling point of PEG 200 lying at $200\text{ }^{\circ}\text{C}$ under atmospheric pressure [61] and the known leaching of PEG from the blend matrix [62]. For blends of fully miscible polymers, the expected glass transition temperature for each mass fraction can be predicted using the Couchman equation (Equation (2)) [63] and the Fox equation (Equation (3)) [64,65]. The glass transition temperatures and the changes in heat capacities from the glassy to the rubbery state in the homopolymers were used in the equations.

$$\ln(T_g/T_{g,I}) = \frac{w_{II}\Delta c_{p,II}\ln(T_{g,II}/T_{g,I})}{w_I\Delta c_{p,I} + w_{II}\Delta c_{p,II}} \quad (2)$$

$$\frac{1}{T_g} = \frac{w_I}{T_{g,I}} + \frac{w_{II}}{T_{g,II}} \quad (3)$$

where

- w_I = mass fraction of polymer I;
- $c_{p,I}$ = heat capacity of polymer I;
- $T_{g,I}$ = glass transition temperature of polymer I;
- w_{II} = mass fraction of polymer II;
- $c_{p,II}$ = heat capacity of polymer II;
- $T_{g,II}$ = glass transition temperature of polymer II.

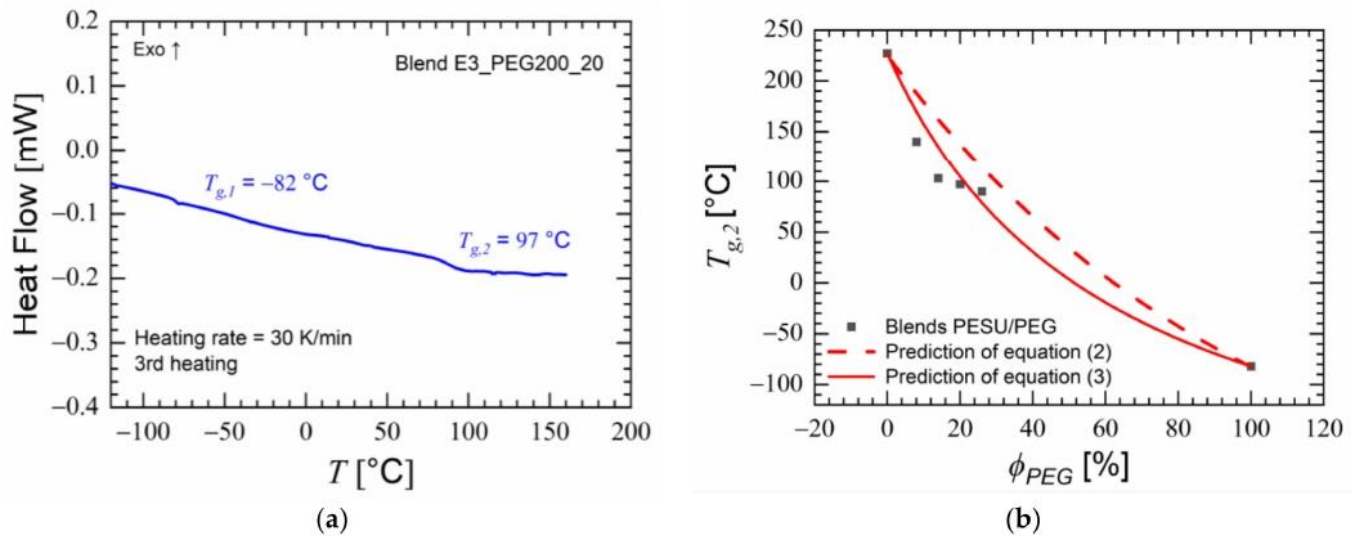


Figure 5. (a) Heat flow measured using differential scanning calorimetry (DSC) during the third heating cycle of blend E3_PEG200_20 showed the occurrence of two glass transitions; (b) observed second glass transitions ($T_{g,2}$) of PESU/PEG blends versus weight percentage of PEG and the predictions from Equations (2) and (3).

Predictions of Equations (2) and (3) did not accurately predict the glass transition temperatures of the blends at various weight compositions. Compliance with these equations would indicate the formation of homogeneous, single-phase polymer blends [14,64,66]. However, the glass transitions observable in Figure 5b were close to the values predicted by Equation (2), and their decrease with an increase in PEG content provided an indication of some degree of miscibility between the two polymers. The evaluation and quantification of miscibility were undertaken by analyzing the rheological measurements of the blends.

Figure 6a shows that the complex and loss moduli increased in a similar way versus angular frequency for blend E3_PEG200_20. Their slopes lay between 0.35 and 0.75. This behavior cannot be described with the Maxwell model where $G' \propto \omega^2$ and $G'' \propto \omega$ hold in the terminal regime. These results correspond to power laws, with both the storage and loss moduli following the power laws $G' \propto \omega^{0.5}$ and $G'' \propto \omega^{0.5}$, indicating microphase separation or another multiphase complex material in the gel state [67]. The data shown in Figure 6a and in Figure S2a–c in the Supplementary Materials for the PESU/PEG blend at a temperature of 160 °C indicate slopes near 0.5 already at high frequencies where evaporation was negligible. This was also an indication that the polymers were not fully miscible [68–71].

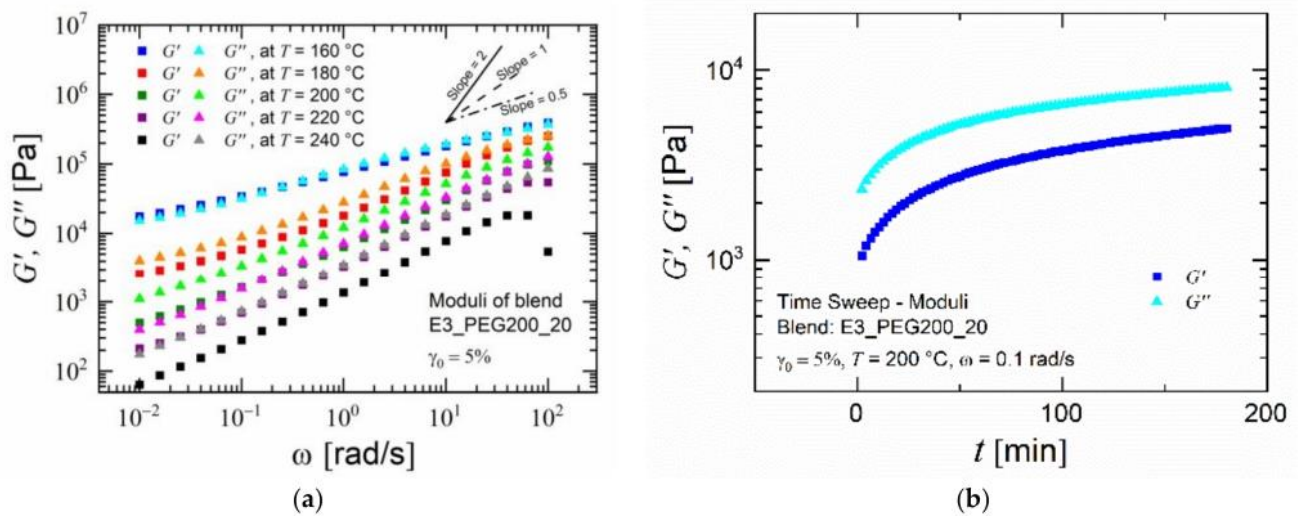


Figure 6. Rheological results for blend E3_PEG200_20: (a) frequency sweep: magnitude of moduli versus angular frequency at various temperatures; (b) time sweep: magnitude of moduli versus time at 200 °C.

As all the rheological measurements were carried out, moving from the highest frequencies to the lowest frequencies, the sample was subjected to its corresponding temperature for approximately 1.5 h. Exposure to temperatures near ± 40 °C of the evaporation temperature of PEG 200 accelerated the leaching of PEG from the samples [72]. This resulted in more accurate values at the highest frequencies, which were relevant for assessing the performance during extrusion, as discussed further below. During the measurements at lower frequencies, the blend samples had a lower net amount of PEG within them than at the previous frequency. This was confirmed by performing time-sweep experiments (Figure 6b). The storage and loss moduli increased equally over time when exposed to a measurement temperature of 200 °C. Plotting a master curve using the time-temperature superposition principle for the blends would not have resulted in accurate values due to the presence of two glass transition temperatures, which indicated heterogeneity, and the large difference between them (>100 K) [73,74]. Rheological measurements at higher temperatures were not pursued due to the rapid evaporation of PEG, which would have resulted in a significant change in the polymer composition over the course of the measurement, thus providing misleading values. The frequency-dependent storage modulus and the loss modulus at various temperatures for PESU and the selected blends were plotted against each other, resulting in a “Han plot” [75]. The resulting plot points were consolidated into a linear fitted curve for lower values of the loss modulus for which the slope values were found. Theoretically, a value of 2 in the low-frequency range indicates a completely homogenous polymeric system, and lower values tend to indicate a non-homogenous mixture [76–80]. As seen in Figure 7, PESU, being a homopolymer, exhibited a slope value near 2. The blend with 8% PEG had a slightly higher slope than the rest of the blend compositions, which had nearly equal slopes around 1.1. Therefore, based on these values and the thermal analysis, it was concluded that PESU and PEG 200 could form a partially miscible system or an even more complex system, such as a gel state.

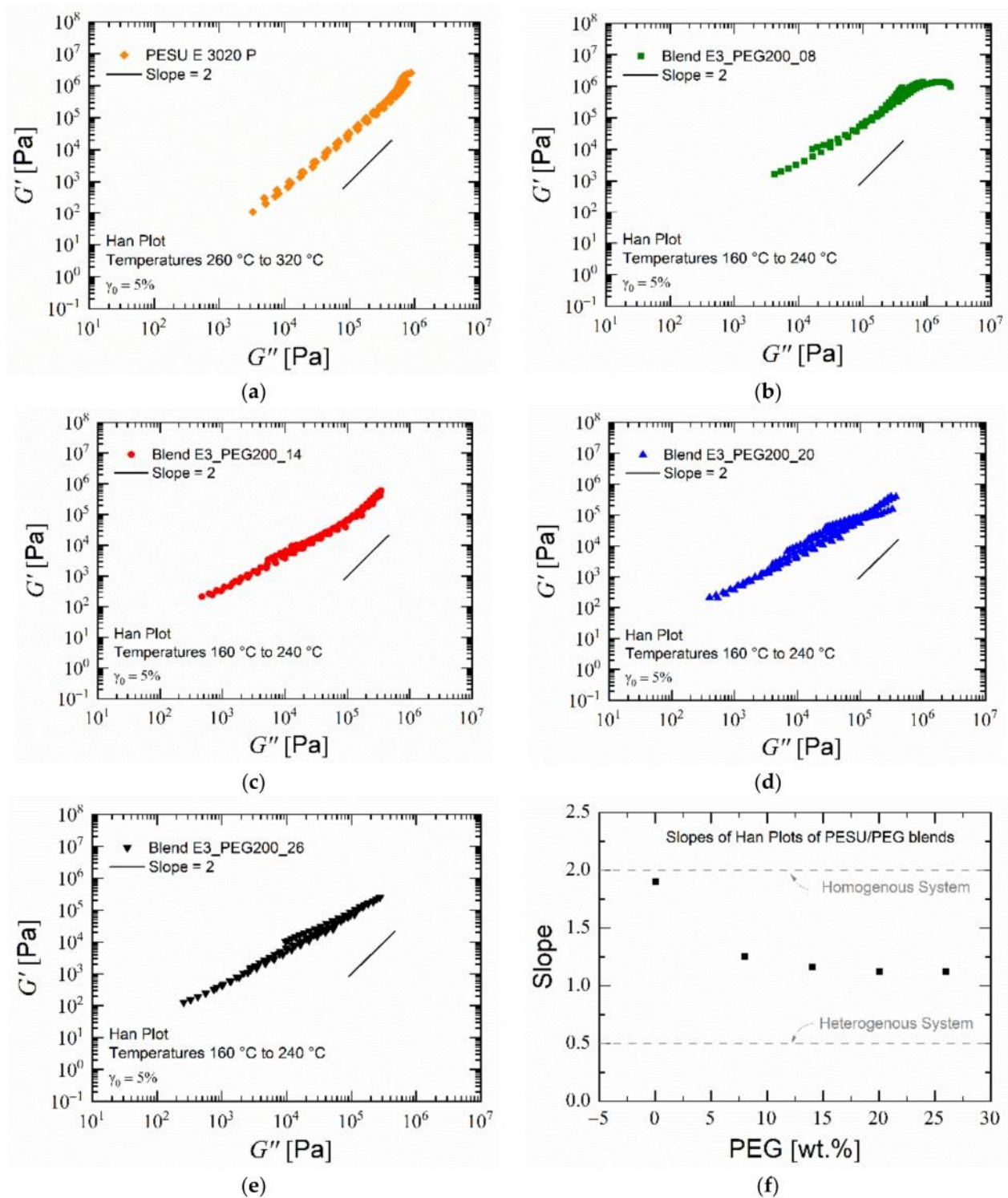


Figure 7. (a–e) Han plots of PESU and blends PESU/PEG200; (f) slopes of Han plots.

Rheological analysis carried out on the PESU/PEG blends showed a decrease in complex viscosity with an increase in PEG content at a given temperature, as seen in Figure 8a. The difference between the viscosities of the blend with 8% PEG and the blend with 14 % PEG was the largest, whereas the difference between the blend with 20% and 26% was the smallest. These differences were similar to those seen in glass transition temperatures in DSC measurements. This provided an indication that, above a certain percentage between 20% and 26%, PESU was fully saturated with PEG and excess PEG

formed a coexisting phase. This was seen in the results for the frequency sweep, as the complex viscosities tended to increase with lower frequencies and the viscosity–frequency curves did not resemble those of typical homopolymers [81–83]. Applying the Cox–Merz rule, as the frequency was replaced by the shear rate, the values of viscosities at shear rates at 100 s^{-1} tended to lie below $10,000 \text{ Pa s}$ [84]. As the data points for this frequency were measured at the beginning, the loss of PEG was minimal and the values confirmed the processibility of these blends in an extruder at $200 \text{ }^\circ\text{C}$ [82,85–89]. Figure 8b shows the influence of temperature on the viscosity of blend E3_PEG200_20. This indicated the temperature range below which this blend could be processed in the foam extruder.

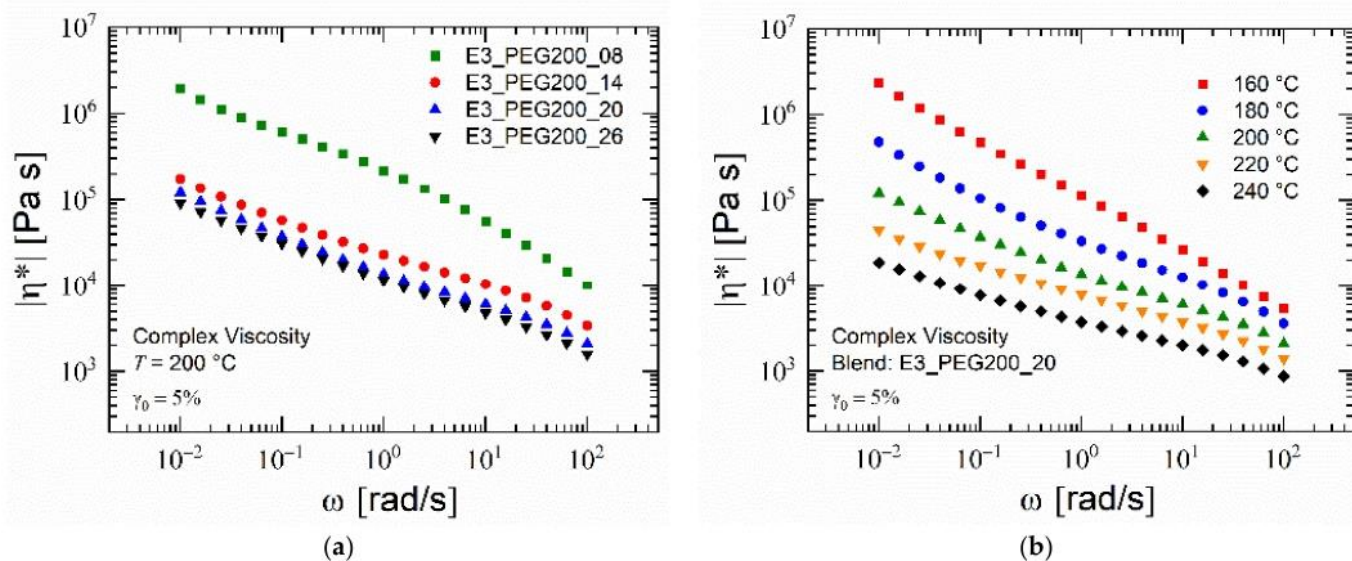


Figure 8. Magnitude of complex viscosity: (a) PESU/PEG200 blends at $200 \text{ }^\circ\text{C}$; (b) blend E3_PEG200_20 at various temperatures.

The kinetic sorption curves for the glassy polymer below T_g can be interpreted as indicating Fickian behavior as a function of the square root of time [90,91]. Similarly, all experiments with pure PESU and with PEG blends resulted in linear plots of the sorption as a function of the square root of time. The influence of PEG content on the CO_2 sorption properties of PESU/PEG blends was evident at all temperatures, as seen in Figure 9. The diffusion coefficient of the blends increased with the increase in PEG content. As seen in Figure 9a, in blend E3_PEG200_20, the magnitude of the increase in the diffusion coefficient with temperature was much higher than the decrease in the total concentration of CO_2 . By plotting the log of the diffusion coefficient versus the inverse of the temperature, as shown in Figure 9b, the values of PESU and blend E3_PEG200_08 fit linearly and could be defined with the Arrhenius equation [62,92]. Blend E3_PEG200_20, however, yielded too high values for the diffusion coefficient at $75 \text{ }^\circ\text{C}$, which did not fit linearly with the other measured temperatures. Plasticization phenomena in the glassy polymer and the existence of rubber phases in the polymer matrix could have caused this high diffusion [55]. This high diffusion coefficient for blend E3_PEG200_20 could be beneficial during foaming to obtain highly porous foams with finer cell sizes [16,36,93].

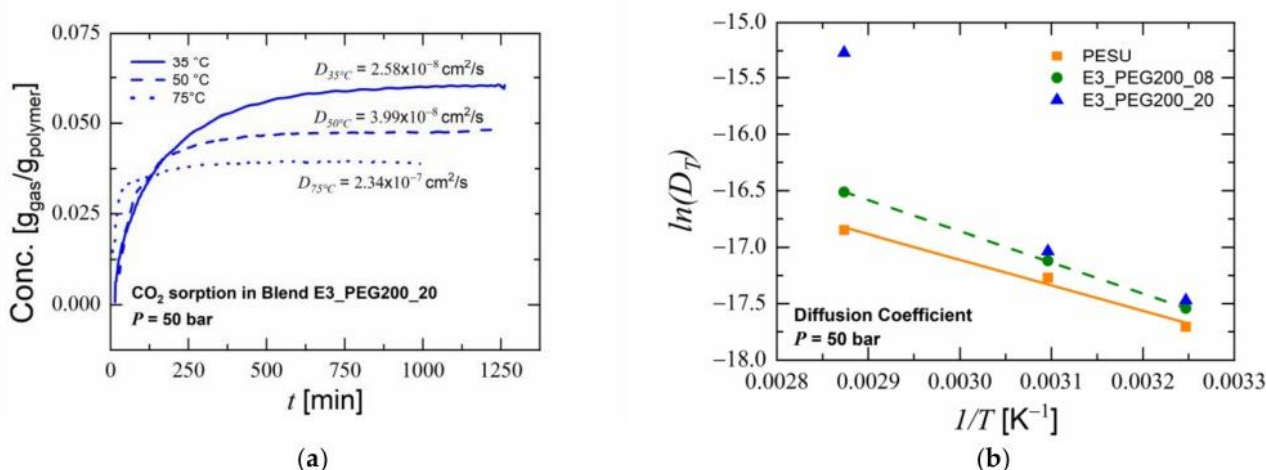


Figure 9. Sorption measurements results: (a) concentration of CO₂ in blend E3_PEG200_20 versus time at various temperatures; (b) Arrhenius plot of diffusion coefficients of blends.

In the foam extruder, the third zone, called the degassing zone, contained a larger internal volume, as the screw's inner diameter was the lowest among the zones. Furthermore, CO₂ and water inlets were present in this zone. For the injection of foaming agents, a high melt pressure should be maintained in this zone. Failure to maintain this pressure causes the foaming agents to find the path of least resistance in the wrong direction of the extruder and escape from the hopper, resulting in blowback. The blended flakes were inserted into the extruder directly. Due to the low apparent density of blend E3_PEG200_08, as seen in Figure S3 in the Supplementary Materials, the difference between the volumes assumed by the blend's flakes and its melt was higher than for the other blends. Therefore, the same mass of flakes that took up the entire screw volume at the hopper could not fill the complete volume of the degassing zone after melting. Therefore, no melt pressure could be generated at this zone. This caused a reverse flow of foaming agents through the hopper, resulting in blowback. Therefore, foam extrusion could not be carried out with blend E3_PEG200_08. Due to their higher apparent densities, blends E3_PEG200_14 and E3_PEG200_20 were successful in increasing the pressure in the degassing zone and, therefore, foam extrusion was possible. Blend E3_PEG200_26 exhibited separation of PEG from the flakes in the initial zones of the extruder, causing flooding of the extruder with liquid PEG. Some amount of PEG remained within the porous structure of the PESU flakes after mixing and could not be absorbed within the PESU matrix. This suggested that 26% PEG was too high an amount to be absorbed into the PESU porous structure of the flakes. The rheological results shown in Figure 8a indicate that, although the percentage weight difference of PEG in the blends was similar, the difference between the viscosities of the blends with E3_PEG200_20 and E3_PEG200_26 was much lower than the difference between E3_PEG200_14 and E3_PEG200_20. Therefore, absorption of PEG 200 within the PESU matrix was limited to a value slightly above 20% and attained saturation. In this way, the upper and lower limits of the PEG200 concentration in the blend for foam extrusion trials were identified.

In trials of the blend E3_PEG200_20 using only CO₂ as the foaming agent, the extruder pressures rose higher than 200 bar at a nozzle temperature equal to or lower than 170 °C. Due to limitations in the pressure generation of CO₂ for injection, it was not possible to conduct trials at these nozzle temperatures. To study the foaming behavior of the blend in the extruder, the nozzle temperature was maintained at 180 °C and CO₂ feed rates of 0.25, 0.50 and 0.75 mL/min were applied. The effect of the CO₂ feed rate can be seen in the SEM micrographs in Figure 10. The higher amount of CO₂ caused more CO₂ to dissolve into the polymer blend, which resulted in a more swollen polymer phase. However, the pressure at the nozzle was not high enough for this amount of CO₂ to achieve high nucleation and, subsequently, higher porosity. The foam created using only CO₂ as the foaming agent

was underwhelming compared to the extruded PESU foam [17]. The CO₂ feed rate of 0.5 mL/min was selected for further experiments since the pore size and porosity were comparatively acceptable, while the operation of the extruder was stable.

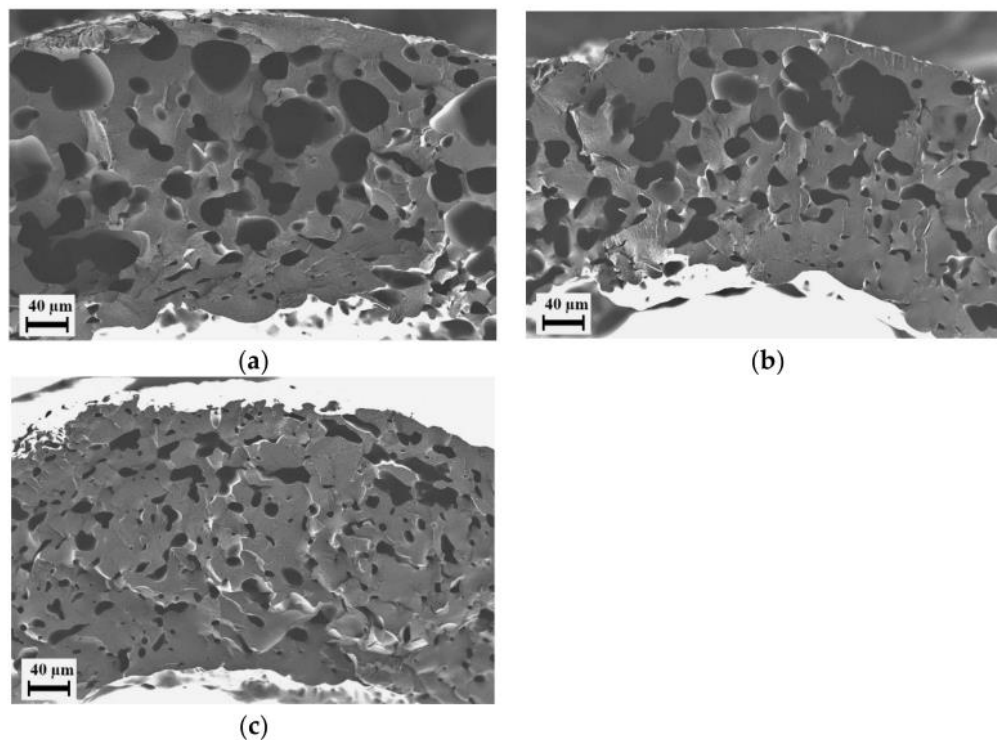


Figure 10. E3_PEG200_20 foams manufactured using only CO₂ as the foaming agent at various CO₂ feed rates: (a) 0.25 mL/min; (b) 0.5 mL/min; (c) 0.75 mL/min. Images show close-up views of the cross-section of the extrudate.

The introduction of water along with CO₂ decreased the viscosity of the melt in the entire extruder. It was possible to process the blend E3_PEG200_20 with CO₂ and water as foaming agents at lower nozzle temperatures up to 145 °C. This agreed well with the results from Evans et al. [49], who found a twentyfold decrease in the viscosity of melts due to the introduction of superheated water into the melt system. The effect of nozzle temperature on the foam quality was studied by injecting equal amounts of CO₂ and water into the foam extruder, as it was identified as one of the most influential extruder settings for the foam quality due to cell nucleation taking place there [16,42,45,94–97]. This was studied for all processable blends; i.e., blends E3_PEG200_14 and E3_PEG200_20. Lower nozzle temperatures led to an increase in the pressure measured in the extruder near the nozzle, as shown in Figure 11. The difference between the pressures of the two blends correlated qualitatively with the difference between their viscosities, as shown in Figure 8a. The same effect on the pressures was expected if the extruder temperatures were set similarly to the nozzle temperatures. This validated our approach of analyzing the rheological results to predict the performance of the extruder. The measurement of pressure took place approximately 10 cm before the nozzle exit. The pressure in the extruder decreased along the longitudinal axis towards the melt exit in the nozzle and was, therefore, lower than the pressure at the pressure-measuring site near the nozzle [89]. Nevertheless, only the nozzle temperatures that led to a pressure lower than 300 bar were used due to safety precautions.

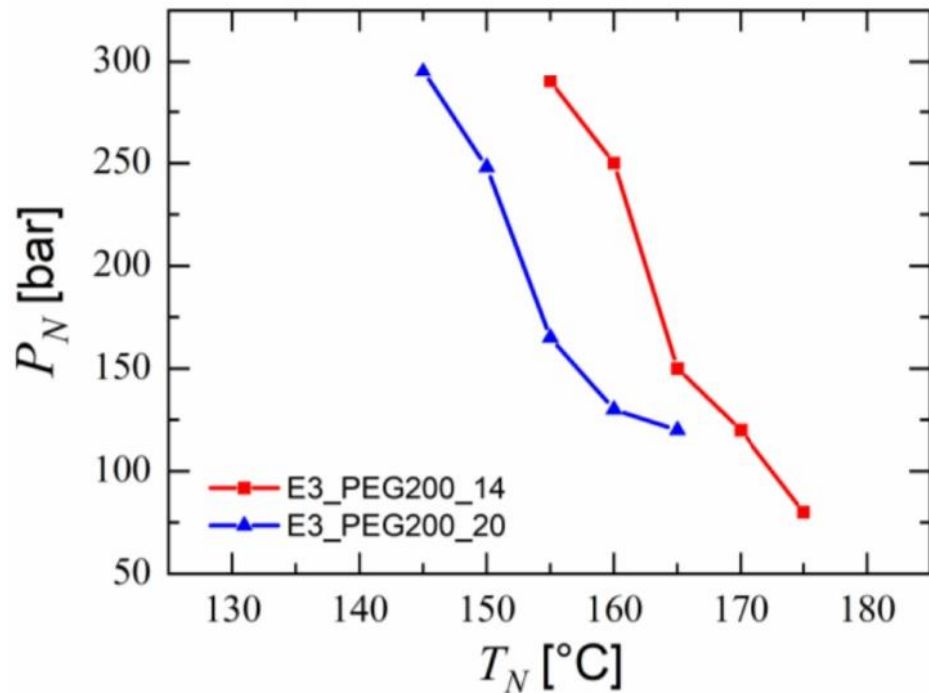


Figure 11. Pressure measured before the nozzle (10 cm) of the foam extruder for PESU/PEG blends at respective nozzle temperatures.

Blend E3_PEG200_14 was processed in the foam extruder at 230 °C and the effect of nozzle temperature was studied between 155 °C and 175 °C, whereas blend E3_PEG200_20 was processed in the foam extruder at 200 °C and the effect of nozzle temperature was studied between 145 °C and 165 °C. Comparing the SEM micrographs in Figures 12 and 13, blend E3_PEG200_20 provided better foam than blend E3_PEG200_14 at lower nozzle temperatures. The effect of nozzle temperature can be seen in both cases, with lower nozzle temperatures yielding higher nucleation and porosity. The lowest nozzle temperature for each blend provided the smallest cell size and highest porosity, as seen in Figure 14. The porosity at higher nozzle temperatures for both materials was slightly higher than the lower adjacent temperature due to the formation of large pores that were essentially macro-cellular in nature. This occurred as the higher nozzle temperature led to lower viscosity, causing the nucleated pores to coalesce and form larger pores in the extrudate. This explains the increases after 155 °C and 170 °C for E3_PEG200_14 and E3_PEG200_20, respectively. At 145 °C, blend E3_PEG200_20 yielded uniform microcellular foam with an average cell size of 5 μm and a porosity of 51%. This average cell size was smaller than those found in the literature on extruded foams obtained from pristine polymers, as the lowest average cell size for the polystyrene foams produced by Han et al. was approximately 7 μm [41,98]. Lee et al. achieved an average cell size of 5 μm using foam extrusion, but they used LDPE/clay nanocomposites [99]. The porosity value was, however, lower compared to the values in the literature [43,100]. The cells seen in Figure 13b appear to be interconnected, and the foam can be classified as open-celled foam [37]. Furthermore, the dye uptake test revealed uptake of the solution of 1-1 methylene blue in ethanol due to the color changing from white to blue. This indicated that the capillary effect enabled the absorption of the solution into the foam, thus confirming the open cellularity [101–103].

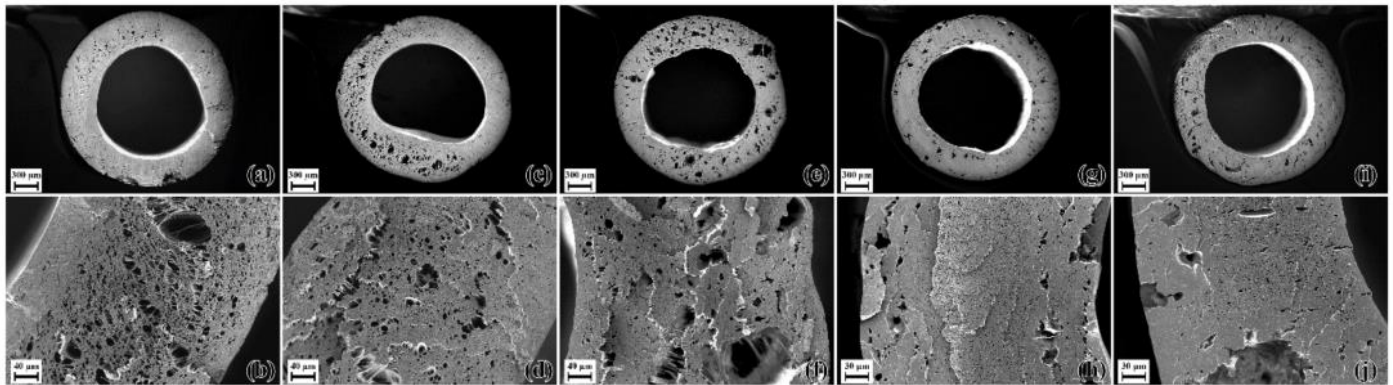


Figure 12. E3_PEG200_14 foams at various nozzle temperatures (T_N): (a,b) $T_N = 155$ °C; (c,d) $T_N = 160$ °C; (e,f) $T_N = 165$ °C; (g,h) $T_N = 170$ °C; (i,j) $T_N = 175$ °C. The images of the entire cross-sections of the extrudates are given, along with close-up views of the cross-sections of the extrudate.

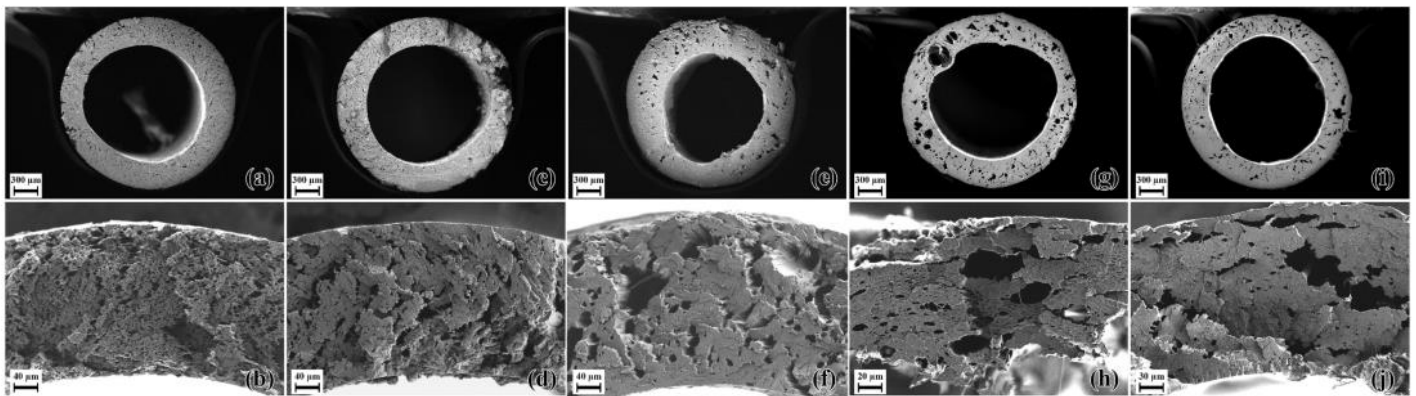


Figure 13. E3_PEG200_20 foams at various nozzle temperatures (T_N): (a,b) $T_N = 145$ °C; (c,d) $T_N = 150$ °C; (e,f) $T_N = 155$ °C; (g,h) $T_N = 160$ °C; (i,j) $T_N = 165$ °C. The images of the entire cross-sections of the extrudates are given, along with close-up views of the cross-sections of the extrudate.

By carrying out tensile tests on the foamed extrudates of blend E3_PEG200_20, the effect of nozzle temperature on the mechanical properties of the foams was observed. Stress versus strain curves, as seen in Figure 15, indicated that a decrease in nozzle temperature led to a lower E modulus while decreasing the tensile strength. However, an exception occurred for the nozzle temperature 160 °C, which led to a higher tensile strength than 165 °C. This can be correlated with the increase in the overall porosity due to larger pores, as seen in Figure 14, but, at the same time, more volume was achieved without pores. This mechanical analysis also showed that an increase in porosity increased the ductility but also decreased the tensile strength significantly.

The cell walls of this foam were porous on their own at the nanocellular level, as seen in Figure 16. This phenomenon has been previously observed in batch foaming in several studies [11,14,104]. The expansion of microcellular cells in foam during foam expansion expresses the tension within the polymer and causes stretching. This stretching leads to fibril-like structures that remain connected to each other and pores are created between them. In a previous work, it was possible to control the pore size and expansion of these structures in PESU/PVP foams manufactured using batch foaming [14]. This was beyond the scope of this work. We suspected that a similar process took place where the bubble growth occurred as the extrudate exited the foam extruder, resulting in stretching of fibrils within the polymer melt and, thus, causing this structure to form. This is the first instance that such a nanocellular structure has been observed in a foam created via extrusion. The

pores on the cell walls of microcells were not considered when measuring the average cell size of the complete foams.

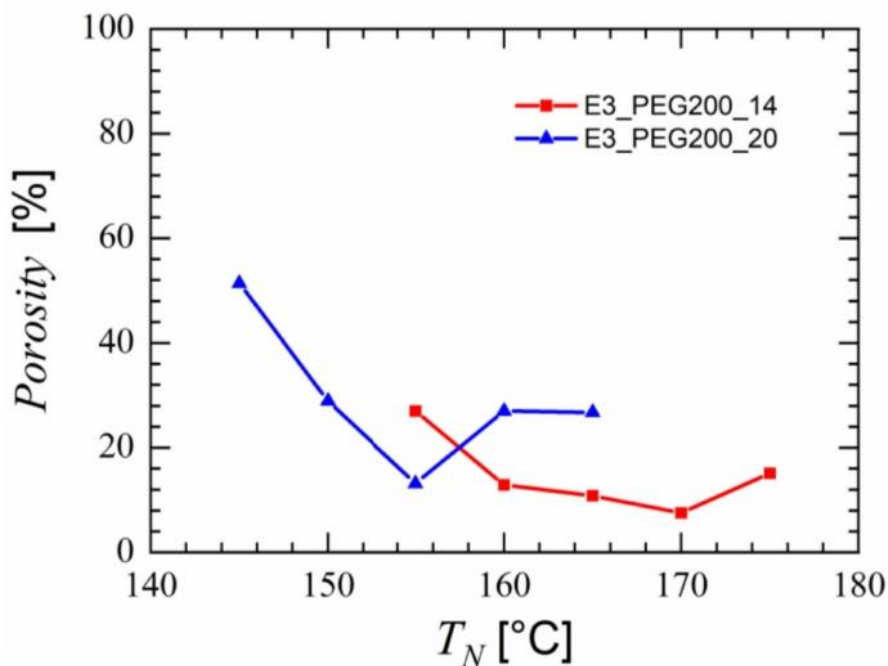


Figure 14. Porosities of foams obtained from the blends E3_PEG200_14 and E3_PEG200_20 at different nozzle temperatures during foam extrusion.

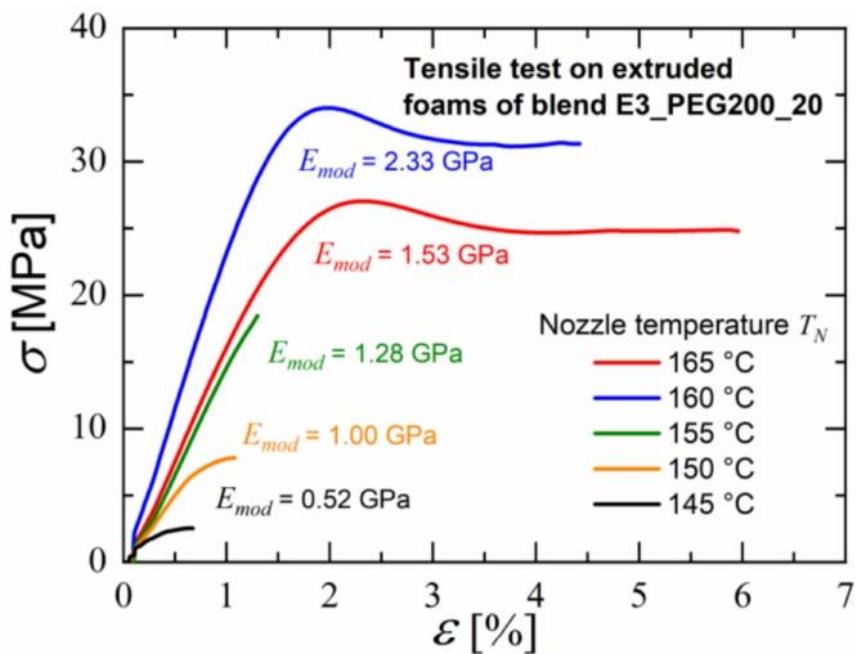


Figure 15. Tensile tests of foamed extrudates of blend E3_PEG200_20 at different nozzle temperatures during foam extrusion.

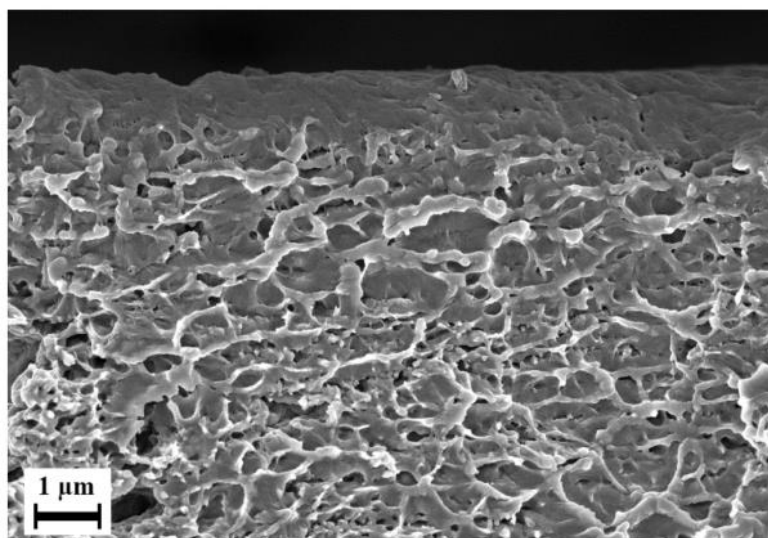


Figure 16. Porous structure observed inside the microcellular foam of the blend E3_PEG200_20.

Comparing Figure 10 with Figure 13, the improvement in foam quality due to the usage of water along with CO₂ as a foaming agent was very significant. This supports the findings of other research, where the usage of water along with CO₂ led to increased porosity and low pore size [13,14,48]. When water was injected into the extruder, it was in a superheated phase, as the extruder possessed pressures in the range of 100–300 bar and temperatures around 200 °C. Superheated water has a polarity similar to that of organic solvents [105] and, thus, aids in pore formation [49]. The presence of the nanocellular pores, as seen in Figure 15, may also have been observed as a result of the removal of PEG from the polymer matrix due to superheated water, similarly to the phase inversion process, or due to evaporation. The thermal and chemical behavior of the produced extrudate was further investigated.

The spectroscopical analysis provided some more information regarding the blending of PEG with PESU after the extrusion process. A comparison of the peaks of PESU in the FTIR spectra of blend E3_PEG200_20 and its extruded foam, as shown in Figure 17, indicated no changes in the characteristic vibrations of PESU and PEG. This indicated that no chemical reactions took place. Since the principle peaks of PESU remained similar in both the blend and the extrudate, the chemical stability and resistance of PESU were retained in the extruded foam. Comparing the DSC measurement of the blend's foam with the blend, an increase of 26 °C was seen after foam extrusion (see Figure S4 in the Supplementary Materials). The amount of PEG appeared to have been reduced, most likely due to evaporation, as the extruder temperatures were near the boiling point of the PEG. This change was also visible in the FTIR spectrum, as the intensities of PEG peaks in the blend's extruded foam were slightly lower than in the original blend. This also agreed with the observations from the rheological measurements discussed above, since the low molecular weight of PEG enables its leaching from the polymer matrix [72]. This effect would be beneficial for the production of extruded porous hollow fibers based on PESU via foam extrusion.

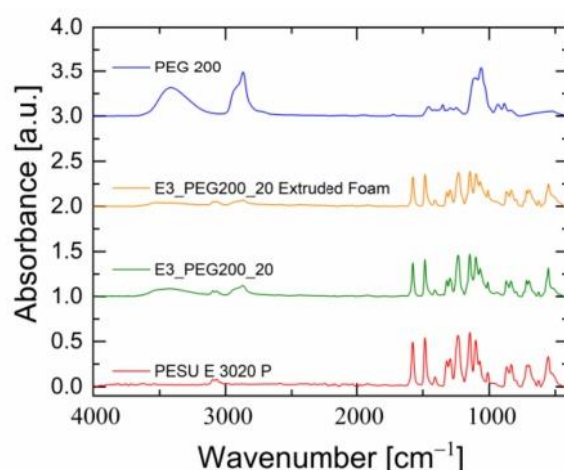


Figure 17. FTIR spectra of PESU E 3020 P, blend E3_PEG200_20, the extruded foam of blend E3_PEG200_20 and PEG200.

4. Conclusions

PESU/PEG blends were manufactured using the absorption of low-molecular-weight liquid PEG into PESU by taking advantage of the porous structure of the PESU flakes. The polymers were partially miscible, as shown by thermal and rheological measurements. Blends with suitable compositions could be extruded. The sorption of CO₂ in selected blends was investigated, and it was found that PEG increased the diffusion coefficient of the blend, and it essentially increased with increases in temperature, providing insight into the foaming characteristics of the blends. Blend PESU/PEG 80/20 was processable in a foam extruder at 200 °C; i.e., 150 °C lower than the extruder temperature required for pure PESU. The use of water along with CO₂ as the foaming agent was confirmed to lower the viscosity of the polymer–foaming agent mixture in the extruder even more than when using only CO₂ and resulted in highly porous foams with smaller cell sizes. At certain process settings, the PESU/PEG 80/20 blend provided the lowest average pore size of 5 μm and a porosity of 51%. The mechanical properties of certain foams were also evaluated, and it was found that an increase in porosity led to a slight increase in the ductility but, at the same time, a significant loss in tensile strength. FTIR measurements confirmed the retention of the PESU chemical structure in the produced foams, but a certain amount of PEG was lost due to evaporation during the foam extrusion; however, this was not problematic due to the aim of obtaining porous hollow fibers later on.

Supplementary Materials: The following supporting information can be downloaded at: <https://www.mdpi.com/article/10.3390/polym15010118/s1>. Figure S1: Gel permeation chromatography for PESU E 3010 and E 3020 P. The molecular weight estimation was based on calibration with polystyrene standards; Figure S2: Rheological investigations of the PESU/PEG200 blends: storage modulus G' and loss modulus G'' versus angular frequency at various temperatures for blend (a) E3_PEG200_08, (b) E3_PEG200_14 and (c) E3_PEG200_26; Figure S3: Apparent densities of PESU E 3010 granules, PESU E 3020 P flakes and PESU/PEO blend flakes; Figure S4: DSC third heating cycle for foam of blend E3_PEG200_20; extrusion foamed using CO₂ and water.

Author Contributions: Conceptualization and methodology, A.R., P.G. and U.A.H.; material characterization, A.R. and J.L.; foam extrusion trials, A.R. and J.K.; writing—original draft preparation, A.R.; writing—review and editing, A.R., P.G., J.K., J.L., U.A.H. and V.A.; analysis of data and visualization, A.R. and J.L.; scientific supervision, P.G. and V.A. All authors have read and agreed to the published version of the manuscript.

Funding: This research received no external funding.

Institutional Review Board Statement: Not applicable.

Informed Consent Statement: Not applicable.

Data Availability Statement: The characterization data are available upon request from the authors.

Acknowledgments: The authors thank Ivonne Ternes (thermal analysis), Kristian Buhr (rheology), Maren Brinkmann (GPC), Martin Held, Anke-Lisa Höhme, Erik Schneider, Evgeni Sperling (microscopy) and Sarah Glaß (scientific discussions). The donations of PESU by Oliver Gronwald and Erik Gubbels (BASF SE), along with the discussions with Oliver Gronwald and Martin Weber (BASF SE) during the initial stage of this work, are gratefully acknowledged.

Conflicts of Interest: The authors declare no conflict of interest.

Nomenclature

Symbol	Parameter	Unit
T_g	Glass transition temperature	K
w	Mass fraction of polymer	%
c_p	Heat capacity of polymer	mW
t	Time	s
M_t	Mass of gas absorbed by sample at time t	g
M_∞	Mass of gas absorbed by sample at time $t \rightarrow \infty$; i.e., equilibrium	g
ρ_{apparent}	Apparent density	g/mL
T_{ext}	Extruder temperature	°C
T_N	Nozzle temperature	°C
P_N	Nozzle pressure	bar
G'	Storage modulus	Pa
G''	Loss modulus	Pa
ω	Angular frequency	rad/s
$ \eta^* $	Complex viscosity	Pa s

References

- Giesa, R.; Schmidt, H.W. High-temperature Stable Polymers. In *Encyclopedia of Materials: Science and Technology*; Buschow, K.H.J., Cahn, R.W., Flemings, M.C., Ilschner, B., Kramer, E.J., Mahajan, S., Veyssi re, P., Eds.; Elsevier: Oxford, UK, 2001; pp. 3803–3806. [[CrossRef](#)]
- Lutz, H. 2.06—Ultrafiltration: Fundamentals and Engineering. In *Comprehensive Membrane Science and Engineering*; Drioli, E., Giorno, L., Eds.; Elsevier: Oxford, UK, 2010; pp. 115–139. [[CrossRef](#)]
- Biernat, U. *Threepart Sandwich, One Thermoplastic, Many Possibilities*; BASF SE: Ludwigshafen, Germany, 2018.
- BASF. *Ultrason®(Psu, Pesu, Ppsu)—The Specialty Plastic for High-Quality Parts*; BASF SE: Ludwigshafen, Germany, 2020.
- Tsehaye, M.T.; Velizarov, S.; Van der Bruggen, B. Stability of polyethersulfone membranes to oxidative agents: A review. *Polym. Degrad. Stabil.* **2018**, *157*, 15–33. [[CrossRef](#)]
- Qi, K.; Huang, R. 3—Polyethersulfone (PES) and Its Processing. In *Advanced Polymer Processing Operations*; Cheremisinoff, N.P., Ed.; William Andrew Publishing: Westwood, NJ, USA, 1998; pp. 69–99. [[CrossRef](#)]
- Krause, B.; Boerrigter, M.E.; van der Vegt, N.F.A.; Strathmann, H.; Wessling, M. Novel open-cellular polysulfone morphologies produced with trace concentrations of solvents as pore opener. *J. Membr. Sci.* **2001**, *187*, 181–192. [[CrossRef](#)]
- Krause, B.; van der Vegt, N.F.A.; Wessling, M. New ways to produce porous polymeric membranes by carbon dioxide foaming. *Desalination* **2002**, *144*, 5–7. [[CrossRef](#)]
- Krause, B.; Diekmann, K.; van der Vegt, N.F.A.; Wessling, M. Open nanoporous morphologies from polymeric blends by carbon dioxide foaming. *Macromolecules* **2002**, *35*, 1738–1745. [[CrossRef](#)]
- Sorrentino, L.; Aurilia, M.; Iannace, S. Polymeric Foams from High-Performance Thermoplastics. *Adv. Polym. Technol.* **2011**, *30*, 234–243. [[CrossRef](#)]
- Guo, H.M.; Nicolae, A.; Kumar, V. Fabrication of high temperature polyphenylsulfone nanofoams using high pressure liquid carbon dioxide. *Cell Polym.* **2016**, *35*, 119–142. [[CrossRef](#)]
- Guo, H.M.; Nicolae, A.; Kumar, V. Solid-state microcellular and nanocellular polysulfone foams. *J. Polym. Sci. Pol. Phys.* **2015**, *53*, 975–985. [[CrossRef](#)]
- Owusu-Nkwantabisah, S.; Staudt, C.; Lesser, A.J. Synergy of supercritical CO₂ and superheated H₂O for enhanced processability of polyethersulfone towards open cell foams. *Polym. Eng. Sci.* **2018**, *58*, 1108–1114. [[CrossRef](#)]
- Raje, A.; Buhr, K.; Koll, J.; Lilleparg, J.; Abetz, V.; Handge, U.A. Open-Celled Foams of Polyethersulfone/Poly(N-vinylpyrrolidone) Blends for Ultrafiltration Applications. *Polymers* **2022**, *14*, 1177. [[CrossRef](#)]
- Jin, F.-L.; Zhao, M.; Park, M.; Park, S.-J. Recent Trends of Foaming in Polymer Processing: A Review. *Polymers* **2019**, *11*, 953. [[CrossRef](#)]

16. Lee, S.T. *Foam Extrusion*, 2nd ed.; Polymeric Foams, Lee, S.T., Park, C.B., Eds.; CRC Press: Boca Raton, FL, USA, 2014; p. 624. [[CrossRef](#)]
17. Huang, Q. Lösemittelfreie Herstellung von Porösen Polymeren Membranen Durch Schaumextrusion. Ph.D. Thesis, Universität Hamburg, Hamburg, Germany, 2000. Available online: <https://ediss.sub.uni-hamburg.de/bitstream/ediss/1334/1/Dissertation-Huang.PDF> (accessed on 3 November 2022).
18. Ruckdäschel, H.; Gutmann, P.; Altstädt, V.; Schmalz, H.; Müller, A.H.E. Foaming of Microstructured and Nanostructured Polymer Blends. In *Complex Macromolecular Systems I*; Müller, A.H.E., Schmidt, H.-W., Eds.; Springer: Berlin/Heidelberg, Germany, 2010; pp. 199–252. [[CrossRef](#)]
19. Bärwinkel, S.; Bahrami, R.; Löbbling, T.I.; Schmalz, H.; Müller, A.H.E.; Altstädt, V. Polymer Foams Made of Immiscible Polymer Blends Compatibilized by Janus Particles—Effect of Compatibilization on Foam Morphology. *Adv. Eng. Mater.* **2016**, *18*, 814–825. [[CrossRef](#)]
20. Kong, W.-I.; Bao, J.-B.; Wang, J.; Hu, G.-H.; Xu, Y.; Zhao, L. Preparation of open-cell polymer foams by CO₂ assisted foaming of polymer blends. *Polymer* **2016**, *90*, 331–341. [[CrossRef](#)]
21. Haurat, M.; Dumon, M. Amorphous Polymers' Foaming and Blends with Organic Foaming-Aid Structured Additives in Supercritical CO₂, a Way to Fabricate Porous Polymers from Macro to Nano Porosities in Batch or Continuous Processes. *Molecules* **2020**, *25*, 5320. [[CrossRef](#)] [[PubMed](#)]
22. Krause, B.; Wessling, M.; Göhl, H.; Storr, M. *Membrane and Use Thereof*; European Patent Office, Ed.; Gambro Lundia AB: Lund, Germany, 2020.
23. Yoshida, M.; Prasad, P.N. Fabrication of channel waveguides from sol-gel-processed polyvinylpyrrolidone/SiO₂ composite materials. *Appl. Opt.* **1996**, *35*, 1500–1506. [[CrossRef](#)] [[PubMed](#)]
24. Raviv, U.; Klein, J. 2.24—Adhesion, Friction, and Lubrication between Polymer-Bearing Surfaces. In *Polymer Science: A Comprehensive Reference*; Matyjaszewski, K., Möller, M., Eds.; Elsevier: Amsterdam, The Netherlands, 2012; pp. 607–628. [[CrossRef](#)]
25. Ibrahim, M.S.; El-Wassefy, N.A.; Farahat, D.S. 8—Biocompatibility of dental biomaterials. In *Biomaterials for Oral and Dental Tissue Engineering*; Tayebi, L., Moharamzadeh, K., Eds.; Woodhead Publishing: Sawston, UK, 2017; pp. 117–140. [[CrossRef](#)]
26. Porter, S.; Sackett, G.; Liu, L. Chapter 33—Development, Optimization, and Scale-up of Process Parameters: Pan Coating. In *Developing Solid Oral Dosage Forms*; Qiu, Y., Chen, Y., Zhang, G.G.Z., Liu, L., Porter, W.R., Eds.; Academic Press: San Diego, CA, USA, 2009; pp. 761–805. [[CrossRef](#)]
27. Shah, H.; Jain, A.; Laghate, G.; Prabhudesai, D. Chapter 32—Pharmaceutical excipients. In *Remington*, 23rd ed.; Adejare, A., Ed.; Academic Press: Cambridge, MA, USA, 2021; pp. 633–643. [[CrossRef](#)]
28. Hutanu, D.; Frishberg, M.D.; Guo, L.; Darie, C.C. Recent Applications of Polyethylene Glycols (PEGs) and PEG Derivatives. *Mod. Chem. Appl.* **2014**, *2*, 1–6. [[CrossRef](#)]
29. Dimitrov, I.; Tsvetanov, C.B. 4.27—Oligomeric Poly(ethylene oxide)s. Functionalized Poly(ethylene glycol)s. PEGylation. In *Polymer Science: A Comprehensive Reference*; Matyjaszewski, K., Möller, M., Eds.; Elsevier: Amsterdam, The Netherlands, 2012; pp. 679–693. [[CrossRef](#)]
30. Gronwald, O.; Frost, I.; Ulbricht, M.; Shalmani, A.K.; Panglisch, S.; Grunig, L.; Handge, U.A.; Abetz, V.; Heijnen, M.; Weber, M. Hydrophilic poly(phenylene sulfone) membranes for ultrafiltration. *Sep. Purif. Technol.* **2020**, *250*, 117107. [[CrossRef](#)]
31. Hao, Y.; Liang, C.; Moriya, A.; Matsuyama, H.; Maruyama, T. Visualization of Protein Fouling inside a Hollow Fiber Ultrafiltration Membrane by Fluorescent Microscopy. *Ind. Eng. Chem. Res.* **2012**, *51*, 14850–14858. [[CrossRef](#)]
32. Barry, E.; Mane, A.U.; Libera, J.A.; Elam, J.W.; Darling, S.B. Advanced oil sorbents using sequential infiltration synthesis. *J. Mater. Chem. A* **2017**, *5*, 2929–2935. [[CrossRef](#)]
33. Gronwald, O.; Weber, M. AGNIQUE AMD 3L as green solvent for polyethersulfone ultrafiltration membrane preparation. *J. Appl. Polym. Sci.* **2020**, *137*, 48419. [[CrossRef](#)]
34. Anastas, P.T.; Warner, J.C. Green chemistry. *Frontiers* **1998**, *640*, 1998.
35. Redlich, C.A.; Beckett, W.S.; Sparer, J.; Barwick, K.W.; Riely, C.A.; Miller, H.; Sigal, S.L.; Shalat, S.L.; Cullen, M.R. Liver-disease associated with occupational exposure to the solvent dimethylformamide. *Ann. Intern. Med.* **1988**, *108*, 680–686. [[CrossRef](#)] [[PubMed](#)]
36. Gutmann, P.; Hildebrandt, K.; Altstädt, V.; Müller, A.H.E. Foaming of an Immiscible Blend System Using Organic Liquids as Blowing Agents. *J. Cell. Plast.* **2010**, *46*, 239–258. [[CrossRef](#)]
37. Okolieocha, C.; Raps, D.; Subramaniam, K.; Altstädt, V. Microcellular to nanocellular polymer foams: Progress (2004–2015) and future directions—A review. *Eur. Polym. J.* **2015**, *73*, 500–519. [[CrossRef](#)]
38. Hwang, Y.D.; Cha, S.W. The relationship between gas absorption and the glass transition temperature in a batch microcellular foaming process. *Polym. Test.* **2002**, *21*, 269–275. [[CrossRef](#)]
39. Sauceau, M.; Fages, J.; Common, A.; Nikitine, C.; Rodier, E. New challenges in polymer foaming: A review of extrusion processes assisted by supercritical carbon dioxide. *Prog. Polym. Sci.* **2011**, *36*, 749–766. [[CrossRef](#)]
40. Jacobs, L.J.M. Carbon Dioxide as a Sustainable Means to Control Polymer Foam Morphology. Ph.D. Thesis, Technische Universiteit Eindhoven, Eindhoven, The Netherlands, 2008. Available online: <https://research.tue.nl/en/publications/carbon-dioxide-as-a-sustainable-means-to-control-polymer-foam-mor> (accessed on 3 November 2022).
41. Han, X.; Koelling, K.W.; Tomasko, D.L.; Lee, L.J. Continuous microcellular polystyrene foam extrusion with supercritical CO₂. *Polym. Eng. Sci.* **2002**, *42*, 2094–2106. [[CrossRef](#)]

42. Park, C.B.; Behraves, A.H.; Venter, R.D. Low density microcellular foam processing in extrusion using CO₂. *Polym. Eng. Sci.* **1998**, *38*, 1812–1823. [[CrossRef](#)]
43. Chauvet, M.; Sauceau, M.; Fages, J. Extrusion assisted by supercritical CO₂: A review on its application to biopolymers. *J. Supercrit. Fluids* **2017**, *120*, 408–420. [[CrossRef](#)]
44. Michaeli, W.; Heinz, R. Foam extrusion of thermoplastic polyurethanes (TPU) using CO₂ as a blowing agent. *Macromol. Mater. Eng.* **2000**, *284–285*, 35–39. [[CrossRef](#)]
45. Yeh, S.-K.; Yang, S.-H.; Han, L.; Liu, H.-Y.; Liao, Y.-S.; Chang, Y.-C. Foam extrusion of polypropylene–rice husk composites using CO₂ as the blowing agent. *J. Cell. Plast.* **2019**, *55*, 401–419. [[CrossRef](#)]
46. Mi, H.-Y.; Jing, X.; Liu, Y.; Li, L.; Li, H.; Peng, X.-F.; Zhou, H. Highly Durable Superhydrophobic Polymer Foams Fabricated by Extrusion and Supercritical CO₂ Foaming for Selective Oil Absorption. *ACS Appl. Mater. Interfaces* **2019**, *11*, 7479–7487. [[CrossRef](#)] [[PubMed](#)]
47. Sun, H.L.; Sur, G.S.; Mark, J.E. Microcellular foams from polyethersulfone and polyphenylsulfone—Preparation and mechanical properties. *Eur. Polym. J.* **2002**, *38*, 2373–2381. [[CrossRef](#)]
48. Schulze, M.; Handge, U.A.; Abetz, V. Preparation and characterisation of open-celled foams using polystyrene-*b*-poly(4-vinylpyridine) and poly(4-methylstyrene)-*b*-poly(4-vinylpyridine) diblock copolymers. *Polymer* **2017**, *108*, 400–412. [[CrossRef](#)]
49. Evans, G.C.; Lesser, A.J. Processing polyamides with superheated water. *J. Polym. Sci. Part B Polym. Phys.* **2018**, *56*, 803–813. [[CrossRef](#)]
50. Papageorgiou, G.Z.; Bikiaris, D.N. Crystallization and melting behavior of three biodegradable poly(alkylene succinates). A comparative study. *Polymer* **2005**, *46*, 12081–12092. [[CrossRef](#)]
51. Halder, K.; Khan, M.M.; Grünauer, J.; Shishatskiy, S.; Abetz, C.; Filiz, V.; Abetz, V. Blend membranes of ionic liquid and polymers of intrinsic microporosity with improved gas separation characteristics. *J. Membr. Sci.* **2017**, *539*, 368–382. [[CrossRef](#)]
52. Schulze, M.; Handge, U.A.; Rangou, S.; Lillepär, J.; Abetz, V. Thermal properties, rheology and foams of polystyrene-block-poly(4-vinylpyridine) diblock copolymers. *Polymer* **2015**, *70*, 88–99. [[CrossRef](#)]
53. Wang, J.S.; Kamiya, Y. Concurrent Measurements of Sorption and Dilation Isotherms and Diffusivity for Polysulfone Membrane Carbon-Dioxide System. *J. Membr. Sci.* **1995**, *98*, 69–76. [[CrossRef](#)]
54. Barrer, R.M. Diffusivities in Glassy-Polymers for the Dual Mode Sorption Model. *J. Membr. Sci.* **1984**, *18*, 25–35. [[CrossRef](#)]
55. Frisch, H.L. Sorption and Transport in Glassy-Polymers—Review. *Polym. Eng. Sci.* **1980**, *20*, 2–13. [[CrossRef](#)]
56. Höhme, C.; Filiz, V.; Abetz, C.; Georgopoulos, P.; Scharnagl, N.; Abetz, V. Postfunctionalization of Nanoporous Block Copolymer Membranes via Click Reaction on Polydopamine for Liquid Phase Separation. *ACS Appl. Nano Mater.* **2018**, *1*, 3124–3136. [[CrossRef](#)]
57. Georgopoulos, P.; Eichner, E.; Filiz, V.; Handge, U.A.; Schneider, G.A.; Heinrich, S.; Abetz, V. Improvement of mechanical properties by a polydopamine interface in highly filled hierarchical composites of titanium dioxide particles and poly(vinyl butyral). *Compos. Sci. Technol.* **2017**, *146*, 73–82. [[CrossRef](#)]
58. Cassagnau, P.; Courmont, M.; Melis, F.; Puaux, J.P. Study of mixing of liquid/polymer in twin screw extruder by residence time distribution. *Polym. Eng. Sci.* **2005**, *45*, 926–934. [[CrossRef](#)]
59. Naeini, A.T. Visualization of the Crystallization in Foam Extrusion Process. *Theory Comput. Syst. Math. Syst. Theory* **2012**, *14*, 1–93.
60. Maruhashi, Y.; Iida, S. Transparency of polymer blends. *Polym. Eng. Sci.* **2001**, *41*, 1987–1995. [[CrossRef](#)]
61. *Safety Data Sheet—Polyethylene Glycol 200 for Synthesis*; Sigma-Aldrich: St. Louis, MO, USA, 2021.
62. Lillepär, J.; Georgopoulos, P.; Shishatskiy, S. Stability of blended polymeric materials for CO₂ separation. *J. Membr. Sci.* **2014**, *467*, 269–278. [[CrossRef](#)]
63. Couchman, P.R. The Glass-Transition of Compatible Blends. *Polym. Eng. Sci.* **1987**, *27*, 618–621. [[CrossRef](#)]
64. Fox, T.G. Influence of diluent and of copolymer composition on the glass temperature of a polymer system. *Bull. Am. Phys. Soc.* **1956**, *1*, 123.
65. Georgopoulos, P.; Handge, U.A.; Abetz, C.; Abetz, V. Influence of block sequence and molecular weight on morphological, rheological and dielectric properties of weakly and strongly segregated styrene-isoprene triblock copolymers. *Polymer* **2016**, *104*, 279–295. [[CrossRef](#)]
66. Couchman, P.R. Compositional variation of glass-transition temperatures. 2. Application of thermodynamic theory to compatible polymer blends. *Macromolecules* **1978**, *11*, 1156–1161. [[CrossRef](#)]
67. Sailer, C.; Weber, M.; Steininger, H.; Handge, U.A. Grafting of polyamide 6 on a styrene-acrylonitrile maleic anhydride terpolymer: Melt rheology at the critical gel state. *Rheol. Acta* **2009**, *48*, 579–588. [[CrossRef](#)]
68. Asthana, H.; Jayaraman, K. Rheology of Reactively Compatibilized Polymer Blends with Varying Extent of Interfacial Reaction. *Macromolecules* **1999**, *32*, 3412–3419. [[CrossRef](#)]
69. Stadler, R.; Freitas, L.D.; Krieger, V.; Klotz, S. Influence of the Phase-Separation on the Linear Viscoelastic Properties of a Polystyrene Poly(vinyl Methyl-Ether) Blend. *Polymer* **1988**, *29*, 1643–1647. [[CrossRef](#)]
70. Bates, F.S. Block Copolymers near the Microphase Separation Transition. 2. Linear Dynamic Mechanical-Properties. *Macromolecules* **1984**, *17*, 2607–2613. [[CrossRef](#)]
71. Mani, S.; Malone, M.F.; Winter, H.H. Influence of Phase-Separation on the Linear Viscoelastic Behavior of a Miscible Polymer Blend. *J. Rheol.* **1992**, *36*, 1625–1649. [[CrossRef](#)]

72. Lillepär, J.; Georgopoulos, P.; Emmler, T.; Shishatskiy, S. Effect of the reactive amino and glycidyl ether terminated polyethylene oxide additives on the gas transport properties of Pebax® bulk and thin film composite membranes. *RSC Adv.* **2016**, *6*, 11763–11772. [[CrossRef](#)]
73. Urakawa, O.; Ujii, T.; Adachi, K. Dynamic heterogeneity in a miscible poly(vinyl acetate)/poly(ethylene oxide) blend. *J. Non-Cryst. Solids* **2006**, *352*, 5042–5049. [[CrossRef](#)]
74. Kalogerias, I.M. Glass-Transition Phenomena in Polymer Blends. In *Encyclopedia of Polymer Blends*; John Wiley & Sons, Ltd.: Hoboken, NJ, USA, 2016; pp. 1–134. [[CrossRef](#)]
75. Han, C.D.; Kim, J. Rheological Technique for Determining the Order—Disorder Transition of Block Copolymers. *J. Polym. Sci. Pol. Phys.* **1987**, *25*, 1741–1764. [[CrossRef](#)]
76. Yu, Z.X.; Wang, J.; Li, P.H.; Ding, D.C.; Zheng, X.; Hu, C.Q.; Gao, Z.N.; Hu, T.; Gong, X.H.; Wu, C.G. Melt Blending Modification of Commercial Polystyrene with Its Half Critical Molecular Weight, High Ion Content Ionomer, Poly(styrene-ran-cinnamic Acid) Zn Salt, toward Heat Resistance Improvement. *Polymers* **2020**, *12*, 584. [[CrossRef](#)]
77. Walha, F.; Lamnawar, K.; Maazouz, A.; Jaziri, M. Rheological, Morphological and Mechanical Studies of Sustainably Sourced Polymer Blends Based on Poly(Lactic Acid) and Polyamide 11. *Polymers* **2016**, *8*, 61. [[CrossRef](#)]
78. Luo, H.Y.; Han, H.; Chi, H.F.; Li, J.Y.; Zhao, S.M.; Tao, Y.; Hu, H.Q. Research on the viscous flow transition of styrene-isoprene-styrene triblock copolymer by Rheology. *J. Polym. Res.* **2021**, *28*, 160. [[CrossRef](#)]
79. Tian, J.; Yu, W.; Zhou, C. The preparation and rheology characterization of long chain branching polypropylene. *Polymer* **2006**, *47*, 7962–7969. [[CrossRef](#)]
80. Wu, D.; Huang, A.; Fan, J.; Xu, R.; Liu, P.; Li, G.; Yang, S. Effect of blending procedures and reactive compatibilizers on the properties of biodegradable poly(butylene adipate-co-terephthalate)/poly(lactic acid) blends. *J. Polym. Eng.* **2021**, *41*, 95–108. [[CrossRef](#)]
81. Dunstan, D.E. The viscosity-radius relationship for concentrated polymer solutions. *Sci. Rep.* **2019**, *9*, 543. [[CrossRef](#)]
82. John Vlachopoulos, N.D.P. Basic Concepts in Polymer Melt Rheology and Their Importance in Processing. In *Applied Polymer Rheology: Polymeric Fluids with Industrial Applications*; Kontopoulou, M., Ed.; John Wiley & Sons: Hoboken, NJ, USA, 2012; pp. 1–27.
83. Hernández-Alamilla, M.; Valadez-Gonzalez, A. The effect of two commercial melt strength enhancer additives on the thermal, rheological and morphological properties of polylactide. *J. Polym. Eng.* **2016**, *36*, 31–41. [[CrossRef](#)]
84. Roland, C.M. Chapter 6—Rheological Behavior and Processing of Unvulcanized Rubber. In *The Science and Technology of Rubber*, 4th ed.; Mark, J.E., Erman, B., Roland, C.M., Eds.; Academic Press: Boston, MA, USA, 2013; pp. 285–336. [[CrossRef](#)]
85. Vlachopoulos, J.; Strutt, D. The Role of Rheology in Polymer Extrusion. In *Proceedings of the Extrusion Minitex and Conference: From Basics to Recent Developments*, Düsseldorf, Germany, 2003.
86. John Vlachopoulos, N.D.P. *Understanding Rheology and Technology of Polymer Extrusion*; Polydynamics Inc.: Dundas, ON, Canada, 2019.
87. Mitsoulis, E.; Hatzikiriakos, S.G. Rheological Properties Related to Extrusion of Polyolefins. *Polymers* **2021**, *13*, 489. [[CrossRef](#)]
88. Abeykoon, C.; Kelly, A.; Wilkinson, A. *Investigation of Thermal Stability of Non-Newtonian Melt Flows*; Avestia: Orléans, ON, Canada, 2019. [[CrossRef](#)]
89. Han, C.D.; Villamizar, C.A. Studies on structural foam processing I. The rheology of foam extrusion. *Polym. Eng. Sci.* **1978**, *18*, 687–698. [[CrossRef](#)]
90. Di Maio, E.; Iannace, S.; Mensitieri, G. Chapter 6—Mass transport of low molecular weight compounds in polymers. In *Supercritical Fluid Science and Technology*; Di Maio, E., Iannace, S., Mensitieri, G., Eds.; Elsevier: Amsterdam, The Netherlands, 2021; Volume 9, pp. 179–230. [[CrossRef](#)]
91. Berens, A.R. Transport of Plasticizing Penetrants in Glassy Polymers. In *Barrier Polymers and Structures*; American Chemical Society: New York, NY, USA, 1990; Volume 423, pp. 92–110. [[CrossRef](#)]
92. Barrer, R.M.; Rideal, E.K. Permeation, diffusion and solution of gases in organic polymers. *Trans. Faraday Soc.* **1939**, *35*, 628–643. [[CrossRef](#)]
93. Gendron, R. *Thermoplastic Foam Processing: Principles and Development*; CRC Press: Boca Raton, FL, USA, 2004.
94. Standau, T.; Castellón, S.M.; Delavoie, A.; Bonten, C.; Altstädt, V. Effects of chemical modifications on the rheological and the expansion behavior of polylactide (PLA) in foam extrusion. *e-Polymers* **2019**, *19*, 297–304. [[CrossRef](#)]
95. Shabani, A.; Fathi, A.; Erlwein, S.; Altstädt, V. Thermoplastic polyurethane foams: From autoclave batch foaming to bead foam extrusion. *J. Cell. Plast.* **2021**, *57*, 391–411. [[CrossRef](#)]
96. Kalia, K.; Francoeur, B.; Amirkhizi, A.; Ameli, A. In Situ Foam 3D Printing of Microcellular Structures Using Material Extrusion Additive Manufacturing. *ACS Appl. Mater. Interfaces* **2022**, *14*, 22454–22465. [[CrossRef](#)] [[PubMed](#)]
97. Doyle, L. Extrusion foaming behavior of polybutene-1. Toward single-material multifunctional sandwich structures. *J. Appl. Polym. Sci.* **2022**, *139*, 51816. [[CrossRef](#)]
98. Azdast, T.; Hasanzadeh, R. Increasing cell density/decreasing cell size to produce microcellular and nanocellular thermoplastic foams: A review. *J. Cell. Plast.* **2021**, *57*, 769–797. [[CrossRef](#)]
99. Lee, Y.H.; Wang, K.H.; Park, C.B.; Sain, M. Effects of clay dispersion on the foam morphology of LDPE/clay nanocomposites. *J. Appl. Polym. Sci.* **2007**, *103*, 2129–2134. [[CrossRef](#)]

100. Nikitine, C.; Rodier, E.; Sauceau, M.; Letourneau, J.-J.; Fages, J. Controlling the structure of a porous polymer by coupling supercritical CO₂ and single screw extrusion process. *J. Appl. Polym. Sci.* **2010**, *115*, 981–990. [[CrossRef](#)]
101. Minju, N.; Jobin, G.; Savithri, S.; Ananthakumar, S. Double-Silicate Derived Hybrid Foams for High-Capacity Adsorption of Textile Dye Effluent: Statistical Optimization and Adsorption Studies. *Langmuir* **2019**, *35*, 9382–9395. [[CrossRef](#)]
102. Galzerano, B.; Cabello, C.I.; Muñoz, M.; Buonocore, G.G.; Aprea, P.; Liguori, B.; Verdolotti, L. Fabrication of Green Diatomite/Chitosan-Based Hybrid Foams with Dye Sorption Capacity. *Materials* **2020**, *13*, 3760. [[CrossRef](#)]
103. Novais, R.M.; Pullar, R.C.; Labrincha, J.A. Geopolymer foams: An overview of recent advancements. *Prog. Mater. Sci.* **2020**, *109*, 100621. [[CrossRef](#)]
104. Gong, P.J.; Taniguchi, T.; Ohshima, M. Nanoporous structure of the cell walls of polycarbonate foams. *J. Mater. Sci.* **2014**, *49*, 2605–2617. [[CrossRef](#)]
105. Smith, R.M. Extractions with superheated water. *J. Chromatogr. A* **2002**, *975*, 31–46. [[CrossRef](#)]

Disclaimer/Publisher’s Note: The statements, opinions and data contained in all publications are solely those of the individual author(s) and contributor(s) and not of MDPI and/or the editor(s). MDPI and/or the editor(s) disclaim responsibility for any injury to people or property resulting from any ideas, methods, instructions or products referred to in the content.

6.3. Article 3: A Novel Organic Solvent-Free Method for Manufacturing Polyethersulfone Hollow Fiber Membranes using Melt Extrusion

Authors: Aniket Raje, Joachim Koll, Erik S. Schneider, Prokopios Georgopoulos.

The hollow fibers manufactured using the optimum blend combination in Article 2, when tested for permeability using the same experimental setup as in Article 3, yielded high water flux, as shown in Figure 27.

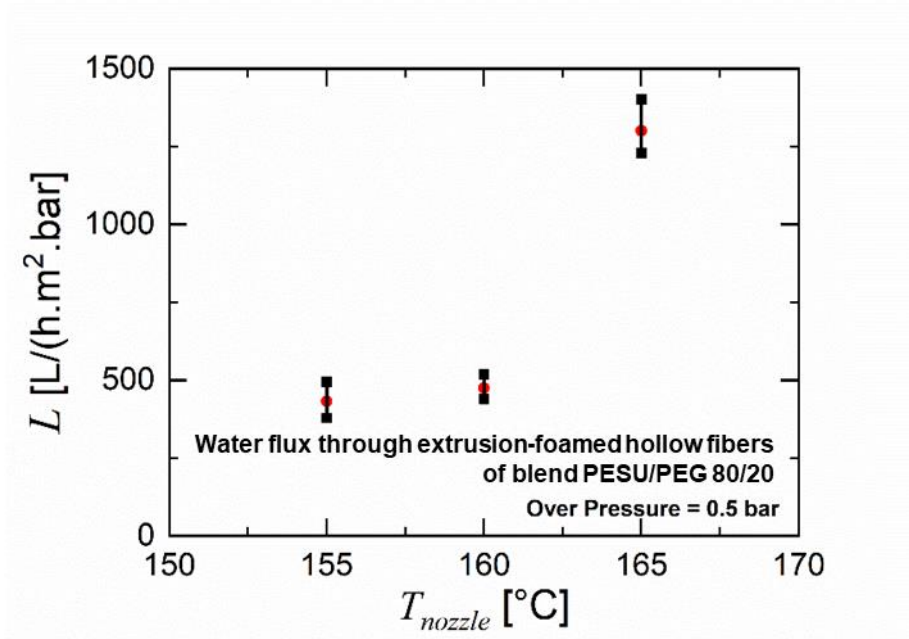


Figure 27: Water flux through the extrusion foamed hollow fibers of blend PESU/PEG 80/20 produced at various nozzle temperatures. Hollow fibers produced at $T_{Nozzle} = 145$ °C and 150 °C, due to low tensile strength, could not bear any water pressure above ATP and thus could not be tested for water flux.

As expected from the average pore size of these fibers, there was no retention of any molecules of PEO when tested for retention.

On the cell walls of the PESU/PEG foam, a nanocellular structure, as shown in Figure 16 of Article 2, was seen as a first in foam extrusion. As such a structure was reported multiple times in literature for polymer foams manufactured using batch foaming process, the reasoning behind it in this case of foam extrusion was hypothesized to be similar, i.e.,

the stretching caused due to microcellular foam expansion leading to the formation of nanocellular pores. However, as the goal of scaling the process to a continuous open-celled foam production in hollow fibers was achieved, the study was concluded without exploring the nanocellular pores in detail.

As the task for the third step of this work was developing continuous hollow fiber membranes capable of ultrafiltration, the nanocellular pores found in the previous step were of interest. However, contrary to the hypothesized explanation, pores with average pore sizes smaller than $1\mu\text{m}$ were found uniformly distributed in the extrudate of the same blend, i.e., PESU/PEG 80/20, without the involvement of any foaming agents.

This phenomenon was studied in detail and was instrumentalized in more porous extruded hollow fibers by developing a ternary polymer blend of PESU/PEG/PVP. The know-how gained from Article 1 on PESU/PVP blends and the absorption blending technique used in Article 2 for PESU/PEG blends were highly beneficial in developing this ternary blend. Furthermore, the effect of various blend combinations and extruder settings on the morphology of these extruded hollow fibers was studied by conducting pore analysis using SEM. However, the hollow fibers were impermeable to water due to their solid outer surface and non-interconnected pores.

As PEG and PVP, both water-soluble polymers, were washed out by immersing the extruded hollow fibers into an aqueous solution of NaOCl, the internal porosity of the hollow fibers increased, allowing interconnected microcellular pores and a porous outer surface with average pore size $\sim 50\text{ nm}$ was obtained. This significant difference between the pores on the outer surface and the rest of the hollow fiber was due to the difference in the composition of the polymer blend between the outer surface and the rest of the fiber occurring during extrusion and the different dissolution mechanisms of PEG and PVP in aqueous NaOCl. This synergistically allowed the extruded hollow fibers to have a separation layer on the outer surface. Thus, along with a decent water flux, these hollow

fiber membranes revealed ultrafiltration capabilities. Moreover, as PEG and PVP were almost washed out of the fibers, these fibers comprised nearly only PESU, allowing for high-temperature stability together with decent mechanical strength.

Thus, continuously produced hollow fiber membranes capable of ultrafiltration were produced without the use of organic solvents, therefore achieving the goal of step 3 of this work successfully.

6.3.1. Author Contributions

Aniket Raje (A.R.), Joachim Koll (J.K.), Erik S. Schneider (E.S.), Prokopios Georgopoulos (P.G.)

Contributions	Authors			
	A.R.	J.K.	E.S.	P.G.
First Author (1) and Corresponding Author (*)	1			*
Conceptualization and methodology	✓			✓
Material and membrane characterization	✓	✓		
Extrusion trials	✓	✓		
SEM and pore analysis			✓	
Writing - original draft preparation	✓			
Writing - review and editing	✓	✓	✓	✓
Analysis of data and graphical visualization	✓			
Scientific supervision				✓

Table 9: Author contributions for article 3.

6.3.2. Funding and Acknowledgements

No external funding was received for this work.

The authors express their gratitude to several individuals and organizations whose contributions have been instrumental in conducting the research. Ivonne Ternes is acknowledged for her assistance with thermal analysis, while Kristian Buhr's skills in rheological measurements proved invaluable. Petra Marten and Maren Brinkmann provided support in the area of GPC, and Barbara Bajer's expertise in pH measurement are greatly appreciated. Martin Held and Evgeni Sperling supported immensely with microscopy, while Sarah Glaß provided valuable scientific insights into polymer membranes.

The authors also extend their gratitude to Volker Abetz for his insightful scientific inputs and ideas, which were instrumental in shaping the research direction.

In addition, the authors would like to acknowledge the generous donations of PESU by Oliver Gronwald and Erik Gubbels from BASF SE.

6.3.3. Publication



A novel organic solvent-free method for manufacturing polyethersulfone hollow fiber membranes using melt extrusion

Aniket Raje, Joachim Koll, Erik S. Schneider, Prokopios Georgopoulos*

Helmholtz-Zentrum Hereon, Institute of Membrane Research, Max-Planck Straße 1, 21502, Geesthacht, Germany

ARTICLE INFO

Keywords:

Organic solvent-free
Polyethersulfone
Ultrafiltration
Melt extrusion
Extruded hollow-fiber membranes

ABSTRACT

Hollow fiber membranes are traditionally manufactured using the spinning process, which takes advantage of the phase separation/inversion for the creation of a porous structure. In this work, the use of melt extrusion led to the fabrication of hollow fiber membranes without the use of organic solvents. Following post-treatment, the fabricated partially dense fibers are transformed into porous fibers. In detail, ternary blends of polyethersulfone/poly(ethylene glycol)/poly(*N*-vinyl pyrrolidone) (PESU/PEG/PVP) were developed by combining a solvent-free liquid mixture of PEG/PVP into PESU. Using a single screw extruder, this blend was melted and extruded using an annular slit nozzle where PEG functioned as a plasticizer, i.e., decreased processing temperatures, while PVP aided in retaining the hollow fiber geometry. These hollow fibers were comprised of uniformly closed pores, occurring due to the expansion and formation of bubbles of evaporating PEG nucleated by PVP during extrusion. By immersing these fibers into an aqueous solution of sodium hypochlorite (NaOCl), PEG and PVP were removed, which led to an open porous structure with pore sizes between 100 nm and 1 μ m throughout the membrane. The outer surfaces of the hollow fibers were found to contain a higher PVP content than the inner surface. As PVP and PESU are miscible, i.e., blended in a single phase, treatment with NaOCl led to the creation of open pores on the outer surface with pore sizes between 10 and 150 nm, thus deeming the outer surface functional as a separation layer. The effect of blend composition, extrusion settings, and post-treatment parameters on membrane morphology, water flux, thermal characteristics, and tensile strength was studied, while after the modification, near-pristine PESU membranes were pursued. A water-flux of 28 L/h m² bar and a molecular weight cut-off (MWCO) of 90%, 75%, and 40% for poly(ethylene oxide) of an average of 1000 kDa, 400 kDa, and 100 kDa molecular weight, respectively, proved that via extrusion it is possible to produce hollow fiber membranes for ultrafiltration without the use of organic solvents.

1. Introduction

Hollow fiber membranes have been widely used and studied in the last four decades as they offer high surface area per unit volume and provide high permeability and selectivity for certain applications [1,2]. They are typically manufactured using the spinning process, which uses phase separation processes such as thermally induced phase separation or the non-solvent induced phase separation (NIPS) process, etc. [3–8]. These processes are widely used due to the possibility of producing hollow fibers on a large scale continuously [9]. This process has been improved over the years and hollow fiber membranes of various pore sizes, porosities, selectivities, and/or permeabilities have been developed using different polymers by various researchers. However, this process makes use of organic solvents as an important component that

aids in the formation of pores through phase inversion. Organic solvents such as *N*-methyl-pyrrolidone (NMP), tetrahydrofuran (THF), *N*, *N*-dimethylformamide (DMF), *N,N*-dimethylacetamide (DMAc) are generally used and their selection depends upon their compatibility with the polymers used. Many organic solvents, due to their harm to health [10] and the environment [11,12], are classified by various regulatory authorities as hazardous and it is advised to reduce their use wherever possible [13–16].

Since the publication of the principles of Green Chemistry in 1998 [17], some researchers have attempted to reduce the number of organic solvents used for membrane manufacturing, while some have suggested using sustainable solvents [18–41]. In the membrane industry, organic solvents are recirculated to avoid their wastage, which consumes high amounts of energy, leading to increased emissions [42–44]. Using salt

* Corresponding author.

E-mail address: prokopios.georgopoulos@hereon.de (P. Georgopoulos).

<https://doi.org/10.1016/j.memsci.2023.121837>

Received 27 March 2023; Received in revised form 26 May 2023; Accepted 9 June 2023

Available online 10 June 2023

0376-7388/© 2023 Elsevier B.V. All rights reserved.

dilution-induced phase separation, researchers have been able to manufacture ultrafiltration and nanofiltration polymer membranes. This process takes advantage of the state of the art of the NIPS process using polyanions and polycations without the use of organic solvents during their processing [45,46]. In this work, the aim is to develop an organic solvent-free hollow fiber membrane manufacturing method for commercially inexpensive polymers that are already proven to function well as membrane materials.

Melt extrusion, a process independent of the use of any organic solvents, is used on a large scale in the plastics industry to manufacture continuous products such as pipes, wire-sheath, tapes, etc. The extruder melts and homogenizes the polymer while the extruder's nozzle shapes it into a desired shape as the polymer extrudate exits the extruder. Most thermoplastic polymers that are solid at room temperature and do not undergo cross-linking or degradation on exposure to heat can be extruded using melt extrusion [47]. For example, melt extrusion of polymers such as polypropylene, polyethylene, polycarbonate, polyvinylchloride, polyamide, polysulfone, among others, has been studied by a number of researchers and implemented in the industry [48–54].

A polymer melt, when extruded through an annular slit nozzle, can produce hollow fibers whose length is not limited since this can be a continuous process, but the diameter is possible to be controlled by the size of the slit nozzle. To use these hollow fibers in liquid separation applications as membranes, they need to be porous, permeable and capable of performing a certain degree of separation of substances included in the liquid. Foam extrusion is a well-established method of manufacturing porous extrudate. At the turn of the century, it was attempted to use foam extrusion to manufacture hollow fibers from commercially available polymers [55,56]. Using melt extrusion coupled with foaming, Huang et al. created hollow fiber membranes from polysulfone with pore sizes between 15 and 20 μm and from polycarbonate with pore sizes between 5 and 10 μm [57,58]. However, for ultrafiltration, pore sizes below 100 nm are necessary [59]. However, even after twenty years, foam extrusion cannot produce open-cellular pores with pore sizes in the nanometer range to use as hollow fiber membranes [54,60–62]. Using batch foaming, without the use of organic solvents, flat sheet membranes capable of ultrafiltration were manufactured [63], but the method is limited to its scale and additionally is a slow and non-continuous process.

Melt extrusion, followed by cold/hot-stretching of the extrudate to create a porous structure has been attempted by some researchers. Permeable flat-sheet and hollow fiber membranes manufactured using this method achieved pore sizes down to 50 nm, and exhibited separation capabilities [64–78]. Similar to foam extrusion, the morphology depends on the polymer type and the extruder settings. However, the tensile force exerted during the stretching also plays a vital role. This method is suitable for semi-crystalline polymers, as the crazing phenomenon responsible for pore creation takes advantage of the crystalline structures [79–82].

In this study, using an annular slit nozzle on a single screw melt-extruder, extruded hollow fibers of a polymeric blend were produced. This blend was developed based on polyethersulfone (PESU), a commercially available polymer, widely used for developing ultrafiltration membranes given its excellent chemical, thermal and structural stability [4–6,8,19,25,83–97]. The other components of this blend are water-soluble polymers, such that, the extruded hollow fibers can be treated using inorganic aqueous solutions for their removal. Removal of the water-soluble polymers would then result in a porous structure. The pore size would depend on the miscibility of the polymers and the porosity of the polymer content will be defined by the content of the water-soluble part.

Due to its known application as a pore-forming agent in polymer membranes, low molecular weight polyethylene glycol (PEG), a water-soluble polymer, is selected [3,9,70,93,98–100]. In a previous study, by absorbing liquid-state low molecular weight PEG into PESU, PESU/PEG blends were manufactured [54]. The availability of PESU in

the form of flakes takes advantage of their porous structure, inducing a capillary effect on the liquid PEG and significantly influencing the absorption of PEG into PESU matrix. The most optimum blend combination found in the study was PESU/PEG 80/20. This blend combination was processable in the extruder at processing temperatures $\sim 120^\circ\text{C}$ lower than that of PESU homopolymer. The miscibility of the PESU/PEG blends was investigated and a partially miscible blend, along with some indications of a gel state, was found. This blend, however, yielded a microcellular foam. In this study, we choose to begin with the same blend and extrude without the use of foaming agents.

The extrudate of this blend is found to contain uniformly distributed closed cells resembling a foam but fails in maintaining the hollow fiber structure. The cause is investigated and based on material characterization, as an improvement, another PESU-miscible polymer Poly(*N*-vinyl pyrrolidone) (PVP) [63] is introduced to the blend, thus creating a ternary blend. This ternary blend, at its optimum combination, yields extruded hollow fibers with higher porosity than the binary PESU/PEG blend and maintained the hollow fiber shape after exiting the extruder nozzle. The optimum blend composition and extruder settings are found and the extruded hollow fibers are treated using an aqueous solution of sodium hypochlorite (NaOCl) such that PEG and PVP are dissolved from the blend and a near-pristine PESU membrane is attained. This increases the overall porosity and also creates open pores on the surface of the hollow fibers that render the extruded hollow fibers permeable to water. The effects of various post-treatment parameters on their characteristics, such as water flux, thermal behavior, porosity, etc., are studied and the most influential post-treatment parameters on the dissolution of various components of the blends are found. The filtration performance of the optimized hollow fiber membrane is tested. Thus using a completely organic-solvent-free manufacturing method, hollow fiber membranes are developed whose performance is comparable to the state-of-the-art ultrafiltration membranes that are manufactured using organic solvents.

2. Experimental

2.1. Materials

Commercial grade PESU BASF Ultrason® E 3020 P was offered by BASF SE (Ludwigshafen, Germany) in the form of flakes. PEG 200 in liquid form was purchased from Sigma Aldrich (Taufkirchen, Germany). PVP BASF Luvitec® K 30 was received from BASF SE in powder form. Sodium hypochlorite (NaOCl) with a label concentration of 12% was purchased from Sigma Aldrich. The concentration of active Cl^- content was determined regularly using titration and the pH using a digital pH measurement device (Mettler Toledo, Gießen, Germany). Ultrapure water having resistivity $>18.2\text{ M}\Omega\text{ cm}^{-1}$ was obtained from a Millipore (Merck, Darmstadt, Germany) Direct-Q® UV water purification system [101].

2.2. Blend production

The absorption blending method used to manufacture PESU/PEG blend was followed as mentioned in another publication [54]. To manufacture PESU/PEG/PVP blends, PEG/PVP solutions were prepared by dissolving PVP powder into PEG liquid by physical mixing in a container for 24 h at room temperature in a fume hood. This PEG/PVP solution was then mixed with PESU flakes, similar to the method used

Table 1
Nomenclature of blends used in this study.

Blend Name	PESU [%]	PEG [%]	PVP [%]
P0	80.0	20	0
P2.5	77.5	20	2.5
P5	75.0	20	5.0
P7.5	72.5	20	7.5

for PESU/PEG blend. The polymer composition of the blends developed is given in Table 1, along with the nomenclature of the blends.

2.3. Material characterization

2.3.1. Differential scanning calorimetry (DSC)

DSC 1 (Mettler Toledo, Gießen, Germany) calorimeter was used for DSC and the software STARE SW 16.20 (Mettler Toledo, Gießen, Germany) was used for data evaluation. A 40 μL aluminum pan was filled with ~ 10 mg of polymer and closed with a mono-perforated lid. The heating-cooling-heating cycles were carried out in a nitrogen atmosphere. The temperature interval for the PEG/PVP solution was -130 to 100 $^{\circ}\text{C}$. The heating/cooling rate for the first two cycles was 10 K min^{-1} and 30 K min^{-1} for the third heating to obtain a pronounced glass transition signal [102]. Glass transition temperature (T_g) was evaluated from the third heating. PESU/PEG and PESU/PEG/PVP blends were measured between -130 and 260 $^{\circ}\text{C}$ at a heating/cooling rate of 20 K min^{-1} and T_g was evaluated from the second heating.

2.3.2. Thermogravimetric analysis (TGA)

TGA was conducted using a TG 209F1 Iris (NETZSCH Gerätebau GmbH, Selb, Germany) to observe the thermal stability of polymers. A heating rate of 10 K min^{-1} was used in a temperature interval of 25 $^{\circ}\text{C}$ – 900 $^{\circ}\text{C}$ under argon gas.

2.3.3. Rheology

For rheological measurements on polymer solutions, 0.67 mL of the solution were measured with a cone-plate geometry tool of an Anton Paar MCR 502 rheometer (Anton Paar, Graz, Austria). Viscosities were measured between the frequencies 0.01 – 100 rad/s at a shear rate of 5% .

2.3.4. Turbidity experiment

Equal parts (1:1 by weight) of PEG 200 and aqueous NaOCl solutions (0.1% , 0.2% , 0.4%) were mixed at room temperature twice. The turbidity was observed at room temperature for all solutions. To observe the turbidity at the post-treatment temperatures chosen in this study, one set of bottles of each concentration was subjected to 45 $^{\circ}\text{C}$ in a controlled water bath. In contrast, another set of bottles was subjected to 70 $^{\circ}\text{C}$ similarly. After 2 h of exposure to this temperature, the turbidity of the solutions was visually observed and noted. This experiment was video recorded for monitoring and observation of changes continuously.

2.4. Extrusion of hollow fibers

Hollow fibers were extruded using the single screw extruder Extrusion 19/25 (Brabender GmbH & Co. KG, Duisburg, Germany). The complete extruder setup consisted of two static mixers with a combined length of 20 cm, one melt pump and an annular slit nozzle, in a horizontal setting. The melt pump's gears were removed so as to take advantage of the melt-travel length offered by the pump's construction, allowing the screw speed to determine the throughput of the extruder. A custom-made 'Tubing die head' (Brabender GmbH & Co. KG, Duisburg, Germany), having a 2 mm opening and 1 mm centered needle was used as the annular slit nozzle (see supporting information Fig. S1). Due to presence of melt-pressures up to 200 bar at the nozzle of the melt-extruder, a mechanically stable bore for carrying a bore fluid was not possible to be constructed at these dimensions. However, for particular polymers at certain nozzle temperatures, the melt would form a hollow fiber profile with 2 mm outer diameter and 1 mm inner diameter, thus eliminating the need for a bore fluid. The nozzle extruded the extrudate onto a flat conveyor belt whose speed was manually adjusted to match the extrudate speed without exerting any tension or resistance. The chosen extruder temperatures, as seen in Table 2 were 100 – 120 K higher than the glass transition temperatures of the blends, as observed in DSC measurements.

Table 2

Extruder process settings for the fabrication of the melt-extruded hollow fiber membranes.

Extrusion settings	Values				
	Polymer blend	Blend P0	Blend P2.5	Blend P5	Blend P7.5
Extruder temperature	200 $^{\circ}\text{C}$	220 $^{\circ}\text{C}$	235 $^{\circ}\text{C}$	Not processable with the extruder	
Nozzle temperature	150 $^{\circ}\text{C}$	150, 160 and 170 $^{\circ}\text{C}$	150, 160, 170, 180 and 190 $^{\circ}\text{C}$		
Screw speed	10 RPM	10 RPM	3, 6 and 10 RPM		
Nozzle outer diameter	2 mm				
Nozzle inner diameter	1 mm				
Bore	Solid needle				
Bore fluid	Not applicable				
Drawing/Stretching	Not used				

2.5. Post-treatment of hollow fibers

The post-treatment was carried out by inserting the extruded hollow fibers into a closed bottle of an aqueous solution of NaOCl. The effects of various concentrations of NaOCl solution, temperature, time and pH on the membrane properties were studied. The concentration range of the solutions was 0.01491 – 0.05964 M, whereas room temperature [103], 45 $^{\circ}\text{C}$ and 70 $^{\circ}\text{C}$ were chosen. Temperatures above 70 $^{\circ}\text{C}$ were avoided due to approaching the glass transition temperature of blend P0 (97 $^{\circ}\text{C}$). The temperature was regulated using a jacket heating setup, ultrapure water was used to dilute NaOCl to the required concentration, and hydrochloric acid was used to change the pH value wherever required. Fig. 1 illustrates the schematics of the extruded hollow fiber fabrication process.

2.6. Hollow fiber membrane characterization

2.6.1. Scanning electron microscopy

Scanning electron microscopy (SEM) was carried out on a Merlin microscope (Carl Zeiss AG, Oberkochen, Germany) at an accelerating voltage between 1 and 3 kV, while the detectors used were a high-efficiency secondary electron (HE-SE2) detector and an in-lens secondary electron detector. Samples of hollow fibers were cross-fractured using liquid nitrogen. For cross-sectional imaging of the entire hollow fiber, samples were cut using a sharp razor blade instead of fracturing in liquid nitrogen. Prior to examination, all specimens were sputter-coated with 1.5 nm of platinum using a CCU-010 coating device (Safematic, Switzerland).

2.6.1.1. Pore analysis. For pore analysis, scanning electron microscope images of freeze-fractured samples were recorded at a magnification of $7000\times$. The SEM images were acquired at an accelerating voltage of 1 keV using the HE-SE2 detector. Before measurement, the freeze-fractured specimens were sputter-coated with 1.5 nm platinum. Pore analysis was performed with the software IMS (Imagic Bildverarbeitung AG, Switzerland). Pore analysis included the measurement of the mean pore diameter (in the following referred to as 'pore size') and the area ratio of pores to the total surface area (in the following referred to as 'porosity'). Pores that projected an area smaller than 2000 nm^2 on the SEM images were excluded from the analysis.

2.6.2. Tensile test

Tensile tests were performed at room temperature using a Zwick Roell Z020 (Zwick Roell, Ulm, Germany) using a load cell of 1 kN. Hollow fibers having a length of 55 mm were used. The hollow fibers

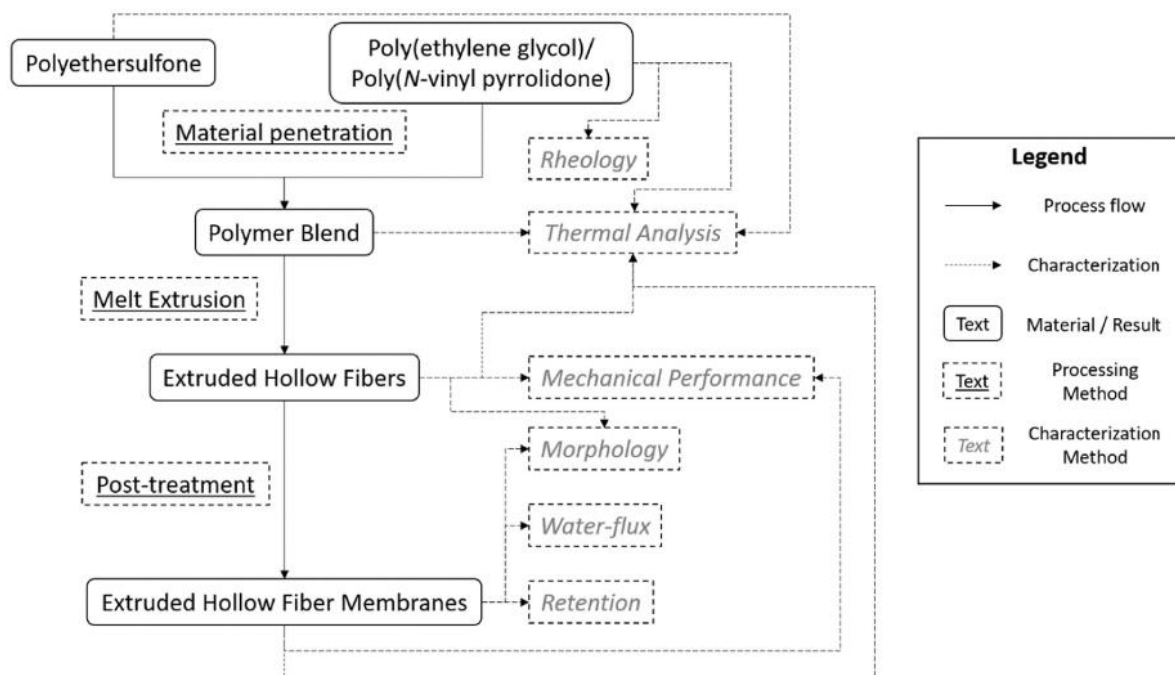


Fig. 1. Melt-extruded hollow fiber membranes preparation procedure.

were dried at 50 °C for 24 h before tensile testing, except for the fibers that were water soaked for 24 h prior to testing.

2.6.3. Water flux

Water flux measurements were performed on individual hollow fiber membranes having lengths between 50 and 70 mm. The measurement setup was an in-house built setup where pressurized ultrapure water was pumped into the fibers in a dead-end setup at 1 bar overpressure for 2 h [104].

2.6.4. Fourier transform infrared spectroscopy

Fourier transform infrared spectroscopy (FTIR) was performed on the inner and outer surface of the extruded hollow fiber membranes using a Bruker Alpha-P, platinum attenuated total reflection equipped with a diamond head (Ettingen, Germany). The measurements were performed by taking 64 scans with a resolution of 4 cm⁻¹ within a spectral range of 400–4000 cm⁻¹.

2.6.5. Retention tests

Retention tests were performed using an in-house built setup at 1 bar overpressure using solutions of 0.02% poly(ethylene oxide) (PEO) with molecular weights equal to $M_w = 8$ kDa, 400 kDa, 100 kDa, and 1000 kDa in ultrapure water [6]. The PEO solutions, feed, retentate and permeate were analyzed using gel permeation chromatography (GPC). The retention coefficient R was calculated using Equation (1), where w_p and w_f are the mass fractions of PEO in permeate and feed solutions, respectively.

$$R = 1 - \frac{w_p}{w_f} \quad (1)$$

3. Results and discussion

The absorption of low molecular weight PEG into PESU to form PESU/PEG blends was possible due to the liquid state of PEG 200 taking advantage of the porous morphology of PESU flakes. Using foam extrusion, the blend P0 is able to produce porous membranes in hollow fiber shape using an annular slit nozzle in foam extrusion [54]. However, in this study, without using any foaming agent, the same blend

could not maintain the shape of the annular slit nozzle after exiting the extruder. The melt's low viscosity at the lowest possible nozzle temperature (T_N) of 150 °C and the absence of a bore fluid, led to the collapse of the hollow fiber structure leading to an extrudate, as shown in Fig. 2(a). At first glance, this blend's extrudate seems improper for further research, but looking at increased magnification in scanning electron microscopy images provides a revelation. Uniformly distributed pores with an average pore size of 270 nm ranging between 70 nm and 700 nm (5th & 95th percentile) across the extrudate, as seen in Fig. 2(b) are observed. This result served as a starting point in exploring the reasoning behind these pores and improving them to create permeable extruded hollow fiber membranes.

As PEG 200 is a liquid, its boiling point lies around 200 °C [105]. Organic liquids, absorbed into polymers are known to behave as foaming agents, thus providing porous morphology in certain foaming methods [106,107]. As the extrusion temperatures are set near or higher than the boiling point of the PEG used, it expands during the extrusion process and leaves behind pores as the blend exits the nozzle. As the extrudate cools down, the PEG reverts to the liquid state and stays in the extrudate, which is then reabsorbed into the PESU matrix. The porous structure remains unchanged due to the increase in the melt-viscosity of the blend due to lower temperatures. The similar thermal decomposition behavior in TGA of the blend P0 and its extrudate, as well as their similar second glass transition temperatures* as shown in Fig. 3(a) and (d), respectively, confirm that the composition of the blend stays the same after extrusion. Removal of one blend component, mainly using organic solvents, to create or increase porosity is a common practice in membrane science. PEG is a water-soluble polymer and can be removed from the blend using water or inorganic solvents such as NaOCl [108,109]. Therefore, the removal of PEG 200 from the P0 blend was pursued by immersing the extrudates in 0.2% aqueous solution of NaOCl for 120 h at 45 °C. This post-treatment caused partial removal of PEG, leading to increased temperature resistance, glass transition temperature and internal porosity as seen in Fig. 3(a), (d) and 4(a-b), respectively. Complete removal was not possible due to the porosity of the extrudate being too low for the NaOCl solution to reach every nook and corner of the extrudate.

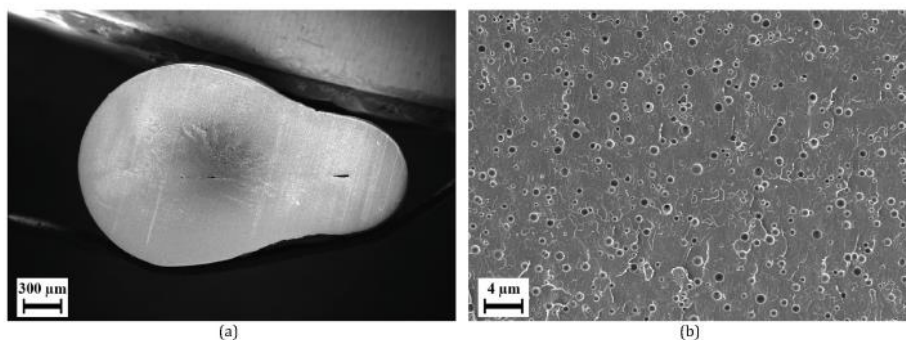


Fig. 2. Scanning electron micrographs of extrudate of blend P0 extruded at $T_N = 150$ °C (a) cross-section (overview); (b) cross-fracture at 2000x magnification.

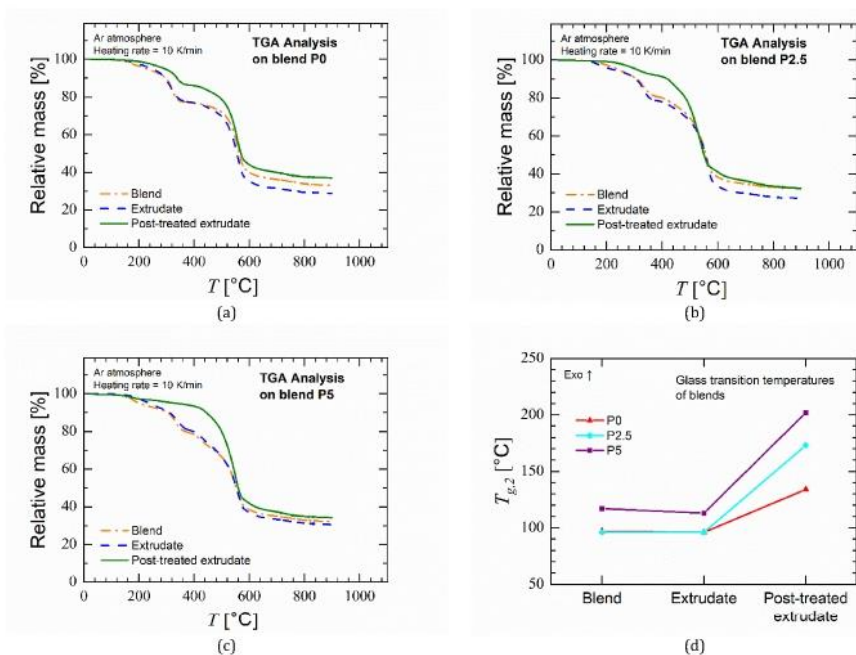


Fig. 3. Thermal analysis of blends P0, P2.5 and P5. TGA Analysis on (a) blend P0; (b) blend P2.5; (c) blend P5; (d) Second glass transition temperature $T_{g,2}$ observed in DSC measurements on the blends, their extrudates and post-treated extrudate.

(*In all blends, there was a visible glass transition of PEG or PEG/PVP; see supporting information in Fig. S2 and in Fig. 3(d), the second glass transition temperature $T_{g,2}$ is shown.).

3.1. Effect of PVP concentration

Decreasing the amount of PEG from PESU/PEG blend might result in the maintenance of the hollow fiber shape at the nozzle. However, as the expansion of PEG creates a porous structure, high amounts of PEG are desirable. In addition, PEG functions as a plasticizer, i.e., it reduces the processing temperatures of the blend. Theoretically, an increase in the amount of water-soluble polymer, i.e., PEG in the blend would appear as a solution to obtain the highest possible porosity during post-treatment. However, processing amounts of PEG larger than 20% in such a blend is not possible in the extruder [54]. Thus to proceed with the same approach, PVP, another water-soluble polymer also used as a pore-forming agent in PESU membranes, was selected [6,84,92,103,110–113]. PVP when blended with PESU increases nucleation and porosity in foams obtained using batch foaming [63]. PVP is also water-soluble in the presence of NaOCl [6,103,112]. The addition of PVP to PEG resulted in a highly viscous PEG/PVP solution. This solution was transparent and had a yellowish color. The measured dynamic viscosities of solutions with 0%, 10%, 20% and 30% PVP in PEG 200 were 56, 545, 2320 and 9787 mPa s, respectively. These percentages correspond to the ratio of PEG and PVP in blends P0, P2.5, P5 and P7.5, respectively. The viscosities of PEG/PVP solutions increase significantly with an increase in PVP content. As the formation of the blend relies on the absorption of liquid into PESU flakes by capillary forces exerted by

the porous flakes as well as their rough surface, a very high viscosity would not be feasible for this method. Therefore, blend formulation will not take place above a certain amount of PVP. Due to the high viscosity of PEG/PVP 70/30 solution (9787 mPa s), PEG/PVP solution was not fully absorbed into PESU. This resulted in the blend P7.5 not being processable as the unabsorbed solution blocked the extruder hopper.

However, the blends P2.5 and P5 were processable in the extruder. The extrudates of blend P2.5 did not form a hollow fiber geometry at the nozzle similar to the blend P0 except for the lowest nozzle temperature, i.e., 150 °C, where the desired geometry was obtained. Extrudates of blend P5 produced a hollow fiber geometry at all nozzle temperatures. PVP is known to cross-link on exposure to high temperatures [114], which causes an increase in the storage modulus, thus increasing elasticity. Therefore, the storage modulus of blends increases with an increase in PVP content allowing the fibers to maintain the shape of the annular slit nozzle, thus producing hollow fibers. The cross-sections of the extrudate from the blends P2.5 and P5 at various nozzle temperatures are shown in the supporting information in Figs. S3 and S4.

As seen in Fig. 4, the scanning electron micrographs of fibers extruded at nozzle temperature 150 °C for the blends P0, P2.5 and P5 reveal that the addition of PVP increases the porosity of the extrudate. This porosity is further increased after post-treatment with an aqueous solution of 0.2% NaOCl at 45 °C for 120 h. The thermal decomposition behavior and the second glass transition temperature observed for the

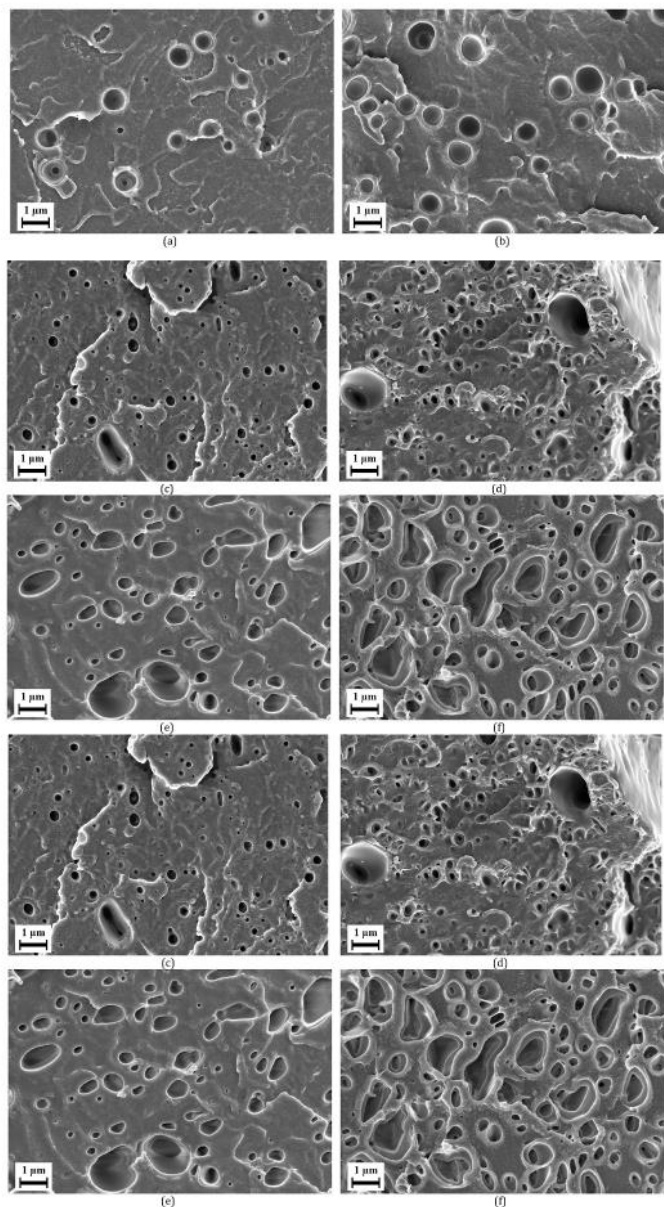


Fig. 4. Scanning electron micrographs of cross-fractured extrudates extruded at $T_N = 150\text{ }^\circ\text{C}$ and $U = 10\text{ RPM}$: (a) non-post-treated extrudate of blend P0; (b) post-treated extrudate of blend P0; (c) non-post-treated extrudate of blend P2.5; (d) Post-treated extrudate of blend P2.5; (e) non-post-treated extrudate of blend P5; (f) post-treated extrudate of blend P5.

extruded hollow fibers, before and after the post-treatment, as shown in Fig. 3, shows that the post-treatment increased the thermal resistance of the fibers for all the blends. This change is more pronounced for the blends with higher concentrations of PVP. As the increase in PVP contributed to increased porosity, NaOCl solution could reach more volume of the material, thus dissolving more larger amount of polymer. The glass transition temperature observed for post-treated extruded hollow fiber of blend P5 is $202\text{ }^\circ\text{C}$, nearest to that of PESU ($228\text{ }^\circ\text{C}$ [63]). With these results, it can be said with confidence that the post-treatment dissolved the PEG and PVP from the extruded hollow fibers of blend P5, thus leading towards highly porous hollow fibers comprising mostly only PESU.

3.2. Effect of extruder speed

To study the influence of extruder screw speed on the extruded

hollow fibers of blend P5, a constant nozzle temperature of $150\text{ }^\circ\text{C}$ was selected and three screw speeds were tried. The extrudates produced at 3 and 6 RPM were too brittle to handle, making a realistic application of them as hollow fiber membranes impossible. However, the ones produced at 10 RPM were more structurally stable. Performing tensile tests of these fibers quantified their structural stability, as seen in Fig. 5(a). The tensile tests revealed very low stress at break below 5 MPa and 9 MPa for fibers produced at a speed of 3 and 6 RPM, respectively, while also a much higher value of 25 MPa for the fibers produced at 10 RPM was observed. A low screw speed means that the foaming agent, PEG in this case, is exposed to the extruder temperature for a longer time leading to higher expansion and the creation of larger pores [115]. In addition, longer exposure of PVP to the extruder temperature causes a higher degree of cross-linking, thus causing the fibers to be stiffer. Fig. 5 (b) shows the tensile test results of extruded hollow fibers produced at $T_N = 150\text{ }^\circ\text{C}$ and compares the tensile strength between untreated hollow fibers and those treated with 0.2% NaOCl at $45\text{ }^\circ\text{C}$ for 120 h. The increased porous structure due to the post-treatment reduces the stress at break by 40%. The tensile performance of an extruded hollow fiber that was soaked in water for 24 h after post-treatment is also investigated to observe the realistic mechanical behavior the fibers would face if applied in a membrane module for water filtration at a certain pressure. The value of stress at break is higher than those found in the literature for polymeric hollow fiber membranes [3,9,85,91], thus confirming the mechanical stability of these hollow fibers when used as membranes.

3.3. Effect of nozzle temperature

By performing pore analysis on extruded hollow fibers, the influence of certain processing parameters on the membrane-relevant properties such as pore size and porosity was determined. Fig. 6(a) shows that with decreasing nozzle temperature, the average pore size decreases and the porosity increases except for the fibers fabricated at $160\text{ }^\circ\text{C}$. In this case, a larger median pore size than that of the fibers made at $150\text{ }^\circ\text{C}$ and $170\text{ }^\circ\text{C}$ as well as the highest porosity can be observed. This is a similar behavior to various foam extrusion studies done where an optimum temperature is found between the highest and lowest possible nozzle temperature [54,115,116]. With a decreased nozzle temperature, the nozzle pressure increases causing more nucleation whereas, the expansion of the pores is restricted due to increase in the viscosity of the melt caused by the decreased temperature, which leads to smaller pore sizes. At $150\text{ }^\circ\text{C}$, although the higher viscosity of the melt caused the pores to remain smaller, the increased pressure was unable to overpower the high viscosity to cause higher porosity, as it did at $T_N = 160\text{ }^\circ\text{C}$. An optimum nozzle temperature is where the pressure inside the extruder is high enough and melt-viscosity low enough to lead to the smallest pore sizes and high porosity.

3.4. Effect of post-treatment

After post-treatment, the increase observed in porosity is similar to hollow fibers extruded at all nozzle temperatures, thus the highest porosity was observed for hollow fibers extruded with $T_N = 160\text{ }^\circ\text{C}$, as seen in Fig. 6(b and c). The extruded hollow fibers did not exhibit any water flux before the post-treatment. However, as Fig. 6(d) shows, after the post-treatment the ones extruded at nozzle temperatures between $150\text{ }^\circ\text{C}$ and $170\text{ }^\circ\text{C}$ did have water flux through them. Nozzle temperature $160\text{ }^\circ\text{C}$ provided the highest water flux and $150\text{ }^\circ\text{C}$ the lowest. The highs and lows of water flux results correspond to the porosity values of the post-treated extruded hollow fibers. The fibers extruded at $180\text{ }^\circ\text{C}$ and $190\text{ }^\circ\text{C}$, although they had porosity equal to or higher than the fibers created at $170\text{ }^\circ\text{C}$ after post-treatment, they failed to provide a water flux. This is mainly due to the formation of too large pores that increase the porosity value although interconnections between pores are missing. Therefore, it can be said that, for the extruded hollow fibers that are

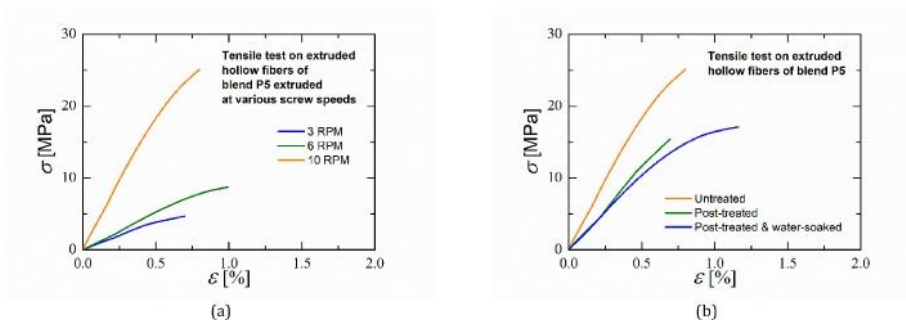


Fig. 5. Tensile tests on extruded hollow fibers: (a) effect of rotational speed of extruder screw on the tensile strength of extruded hollow fibers of blend P5; (b) comparison between non-post-treated and post-treated extruded hollow fiber.

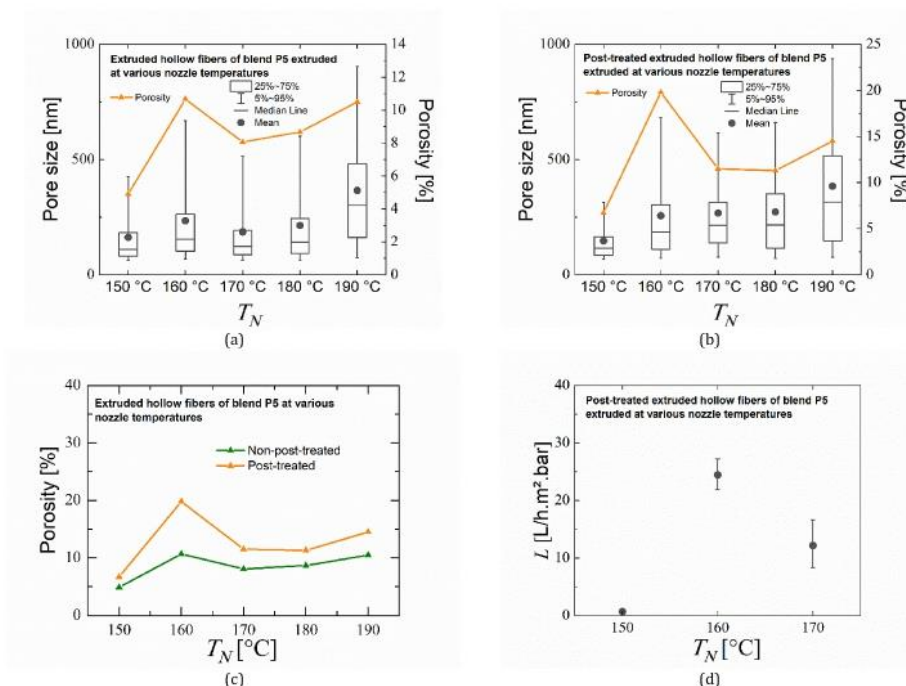


Fig. 6. Effect of extrusion process settings on extruded hollow fibers of blend P5. (a) Pore size distribution and porosity versus nozzle temperature (T_N) of untreated extruded hollow fibers; (b) Pore size distribution and porosity versus T_N of post-treated extruded hollow fibers; (c) Comparison of porosity versus T_N of post-treated hollow fiber membranes; (d) Water flux versus T_N of post-treated hollow fiber membranes.

permeable, the porosity values correspond directly to the amount of water flux. The obtained water flux at certain process settings provides the first indication of the possible usage of these porous hollow fibers as membranes.

Fig. 7 shows the scanning electron micrographs of post-treated extruded hollow fibers of blend P5. In Fig. 7(b), the cross-sectional micrograph shows that the internal pores are partially connected to each other. These connections could also have led to higher pore sizes detected during pore analysis as an increased average and median pore size is seen for fibers extruded at this temperature in Fig. 6(b). The pores on the inner and the outer surface in Fig. 7(c) and (d), respectively, together with the cross-sectional pores, facilitate the permeability of water through these fibers, as seen in the water flux results of Fig. 6(d). The inner surface appears rough with pore sizes ranging from a few hundred nanometers to a few micrometers. However, the pores on the outer surface are much smaller, i.e., below 150 nm. The rough surfaces does not allow for a correct measurement during pore analysis and therefore are not measurable similarly to the cross-sectional pores. During extrusion, at the annular slit nozzle, the outer surface of the fiber is directly exposed to the metallic surface throughout the nozzle that is actively tempered, while the internal pin that aids in the formation of

the hollow fiber geometry is not. This exposes the outer surface of the extrudate to a higher temperature than the inner surface. Therefore, as PEG is known to leach out of the blend and evaporate at temperatures near to its boiling point [54,117], the outer surface has a much lower amount of PEG than the rest of the hollow fiber. After evaporation of PEG from the outer surface, mostly PESU and PVP remain, whose blend is miscible [63]. Due to the complete miscibility of PESU/PVP, removal of PVP through post-treatment yields a pore size of less than 100 nm. The partial miscibility of PESU/PEG/PVP blend as observed due to the presence of two glass transitions in DSC measurements, causes the rest of the hollow fiber, including the inner surface, to yield a larger pore size. Also, the shear stress on the outer surface occurring during extrusion produces a layer of dense polymer [4], avoiding any foaming to take place from the remnants of PEG. Therefore, due to this dense surface, the non-post-treated extruded hollow fibers had no water flux. Measurement of the exact temperatures of the metal surfaces of the nozzle was not possible due to the very small nozzle dimensions between 1 and 2 mm.

By performing FT-IR spectroscopy on the inner and outer surfaces of untreated extruded hollow fibers, the qualitative content estimation of PVP can be identified. Fig. 8 clearly indicates a difference between the

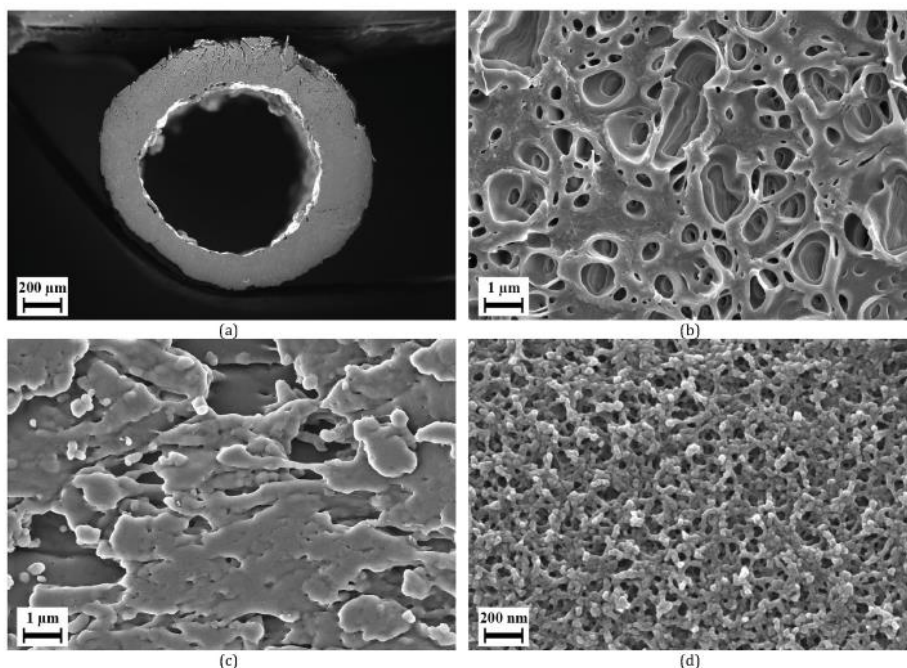


Fig. 7. Scanning electron micrographs of extruded hollow fiber of blend P5 extruded at $T_N = 160\text{ }^\circ\text{C}$ and post-treated using an aqueous solution of 0.2% NaOCl for 120 h at $45\text{ }^\circ\text{C}$: (a) cross-section image of the whole fiber, (b) cross-fracture showing the interior of the fiber wall, (c) inner surface and (d) outer surface of the hollow fiber.

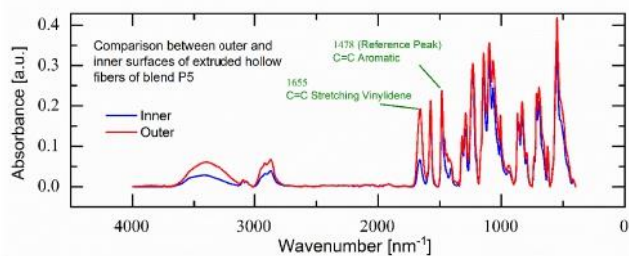


Fig. 8. FT-IR absorbance (arbitrary units (a.u.)) on the outer (red curve) and inner (blue curve) surface of extruded hollow fibers. (For interpretation of the references to color in this figure legend, the reader is referred to the Web version of this article.)

intensity of the principle vibrations of PVP (at 1655 nm^{-1}) between the inner and outer surface when a principal PESU vibration is taken as a reference. These measurements support the above hypothesis related to surface pore formation, as the outer surface has a higher amount of PVP content than the inner surface. The pores on the outer surface of the hollow fibers are not present uniformly throughout the fiber and non-porous areas exist on the outer surface of the post-treated hollow fibers, as shown in supporting information Fig. S6. This leads to a lower water flux, as shown in Fig. 6(d), than the PESU ultrafiltration hollow fiber membranes in literature [3,5,7,85,118,119].

To optimize the hollow fibers even further in obtaining higher porosity and flux thereof, the influence of post-treatment parameters is investigated. It can be theoretically appealing to dissolve the water-soluble polymers only partially, thus obtaining much better separation performance due to the smaller pore sizes. However, for filtration applications where water or water-based substances are used, the flux through the membrane would eventually cause the remaining water-soluble polymers to leach out of the fibers, thus increasing the pore sizes and not delivering the expected separation performance. Therefore, complete or near-complete dissolution of the water-soluble polymers is aimed during the post-treatment. The amount of time taken for

0.2% NaOCl to dissolve PEG and PVP from the extruded hollow fibers can be visualized by the change in glass transition temperature over time in Fig. 9. The closer the glass transition temperature is to that of PESU ($228\text{ }^\circ\text{C}$ [63]), the less amount of PEG and PVP are present in the fibers. The glass transition temperature of the fiber remains unchanged between 100 h and 120 h, which indicates that there is no change seen in the polymer composition of the extruded hollow fiber. Therefore, the initially selected time of 120 h is ideal for this concentration to ensure maximum dissolution.

Fig. 10 shows the effect of the post-treatment temperature on the characteristics of the extruded hollow fibers. At 0.2% concentration, although the pore sizes do not change significantly with increasing temperature, the internal porosity peaks at $45\text{ }^\circ\text{C}$ where the water flux is also at the highest. Fig. 11 shows the effect of the concentration of an

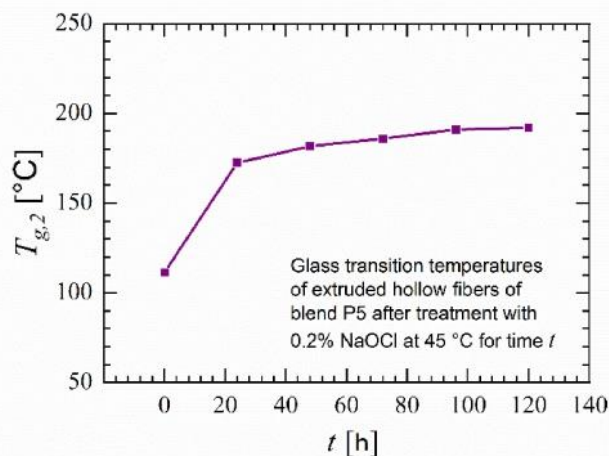


Fig. 9. Effect of the post-treatment time on the glass transition temperature of the extruded hollow fibers when treated with an aqueous solution of 0.2% NaOCl at $45\text{ }^\circ\text{C}$.

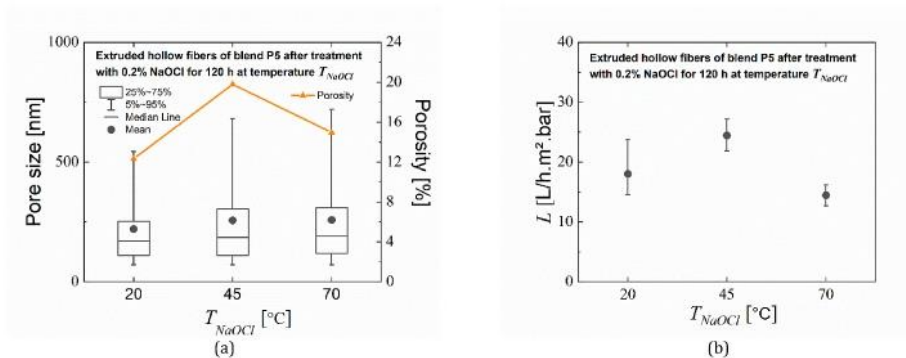


Fig. 10. Effect of temperature on the extruded hollow fibers treated with aqueous solution of 0.2% NaOCl for 120 h. (a) Pore size distribution and porosity; (b) Water flux.

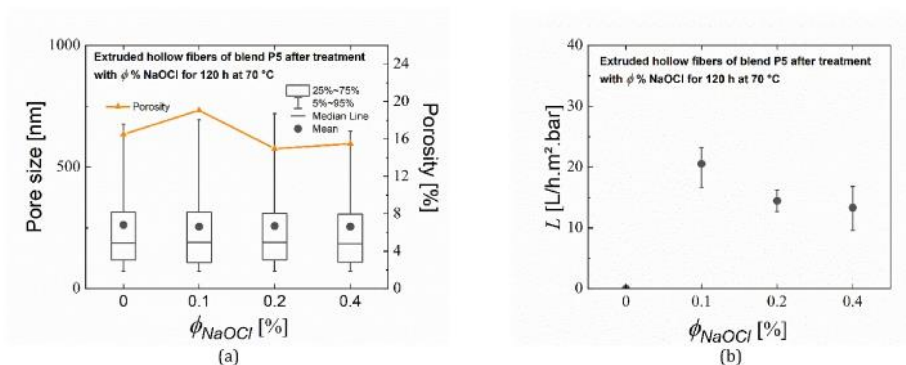


Fig. 11. Effect of concentration of NaOCl aqueous solution on the extruded hollow fibers after 120 h at 70 °C. (a) Pore size distribution and porosity; (b) Water flux.

aqueous solution of NaOCl on the fiber characteristics at 70 °C. Here as well, the concentration providing the highest internal porosity and highest water flux is the same. However, it appears that the solution concentration does not have any noticeable effect on the internal pore sizes of the extruded hollow fibers. Internal porosities for all concentrations are of a similar order, i.e., between 15 and 20%. However, this internal porosity is unable to allow water flux through the hollow fibers when post-treated at 0% concentration, i.e., only water. As discussed earlier, the outer surface of the fibers becomes porous by the sole dissolution of PVP from PESU/PVP blend. Although pure water can dissolve PVP as a homopolymer, it is unable to dissolve it from the PESU/PVP surface of the fibers in contrast to the aqueous solution of NaOCl. This can be confirmed by observing the SEM of the outer surface of this water post-treated fiber in Fig. S7 of supporting information, which is non-porous. Therefore, failure of dissolution of PVP from the outer surface leads towards non-permeability of the extruded hollow fibers treated with pure water. Fig. 12 shows the effect of the pH of 0.1%

solution of NaOCl on the fiber characteristics at 70 °C. The internal porosity, pore size distribution and water flux are highest at 12.35 pH value. However, the median and average internal pore sizes are not significantly different.

By comparing selected data from the above results, as visualized in Fig. 13, it can be observed that the effect of temperature on the porosity and the water flux of the extruded hollow fibers is different at different concentrations of NaOCl. As discussed earlier, NaOCl is the major driving force for the dissolution of PVP from the fibers than water, whereas the dissolution of PEG is dependent on both water and NaOCl. However, the lowest critical solution temperature (LCST) for the solution of PEG and aqueous NaOCl is different for different concentrations of NaOCl. This temperature affects the dissolution of PEG into NaOCl solution at the treatment temperature, thus affecting the formation and expansion of pores. This was qualitatively verified by carrying out turbidity experiments on solutions of equal amounts of PEG and aqueous solution of NaOCl at various concentrations at different temperatures.

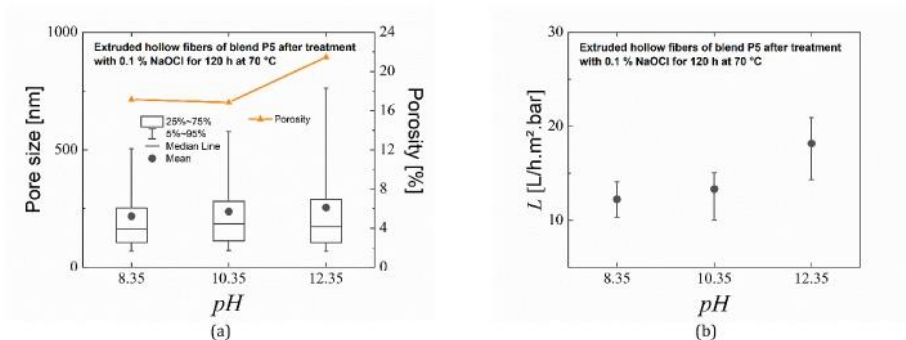


Fig. 12. Effect of pH of 0.1% NaOCl aqueous solution on the extruded hollow fibers after 120 h at 45 °C. (a) Pore size distribution and porosity; (b) Water flux.

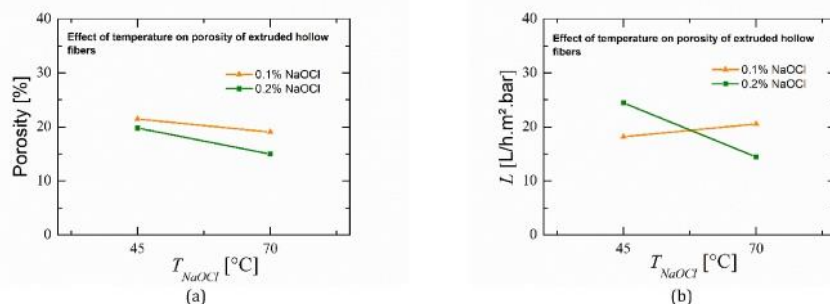


Fig. 13. Effects of temperature at different concentrations of NaOCl for 120 h on the extruded hollow fibers' characteristics. (a) Pore size distribution and porosity; (b) Average water flux.

As shown in Fig. 14, the solution with 0.4% NaOCl was turbid at all temperatures, the solution with 0.2% NaOCl was turbid at 70 °C and the 0.1% NaOCl solution was clear at all measured temperatures. As the 0.2% NaOCl solution failed to dissolve PEG at 70 °C completely, the internal porosity remained low, thus causing lower water flux to occur. For 0.1% NaOCl, complete dissolution of the same amount of PEG is possible at both 45 and 70 °C, which causes the porosity and water flux of the fibers not to show a significant difference. At 45 °C, although the internal porosity of the fibers treated with 0.1% and 0.2% concentrations of NaOCl remains similar, the water flux is higher for 0.2%. As NaOCl facilitates the dissolution of PVP from the outer surface, creating open pores while its higher concentrations yield a better flux. As 0.4% NaOCl fails to dissolve enough PEG from the fiber itself, it fails to increase the internal porosity, thus causing a lower water flux.

3.5. Performance of an optimized extruded hollow fiber membrane

This investigation shows that 0.2% NaOCl at 45 °C for 120 h can assist in the highest dissolution of PVP. Still, the highest dissolution of PEG is possible at higher temperatures with pure water. Therefore, an extruded hollow fiber of blend P5 extruded at $T_N = 160$ °C with a screw speed of 10 RPM when immersed in 0.2% NaOCl at 45 °C for 120 h and then immersed with pure water at 70 °C for 120 h should aid in the maximum possible dissolution of the water-soluble components of the extruded hollow fiber. A fiber treated using these parameters yielded the highest water flux measured till now of 28 L/h.m².bar and the highest glass transition temperature measured till now of 206 °C during the second heating in DSC measurement. This showed that the water-soluble components were dissolved at most and the highest possible porosity was achieved. This glass transition temperature is similar to that found

in the literature for PESU hollow fiber membranes prepared using wet spinning [4].

In order to validate this extruded hollow fiber for membrane applications, retention tests were carried out to observe the separation of molecules of poly(ethylene oxide) of various molecular weights dissolved in water. Fig. 15 shows the retention coefficients obtained by this post-treated extruded hollow fiber for different molecular weights of PEO.

The hollow fiber membrane provides a retention coefficient of 0.9, i. e., 90% molecular weight cut-off (MWCO) for molecules of PEO 1000 kDa. This confirms that the post-treated extruded hollow fibers are capable of ultrafiltration [90,120,121]. The retention coefficient decreases with a decrease in the PEO molecular weight. In addition, due to the outer surface not being completely open, the water-flux is low. The retention and water-flux are lower than those found in the literature with fibers manufactured using conventional methods involving organic solvents and semi-crystalline melt-extruded membranes fabricated by stretching [3,5,7,32,64–78,85,118,119,122,123]. However, the development of porous hollow fibers, capable of performing ultrafiltration and having a measurable flux, from an entirely new method, which does not use organic solvents, neither utilizes melt-state compounding for developing the blend, nor has to be processed at the processing temperatures of PESU, i. e., 300–350 °C, provides a gateway towards various studies involving optimizations of each aspect of this process.

3.6. Future scope

In future studies, to maximize performance or develop other membrane applications, other polymers could be used instead of the ones

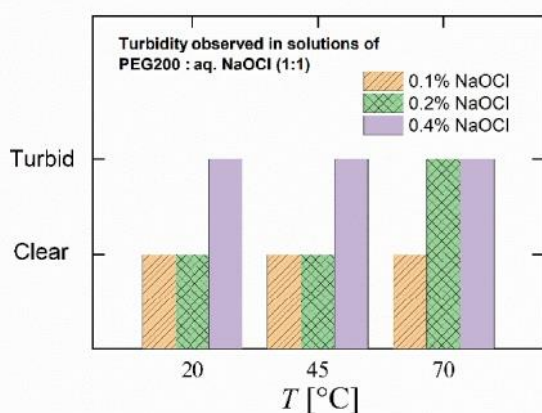


Fig. 14. Clarity/turbidity observed during turbidity experiment at different concentrations of NaOCl on equal parts PEG 200.

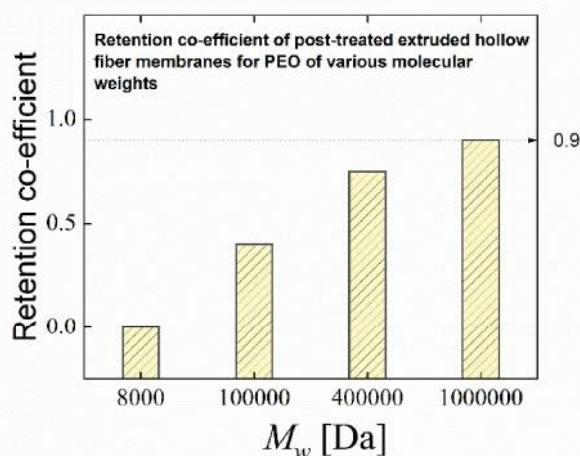


Fig. 15. Retention test results: Retention coefficients versus molecular weights of PEO permeating the extruded hollow fiber membrane.

used here. One could use another molecular weight of PESU or a different water-insoluble polymer than PESU, such as polyacrylonitrile (PAN), etc., other water-soluble polymers could replace PEG, PVP or both; post-treatment with water-based solutions other than NaOCl can be experimented with depending on the polymer; an overall optimization of materials and process could speed up the membrane fabrication. Furthermore, as the separation layer is on the outer surface of the hollow fiber membrane, more precise membrane characterization can be carried out by performing outside-inside water flux and retention measurements. The recovery of PEG and PVP from the aqueous NaOCl solution after post-treatment will lead towards a highly sustainable process, whereas a better combination of polymers could yield enough porosity such that performing post-treatment to enable water permeability is not required. This, however, is out of the scope of this work. This method can also be used to produce extruded flat-sheet ultrafiltration membranes by using a flat slit nozzle at the extruder.

4. Conclusion

The discovery of uniformly distributed pores in the extrudate of blends of polyethersulfone/poly(ethylene glycol) (PESU/PEG) led towards a series of improvements to porous hollow fiber membranes that indicated ultrafiltration capabilities. A ternary blend of PESU/PEG/Poly (*N*-vinyl pyrrolidone) (PESU/PEG/PVP) was developed whose extruded hollow fibers were treated with aqueous solution of sodium hypochlorite (NaOCl). The blend was produced through material penetration method, using neither organic solvents nor melt-state compounding. It was found that the addition of PVP to the PESU/PEG blend matrix resulted in the extruder retaining the hollow fiber shape due to added elasticity. This also resulted in an increase of porosity that was further increased by the treatment with NaOCl after which water-permeability was obtained. Effects of various process settings such as extruder screw speed, nozzle temperature, post-treatment time, temperature, concentration, pH on the extruded hollow fibers's properties such as pore size, porosity and waterflux were investigated. Complete or near complete dissolution of PEG and PVP was aimed and the glass transition temperature of the post-treated hollow fiber was used as an indicator to determine the saturation time where near-PESU hollow fibers remained. A non-linear effect of temperature was seen on the fiber characteristics for certain concentrations of NaOCl. Turbidity measurements concluded that PEG and PVP have different mechanisms of dissolution that depend upon the concentration of the NaOCl solution, such as the insolubility of PEG at higher concentrations of NaOCl at higher temperatures. The outer surface with a very high concentration of PVP delivered nano-cellular open pores connected to the larger internal pores of the rest of the fiber, with higher concentration of PEG. The synergetic performance of PEG and PVP was instrumental in creating the separation layer that resulted in the optimized fiber having a 90% MWCO for PEO 1000 kDa and reasonable filtration for lower PEO molecular weights. The produced hollow fiber membranes do not possess the state-of-the-art performance of those produced using other methods involving organic solvents. However this novel method delivers membranes in hollow fiber geometry with a decent water flux of 28 L/h·m²·bar and ultrafiltration performance in one single study, providing a dawn of opportunities towards realizing state of the art performance. This method, of producing hollow fiber ultrafiltration membranes without using organic solvents, brings membrane science one step closer towards reaching sustainability; whereas future improvements, such as the recovery of PEG and PVP after post-treatment, or material/process optimizations deeming the post-treatment unnecessary, would make total sustainability attainable.

Author contributions

Conceptualization and methodology, A.R. and P.G.; Material and membrane characterization, A.R. and J.K.; extrusion trials, A.R. and J.K.; SEM and pore analysis, E.S.; writing-original draft preparation, A.R.;

writing - review and editing, A.R., P.G., J.K. and E.S. ; analysis of data and graphical visualization, A.R.; scientific supervision, P.G.; All authors have read and agreed to the published version of the manuscript.

Declaration of competing interest

The authors declare that they have no known competing financial interests or personal relationships that could have appeared to influence the work reported in this paper.

Data availability

Data will be made available on request.

Acknowledgments

The authors thank Ivonne Ternes (thermal analysis), Kristian Buhr (rheology), Petra Marten, Maren Brinkmann (GPC), Barbara Bajer (pH measurement), Martin Held, Evgeni Sperling (microscopy), and Sarah Glaß (scientific discussions). The authors greatly acknowledge Volker Abetz for his scientific input and ideas. The donation of PESU and PVP by Oliver Gronwald and Erik Gubbels (BASF SE) is gratefully acknowledged.

Appendix A. Supplementary data

Supplementary data to this article can be found online at <https://doi.org/10.1016/j.memsci.2023.121837>.

References

- [1] Xiaoyao Tan, Shaomin Liu, K. Li, Preparation and characterization of inorganic hollow fiber membranes, *J. Membr. Sci.* 188 (1) (2001) 87–95, [https://doi.org/10.1016/S0376-7388\(01\)00369-6](https://doi.org/10.1016/S0376-7388(01)00369-6).
- [2] Dongliang Wang, K. Li, W.K. Teo, Preparation and characterization of polyvinylidene fluoride (pvdf) hollow fiber membranes, *J. Membr. Sci.* 163 (2) (1999) 211–220, [https://doi.org/10.1016/S0376-7388\(99\)00181-7](https://doi.org/10.1016/S0376-7388(99)00181-7).
- [3] X.Y. Fu, H. Matsuyama, M. Teramoto, H. Nagai, Preparation of polymer blend hollow fiber membrane via thermally induced phase separation, *Separ. Purif. Technol.* 52 (2) (2006) 363–371, <https://doi.org/10.1016/j.seppur.2006.05.018>.
- [4] Tai-Shung Chung, Jian-Jun Qin, Juan Gu, Effect of shear rate within the spinneret on morphology, separation performance and mechanical properties of ultrafiltration polyethersulfone hollow fiber membranes, *Chem. Eng. Sci.* 55 (6) (2000) 1077–1091, [https://doi.org/10.1016/S0009-2509\(99\)00371-1](https://doi.org/10.1016/S0009-2509(99)00371-1).
- [5] Zhen-Liang Xu, F. Alsahy Qusay, Polyethersulfone (pes) hollow fiber ultrafiltration membranes prepared by pes/non-solvent/nmp solution, *J. Membr. Sci.* 233 (1) (2004) 101–111, <https://doi.org/10.1016/j.memsci.2004.01.005>.
- [6] L. Grunig, U.A. Handge, J. Koll, O. Gronwald, M. Weber, B. Hankiewicz, N. Scharnagl, V. Abetz, Hydrophilic dual layer hollow fiber membranes for ultrafiltration, *Membranes* 10 (2020) 7, <https://doi.org/10.3390/membranes10070143>.
- [7] K. Sankhala, J. Koll, M. Radjabian, U.A. Handge, V. Abetz, A pathway to fabricate hollow fiber membranes with isoporous inner surface, *Adv. Mater. Interfac.* 4 (2017) 7, <https://doi.org/10.1002/admi.201600991>.
- [8] N. Noor, J. Koll, N. Scharnagl, C. Abetz, V. Abetz, Hollow fiber membranes of blends of polyethersulfone and sulfonated polymers, *Membranes* 8 (2018) 3, <https://doi.org/10.3390/membranes8030054>.
- [9] Qinglei Zhang, Xiaolong Lu, Lihua Zhao, Preparation of polyvinylidene fluoride (pvdf) hollow fiber hemodialysis membranes, *Membranes* (2014) 1, <https://doi.org/10.3390/membranes4010081>.
- [10] J. Donald Millar, Organic Solvent Neurotoxicity, Center for Disease Control (CDC), 1987. <https://www.cdc.gov/niosh/docs/87-104/default.html>.
- [11] Hang Mei, Huajing Liu, Qianqian Shang, Ying Dong, Stig Pedersen-Bjergaard, Chuxiu Huang, Xiantao Shen, Organic-solvent-free electromembrane extraction based on semi-interpenetrating polymer networks, *Green Chem.* 23 (4) (2021) 1782–1793, <https://doi.org/10.1039/D1GC00148E>.
- [12] Mayamin Razali, Jeong F. Kim, Martin Attfield, Peter M. Budd, Enrico Dioli, Moo Lee Young, Gyorgy Szekeely, Sustainable wastewater treatment and recycling in membrane manufacturing, *Green Chem.* 17 (12) (2015) 5196–5205, <https://doi.org/10.1039/C5GC01937K>.
- [13] "Preventing Adverse Health Effects from Exposure To: Dimethylformamide (Dmf)." The National Institute for Occupational Safety and Health; Centers for Disease Control and Prevention, <https://www.cdc.gov/niosh/docs/90-105/default.html> (accessed 13 February 2022).
- [14] Åkesson, Dr Bengt. "N-Methyl-2-Pyrrolidone." World Health Organization, <https://www.who.int/ipcs/publications/cicad/en/cicad35.pdf> (accessed 13 February 2022).

- [15] "Dimethyl Acetamide." New Jersey Department of Health and Senior Services. <https://nj.gov/health/eoh/rdkweb/documents/fs/0736.pdf>. (Accessed 13 February 2022).
- [16] ECHA, European Chemicals Agency, Formic acid. <https://echa.europa.eu/de/substance-information/-/substanceinfo/100.000.527>. (Accessed 13 February 2022).
- [17] Paul T. Anastas, John C. Warner, *Green Chemistry*, *Frontiers* 640 (1998) 1998.
- [18] A. Figoli, T. Marino, S. Simone, E. Di Nicolò, X.M. Li, T. He, S. Tornaghi, E. Drioli, Towards non-toxic solvents for membrane preparation: a review, *Green Chem.* 16 (9) (2014) 4034–4059, <https://doi.org/10.1039/C4GC00613E>.
- [19] C. Ursino, F. Russo, R.M. Ferrari, M.P. De Santo, E. Di Nicolò, T. He, F. Galiano, A. Figoli, Polyethersulfone hollow fiber membranes prepared with Polarclean® as a more sustainable solvent, *J. Membr. Sci.* 608 (2020), 118216, <https://doi.org/10.1016/j.memsci.2020.118216>.
- [20] Francesca Russo, Francesco Galiano, Francesco Pedace, Fabio Aricò, Figoli Alberto, Dimethyl isosorbide as a green solvent for sustainable ultrafiltration and microfiltration membrane preparation, *ACS Sustain. Chem. Eng.* 8 (1) (2020) 659–668, <https://doi.org/10.1021/acsschemeng.9b06496>.
- [21] Francesco Galiano, Abdulsattar H. Ghanim, Khalid T. Rashid, Tiziana Marino, Silvia Simone, Qusay F. Alsahy, Figoli Alberto, Preparation and characterization of green polylactic acid (pla) membranes for organic/organic separation by pervaporation, *Clean Technol. Environ. Policy* 21 (1) (2019) 109–120, <https://doi.org/10.1007/s10098-018-1621-4>.
- [22] Tiziana Marino, Francesco Galiano, Silvia Simone, Figoli Alberto, DmsolTM as novel non-toxic solvent for polyethersulfone membrane preparation, *Environ. Sci. Pollut. Control Ser.* 26 (15) (2019) 14774–14785, <https://doi.org/10.1007/s11356-018-3575-9>.
- [23] T. Marino, F. Galiano, A. Molino, A. Figoli, New frontiers in sustainable membrane preparation: cyreneTM as green bioderived solvent, *J. Membr. Sci.* 580 (2019) 224–234, <https://doi.org/10.1016/j.memsci.2019.03.034>.
- [24] Francesca Russo, Roberto Castro-Muñoz, Francesco Galiano, Figoli Alberto, Unprecedented preparation of porous Matrimid® 5218 membranes, *J. Membr. Sci.* 585 (2019) 166–174, <https://doi.org/10.1016/j.memsci.2019.05.036>.
- [25] Tiziana Marino, Enrico Blasi, Sergio Tornaghi, Emanuele Di Nicolò, Figoli Alberto, Polyethersulfone membranes prepared with Rhodiasolv®Polarclean as water soluble green solvent, *J. Membr. Sci.* 549 (2018) 192–204, <https://doi.org/10.1016/j.memsci.2017.12.007>.
- [26] Tiziana Marino, Serenella Blefari, Emanuele Di Nicolò, Figoli Alberto, A More Sustainable Membrane Preparation Using Triethyl Phosphate as Solvent 6 (3) (2017) 295–300, <https://doi.org/10.1515/gps-2016-0165>.
- [27] T. Marino, F. Russo, A. Criscuoli, A. Figoli, Tamisolve® nxx as novel solvent for polymeric membrane preparation, *J. Membr. Sci.* 542 (2017) 418–429, <https://doi.org/10.1016/j.memsci.2017.08.038>.
- [28] Alena Randová, Lidmila Bartovská, Pavel Morávek, Pavel Matějka, Miroslava Novotná, Stanislava Matějková, Enrico Drioli, Figoli Alberto, Marek Lanc, Karel Friess, A fundamental study of the physicochemical properties of Rhodiasolv®Polarclean: a promising alternative to common and hazardous solvents, *J. Mol. Liq.* 224 (2016) 1163–1171, <https://doi.org/10.1016/j.molliq.2016.10.085>.
- [29] Hassankiadeh, Naser Tavajohi, Zhaoliang Cui, Ji Hoon Kim, Won Shin Dong, Suk Young Lee, Aldo Sanguineti, Vincenzo Arcella, Moo Lee Young, Enrico Drioli, Microporous poly(vinylidene fluoride) hollow fiber membranes fabricated with polarclean as water-soluble green diluent and additives, *J. Membr. Sci.* 479 (2015) 204–212, <https://doi.org/10.1016/j.memsci.2015.01.031>.
- [30] Jian Chang, Jian Zuo, Liling Zhang, S. Gregory, O'Brien, Tai-Shung Chung, Using green solvent, triethyl phosphate (tep), to fabricate highly porous pvdf hollow fiber membranes for membrane distillation, *J. Membr. Sci.* 539 (2017) 295–304, <https://doi.org/10.1016/j.memsci.2017.06.002>.
- [31] Ho Hyun Wang, Jun Tae Jung, Jeong F. Kim, Seungju Kim, Enrico Drioli, Moo Lee Young, A novel green solvent alternative for polymeric membrane preparation via nonsolvent-induced phase separation (nips), *J. Membr. Sci.* 574 (2019) 44–54, <https://doi.org/10.1016/j.memsci.2018.12.051>.
- [32] Oliver Gronwald, Martin Weber, Agnique amd 3l as green solvent for polyethersulfone ultrafiltration membrane preparation, *J. Appl. Polym. Sci.* 137 (9) (2020), 48419, <https://doi.org/10.1002/app.48419>.
- [33] Naziri Mehrabani, Seyed Ali, Vahid Vatanpour, Koyuncu Ismail, Green solvents in polymeric membrane fabrication: a review, *Separ. Purif. Technol.* 298 (2022), 121691, <https://doi.org/10.1016/j.seppur.2022.121691>.
- [34] Kinnian Jiang, Yong Wai Fen, Jie Gao, Dan-Dan Shao, Shi-Peng Sun, Understanding the role of substrates on thin film composite membranes: a green solvent approach with Tamisolve® nxx, *J. Membr. Sci.* 635 (2021), 119530, <https://doi.org/10.1016/j.memsci.2021.119530>.
- [35] Dooli Kim, Suzana P. Nunes, Green solvents for membrane manufacture: recent trends and perspectives, *Current Opinion in Green and Sustainable Chemistry* 28 (2021), 100427, <https://doi.org/10.1016/j.cogsc.2020.100427>.
- [36] Wei J. Lee, Pei S. Goh, Woei J. Lau, Ahmad F. Ismail, Nidal Hilal, Green approaches for sustainable development of liquid separation membrane, *Membranes* (2021) 4, <https://doi.org/10.3390/membranes11040235>.
- [37] Marcello Pagliero, Antonio Comite, Camilla Costa, Ilaria Rizzardi, Omar Soda, A single step preparation of photothermally active polyvinylidene fluoride membranes using triethyl phosphate as a green solvent for distillation applications, *Membranes* (2021) 11, <https://doi.org/10.3390/membranes11110896>.
- [38] Yuanhui Tang, Mufei Li, Yakai Lin, Lin Wang, Fangyu Wu, Xiaolin Wang, A novel green diluent for the preparation of poly(4-methyl-1-pentene) membranes via a thermally-induced phase separation method, *Membranes* (2021) 8, <https://doi.org/10.3390/membranes11080622>.
- [39] Dong Zou, Suzana P. Nunes, Ivo F.J. Vankelecom, Figoli Alberto, Moo Lee Young, Recent advances in polymer membranes employing non-toxic solvents and materials, *Green Chem.* 23 (24) (2021) 9815–9843, <https://doi.org/10.1039/D1GC03318B>.
- [40] Angela Dedvukaj, Peter Van den Mooter, Ivo F.J. Vankelecom, Solvent-resistant uv-cured polysulfone support membranes using a green solvent, *Membranes* (2022) 1, <https://doi.org/10.3390/membranes12010001>.
- [41] Rifan Hardian, Abdulaziz Alammari, Tibor Holtzl, Gyorgy Szekely, Fabrication of sustainable organic solvent nanofiltration membranes using cellulose-chitosan biopolymer blends, *J. Membr. Sci.* 658 (2022), 120743, <https://doi.org/10.1016/j.memsci.2022.120743>.
- [42] J.D. Seader, J.S. Sirolo, S.D. Bamicki, *Distillation*, in: W. Don, H. Perry Green Robert, O. James (Eds.), *Perry's Chemical Engineers' Handbook*, McGraw-Hill, Maloney, 1997. ISBN 0-07-049841-5.
- [43] M.A. Gadalla, Z. Olujic, P.J. Jansens, M. Jobson, R. Smith, Reducing CO₂ emissions and energy consumption of heat-integrated distillation systems, *Environ. Sci. Technol.* 39 (17) (2005) 6860–6870, <https://doi.org/10.1021/es049795q>.
- [44] Karina Schuldt, Torsten Brinkmann, Prokopios Georgopoulos, Zero-discharge process for recycling of tetrahydrofuran–water mixtures, *Processes* (2021) 5, <https://doi.org/10.3390/pr9050729>.
- [45] Johannes Kamp, Stephan Emonds, Julian Borowec, Maria Adelaida Restrepo Toro, Matthias Wessling, On the organic solvent free preparation of ultrafiltration and nanofiltration membranes using polyelectrolyte complexation in an all aqueous phase inversion process, *J. Membr. Sci.* 618 (2021), 118632, <https://doi.org/10.1016/j.memsci.2020.118632>.
- [46] Stephan Emonds, Johannes Kamp, Julian Borowec, Hannah Roth, Matthias Wessling, Polyelectrolyte complex tubular membranes via a salt dilution induced phase inversion process, *Adv. Eng. Mater.* 23 (5) (2021), 2001401, <https://doi.org/10.1002/adem.202001401>.
- [47] C. Rauwendaal, *Polymer Extrusion*, Carl Hanser Verlag GmbH & Company KG, 2014.
- [48] Sarita J. Charde, Shiriram S. Sonawane, Shirish H. Sonawane, Shimpi Navin, Influence of functionalized calcium carbonate nanofillers on the properties of melt-extruded polycarbonate composites, *Chem. Eng. Commun.* 205 (4) (2018) 492–505, <https://doi.org/10.1080/00986445.2017.1404459>.
- [49] Abdullah Demirci, Teke Ismail, Goger Ali, Elif Cambaz, John Vlachopoulos, Gelation of poly(vinyl chloride) inside a single screw extruder and its effect on product properties, *J. Vinyl Addit. Technol.* 25 (S1) (2019) E174–E180, <https://doi.org/10.1002/vnl.21676>.
- [50] A. Elsanbagh, L. Steuernagel, J. Ring, Natural fibre/Pa6 composites with flame retardance properties: extrusion and characterisation, *Compos. B Eng.* 108 (2017) 325–333, <https://doi.org/10.1016/j.compositesb.2016.10.012>.
- [51] Xiaodong Zhai, Xinyu Wang, Junjun Zhang, Zhikun Yang, Yue Sun, Zhihua Li, Xiaowei Huang, Melvin Holmes, Yunyun Gong, Megan Povey, Jiyong Shi, Xiaobo Zou, Extruded low density polyethylene-curcumin film: a hydrophobic ammonia sensor for intelligent food packaging, *Food Packag. Shelf Life* 26 (2020), 100595, <https://doi.org/10.1016/j.fpsl.2020.100595>.
- [52] Huang Pengke, Yaozhuo Su, Fei Wu, C. Lee Patrick, Haibin Luo, Xiaoqin Lan, Zhang Liyang, Shen Bin, Wang Long, Zheng Wenge, Extruded polypropylene foams with radially gradient porous structures and selective filtration property via supercritical CO₂ foaming, *J. CO₂ Util.* 60 (2022), 101995, <https://doi.org/10.1016/j.jcou.2022.101995>.
- [53] BASF, "Polyamides for extrusion." BASF SE. https://chemicals.basf.com/global/en/Monomers/polyamide_intermediates/polyamide_for_extrusions.html. (Accessed 17 April 2023).
- [54] Aniket Raje, Prokopios Georgopoulos, Joachim Koll, Jelena Lillepär, Ulrich A. Handge, Volker Abetz, Open-celled foams from polyethersulfone/poly(ethylene glycol) blends using foam extrusion, *Polymers* 15 (1) (2023) 118, <https://doi.org/10.3390/polym15010118>.
- [55] Quan Huang, Lösemittelfreie Herstellung Von Porösen Polymeren Membranen Durch Schaumextrusion. Doctoral Thesis, Doctorate, Universität Hamburg, Hamburg, 2000. Online: <https://ediss.sub.uni-hamburg.de/bitstream/ediss/1334/1/Dissertation-Huang.PDF>.
- [56] Q. Huang, D. Paul, B. Seibig, Advances in solvent-free manufacturing of polymer membranes, *Membr. Technol.* 140 (2001) (2001) 6–9, [https://doi.org/10.1016/S0958-2118\(01\)80394-3](https://doi.org/10.1016/S0958-2118(01)80394-3).
- [57] Q. Huang, R. Klötzer, B. Seibig, D. Paul, Extrusion of microcellular polysulfone using chemical blowing agents, *J. Appl. Polym. Sci.* 69 (9) (1998) 1753–1760, [https://doi.org/10.1002/\(SICI\)1097-4628\(19980829\)69:9<1753::AID-APP9>3.0.CO;2-A](https://doi.org/10.1002/(SICI)1097-4628(19980829)69:9<1753::AID-APP9>3.0.CO;2-A).
- [58] Huang Quan, Seibig Bernd, Dieter Paul, Polycarbonate hollow fiber membranes by melt extrusion, *J. Membr. Sci.* 161 (1) (1999) 287–291, [https://doi.org/10.1016/S0376-7388\(99\)00122-2](https://doi.org/10.1016/S0376-7388(99)00122-2).
- [59] Abeer Khan, Jafar Ali, Syed Umair Ullah Jamil, Nadia Zahra, T.B. Tayaba, Muhammad Javed Iqbal, Waseem Hassan, Chapter 22 - removal of micropollutants, in: *Environmental Micropollutants*, Edited by Muhammad Zaffar Hashmi, Shuhong Wang and Zulkifli Ahmed, 443–61, Elsevier, 2022, <https://doi.org/10.1016/B978-0-323-90555-8.00012-X>.
- [60] Xiangmin Han, Kurt W. Koelling, David L. Tomasko, L. James Lee, Continuous microcellular polystyrene foam extrusion with supercritical CO₂, *Polym. Eng. Sci.* 42 (11) (2002) 2094–2106, <https://doi.org/10.1002/pen.11100>.

- [61] Taher Azdast, Rezgar Hasanzadeh, Increasing cell density/decreasing cell size to produce microcellular and nanocellular thermoplastic foams: a review, *J. Cell. Plast.* 57 (5) (2021) 769–797, <https://doi.org/10.1177/0021955x20959301>.
- [62] Y.H. Lee, K.H. Wang, C.B. Park, M. Sain, Effects of clay dispersion on the foam morphology of ldpe/clay nanocomposites, *J. Appl. Polym. Sci.* 103 (4) (2007) 2129–2134, <https://doi.org/10.1002/app.24908>.
- [63] A. Raje, K. Buhr, J. Koll, J. Lilleparg, V. Abetz, U.A. Handge, Open-celled foams of polyethersulfone/poly(N-vinylpyrrolidone) blends for ultrafiltration applications, *Polymers* 14 (6) (2022), <https://doi.org/10.3390/polym14061177>.
- [64] Jae-Jin Kim, Tae-Seok Jang, Young-Don Kwon, Un Young Kim, Sung Soo Kim, Structural study of microporous polypropylene hollow fiber membranes made by the melt-spinning and cold-stretching method, *J. Membr. Sci.* 93 (3) (1994) 209–215, [https://doi.org/10.1016/0376-7388\(94\)00070-0](https://doi.org/10.1016/0376-7388(94)00070-0).
- [65] C. Chandavasu, M. Xanthos, K.K. Sirkar, C.G. Gogos, Fabrication of microporous polymeric membranes by melt processing of immiscible blends, *J. Membr. Sci.* 211 (1) (2003) 167–175, [https://doi.org/10.1016/S0376-7388\(02\)00032-7](https://doi.org/10.1016/S0376-7388(02)00032-7).
- [66] M. Xanthos, C. Chandavasu, K.K. Sirkar, C.G. Gogos, Melt processed microporous films from compatibilized immiscible blends with potential as membranes, *Polym. Eng. Sci.* 42 (4) (2002) 810–825, <https://doi.org/10.1002/pen.10993>.
- [67] C. Chandavasu, M. Xanthos, K.K. Sirkar, C.G. Gogos, Preparation of microporous films from immiscible blends via melt processing, *J. Plast. Film Sheeting* 16 (4) (2000) 288–300, <https://doi.org/10.1106/VEHN-PMN3-Q6RE-FUH9>.
- [68] Dawei Ji, Yifei Gao, Wanning Wang, Haowei Feng, Kaikai Chen, Changfa Xiao, Green preparation of pvdf hollow fiber membranes with multiple pore structure via melt spinning method for oil/water separation, *J. Environ. Chem. Eng.* 10 (5) (2022), 108337, <https://doi.org/10.1016/j.jece.2022.108337>.
- [69] D. Ji, C. Xiao, K. Chen, F. Zhou, Y. Gao, T. Zhang, H. Ling, Solvent-free green fabrication of pvdf hollow fiber mf membranes with controlled pore structure via melt-spinning and stretching, *J. Membr. Sci.* 621 (2021), <https://doi.org/10.1016/j.memsci.2020.118953>.
- [70] D. Ji, C. Xiao, S. An, K. Chen, Y. Gao, F. Zhou, T. Zhang, Completely green and sustainable preparation of pvdf hollow fiber membranes via melt-spinning and stretching method, *J. Hazard Mater.* 398 (2020), <https://doi.org/10.1016/j.jhazmat.2020.122823>.
- [71] L. Zou, G. Zhang, J. Yu, Desirable pvdf hollow fiber membrane engineered with synergism between small molecular weight additives for dcmd treating of a hypersaline brine, *J. Water Proc. Eng.* 45 (2022), <https://doi.org/10.1016/j.jwpe.2021.102528>.
- [72] G. Liang, W. Fang, J. Li, S. Guo, Micropore Formation and crystalline evolution during biaxial stretching process of ipp film constructed of ordered and continuous B-transcrystallinity, *J. Membr. Sci.* 636 (2021), <https://doi.org/10.1016/j.memsci.2021.119558>.
- [73] Q. Liu, Q. Yang, Y. Zhou, M. Zhao, Y. Shen, F. Zhou, R.H. Gong, B. Deng, A facile method of preparing highly porous polylactide microfibers, *J. Appl. Polym. Sci.* 135 (2018) 7, <https://doi.org/10.1002/app.45860>.
- [74] J. Hao, Z. Fan, C. Xiao, J. Zhao, H. Liu, L. Chen, Effect of stretching on continuous oil/water separation performance of polypropylene hollow fiber membrane, *Iran. Polym. J. (Engl. Ed.)* 26 (12) (2017) 941–948, <https://doi.org/10.1007/s13726-017-0566-5>.
- [75] H. Shao, F. Wei, B. Wu, K. Zhang, Y. Yao, S. Liang, S. Qin, Effects of annealing stress field on the structure and properties of polypropylene hollow fiber membranes made by stretching, *RSC Adv.* 6 (6) (2016) 4271–4279, <https://doi.org/10.1039/c5ra21785g>.
- [76] Q.L. Huang, Y.J. Wu, C.F. Xiao, K.K. Chen, L. Song, Z. Liu, Effects of post-treatment on the structure and properties of pvdf/pep blend hollow fiber membranes, *RSC Adv.* 5 (94) (2015) 77407–77416, <https://doi.org/10.1039/c5ra13565f>.
- [77] T.H. Kim, K.Y. Jee, Y.T. Lee, The improvement of water flux and mechanical strength of pvdf hollow fiber membranes by stretching and annealing conditions, *Macromol. Res.* 23 (7) (2015) 592–600, <https://doi.org/10.1007/s13233-015-3087-0>.
- [78] S.W. Han, S.M. Woo, D.J. Kim, O.O. Park, S.Y. Nam, Effect of annealing on the morphology of porous polypropylene hollow fiber membranes, *Macromol. Res.* 22 (6) (2014) 618–623, <https://doi.org/10.1007/s13233-014-2087-9>.
- [79] Jingxing Feng, Guojun Zhang, Kari MacInnis, Andrew Olah, Eric Baer, Structure-property relationships of microporous membranes produced by biaxial orientation of compatibilized pp/nylon 6 blends, *Polymer* 145 (2018) 148–156, <https://doi.org/10.1016/j.polymer.2018.05.005>.
- [80] Dajun Luo, Gaoyi Xie, Shuhao Qin, The hydrophilic polypropylene/poly(ethylene-co-vinyl alcohol) hollow fiber membrane with bimodal microporous structure prepared by melt-spinning and stretching, *Separ. Purif. Technol.* 274 (2021), 118890, <https://doi.org/10.1016/j.seppur.2021.118890>.
- [81] X.M. Tan, D. Rodrigue, A review on porous polymeric membrane preparation. Part II: production techniques with polyethylene, polydimethylsiloxane, polypropylene, polyimide, and polytetrafluoroethylene, *Polymers* 11 (2019) 8, <https://doi.org/10.3390/polym11081310>.
- [82] A.A.I.A.S. Komaladewi, P.T.P. Aryanti, G. Lugito, I. Wayan Surata, I. Gede Wenten, Recent progress in microfiltration polypropylene membrane fabrication by stretching method, *E3S Web of Conferences* 67 (2018), <https://doi.org/10.1051/e3sconf/20186703018>.
- [83] U.A. Handge, O. Gronwald, M. Weber, J. Koll, C. Abetz, B. Hankiewicz, V. Abetz, Fabrication of membranes of polyethersulfone and poly(N-vinyl pyrrolidone): influence of glycerol on processing and transport properties, *Polym. Int.* 69 (5) (2020) 502–512, <https://doi.org/10.1002/pi.5984>.
- [84] Y. Dai, J. Wang, P.P. Tao, R.H. He, Various hydrophilic carbon dots doped high temperature proton exchange composite membranes based on polyvinylpyrrolidone and polyethersulfone, *J. Colloid Interface Sci.* 553 (2019) 503–511, <https://doi.org/10.1016/j.jcis.2019.06.020>.
- [85] Min Liu, Anne Ladegaard Skov, Sheng-Hui Liu, Li-Yun Yu, Zhen-liang Xu, A Facile Way to Prepare Hydrophilic Homogeneous Pes Hollow Fiber Membrane via Non-solvent Assisted Reverse Thermally Induced Phase Separation (Rtips) Method, *Polymers*, 2019, p. 2, <https://doi.org/10.3390/polym11020269>.
- [86] N. Noor, J. Koll, N. Scharnagl, C. Abetz, V. Abetz, Hollow fiber membranes of blends of polyethersulfone and sulfonated polymers, *Membranes* 8 (2018) 3, <https://doi.org/10.3390/membranes8030054>.
- [87] M.T. Tsehaye, S. Velizarov, B. Van der Bruggen, Stability of polyethersulfone membranes to oxidative agents: a review, *Polym. Degrad. Stabil.* 157 (2018) 15–33, <https://doi.org/10.1016/j.polymdegradstab.2018.09.004>.
- [88] T. Mantel, P. Benne, S. Parsin, M. Ernst, Electro-conductive composite gold-polyethersulfone-ultrafiltration-membrane: characterization of membrane and natural organic matter (nom) filtration performance at different in-situ applied surface potentials, *Membranes* 8 (2018), <https://doi.org/10.3390/membranes8030064>.
- [89] D. Kim, H. Vovusha, U. Schwingenschlogl, S.P. Nunes, Polyethersulfone flat sheet and hollow fiber membranes from solutions in ionic liquids, *J. Membr. Sci.* 539 (2017) 161–171, <https://doi.org/10.1016/j.memsci.2017.06.001>.
- [90] X.F. Fang, J.S. Li, X. Li, S.L. Pan, X. Zhang, X.Y. Sun, J.Y. Shen, W.Q. Han, L. J. Wang, Internal pore decoration with polydopamine nanoparticle on polymeric ultrafiltration membrane for enhanced heavy metal removal, *Chem. Eng. J.* 314 (2017) 38–49, <https://doi.org/10.1016/j.cej.2016.12.125>.
- [91] Nasrul Arahman, Sri Mulyati, Mirna Rahmah Lubis, Fachrul Razi, Ryoosuke Takagi, Hideto Matsuyama, Modification of polyethersulfone hollow fiber membrane with different polymeric additives, *Membr. Water Treat* 7 (no. 4) (2016) 355–365, <https://doi.org/10.12989/mwt.2016.7.4.355>.
- [92] S.A. Al Malek, M.N. Abu Seman, D. Johnson, N. Hilal, Formation and characterization of polyethersulfone membranes using different concentrations of polyvinylpyrrolidone, *Desalination* 288 (2012) 31–39, <https://doi.org/10.1016/j.desal.2011.12.006>.
- [93] Heru Susanto, Mathias Ulbricht, Characteristics, performance and stability of polyethersulfone ultrafiltration membranes prepared by phase separation method using different macromolecular additives, *J. Membr. Sci.* 327 (1) (2009) 125–135, <https://doi.org/10.1016/j.memsci.2008.11.025>.
- [94] A.F. Ismail, M.I. Mustaffar, R.M. Illias, M.S. Abdullah, Effect of dope extrusion rate on morphology and performance of hollow fibers membrane for ultrafiltration, *Separ. Purif. Technol.* 49 (1) (2006) 10–19, <https://doi.org/10.1016/j.seppur.2005.08.001>.
- [95] L.E. Grunig, U.A. Handge, J. Koll, O. Gronwald, M. Weber, B. Hankiewicz, N. Scharnagl, V. Abetz, Verbesserte hydrophilie von hohlfasermembranen mittels funktionalisierter trennschicht Fur die ultrafiltration dual layer hollow fiber membranes with functionalized separation layer for improved hydrophilicity, *Chem. Ing. Tech.* 93 (9) (2021) 1451–1456, <https://doi.org/10.1002/cite.202100034>.
- [96] U.A. Handge, O. Gronwald, M. Weber, B. Hankiewicz, V. Abetz, Phase behavior and dynamics of pluronic (R)-Based additives in semidilute solutions of poly(ethersulfone) and poly(N-vinyl pyrrolidone): rheological and dynamic light scattering experiments, *Rheol. Acta* 58 (9) (2019) 591–602, <https://doi.org/10.1007/s00397-019-01160-0>.
- [97] K. Sankhala, J. Koll, V. Abetz, Setting the stage for fabrication of self-assembled structures in compact geometries: inside-out isoporous hollow fiber membranes, *ACS Macro Lett.* 7 (7) (2018) 840–845, <https://doi.org/10.1021/acsmacrolett.8b00402>.
- [98] O. Gronwald, I. Frost, M. Ulbricht, A.K. Shalmani, S. Panglisch, L. Grunig, U. A. Handge, V. Abetz, M. Heijnen, M. Weber, Hydrophilic poly(phenylene sulfone) membranes for ultrafiltration, *Separ. Purif. Technol.* 250 (2020), <https://doi.org/10.1016/j.seppur.2020.117107>.
- [99] Yan Hao, Liang Cui, Akihito Moriya, Hideto Matsuyama, Tatsuo Maruyama, Visualization of protein fouling inside a hollow fiber ultrafiltration membrane by fluorescent microscopy, *Ind. Eng. Chem. Res.* 51 (45) (2012) 14850–14858, <https://doi.org/10.1021/ie302111w>.
- [100] Yin Xiuli, Hongbin Cheng, Xiu Wang, Yongxin Yao, Morphology and properties of hollow-fiber membrane made by Pan mixing with small amount of pvdf, *J. Membr. Sci.* 146 (2) (1998) 179–184, [https://doi.org/10.1016/S0376-7388\(98\)00107-0](https://doi.org/10.1016/S0376-7388(98)00107-0).
- [101] Katharina Nieswandt, Prokopios Georgopoulos, Volker Abetz, Well-defined polyvinylpyridine-block-polystyrene diblock copolymers via raft aqueous-alcoholic dispersion polymerization: synthesis and isoporous thin film morphology, *Polym. Chem.* 12 (15) (2021) 2210–2221, <https://doi.org/10.1039/D1PY00074H>.
- [102] George Z. Papageorgiou, Dimitris N. Bikiaris, Crystallization and melting behavior of three biodegradable poly(alkylene succinates). A comparative study, *Polymer* 46 (26) (2005) 12081–12092, <https://doi.org/10.1016/j.polymer.2005.10.073>.
- [103] G. Dibrov, G. Kagramanov, V. Sudin, E. Grushevenko, A. Yushkin, A. Volkov, Influence of sodium hypochlorite treatment on pore size distribution of polysulfone/polyvinylpyrrolidone membranes, *Membranes* 10 (2020) 11, <https://doi.org/10.3390/membranes10110356>.
- [104] M. Radjabian, J. Koll, K. Buhr, U. Vainio, C. Abetz, U.A. Handge, V. Abetz, Tailoring the morphology of self-assembled block copolymer hollow fiber membranes, *Polymer* 55 (13) (2014) 2986–2997, <https://doi.org/10.1016/j.polymer.2014.04.041>.
- [105] Safety Data Sheet - Polyethylene Glycol 200 for Synthesis, Sigma-Aldrich, 2021.

- [106] Peter Gutmann, Klaus Hildebrandt, Volker Altstädt, H. Axel, E. Müller, Foaming of an immiscible blend system using organic liquids as blowing agents, *J. Cell. Plast.* 46 (3) (2010) 239–258, <https://doi.org/10.1177/0021955x09352138>.
- [107] F. Lu, H. Liu, C. Xiao, X. Wang, K. Chen, H. Huang, Effect of on-line stretching treatment on the structure and performance of polyvinyl chloride hollow fiber membranes, *RSC Adv.* 9 (12) (2019) 6699–6707, <https://doi.org/10.1039/c9ra00265k>.
- [108] U. Raviv, J. Klein, 2.24 - adhesion, friction, and lubrication between polymer-bearing surfaces, in: Krzysztof Matyjaszewski, Martin Möller (Eds.), *Polymer Science: A Comprehensive Reference*, Elsevier, Amsterdam, 2012, pp. 607–628, <https://doi.org/10.1016/B978-0-444-53349-4.00048-0>.
- [109] Mohamed S. Ibrahim, Noha A. El-Wasefy, Dina S. Farahat, 8 - biocompatibility of dental biomaterials, in: *Biomaterials for Oral and Dental Tissue Engineering* 117–40, Woodhead Publishing, 2017, <https://doi.org/10.1016/B978-0-08-100961-1.00008-6>. Lobat Tayebi and Keyvan Moharamzadeh.
- [110] B. Jaleh, E. Zare, S. Azizian, O. Qanati, M. Nasrollahzadeh, R.S. Varma, Preparation and characterization of polyvinylpyrrolidone/polysulfone ultrafiltration membrane modified by graphene oxide and titanium dioxide for enhancing hydrophilicity and antifouling properties, *J. Inorg. Organomet. Polym. Mater.* 30 (6) (2020) 2213–2223, <https://doi.org/10.1007/s10904-019-01367-x>.
- [111] J. Zhang, S. Chen, H.J. Bai, S.F. Lu, Y. Xiang, S.P. Jiang, Effects of phosphotungstic acid on performance of phosphoric acid doped polyethersulfone-polyvinylpyrrolidone membranes for high temperature fuel cells, *Int. J. Hydrogen Energy* 46 (19) (2021) 11104–11114, <https://doi.org/10.1016/j.ijhydene.2020.07.082>.
- [112] O. Gronwald, M. Weber, Agnique amd 3l as green solvent for polyethersulfone ultrafiltration membrane preparation, *J. Appl. Polym. Sci.* 137 (2020) 9, <https://doi.org/10.1002/app.48419>.
- [113] D. Aili, M.R. Kraglund, J. Tavacoli, C. Chatzichristodoulou, J.O. Jensen, Polysulfone-polyvinylpyrrolidone blend membranes as electrolytes in alkaline water electrolysis, *J. Membr. Sci.* 598 (2020), <https://doi.org/10.1016/j.memsci.2019.117674>.
- [114] Makoto Yoshida, Paras N. Prasad, Fabrication of channel waveguides from sol-gel-processed polyvinylpyrrolidone/sio2 composite materials, *Appl. Opt.* 35 (9) (1996) 1500–1506, <https://doi.org/10.1364/AO.35.001500>.
- [115] Shu-Kai Yeh, Ssu-Hsuan Yang, Long Han, Hung-Yun Liu, Yi-Syun Liao, Yi-Chun Chang, Foam extrusion of polypropylene-rice husk composites using Co2 as the blowing agent, *J. Cell. Plast.* 55 (4) (2019) 401–419, <https://doi.org/10.1177/0021955x19839744>.
- [116] Chul B. Park, Amir H. Behraves, D. Venter Ronald, Low density microcellular foam processing in extrusion using Co2, *Polym. Eng. Sci.* 38 (11) (1998) 1812–1823, <https://doi.org/10.1002/pen.10351>.
- [117] Jelena Lillepär, Prokopios Georgopoulos, Sergey Shishatskiy, Stability of blended polymeric materials for Co2 separation, *J. Membr. Sci.* 467 (2014) 269–278, <https://doi.org/10.1016/j.memsci.2014.05.039>.
- [118] Z.Y. Chu, K.K. Chen, C.F. Xiao, D.W. Ji, H.Y. Ling, M.Y. Li, H.L. Liu, Improving pressure durability and fractionation property via reinforced pes loose nanofiltration hollow fiber membranes for textile wastewater treatment, *J. Taiwan Inst. Chem. Eng.* 108 (2020) 71–81, <https://doi.org/10.1016/j.jtice.2019.12.009>.
- [119] Yi Jiang, Qingqing Zeng, Pratim Biswas, John D. Fortner, Graphene oxides as nanofillers in polysulfone ultrafiltration membranes: shape matters, *J. Membr. Sci.* 581 (2019) 453–461, <https://doi.org/10.1016/j.memsci.2019.03.056>.
- [120] Youcai Zhao, Chapter 2 - physical and chemical treatment processes for leachate, in: Youcai Zhao (Ed.), *Pollution Control Technology for Leachate from Municipal Solid Waste*, Butterworth-Heinemann, 2018, pp. 31–183, <https://doi.org/10.1016/B978-0-12-815813-5.00002-4>.
- [121] Eric K. Lee, W.J. Koros, Membranes, synthetic, applications, in: Robert A. Meyers (Ed.), *Encyclopedia of Physical Science and Technology*, third ed., Academic Press, New York, 2003, pp. 279–344, <https://doi.org/10.1016/B0-12-227410-5/00419-1>.
- [122] T. Hliavitskaya, T. Plisko, A. Bilydukevich, F. Lipnizki, G. Rodrigues, M. Sjolín, Modification of pes ultrafiltration membranes by cationic polyelectrolyte praestol 859: characterization, performance and application for purification of hemicellulose, *Chem. Eng. Res. Des.* 162 (2020) 187–199, <https://doi.org/10.1016/j.cherd.2020.08.008>.
- [123] Nazanin Nasrollahi, Vahid Vatanpour, Soheil Aber, Mahmoodi Niyaz Mohammad, Preparation and characterization of a novel polyethersulfone (pes) ultrafiltration membrane modified with a cuo/zno nanocomposite to improve permeability and antifouling properties, *Separ. Purif. Technol.* 192 (2018) 369–382, <https://doi.org/10.1016/j.seppur.2017.10.034>.

7. Discussions

The process of polymer foaming was successful in manufacturing ultrafiltration membranes, both as flat-sheet and hollow fiber membranes. Blending a high-performance water-insoluble polymer with water-soluble polymers, foaming the said blend continuously, and removing the water-soluble polymer using aqueous inorganic solutions, created water-permeable membranes capable of ultrafiltration.

Previously not tried combinations of many state-of-the-art techniques led to the achievements of this work. However, certain novel ideas were implemented as well, such as,

- A method to avoid non-foamed skin layer in batch foaming.
- A method of creating a polymer blend using material penetration by taking advantage of the major polymer's porous flakes and the minor polymer's liquid state.
- Foam extrusion using CO₂ and H₂O as co-blowing agents.

7.1. Summary of Findings of This Work

The published articles, as well as the brief information provided in Section 6, provide an apt summary of the results and findings based on the goals set for each step of this work.

However, various scientific findings could be significant individually for further research. Therefore, the following list is provided to assist the reader in distinguishing the inferences individually.

- The complete miscibility of PESU and PVP was confirmed.
- Blending PESU (Avg. $M_w = 65000$ Da) and PVP K 30 using compounding works only up to certain grams of the blend. Afterward, due to crosslinking and decomposition of PVP, the extruder undergoes problems.
- PESU/PVP's foam, manufactured using batch foaming where CO₂ and water as co-foaming agents are used, shows a dual foam structure, i.e., microcellular closed-celled foam with nanocellular open pores on its cell walls. Both these morphologies are codependent and can be controlled by the process parameters.
- The non-foamed skin layer occurring on polymer samples subjected to batch foaming can be bypassed by sticking another removable or dissolvable material on the sample surface and foaming them together.
- Aqueous solution of sodium hypochlorite can dissolve PVP K 30 from the surface of a compression molded sample made of blend PESU/PVP creating nanocellular blind pores.

- A disc sample comprising a PESU (Avg. $M_w = 65000$ Da) / PVP K 30 (68/32) blend, enclosed on both sides with compression molded PVP K 90, when batch foamed using CO₂ and water as co-foaming agents, yields a nanocellular open-celled foam. The foamed sample can be accessed by dissolving the PVP K 90 enclosure in aqueous solution of sodium hypochlorite. This sample provides a water flux and possesses ultrafiltration capabilities.
- PESU flakes' porous nature can assist the absorption of liquid PEG 200 into the PESU matrix, leading toward a partially miscible blend. The highest amount of PEG absorbable was between 20% and 26%. This method eliminates the use of compounding or organic solvents.
- The plasticizing nature of PEG causes the glass transition of the blend to be 100-120 °C lower than PESU homopolymer, translating into a reduction of the processing temperatures in the extruder.
- Using water and CO₂ as co-foaming agents in extrusion increases porosity and cell uniformity.
- PESU (Avg. $M_w = 65000$ Da) / PEG 200 (80/20) blend produces open-celled foam with an average cell size of 5 μm at the optimum process settings using CO₂ and water as co-foaming agents in foam extrusion.
- With increasing porosity, the tensile strength of a foam decreases while its ductility increases.

- Without any foaming agent, PESU/PEG blend's extrudates possess uniformly distributed closed-cell foam-like morphology. The reason is the expansion and reabsorption of PEG into the blend matrix during the extrusion process.
- PVP K 30 powder can be dissolved in liquid PEG, forming a highly viscous transparent yellowish solution. This solution can be absorbed in PESU flakes forming a PESU/PEG/PVP blend similar to PESU/PEG blend.
- The miscibility of PESU, PEG and PVP can be visualized by the illustration in Figure 28.

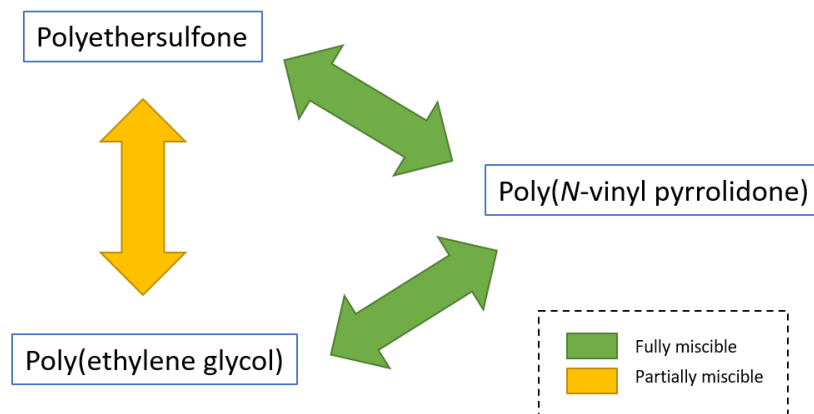


Figure 28: Illustration showing mutual miscibility of polymers based on the findings of this work.

- Similar to PESU/PEG blend's extrudates, PESU/PEG/PVP blend's extrudates also demonstrate foam-like morphology. However, with higher porosity.

- The desired hollow fiber shape is not maintained when using an annular slit nozzle in extruding PESU/PEG blend. However, PESU/PEG/PVP's extrudates maintain a hollow fiber shape due to increased elasticity from adding PVP.
- Using aqueous solution of NaOCl, PEG and PVP can be washed out of the PESU/PEG/PVP blend's extruded hollow fibers, leading to higher porosity, cell interconnection, and water-permeability.
- PEG and PVP have different temperatures of optimum dissolution in aqueous solution of NaOCl. This dissolution depends on the concentration of NaOCl, temperature, pH, etc.
- Leaching out of PEG from the outer surface of the extruded PESU/PEG/PVP hollow fibers due to high nozzle temperatures causes the outer surface of the extruded hollow fibers to have a higher concentration of PVP than PEG.
- The complete miscibility of PESU and PVP, leading towards a dispersion of respective polymers within a few nanometers, causes the PVP-rich outer surface to exhibit a nanocellular porous structure when PVP is washed out by sodium hypochlorite. Whereas the partial miscibility of PESU and PEG, leading towards a dispersion of the respective polymers in a few micrometers, causes the rest of the extruded hollow fiber, richer in PEG content, to exhibit a microcellular porous structure.
- Post-treatment of an extruded PESU/PEG/PVP hollow fiber with aqueous solution of NaOCl using an optimum combination of process parameters leads to formation of separation layer with an average pore size of 50 nm and

interconnected internal pores. This causes the hollow fibers to be permeable to water and display ultrafiltration capabilities.

7.2. Future Scope

The foams manufactured in this work can be directly implemented as ultrafiltration membranes, especially the continuously manufactured hollow fibers from Article 3. Ultrafiltration membranes were manufactured using pre-existing techniques of polymer foaming without the use of organic solvents.

However, these membranes have lower performance than the state-of-the-art ultrafiltration membranes manufactured using techniques involving organic solvents. This realization is out of the scope of this work; however, material and process optimizations can be pursued to improve the performance of these membranes to match or exceed the state-of-the-art. Article 3 provides some ideas that could be implemented to increase the efficiency of the developed process and improve product performance.

Not only membrane science but a wide range of polymer research and industry can gain from the findings and developments of this work. For example, nanocellular open-celled foams not only aid in ultrafiltration applications but also can be implemented for heat exchange applications taking advantage of the Knudsen effect. (Krause *et al.*, 2001)

Apart from eliminating the need for organic solvents in manufacturing ultrafiltration membranes, other developments from this work can also be implemented as sustainable solutions. These developments include energy-saving techniques such as reducing processing temperature using a plasticizer, eliminating compounding extruder for blending polymers, and excluding a physical blowing agent from foam extrusion using a blend component from a ternary blend to act as a blowing agent additionally.

8. Bibliography

Abdul Latif, A.A. *et al.* (2021) ‘Multicomponent Spiral Wound Membrane Separation Model for CO₂ Removal from Natural Gas’, *Membranes*, 11(9). Available at: <https://doi.org/10.3390/membranes11090654>.

Abetz, V. *et al.* (2014) ‘Formation of isoporous block copolymer Membranes in flat and hollow fibre geometries’, *Abstracts of Papers of the American Chemical Society*, 248. Available at: <https://doi.org/10.1002/marc.201400556>.

Abetz, V. (2015) ‘Isoporous Block Copolymer Membranes’, *Macromolecular Rapid Communications*, 36(1), pp. 10–22. Available at: <https://doi.org/10.1002/marc.201400556>.

Abetz, V., Brinkmann, T. and Sözbilir, M. (2021) ‘Fabrication and function of polymer membranes’, 3(2), pp. 141–154. Available at: <https://doi.org/10.1515/cti-2020-0023>.

Agilent Technologies (2015) ‘An Introduction to Gel Permeation Chromatography and Size Exclusion Chromatography’. Agilent Technologies. Available at: <https://www.agilent.com/cs/library/primers/Public/5990-6969EN%20GPC%20SEC%20Chrom%20Guide.pdf> (Accessed: 11 April 2023).

Ahmad, A.L. *et al.* (2010) ‘CO₂ removal using membrane gas absorption’, *International Journal of Greenhouse Gas Control*, 4(3), pp. 495–498. Available at: <https://doi.org/10.1016/j.ijggc.2009.12.003>.

Ahmad, A.L., Otitoju, T.A. and Ooi, B.S. (2019) ‘Hollow fiber (HF) membrane fabrication: A review on the effects of solution spinning conditions on morphology and performance’, *Journal of Industrial and Engineering Chemistry*, 70, pp. 35–50. Available at: <https://doi.org/10.1016/j.jiec.2018.10.005>.

Aili, D. *et al.* (2020) ‘Polysulfone-polyvinylpyrrolidone blend membranes as electrolytes in alkaline water electrolysis’, *Journal of Membrane Science*, 598. Available at: <https://doi.org/10.1016/j.memsci.2019.117674>.

- Åkesson, B. (2001) *N-methyl-2-pyrrolidone*. Geneva: World health organization (Concise international chemical assessment document, 35). Available at: <https://apps.who.int/iris/handle/10665/42404> (Accessed: 24 June 2023).
- Al Aani, S., Mustafa, T.N. and Hilal, N. (2020) 'Ultrafiltration membranes for wastewater and water process engineering: A comprehensive statistical review over the past decade', *Journal of Water Process Engineering*, 35, p. 101241. Available at: <https://doi.org/10.1016/j.jwpe.2020.101241>.
- Al Malek, S.A. *et al.* (2012) 'Formation and characterization of polyethersulfone membranes using different concentrations of polyvinylpyrrolidone', *Desalination*, 288, pp. 31–39. Available at: <https://doi.org/10.1016/j.desal.2011.12.006>.
- Alavijeh, H.N. and Baltus, R.E. (2022) 'Transmission of poly(dT60) single-stranded DNA through polycarbonate track-etched ultrafiltration membranes', *Biotechnology Progress*, n/a(n/a), p. e3315. Available at: <https://doi.org/10.1002/btpr.3315>.
- Arumugham, T. *et al.* (2021) 'Recent developments in porous ceramic membranes for wastewater treatment and desalination: A review', *Journal of Environmental Management*, 293, p. 112925. Available at: <https://doi.org/10.1016/j.jenvman.2021.112925>.
- Ashland (2013) *Polyvinylpyrrolidone polymers, PVP K-series chemistry: PVP polymers and VP derivatives*. Available at: <https://www.ashland.com/industries/personal-and-home-care/home-i-and-i/pvp-k-series> (Accessed: 24 June 2023).
- Baker, R.W. (2012) *Membrane Technology and Applications, Third Edition*. John Wiley & Sons, Ltd. Available at: <https://www.wiley.com/en-us/Membrane+Technology+and+Applications,+3rd+Edition-p-9781118359686> (Accessed: 4 May 2023).
- Barrer, R.M. (1984) 'Diffusivities in Glassy-Polymers for the Dual Mode Sorption Model', *Journal of Membrane Science*, 18(Mar), pp. 25–35. Available at: [https://doi.org/10.1016/S0376-7388\(00\)85023-1](https://doi.org/10.1016/S0376-7388(00)85023-1).
- Barrer, R.M. and Rideal, E.K. (1939) 'Permeation, diffusion and solution of gases in organic polymers', *Transactions of the Faraday Society*, 35, pp. 628–643. Available at: <https://doi.org/10.1039/tf9393500628>.

Bärwinkel, S. *et al.* (2016) ‘Polymer Foams Made of Immiscible Polymer Blends Compatibilized by Janus Particles—Effect of Compatibilization on Foam Morphology’, *Advanced Engineering Materials*, 18(5), pp. 814–825. Available at: <https://doi.org/10.1002/adem.201500387>.

BASF SE (2022) *Ultrason® (PSU, PESU, PPSU) – The Specialty Plastic for High-quality Parts*. Available at: https://plastics-rubber.basf.com/northamerica/en/performance_polymers/products/ultrason.html (Accessed: 4 July 2022).

BASF SE (2023) *Povidones, Copovidones, and Crospovidones for Pharmaceutical Products*, *BASF Pharma*. Available at: <https://pharma.basf.com/chemistry/povidones-copovidones-crospovidones> (Accessed: 13 March 2023).

Bazrafshan, N. *et al.* (2021) ‘Preparation and modification of low-fouling ultrafiltration membranes for cheese whey treatment by membrane bioreactor’, *Case Studies in Chemical and Environmental Engineering*, 4, p. 100137. Available at: <https://doi.org/10.1016/j.cscee.2021.100137>.

Biernat, U. (2018) *Threepart sandwich, one thermoplastic, many possibilities*. Available at: <https://www.basf.com/no/en/media/news-releases/2018/08/p-18-281.html> (Accessed: 24 June 2023).

Brincat, J.-P. *et al.* (2016) ‘A review of the state-of-the-art in air filtration technologies as may be applied to cold storage warehouses’, *Trends in Food Science & Technology*, 50, pp. 175–185. Available at: <https://doi.org/10.1016/j.tifs.2016.01.015>.

Bruker (2023) *Guide to FT-IR Spectroscopy*. Available at: <https://www.bruker.com/en/products-and-solutions/infrared-and-raman/ft-ir-routine-spectrometer/what-is-ft-ir-spectroscopy.html> (Accessed: 29 July 2023).

Bühler, V. (2005) *Polyvinylpyrrolidone Excipients for Pharmaceuticals*, *SpringerLink*. Berlin, Germany: Springer. Available at: <https://link.springer.com/book/10.1007/b138598> (Accessed: 1 July 2023).

Car, A. *et al.* (2008) ‘Pebax®/polyethylene glycol blend thin film composite membranes for CO₂ separation: Performance with mixed gases’, *Separation and Purification Technology*, 62(1), pp. 110–117. Available at: <https://doi.org/10.1016/j.seppur.2008.01.001>.

Cassagnau, P. *et al.* (2005) ‘Study of mixing of liquid/polymer in twin screw extruder by residence time distribution’, *Polymer Engineering and Science*, 45(7), pp. 926–934. Available at: <https://doi.org/10.1002/pen.20346>.

Castro-Muñoz, R. *et al.* (2020) ‘Membrane technologies assisting plant-based and agro-food by-products processing: A comprehensive review’, *Trends in Food Science & Technology*, 95, pp. 219–232. Available at: <https://doi.org/10.1016/j.tifs.2019.12.003>.

CDC (1990) *Preventing adverse health effects from exposure to: Dimethylformamide (DMF)*. Available at: <https://www.cdc.gov/niosh/docs/90-105/default.html> (Accessed: 24 June 2023).

Chamberland, J. *et al.* (2019) ‘Influence of feed temperature to biofouling of ultrafiltration membrane during skim milk processing’, *International Dairy Journal*, 93, pp. 99–105. Available at: <https://doi.org/10.1016/j.idairyj.2019.02.005>.

Chandavas, C. *et al.* (2003) ‘Fabrication of microporous polymeric membranes by melt processing of immiscible blends’, *Journal of Membrane Science*, 211(1), pp. 167–175. Available at: [https://doi.org/10.1016/S0376-7388\(02\)00032-7](https://doi.org/10.1016/S0376-7388(02)00032-7).

Chauvet, M., Sauceau, M. and Fages, J. (2017) ‘Extrusion assisted by supercritical CO₂: A review on its application to biopolymers’, *The Journal of Supercritical Fluids*, 120, pp. 408–420. Available at: <https://doi.org/10.1016/j.supflu.2016.05.043>.

Choi, O., Ingole, P.G. and Park, C.H. (2022) ‘Precision-aiming tuning of membranes prepared by NIPS and its performance enhancement’, *Journal of Cleaner Production*, 365, p. 132858. Available at: <https://doi.org/10.1016/j.jclepro.2022.132858>.

Coats, A.W. and Redfern, J.P. (1963) ‘Thermogravimetric analysis. A review’, *Analyst*, 88(1053), pp. 906–924. Available at: <https://doi.org/10.1039/AN9638800906>.

Costeux, S. *et al.* (2015) ‘Experimental study and modeling of nanofoams formation from single phase acrylic copolymers’, *Journal of Cellular*

Plastics, 51(2), pp. 197–221. Available at:
<https://doi.org/10.1177/0021955x14531972>.

Dai, Y. *et al.* (2019) ‘Various hydrophilic carbon dots doped high temperature proton exchange composite membranes based on polyvinylpyrrolidone and polyethersulfone’, *Journal of Colloid and Interface Science*, 553, pp. 503–511. Available at:
<https://doi.org/10.1016/j.jcis.2019.06.020>.

Davis, J.R. (2004) *Tensile Testing, 2nd Edition*. ASM International. Available at: <https://books.google.de/books?id=5uRIb3emLY8C> (Accessed: 1 July 2023).

Dibrov, G. *et al.* (2020) ‘Influence of sodium hypochlorite treatment on pore size distribution of polysulfone/polyvinylpyrrolidone membranes’, *Membranes*, 10(11). Available at:
<https://doi.org/10.3390/membranes10110356>.

Dimitrov, I. and Tsvetanov, C.B. (2012) ‘4.27 - Oligomeric Poly(ethylene oxide)s. Functionalized Poly(ethylene glycol)s. PEGylation’, in K. Matyjaszewski and M. Möller (eds) *Polymer Science: A Comprehensive Reference*. Amsterdam: Elsevier, pp. 679–693. Available at:
<https://doi.org/10.1016/B978-0-444-53349-4.00100-X>.

Dong, X. *et al.* (2021) ‘Polymers and Solvents Used in Membrane Fabrication: A Review Focusing on Sustainable Membrane Development’, *Membranes*, 11(5). Available at:
<https://doi.org/10.3390/membranes11050309>.

Doyle, L. (2022) ‘Extrusion foaming behavior of polybutene-1. Toward single-material multifunctional sandwich structures’, *Journal of Applied Polymer Science*, 139(12), p. 51816. Available at:
<https://doi.org/10.1002/app.51816>.

Drioli, E., Giorno, L. and Fontananova, E. (2017) *Comprehensive Membrane Science and Engineering*. Second. Elsevier. Available at: https://books.google.de/books?hl=en&lr=&id=6-xGDgAAQBAJ&oi=fnd&pg=PP1&dq=membrane+science&ots=49A1JNUbuF&sig=I2Pw0ICj9pdL7licryUrCEUhtF4&redir_esc=y#v=onepage&q=membrane%20science&f=false (Accessed: 1 July 2023).

- Drzeżdżon, J. *et al.* (2019) ‘Characterization of polymers based on differential scanning calorimetry based techniques’, *TrAC Trends in Analytical Chemistry*, 110, pp. 51–56. Available at: <https://doi.org/10.1016/j.trac.2018.10.037>.
- Ebnesajjad, S. (2015) ‘12 - Fabrication and Processing of Polytetrafluoroethylene Dispersions’, in S. Ebnesajjad (ed.) *Fluoroplastics (Second Edition)*. Oxford: William Andrew Publishing, pp. 278–299. Available at: <https://doi.org/10.1016/B978-1-4557-3199-2.00012-4>.
- Ellson, R. *et al.* (2005) ‘In situ DMSO hydration measurements of HTS compound libraries.’, *Combinatorial chemistry & high throughput screening*, 8(6), pp. 489–498. Available at: <https://doi.org/10.2174/1386207054867382>.
- Emonds, S. *et al.* (2021) ‘Polyelectrolyte Complex Tubular Membranes via a Salt Dilution Induced Phase Inversion Process’, *Advanced Engineering Materials*, 23(5), p. 2001401. Available at: <https://doi.org/10.1002/adem.202001401>.
- European Union (2023) *OECD Portal on Per and Poly Fluorinated Chemicals, REACH restrictions*. Available at: <https://www.oecd.org/chemicalsafety/portal-perfluorinated-chemicals/countryinformation/european-union.htm> (Accessed: 29 July 2023).
- Fang, X.F. *et al.* (2015) ‘Polyethyleneimine, an effective additive for polyethersulfone ultrafiltration membrane with enhanced permeability and selectivity’, *Journal of Membrane Science*, 476, pp. 216–223. Available at: <https://doi.org/10.1016/j.memsci.2014.11.021>.
- Feng, J. *et al.* (2018) ‘Structure-property relationships of microporous membranes produced by biaxial orientation of compatibilized PP/Nylon 6 blends’, *Polymer*, 145, pp. 148–156. Available at: <https://doi.org/10.1016/j.polymer.2018.05.005>.
- Ferry, J.D. (1936) ‘Ultrafilter Membranes and Ultrafiltration.’, *Chemical Reviews*, 18(3), pp. 373–455. Available at: <https://doi.org/10.1021/cr60061a001>.

Figoli, A. *et al.* (2014) 'Towards non-toxic solvents for membrane preparation: a review', *Green Chemistry*, 16(9), pp. 4034–4059. Available at: <https://doi.org/10.1039/C4GC00613E>.

Francolini, I., Hall-Stoodley, L. and Stoodley, P. (2020) '2.2.8 - Biofilms, Biomaterials, and Device-Related Infections', in W.R. Wagner *et al.* (eds) *Biomaterials Science (Fourth Edition)*. Academic Press, pp. 823–840. Available at: <https://doi.org/10.1016/B978-0-12-816137-1.00054-4>.

Frisch, H.L. (1980) 'Sorption and transport in glassy polymers-a review', *Polymer Engineering and Science*, 20(1), pp. 2–13. Available at: <https://doi.org/10.1002/pen.760200103>.

Fu, X. *et al.* (2006) 'Preparation of polymer blend hollow fiber membrane via thermally induced phase separation', *Separation and Purification Technology*, 52(2), pp. 363–371. Available at: <https://doi.org/10.1016/j.seppur.2006.05.018>.

Gabbott, P. (2008) *Principles and Applications of Thermal Analysis*. Wiley. Available at: <https://www.wiley.com/en-us/Principles+and+Applications+of+Thermal+Analysis-p-9780470698129> (Accessed: 1 July 2023).

Gaborieau, M. and Castignolles, P. (2011) 'Size-exclusion chromatography (SEC) of branched polymers and polysaccharides', *Analytical and Bioanalytical Chemistry*, 399(4), pp. 1413–1423. Available at: <https://doi.org/10.1007/s00216-010-4221-7>.

Gadalla, M.A. *et al.* (2005) 'Reducing CO₂ emissions and energy consumption of heat-integrated distillation systems', *Environmental Science and Technology*, 39(17), pp. 6860–70. Available at: <https://doi.org/10.1021/es049795q>.

Galiano, F. (2015) 'Casting Solution', in E. Drioli and L. Giorno (eds) *Encyclopedia of Membranes*. Berlin, Heidelberg: Springer Berlin Heidelberg, pp. 1–1. Available at: https://doi.org/10.1007/978-3-642-40872-4_1870-3.

Gama, N.V., Ferreira, A. and Barros-Timmons, A. (2018) 'Polyurethane Foams: Past, Present, and Future', *Materials*, 11(10). Available at: <https://doi.org/10.3390/ma11101841>.

Gendron, R. (ed.) (2004) *Thermoplastic Foam Processing*. 0 edn. CRC Press. Available at: <https://doi.org/10.1201/9780203502167>.

Georgopoulos, P. *et al.* (2016) 'Influence of block sequence and molecular weight on morphological, rheological and dielectric properties of weakly and strongly segregated styrene-isoprene triblock copolymers', *Polymer*, 104, pp. 279–295. Available at: <https://doi.org/10.1016/j.polymer.2016.02.039>.

Giesa, R. and Schmidt, H.W. (2001) 'High-temperature Stable Polymers', in K.H.J. Buschow *et al.* (eds) *Encyclopedia of Materials: Science and Technology*. Oxford: Elsevier, pp. 3803–3806. Available at: <https://doi.org/10.1016/B0-08-043152-6/00677-X>.

Giles, H.F., Wagner, J.R. and Mount, E.M. (2005) '3 - Single Screw Extruder: Equipment', in H.F. Giles, J.R. Wagner, and E.M. Mount (eds) *Extrusion*. Norwich, NY: William Andrew Publishing, pp. 13–34. Available at: <https://doi.org/10.1016/B978-081551473-2.50004-0>.

Glass, S. *et al.* (2021) 'Amine-Terminated PAN Membranes as Anion-Adsorber Materials', *Chemie Ingenieur Technik*, 93(9), pp. 1396–1400. Available at: <https://doi.org/10.1002/cite.202100037>.

Gong, P.J., Taniguchi, T. and Ohshima, M. (2014) 'Nanoporous structure of the cell walls of polycarbonate foams', *Journal of Materials Science*, 49(6), pp. 2605–2617. Available at: <https://doi.org/10.1007/s10853-013-7959-4>.

Göthlich, A., Koltzenburg, S. and Schornick, G. (2005) 'Funktionale Polymere im Alltag: Vielseitig', *Chemie in unserer Zeit*, 39(4), pp. 262–273. Available at: <https://doi.org/10.1002/ciuz.200400346>.

Gronwald, O. *et al.* (2020) 'Hydrophilic poly(phenylene sulfone) membranes for ultrafiltration', *Separation and Purification Technology*, 250. Available at: <https://doi.org/10.1016/j.seppur.2020.117107>.

Gronwald, O. and Weber, M. (2020) 'AGNIQUE AMD 3L as green solvent for polyethersulfone ultrafiltration membrane preparation', *Journal of Applied Polymer Science*, 137(9). Available at: <https://doi.org/10.1002/app.48419>.

- Grünig, L. *et al.* (2020) 'Hydrophilic dual layer hollow fiber membranes for ultrafiltration', *Membranes*, 10(7). Available at: <https://doi.org/10.3390/membranes10070143>.
- Gu, B. *et al.* (2020) 'On the influence of pore connectivity on performance of membrane filters', *Journal of Fluid Mechanics*, 902, p. A5. Available at: <https://doi.org/10.1017/jfm.2020.520>.
- Guan, R. *et al.* (2006) 'Effect of casting solvent on the morphology and performance of sulfonated polyethersulfone membranes', *Journal of Membrane Science*, 277(1), pp. 148–156. Available at: <https://doi.org/10.1016/j.memsci.2005.10.025>.
- Guo, H.M. and Kumar, V. (2015) 'Effect of glass transition temperature and saturation temperature on the solid-state microcellular foaming of cyclic olefin copolymer', *Journal of Applied Polymer Science*, 132(28). Available at: <https://doi.org/10.1002/app.42226>.
- Guo, H.M., Nicolae, A. and Kumar, V. (2015) 'Solid-state microcellular and nanocellular polysulfone foams', *Journal of Polymer Science Part B-Polymer Physics*, 53(14), pp. 975–985. Available at: <https://doi.org/10.1002/polb.23719>.
- Guo, H.M., Nicolae, A. and Kumar, V. (2016) 'Fabrication of high temperature polyphenylsulfone nanofoams using high pressure liquid carbon dioxide', *Cellular Polymers*, 35(3), pp. 119–142. Available at: <https://doi.org/10.1177/026248931603500302>.
- Gutmann, P. *et al.* (2010) 'Foaming of an Immiscible Blend System Using Organic Liquids as Blowing Agents', *Journal of Cellular Plastics*, 46(3), pp. 239–258. Available at: <https://doi.org/10.1177/0021955x09352138>.
- Haaf, F., Sanner, A. and Straub, F. (1985) 'Polymers of N-Vinylpyrrolidone: Synthesis, Characterization and Uses', *Polymer Journal*, 17(1), pp. 143–152. Available at: <https://doi.org/10.1295/polymj.17.143>.
- Haenelt, T.G. *et al.* (2014) 'Morphology and elasticity of polystyrene-block-polyisoprene diblock copolymers in the melt', *Korea-Australia Rheology Journal*, 26(3), pp. 263–275. Available at: <https://doi.org/10.1007/s13367-014-0031-3>.

Halder, K. *et al.* (2017) ‘Blend membranes of ionic liquid and polymers of intrinsic microporosity with improved gas separation characteristics’, *Journal of Membrane Science*, 539, pp. 368–382. Available at: <https://doi.org/10.1016/j.memsci.2017.06.022>.

Halder, K. *et al.* (2018) ‘Investigation of gas transport and other physical properties in relation to the bromination degree of polymers of intrinsic microporosity’, *Journal of Polymer Science Part A: Polymer Chemistry*, 56(24), pp. 2752–2761. Available at: <https://doi.org/10.1002/pola.29262>.

Han, C.D., Kim, Y.W. and Malhotra, K.D. (1976) ‘A study of foam extrusion using a chemical blowing agent’, *Journal of Applied Polymer Science*, 20(6), pp. 1583–1595. Available at: <https://doi.org/10.1002/app.1976.070200615>.

Han, X. *et al.* (2002) ‘Continuous microcellular polystyrene foam extrusion with supercritical CO₂’, *Polymer Engineering & Science*, 42(11), pp. 2094–2106. Available at: <https://doi.org/10.1002/pen.11100>.

Hao, Y. *et al.* (2012) ‘Visualization of Protein Fouling inside a Hollow Fiber Ultrafiltration Membrane by Fluorescent Microscopy’, *Industrial & Engineering Chemistry Research*, 51(45), pp. 14850–14858. Available at: <https://doi.org/10.1021/ie302111w>.

Haurat, M. and Dumon, M. (2020) ‘Amorphous Polymers’ Foaming and Blends with Organic Foaming-Aid Structured Additives in Supercritical CO₂, a Way to Fabricate Porous Polymers from Macro to Nano Porosities in Batch or Continuous Processes’, *Molecules*, 25(22), p. 5320. Available at: <https://doi.org/10.3390/molecules25225320>.

Höhne, G.W.H. (1999) ‘High pressure differential scanning calorimetry on polymers’, *Thermochimica Acta*, 332(2), pp. 115–123. Available at: [https://doi.org/10.1016/S0040-6031\(99\)00066-0](https://doi.org/10.1016/S0040-6031(99)00066-0).

Huang, E. *et al.* (2016) ‘Effect of Unexpected CO₂’s Phase Transition on the High-Pressure Differential Scanning Calorimetry Performance of Various Polymers’, *ACS Sustainable Chemistry & Engineering*, 4(3), pp. 1810–1818. Available at: <https://doi.org/10.1021/acssuschemeng.6b00008>.

Huang, Q. (2000) *Lösemitelfreie Herstellung von porösen polymeren Membranen durch Schaumextrusion*. Universität Hamburg. Available at:

<https://ediss.sub.uni-hamburg.de/handle/ediss/1334> (Accessed: 24 June 2023).

Hutanu, D. (2014) ‘Recent Applications of Polyethylene Glycols (PEGs) and PEG Derivatives’, *Modern Chemistry & Applications*, 02(02). Available at: <https://doi.org/10.4172/2329-6798.1000132>.

Ibrahim, M.S., El-Wassefy, N.A. and Farahat, D.S. (2017) ‘8 - Biocompatibility of dental biomaterials’, in L. Tayebi and K. Moharamzadeh (eds) *Biomaterials for Oral and Dental Tissue Engineering*. Woodhead Publishing, pp. 117–140. Available at: <https://shorturl.at/btBF2> (Accessed: 1 July 2023).

ILO and WHO (2021) *N-METHYL-2-PYRROLIDONE*. Available at: http://www.ilo.org/dyn/icsc/showcard.display?p_card_id=0513&p_version=1&p_lang=en (Accessed: 3 March 2023).

Jaleh, B. *et al.* (2020) ‘Preparation and Characterization of Polyvinylpyrrolidone/Polysulfone Ultrafiltration Membrane Modified by Graphene Oxide and Titanium Dioxide for Enhancing Hydrophilicity and Antifouling Properties’, *Journal of Inorganic and Organometallic Polymers and Materials*, 30(6), pp. 2213–2223. Available at: <https://doi.org/10.1007/s10904-019-01367-x>.

Jiang, J. *et al.* (2021) ‘Microcellular injection molding of polymers: a review of process know-how, emerging technologies, and future directions’, *Current Opinion in Chemical Engineering*, 33, p. 100694. Available at: <https://doi.org/10.1016/j.coche.2021.100694>.

Jin, F.-L. *et al.* (2019) ‘Recent Trends of Foaming in Polymer Processing: A Review’, *Polymers*, 11(6). Available at: <https://doi.org/10.3390/polym11060953>.

Jung, P.U. (2014) *Development of Innovative Gas-assisted Foam Injection Molding Technology*. Available at: <https://tspace.library.utoronto.ca/handle/1807/43608> (Accessed: 1 July 2023).

Kabir, Md.E., Saha, M.C. and Jeelani, S. (2006) ‘Tensile and fracture behavior of polymer foams’, *Materials Science and Engineering: A*, 429(1), pp. 225–235. Available at: <https://doi.org/10.1016/j.msea.2006.05.133>.

- Kalia, K. *et al.* (2022) ‘In Situ Foam 3D Printing of Microcellular Structures Using Material Extrusion Additive Manufacturing’, *ACS Applied Materials & Interfaces*, 14(19), pp. 22454–22465. Available at: <https://doi.org/10.1021/acsami.2c03014>.
- Kalogerias, I.M. (2016) ‘Glass-Transition Phenomena in Polymer Blends’, in *Encyclopedia of Polymer Blends*, pp. 1–134. Available at: <https://doi.org/10.1002/9783527653966.ch1>.
- Kamp, J. *et al.* (2021) ‘On the organic solvent free preparation of ultrafiltration and nanofiltration membranes using polyelectrolyte complexation in an all aqueous phase inversion process’, *Journal of Membrane Science*, 618, p. 118632. Available at: <https://doi.org/10.1016/j.memsci.2020.118632>.
- Khemani, K.C. (1997) ‘Polymeric Foams: An Overview’, in *Polymeric Foams*. American Chemical Society (ACS Symposium Series, 669), pp. 1–7. Available at: <https://doi.org/10.1021/bk-1997-0669.ch001>.
- Kim, J.F. *et al.* (2016) ‘Thermally induced phase separation and electrospinning methods for emerging membrane applications: A review’, *AIChE Journal*, 62(2), pp. 461–490. Available at: <https://doi.org/10.1002/aic.15076>.
- Kim, J.-J. *et al.* (1994) ‘Structural study of microporous polypropylene hollow fiber membranes made by the melt-spinning and cold-stretching method’, *Journal of Membrane Science*, 93(3), pp. 209–215. Available at: [https://doi.org/10.1016/0376-7388\(94\)00070-0](https://doi.org/10.1016/0376-7388(94)00070-0).
- Kim, Y. *et al.* (2011) ‘Origins of the failure of classical nucleation theory for nanocellular polymer foams’, *Soft Matter*, 7(16), pp. 7351–7358. Available at: <https://doi.org/10.1039/C1SM05575E>.
- Klingberg, P. *et al.* (2019) ‘Separation of Carbon Dioxide from Real Power Plant Flue Gases by Gas Permeation Using a Supported Ionic Liquid Membrane: An Investigation of Membrane Stability’, *Membranes*, 9(3). Available at: <https://doi.org/10.3390/membranes9030035>.
- Kong, W. *et al.* (2016) ‘Preparation of open-cell polymer foams by CO₂ assisted foaming of polymer blends’, *Polymer*, 90, pp. 331–341. Available at: <https://doi.org/10.1016/j.polymer.2016.03.035>.

- Kong, Y. and Hay, J.N. (2002) 'The measurement of the crystallinity of polymers by DSC', *Polymer*, 43(14), pp. 3873–3878. Available at: [https://doi.org/10.1016/S0032-3861\(02\)00235-5](https://doi.org/10.1016/S0032-3861(02)00235-5).
- Krause, B. *et al.* (2001) 'Novel open-cellular polysulfone morphologies produced with trace concentrations of solvents as pore opener', *Journal of Membrane Science*, 187(1–2), pp. 181–192. Available at: [https://doi.org/10.1016/S0376-7388\(01\)00329-5](https://doi.org/10.1016/S0376-7388(01)00329-5).
- Krause, B., van der Vegt, N.F.A. and Wessling, M. (2002) 'New ways to produce porous polymeric membranes by carbon dioxide foaming', *Desalination*, 144(1–3), pp. 5–7. Available at: [https://doi.org/10.1016/S0011-9164\(02\)00280-1](https://doi.org/10.1016/S0011-9164(02)00280-1).
- Kumar, V. and Weller, J.E. (1994) 'A model for the unfoamed skin on microcellular foams', *Polymer Engineering & Science*, 34(3), pp. 169–173. Available at: <https://doi.org/10.1002/pen.760340302>.
- Lalia, B.S. *et al.* (2013) 'A review on membrane fabrication: Structure, properties and performance relationship', *Desalination*, 326, pp. 77–95. Available at: <https://doi.org/10.1016/j.desal.2013.06.016>.
- Lee, C.H. *et al.* (2000) 'Growth of gas bubbles in the foam extrusion process', *Advances in Polymer Technology*, 19(2), pp. 97–112. Available at: [https://doi.org/10.1002/\(SICI\)1098-2329\(200022\)19:2<97::AID-ADV3>3.0.CO;2-B](https://doi.org/10.1002/(SICI)1098-2329(200022)19:2<97::AID-ADV3>3.0.CO;2-B).
- Lee, J.K. and Han, C.D. (2000) 'Evolution of polymer blend morphology during compounding in a twin-screw extruder', *Polymer*, 41(5), pp. 1799–1815. Available at: [https://doi.org/10.1016/S0032-3861\(99\)00325-0](https://doi.org/10.1016/S0032-3861(99)00325-0).
- Lee, S.-T. and Park, C.B. (eds) (2014) *Foam extrusion: principles and practice*. Second Edition. Boca Raton: CRC Press (Polymeric foams series). Available at: <https://shorturl.at/fkmvV> (Accessed: 1 July 2023).
- Liguori, S. *et al.* (2020) 'Opportunities and challenges of low-carbon hydrogen via metallic membranes', *Progress in Energy and Combustion Science*, 80, p. 100851. Available at: <https://doi.org/10.1016/j.pecs.2020.100851>.
- Lillepärq, J., Georgopoulos, P. and Shishatskiy, S. (2014) 'Stability of blended polymeric materials for CO₂ separation', *Journal of Membrane*

Science, 467, pp. 269–278. Available at:
<https://doi.org/10.1016/j.memsci.2014.05.039>.

Liu, F. *et al.* (2011) ‘Progress in the production and modification of PVDF membranes’, *Journal of Membrane Science*, 375(1), pp. 1–27. Available at:
<https://doi.org/10.1016/j.memsci.2011.03.014>.

Liu, M. *et al.* (2016) ‘Formation of microporous polymeric membranes via thermally induced phase separation: A review’, *Frontiers of Chemical Science and Engineering*, 10(1), pp. 57–75. Available at:
<https://doi.org/10.1007/s11705-016-1561-7>.

Liu, M. *et al.* (2019) ‘A Facile Way to Prepare Hydrophilic Homogeneous PES Hollow Fiber Membrane via Non-Solvent Assisted Reverse Thermally Induced Phase Separation (RTIPS) Method’, *Polymers*, 11(2). Available at:
<https://doi.org/10.3390/polym11020269>.

Luo, D., Xie, G. and Qin, S. (2021) ‘The hydrophilic polypropylene/poly(ethylene-co-vinyl alcohol) hollow fiber membrane with bimodal microporous structure prepared by melt-spinning and stretching’, *Separation and Purification Technology*, 274, p. 118890. Available at: <https://doi.org/10.1016/j.seppur.2021.118890>.

Lutz, H. (2010) ‘2.06 - Ultrafiltration: Fundamentals and Engineering’, in E. Drioli and L. Giorno (eds) *Comprehensive Membrane Science and Engineering*. Oxford: Elsevier, pp. 115–139. Available at:
<https://doi.org/10.1016/B978-0-08-093250-7.00037-2>.

Ma, Y. *et al.* (2011) ‘Effect of PEG additive on the morphology and performance of polysulfone ultrafiltration membranes’, *Desalination*, 272(1), pp. 51–58. Available at:
<https://doi.org/10.1016/j.desal.2010.12.054>.

Mantel, T. *et al.* (2022) ‘Adsorptive dead-end filtration for removal of Cr(vi) using novel amine modified polyacrylonitrile ultrafiltration membranes’, *Environmental Science: Water Research & Technology*, 8(12), pp. 2981–2993. Available at: <https://doi.org/10.1039/D2EW00570K>.

Mettler-Toledo (2022) *High Pressure Differential Scanning Calorimetry*, Mettler-Toledo International Inc. Mettler-Toledo International Inc. Available at:

https://www.mt.com/de/en/home/products/Laboratory_Analytics_Browse/TA_Family_Browse/HP_DSC.html (Accessed: 15 March 2023).

Michler, S. (2016) 'Atlas of Polymer Structures', in G.H. Michler (ed.) *Atlas of Polymer Structures*. Hanser, p. I–IX. Available at: <https://doi.org/10.3139/9781569905586.fm>.

Miller, D., Chatchaisucha, P. and Kumar, V. (2009) 'Microcellular and nanocellular solid-state polyetherimide (PEI) foams using sub-critical carbon dioxide I. Processing and structure', *Polymer*, 50(23), pp. 5576–5584. Available at: <https://doi.org/10.1016/j.polymer.2009.09.020>.

Miyake, A. (1960) 'Extension of the Schulz-Zimm molecular weight distribution function', *Journal of Polymer Science*, 45(145), pp. 230–232. Available at: <https://doi.org/10.1002/pol.1960.1204514525>.

Mokhtari Motameni Shirvan, M., Famili, M.H.N. and Golbang, A. (2016) 'A Review on the Application of Nucleation Theories in Thermoplastic Foams', *Plastic and Polymer Technology*, 4(0), p. 11. Available at: <https://doi.org/10.14355/papt.2016.04.002>.

Monge, S., Darcos, V. and Haddleton, D.M. (2004) 'Effect of DMSO used as solvent in copper mediated living radical polymerization', *Journal of Polymer Science Part A: Polymer Chemistry*, 42(24), pp. 6299–6308. Available at: <https://doi.org/10.1002/pola.20403>.

Moore, J.C. (1964) 'Gel permeation chromatography. I. A new method for molecular weight distribution of high polymers', *Journal of Polymer Science Part A: General Papers*, 2(2), pp. 835–843. Available at: <https://doi.org/10.1002/pol.1964.100020220>.

Murugan, R. *et al.* (2021) 'Ultrafiltration in critically ill patients treated with kidney replacement therapy', *Nature Reviews Nephrology*, 17(4), pp. 262–276. Available at: <https://doi.org/10.1038/s41581-020-00358-3>.

Naya, S. *et al.* (2013) 'New method for estimating shift factors in time–temperature superposition models', *Journal of Thermal Analysis and Calorimetry*, 113(2), pp. 453–460. Available at: <https://doi.org/10.1007/s10973-013-3193-1>.

NETZSCH (2023a) *A Basic Introduction to Rheology*. Available at: <https://analyzing->

testing.netzsch.com/_Resources/Persistent/6/b/3/4/6b34154e1f16c2b8198c1f4a6fa3ac2cd2ce0eb9/WP_A_Basic_Introduction_to_Rheology.pdf (Accessed: 28 March 2023).

NETZSCH (2023b) ‘Differential Scanning Calorimetry (DSC)’, *NETZSCH - Analyzing and Testing. Leading in Thermal Analysis, Rheology and Fire Testing* [Preprint]. Available at: <https://analyzing-testing.netzsch.com/en/contract-testing/methods/differential-scanning-calorimetry-dsc> (Accessed: 15 March 2023).

Ng, H.M. *et al.* (2018) ‘Thermogravimetric Analysis of Polymers’, in *Encyclopedia of Polymer Science and Technology*, pp. 1–29. Available at: <https://doi.org/10.1002/0471440264.pst667>.

Noor, N. *et al.* (2018) ‘Hollow Fiber Membranes of Blends of Polyethersulfone and Sulfonated Polymers’, *Membranes*, 8(3). Available at: <https://doi.org/ARTN 54 10.3390/membranes8030054>.

Norddahl, B. *et al.* (2021) ‘Chapter 6 - Membrane-based technology for methane separation from biogas’, in N. Aryal *et al.* (eds) *Emerging Technologies and Biological Systems for Biogas Upgrading*. Academic Press, pp. 117–157. Available at: <https://doi.org/10.1016/B978-0-12-822808-1.00006-4>.

Nunes, S.P. *et al.* (2020) ‘Thinking the future of membranes: Perspectives for advanced and new membrane materials and manufacturing processes’, *Journal of Membrane Science*, 598, p. 117761. Available at: <https://doi.org/10.1016/j.memsci.2019.117761>.

Okolieocha, C. *et al.* (2015) ‘Microcellular to nanocellular polymer foams: Progress (2004-2015) and future directions - A review’, *European Polymer Journal*, 73, pp. 500–519. Available at: <https://doi.org/10.1016/j.eurpolymj.2015.11.001>.

Osswald, T. and Rudolph, N. (2015) ‘Polymer Rheology’, in T. Osswald and N. Rudolph (eds) *Polymer Rheology*. Hanser, p. I–XI. Available at: <https://doi.org/10.3139/9781569905234.fm>.

Owusu-Nkwantabisah, S., Staudt, C. and Lesser, A.J. (2018) ‘Synergy of supercritical CO₂ and superheated H₂O for enhanced processability of polyethersulfone towards open cell foams’, *Polymer Engineering and*

Science, 58(7), pp. 1108–1114. Available at:
<https://doi.org/10.1002/pen.24673>.

Oxtoby, D.W. (1998) ‘Nucleation of First-Order Phase Transitions’, *Accounts of Chemical Research*, 31(2), pp. 91–97. Available at:
<https://doi.org/10.1021/ar9702278>.

Pandit, M.P., Vidyāratna, T. and Woodroffe, J.G. (1999) *Kulārṇava Tantra*. Motilal Banarsidass. Available at:
<https://books.google.de/books?id=FWeHQZAZ-goC> (Accessed: 1 July 2023).

Papanicolaou, G.C. and Zaoutsos, S.P. (2011) ‘1 - Viscoelastic constitutive modeling of creep and stress relaxation in polymers and polymer matrix composites’, in R.M. Guedes (ed.) *Creep and Fatigue in Polymer Matrix Composites*. Woodhead Publishing, pp. 3–47. Available at:
<https://doi.org/10.1533/9780857090430.1.3>.

Park, C.B., Behraves, A.H. and Venter, R.D. (1998) ‘Low density microcellular foam processing in extrusion using CO₂’, *Polymer Engineering & Science*, 38(11), pp. 1812–1823. Available at:
<https://doi.org/10.1002/pen.10351>.

Pezeshk, N. *et al.* (2012) ‘Novel modified PVDF ultrafiltration flat-sheet membranes’, *Journal of Membrane Science*, 389, pp. 280–286. Available at: <https://doi.org/10.1016/j.memsci.2011.10.039>.

Pinto, J., Dumon, M. and Rodriguez-Perez, M.A. (2017) ‘9 - Nanoporous polymer foams from nanostructured polymer blends: Preparation, characterization, and properties’, in P.M. Visakh, G. Markovic, and D. Pasquini (eds) *Recent Developments in Polymer Macro, Micro and Nano Blends*. Woodhead Publishing, pp. 237–288. Available at:
<https://doi.org/10.1016/B978-0-08-100408-1.00009-1>.

Porter, S., Sackett, G. and Liu, L. (2009) ‘Chapter 33 - Development, Optimization, and Scale-up of Process Parameters: Pan Coating’, in Y. Qiu *et al.* (eds) *Developing Solid Oral Dosage Forms*. San Diego: Academic Press, pp. 761–805. Available at: <https://doi.org/10.1016/B978-0-444-53242-8.00033-3>.

Pulyalina, A. *et al.* (2018) 'Improved Hydrogen Separation Using Hybrid Membrane Composed of Nanodiamonds and P84 Copolyimide', *Polymers*, 10(8). Available at: <https://doi.org/10.3390/polym10080828>.

Qi, K. and Huang, R. (1998) '3 - Polyethersulfone (PES) and Its Processing', in N.P. Cheremisinoff (ed.) *Advanced Polymer Processing Operations*. Westwood, NJ: William Andrew Publishing, pp. 69–99. Available at: <https://doi.org/10.1016/B978-081551426-8.50006-4>.

Qin, Y. (2016) '5 - Applications of advanced technologies in the development of functional medical textile materials', in Y. Qin (ed.) *Medical Textile Materials*. Woodhead Publishing, pp. 55–70. Available at: <https://doi.org/10.1016/B978-0-08-100618-4.00005-4>.

Radjabian, M. *et al.* (2013) 'Hollow fiber spinning of block copolymers: Influence of spinning conditions on morphological properties', *Polymer*, 54(7), pp. 1803–1812. Available at: <https://doi.org/10.1016/j.polymer.2013.01.033>.

Radjabian, M. *et al.* (2014) 'Tailoring the morphology of self-assembled block copolymer hollow fiber membranes', *Polymer*, 55(13), pp. 2986–2997. Available at: <https://doi.org/10.1016/j.polymer.2014.04.041>.

Rahman, Md.M. *et al.* (2015) 'Influence of Poly(ethylene glycol) Segment Length on CO₂ Permeation and Stability of PolyActive Membranes and Their Nanocomposites with PEG POSS', *ACS Applied Materials & Interfaces*, 7(23), pp. 12289–12298. Available at: <https://doi.org/10.1021/am504223f>.

Rahman, Md.M. (2021) 'Membrane Separation of Gaseous Hydrocarbons by Semicrystalline Multiblock Copolymers: Role of Cohesive Energy Density and Crystallites of the Polyether Block', *Polymers*, 13(23). Available at: <https://doi.org/10.3390/polym13234181>.

Ramli, H. *et al.* (2022) 'Basic principle and good practices of rheology for polymers for teachers and beginners', 4(4), pp. 307–326. Available at: <https://doi.org/10.1515/cti-2022-0010>.

Raviv, U. and Klein, J. (2012) '2.24 - Adhesion, Friction, and Lubrication between Polymer-Bearing Surfaces', in K. Matyjaszewski and M. Möller (eds) *Polymer Science: A Comprehensive Reference*. Amsterdam: Elsevier,

pp. 607–628. Available at: <https://doi.org/10.1016/B978-0-444-53349-4.00048-0>.

Razali, M. *et al.* (2015) ‘Sustainable wastewater treatment and recycling in membrane manufacturing’, *Green Chemistry*, 17(12), pp. 5196–5205. Available at: <https://doi.org/10.1039/C5GC01937K>.

Razzaz, Z., Mohebbi, A. and Rodrigue, D. (2018) ‘Effect of processing conditions on the cellular morphology of polyethylene hollow fiber foams for membrane applications’, *Cellular Polymers*, 37(4–6), pp. 169–188. Available at: <https://doi.org/10.1177/0262489318795967>.

Redlich, C., Beckett, W.S. and Cullen, M.R. (1987) ‘Hepatitis Associated with Occupational Exposure to the Solvent Dimethylformamide’, *Clinical Research*, 35(3), pp. A756–A756.

Redlich, C.A. *et al.* (1987) ‘Dimethylformamide Induced Hepatotoxicity in Factory-Workers’, *Hepatology*, 7(5), pp. 1088–1088.

Redlich, C.A. *et al.* (1988) ‘Liver-disease associated with occupational exposure to the solvent dimethylformamide’, *Annals of Internal Medicine*, 108(5), pp. 680–686. Available at: <https://doi.org/10.7326/0003-4819-108-5-680>.

Rigoli, P.S. *et al.* (2019) ‘Quantification of Aerospace Polymer Blends by Thermogravimetric Analysis and Infrared Spectrometry’, *Journal of Aerospace Technology and Management*, 11. Available at: <https://doi.org/10.5028/jatm.v11.986>.

Roß, N. and Frerich, S.C. (2021) ‘High pressure differential scanning calorimetry of poly(lactic acid) in presence of CO₂ up to 100 MPa’, *Thermochimica Acta*, 706, p. 179076. Available at: <https://doi.org/10.1016/j.tca.2021.179076>.

Rouquerol, J. *et al.* (1994) ‘Recommendations for the characterization of porous solids (Technical Report)’, 66(8), pp. 1739–1758. Available at: <https://doi.org/10.1351/pac199466081739>.

Ruckdäschel, H. *et al.* (2010) ‘Foaming of Microstructured and Nanostructured Polymer Blends’, in A.H.E. Müller and H.-W. Schmidt (eds) *Complex Macromolecular Systems I*. Berlin, Heidelberg: Springer

Berlin Heidelberg, pp. 199–252. Available at:
https://doi.org/10.1007/12_2009_32.

Sambasivam, M., White, R. and Cutting, K. (2016) ‘12 - Exploring the role of polyurethane and polyvinyl alcohol foams in wound care’, in M.S. Ågren (ed.) *Wound Healing Biomaterials*. Woodhead Publishing, pp. 251–260. Available at: <https://doi.org/10.1016/B978-1-78242-456-7.00012-X>.

Sankhala, K. *et al.* (2017) ‘A Pathway to Fabricate Hollow Fiber Membranes with Isoporous Inner Surface’, *Advanced Materials Interfaces*, 4(7). Available at: <https://doi.org/10.1002/admi.201600991>.

Sauceau, M. *et al.* (2011) ‘New challenges in polymer foaming: A review of extrusion processes assisted by supercritical carbon dioxide’, *Progress in Polymer Science*, 36(6), pp. 749–766. Available at: <https://doi.org/10.1016/j.progpolymsci.2010.12.004>.

Schick, C. (2009) ‘Differential scanning calorimetry (DSC) of semicrystalline polymers’, *Analytical and Bioanalytical Chemistry*, 395(6), pp. 1589–1611. Available at: <https://doi.org/10.1007/s00216-009-3169-y>.

Schuldt, K., Brinkmann, T. and Georgopoulos, P. (2021) ‘Zero-Discharge Process for Recycling of Tetrahydrofuran–Water Mixtures’, *Processes*, 9(5). Available at: <https://doi.org/10.3390/pr9050729>.

Schulze, M. *et al.* (2015) ‘Thermal properties, rheology and foams of polystyrene-block-poly(4-vinylpyridine) diblock copolymers’, *Polymer*, 70, pp. 88–99. Available at: <https://doi.org/10.1016/j.polymer.2015.06.005>.

Seader J. D., S.J.S. (1997) ‘Distillation’, in D.W.G. Robert H. Perry (ed.) *Perry's chemical engineers' handbook*. Seven. McGraw-Hill. Available at: <https://www.accessengineeringlibrary.com/content/book/9780071422949> (Accessed: 1 July 2023).

Shabani, A. *et al.* (2021) ‘Thermoplastic polyurethane foams: From autoclave batch foaming to bead foam extrusion’, *Journal of Cellular Plastics*, 57(4), pp. 391–411. Available at: <https://doi.org/10.1177/0021955x20912201>.

Shah, H. *et al.* (2021) ‘Chapter 32 - Pharmaceutical excipients’, in A. Adejare (ed.) *Remington (Twenty-third Edition)*. Academic Press, pp. 633–643. Available at: <https://doi.org/10.1016/B978-0-12-820007-0.00032-5>.

Shi, J., Xu, L. and Qiu, D. (2022) ‘Effective Antifogging Coating from Hydrophilic/Hydrophobic Polymer Heteronetwork’, *Advanced Science*, 9(14), p. 2200072. Available at: <https://doi.org/10.1002/advs.202200072>.

Siddiqui, M.U., Arif, A.F. and Bashmal, S. (2016) ‘Permeability-Selectivity Analysis of Microfiltration and Ultrafiltration Membranes: Effect of Pore Size and Shape Distribution and Membrane Stretching’, *Membranes*, 6(3). Available at: <https://doi.org/10.3390/membranes6030040>.

Singh, R. (2015) ‘Introduction to Membrane Technology’, in *Membrane Technology and Engineering for Water Purification*. Elsevier, pp. 1–80. Available at: <https://doi.org/10.1016/B978-0-444-63362-0.00001-X>.

Skleničková, K. *et al.* (2021) ‘Open-Cell Aliphatic Polyurethane Foams with High Content of Polysaccharides: Structure, Degradation, and Ecotoxicity’, *ACS Sustainable Chemistry & Engineering*, 9(17), pp. 6023–6032. Available at: <https://doi.org/10.1021/acssuschemeng.1c01173>.

Smith, B.C. (2021) *The Infrared Spectra of Polymers, Part I: Introduction, Spectroscopy*. MJH Life Sciences. Available at: <https://www.spectroscopyonline.com/view/the-infrared-spectra-of-polymers-part-i-introduction> (Accessed: 11 April 2023).

Sorrentino, L., Aurilia, M. and Iannace, S. (2011) ‘Polymeric Foams from High-Performance Thermoplastics’, *Advances in Polymer Technology*, 30(3), pp. 234–243. Available at: <https://doi.org/10.1002/adv.20219>.

Spivakov, B. and Shkinev, V. (2005) ‘MEMBRANE TECHNIQUES | Ultrafiltration’, in P. Worsfold, A. Townshend, and C. Poole (eds) *Encyclopedia of Analytical Science (Second Edition)*. Oxford: Elsevier, pp. 524–530. Available at: <https://doi.org/10.1016/B0-12-369397-7/00368-X>.

Standau, T., Zhao, C., *et al.* (2019) ‘Chemical Modification and Foam Processing of Polylactide (PLA)’, *Polymers*, 11(2). Available at: <https://doi.org/10.3390/polym11020306>.

Standau, T., Castellón, S.M., *et al.* (2019) ‘Effects of chemical modifications on the rheological and the expansion behavior of polylactide (PLA) in foam extrusion’, *e-Polymers*, 19(1), pp. 297–304. Available at: <https://doi.org/10.1515/epoly-2019-0030>.

Tabatabaei Naeini, A. (2012) *Visualization of the Crystallization in Foam Extrusion Process*. University of Toronto. Available at: <https://ui.adsabs.harvard.edu/abs/2012MsT.....14T> (Accessed: 1 July 2023).

Tang, D.-S. *et al.* (2009) 'Recovery of protein from brewer's spent grain by ultrafiltration', *Biochemical Engineering Journal*, 48(1), pp. 1–5. Available at: <https://doi.org/10.1016/j.bej.2009.05.019>.

ThermoFischer Scientific (2023) 'Scanning Electron Microscopy | Optical Microscopy - DE'. Available at: <https://www.thermofisher.com/de/de/home/materials-science/learning-center/applications/sem-optical-microscopes-difference.html> (Accessed: 11 April 2023).

Tiron, L.G., Vlad, M. and Baltă, Ș. (2018) 'Research on Hydrophilic Nature of Polyvinylpyrrolidone on Polysulfone Membrane Filtration', *IOP Conference Series: Materials Science and Engineering*, 374(1), p. 012059. Available at: <https://doi.org/10.1088/1757-899X/374/1/012059>.

Toray (2022) 'Gel Permeation Chromatography : GPC | Techniques | Fields | Toray Research Center | TORAY'. Available at: <https://www.toray-research.co.jp/en/technicaldata/techniques/GPC.html> (Accessed: 24 June 2023).

Tree, D.R. *et al.* (2018) 'Marangoni Flows during Nonsolvent Induced Phase Separation', *ACS Macro Letters*, 7(5), pp. 582–586. Available at: <https://doi.org/10.1021/acsmacrolett.8b00012>.

Tshaye, M.T., Velizarov, S. and Van der Bruggen, B. (2018) 'Stability of polyethersulfone membranes to oxidative agents: A review', *Polymer Degradation and Stability*, 157, pp. 15–33. Available at: <https://doi.org/10.1016/j.polymdegradstab.2018.09.004>.

Ulbricht, M. (2006) 'Advanced functional polymer membranes', *Single Chain Polymers*, 47(7), pp. 2217–2262. Available at: <https://doi.org/10.1016/j.polymer.2006.01.084>.

Verreck, G. *et al.* (2006) 'The effect of pressurized carbon dioxide as a plasticizer and foaming agent on the hot melt extrusion process and extrudate properties of pharmaceutical polymers', *The Journal of*

Supercritical Fluids, 38(3), pp. 383–391. Available at:
<https://doi.org/10.1016/j.supflu.2005.11.022>.

Vu, T., LeBlanc, J. and Chou, C.C. (2020) ‘Clarification of sugarcane juice by ultrafiltration membrane: Toward the direct production of refined cane sugar’, *Journal of Food Engineering*, 264, p. 109682. Available at:
<https://doi.org/10.1016/j.jfoodeng.2019.07.029>.

Wang, D., Li, K. and Teo, W.K. (1999) ‘Preparation and characterization of polyvinylidene fluoride (PVDF) hollow fiber membranes’, *Journal of Membrane Science*, 163(2), pp. 211–220. Available at:
[https://doi.org/10.1016/S0376-7388\(99\)00181-7](https://doi.org/10.1016/S0376-7388(99)00181-7).

Wang, G. *et al.* (2018) ‘Lightweight and tough nanocellular PP/PTFE nanocomposite foams with defect-free surfaces obtained using in situ nanofibrillation and nanocellular injection molding’, *Chemical Engineering Journal*, 350, pp. 1–11. Available at:
<https://doi.org/10.1016/j.cej.2018.05.161>.

Wang, H.H. *et al.* (2019) ‘A novel green solvent alternative for polymeric membrane preparation via nonsolvent-induced phase separation (NIPS)’, *Journal of Membrane Science*, 574, pp. 44–54. Available at:
<https://doi.org/10.1016/j.memsci.2018.12.051>.

Wang, J. *et al.* (2014) ‘Fabrication of hydrophilic and sponge-like PVDF/brush-like copolymer blend membranes using triethylphosphate as solvent’, *Chinese Journal of Polymer Science*, 32(2), pp. 143–150. Available at: <https://doi.org/10.1007/s10118-014-1371-7>.

Wang, J.S. and Kamiya, Y. (1995) ‘Concurrent Measurements of Sorption and Dilation Isotherms and Diffusivity for Polysulfone Membrane Carbon-Dioxide System’, *Journal of Membrane Science*, 98(1–2), pp. 69–76. Available at: [https://doi.org/10.1016/0376-7388\(94\)00176-Y](https://doi.org/10.1016/0376-7388(94)00176-Y).

Waters (2023) ‘Calibration of the GPC System | Waters’. Available at: <https://www.waters.com/nextgen/en/education/primers/beginners-guide-to-size-exclusion-chromatography/calibration-of-the-gpc-system1.html> (Accessed: 11 April 2023).

Widyatmoko, I. (2016) ‘14 - Sustainability of bituminous materials’, in J.M. Khatib (ed.) *Sustainability of Construction Materials (Second*

Edition). Woodhead Publishing, pp. 343–370. Available at:
<https://doi.org/10.1016/B978-0-08-100370-1.00014-7>.

Wienk, I.M. *et al.* (1996) ‘Recent advances in the formation of phase inversion membranes made from amorphous or semi-crystalline polymers’, *Journal of Membrane Science*, 113(2), pp. 361–371. Available at:
[https://doi.org/10.1016/0376-7388\(95\)00256-1](https://doi.org/10.1016/0376-7388(95)00256-1).

Worgull, M. (2009) ‘Chapter 3 - Molding Materials for Hot Embossing’, in M. Worgull (ed.) *Hot Embossing*. Boston: William Andrew Publishing, pp. 57–112. Available at: <https://doi.org/10.1016/B978-0-8155-1579-1.50009-4>.

Xanthos, M. *et al.* (2002) ‘Melt processed microporous films from compatibilized immiscible blends with potential as membranes’, *Polymer Engineering & Science*, 42(4), pp. 810–825. Available at:
<https://doi.org/10.1002/pen.10993>.

Xu, X. *et al.* (2013) ‘Bubble nucleation in polymer–CO₂ mixtures’, *Soft Matter*, 9(40), pp. 9675–9683. Available at:
<https://doi.org/10.1039/C3SM51477C>.

Xu, Z.-L. and Alsahy Qusay, F. (2004) ‘Polyethersulfone (PES) hollow fiber ultrafiltration membranes prepared by PES/non-solvent/NMP solution’, *Journal of Membrane Science*, 233(1), pp. 101–111. Available at: <https://doi.org/10.1016/j.memsci.2004.01.005>.

Yang, Z. (2019) *Material Modeling in Finite Element Analysis*, Taylor & Francis. Boca Raton, FL, USA: CRC Press. Available at:
<https://doi.org/10.1201/9780367353216>.

Yeh, S.-K. *et al.* (2019) ‘Foam extrusion of polypropylene–rice husk composites using CO₂ as the blowing agent’, *Journal of Cellular Plastics*, 55(4), pp. 401–419. Available at:
<https://doi.org/10.1177/0021955x19839744>.

Yeh, S.-K. *et al.* (2020) ‘Effect of molecular weight to the structure of nanocellular foams: Phase separation approach’, *Polymer*, 191, p. 122275. Available at: <https://doi.org/10.1016/j.polymer.2020.122275>.

Yin, J., Zhu, G. and Deng, B. (2013) ‘Multi-walled carbon nanotubes (MWNTs)/polysulfone (PSU) mixed matrix hollow fiber membranes for

enhanced water treatment’, *Journal of Membrane Science*, 437, pp. 237–248. Available at: <https://doi.org/10.1016/j.memsci.2013.03.021>.

Youcai, Z. (2018) ‘Chapter 2 - Physical and Chemical Treatment Processes for Leachate’, in Z. Youcai (ed.) *Pollution Control Technology for Leachate from Municipal Solid Waste*. Butterworth-Heinemann, pp. 31–183. Available at: <https://doi.org/10.1016/B978-0-12-815813-5.00002-4>.

Zarrintaj, P. *et al.* (2020) ‘Chapter 18 - Application of compatibilized polymer blends in biomedical fields’, in A. A.R. and S. Thomas (eds) *Compatibilization of Polymer Blends*. Elsevier, pp. 511–537. Available at: <https://doi.org/10.1016/B978-0-12-816006-0.00018-9>.

Zdravkov, B. *et al.* (2007) ‘Pore classification in the characterization of porous materials: A perspective’, 5(2), pp. 385–395. Available at: <https://doi.org/10.2478/s11532-007-0017-9>.

Zhang, J. *et al.* (2021) ‘Effects of phosphotungstic acid on performance of phosphoric acid doped polyethersulfone-polyvinylpyrrolidone membranes for high temperature fuel cells’, *International Journal of Hydrogen Energy*, 46(19), pp. 11104–11114. Available at: <https://doi.org/10.1016/j.ijhydene.2020.07.082>.

Zhang, Q., Lu, X. and Zhao, L. (2014) ‘Preparation of Polyvinylidene Fluoride (PVDF) Hollow Fiber Hemodialysis Membranes’, *Membranes*, 4(1), pp. 81–95. Available at: <https://doi.org/10.3390/membranes4010081>.

Zhang, Y., Rodrigue, D. and Ait-Kadi, A. (2003) ‘High-density polyethylene foams. I. Polymer and foam characterization’, *Journal of Applied Polymer Science*, 90(8), pp. 2111–2119. Available at: <https://doi.org/10.1002/app.12821>.

Zhou, Z. *et al.* (2020) ‘Fabrication of highly permeable polyamide membranes with large “leaf-like” surface nanostructures on inorganic supports for organic solvent nanofiltration’, *Journal of Membrane Science*, 601, p. 117932. Available at: <https://doi.org/10.1016/j.memsci.2020.117932>.

9. Appendix

9.1. Article 1: Open-Celled Foams of Polyethersulfone/Poly(*N*-vinylpyrrolidone) Blends for Ultrafiltration Applications

9.1.1. Graphical Abstract

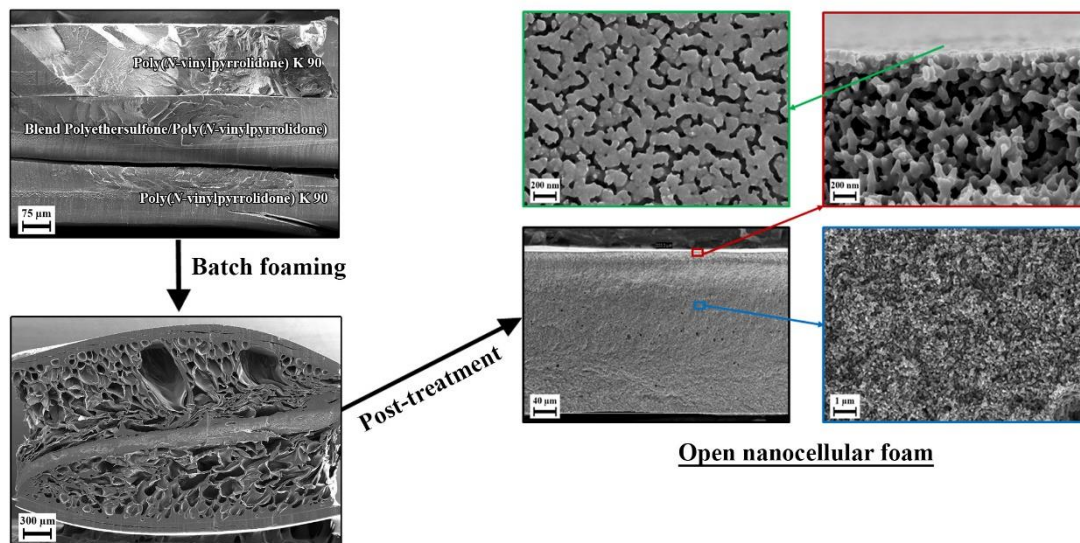


Figure 29: Graphical abstract of article 1.

9.1.2. Miscellaneous Information

Citation:

Raje, Aniket, Kristian Buhr, Joachim Koll, Jelena Lillepär, Volker Abetz, and Ulrich A. Handge. 2022. "Open-Celled Foams of Polyethersulfone/Poly(*N*-vinylpyrrolidone)

Blends for Ultrafiltration Applications" *Polymers* 14, no. 6: 1177.
<https://doi.org/10.3390/polym14061177>

Journal impact factor at the time of publication:

4.967 (15-03-2022)

9.1.3. Supporting Information

(P.T.O.)

Article

Open-Celled Foams of Polyethersulfone/Poly(*N*-vinylpyrrolidone) Blends for Ultrafiltration Applications

Aniket Rajе ¹, Kristian Buhr ¹, Joachim Koll ¹, Jelena Lillepärğ ¹, Volker Abetz ^{1,2} and Ulrich A. Handge ^{1,3*}

¹ Institute of Membrane Research, Helmholtz-Zentrum Hereon, Max-Planck-Strasse 1, 21502 Geesthacht, Germany; aniket.raje@hereon.de (A.R.); kristian.buhr@hereon.de (K.B.); joachim.koll@hereon.de (J.K.); jelena.lillepaerg@hereon.de (J.L.); volker.abetz@hereon.de (V.A.)

² Institute of Physical Chemistry, Universität Hamburg, Grindelallee 117, 20146 Hamburg, Germany

³ Chair of Plastics Technology, Faculty of Mechanical Engineering, TU Dortmund University, Leonhard-Euler-Straße 5, 44227 Dortmund, Germany

* Correspondence: ulrich.handge@tu-dortmund.de; Tel.: +49-231-755-8628

Supporting Information

A – Material Characterization

1. Effect of temperature on solubility

For water solubility tests on PVP K 30, cylindrical samples measuring 8 mm in diameter and 2.3 mm in thickness were prepared using the pressing device Vacuum MR Hei-End (MeltPrep GmbH). Samples, one at a time, were immersed in Millipore water measuring 60 mL in volume. Tests were carried out at temperatures 25 °C, 40 °C, 60 °C and 80 °C with constant stirring using a magnetic stirrer. Time taken for complete dissolution was measured.

The tests showed an increased rate of solubility with increase in temperature. The tests were performed in water, but it is assumed to have a similar effect on a dilute solution of NaOCl.

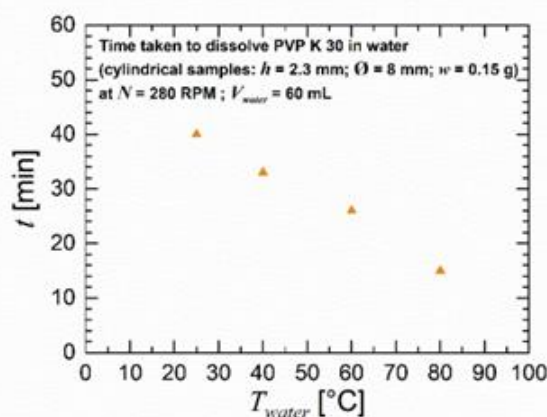


Figure S1. Time taken to dissolve PVP K 30 samples in water at various temperatures

2. Solubility tests in aqueous solution of NaOCl

Solubility tests were carried out for the blends H-8 and H-32 in aqueous solutions of NaOCl. Films of the respective blends of thickness 0.4 mm and width 21 mm were extruded using a twin screw extruder (Brabender, Duisburg, Germany) with a slit die.

Samples of length 25 mm were cut from the respective films. 0.1 wt% NaOCl solution with a pH value 11.5 was used because at this pH value, NaOCl has no interaction with PESU but dissolves PVP K 30 [35]. Two different temperatures, *i.e.* room temperature and 80 °C were chosen. Samples were inserted in the solution in a closed glass bottle at the given temperatures and were subjected to constant stirring using a magnetic stirrer for 48 hours. To wash out residual NaOCl, the samples were rinsed in decalcinated water at 35 °C for 10 minutes, Sodium disulfate ($\text{Na}_2\text{S}_2\text{O}_5$) at room temperature for 10 minutes and finally with decalcified water at 80 °C for 10 minutes. The effect of this treatment was observed using SEM.

Scanning electron micrographs showed no change on the surface of blend H-8 at both room temperatures and 80 °C. Blend H-32 did not undergo any visible change when treated with the NaOCl solution at room temperature. However, at 80 °C, uniform blind open pores appeared on the surface. These pores were of two sizes, smaller pores between 3 nm to 5 nm and larger pores between 20 nm to 50 nm. The depth of the larger pores was limited to approximately 50 nm. This confirms that although PVP is blended with PESU in single phase, it can be removed from the surface through post-treatment thus resulting in a porous structure. If the material is already porous on the inside, these surface pores could function as a selective layer thus implementable in ultrafiltration applications.

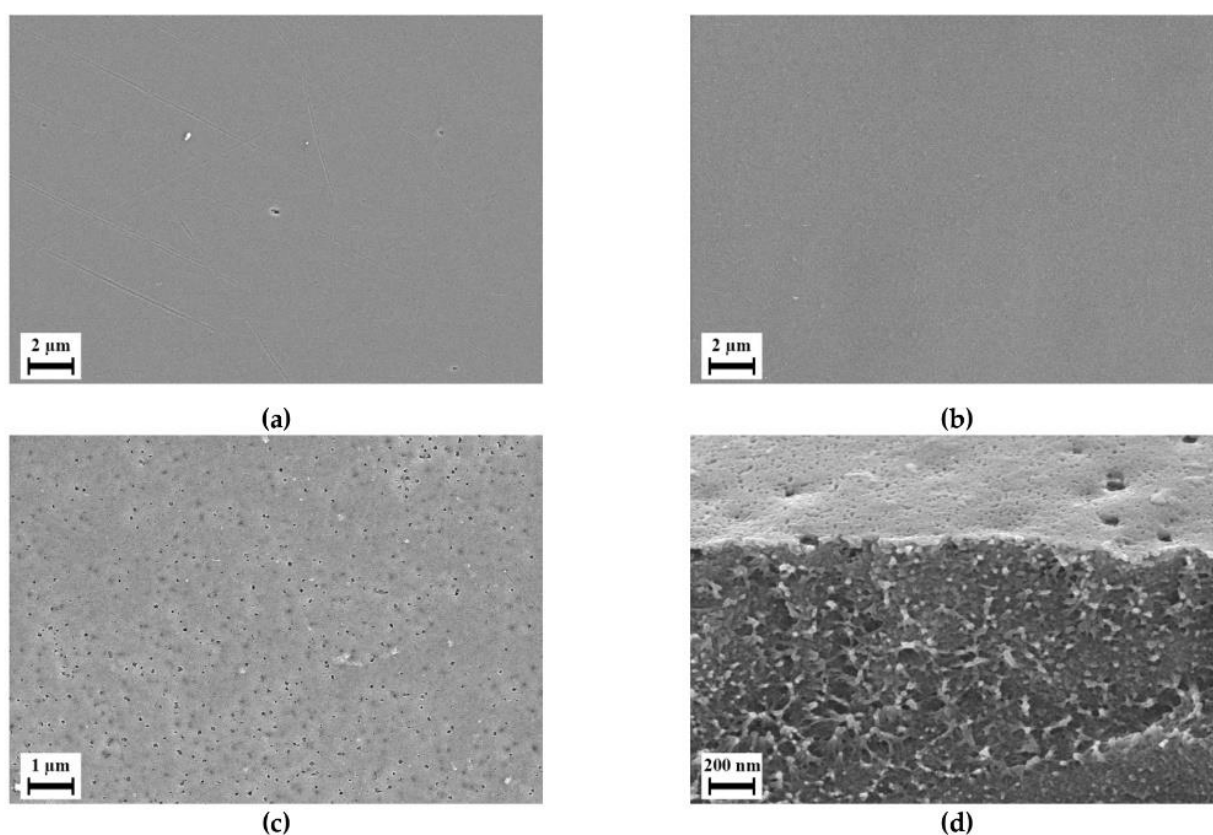


Figure S2. Scanning electron micrographs of post-treated blends in NaOCl at various temperatures: (a) Surface of film of blend H-8 at 80 °C (b) Surface of film of blend H-32 at RT; (c) Surface of film of blend H-32 at 80 °C; (d) Cross-section of film of blend H-32 at 80 °C

3. Infrared spectrometry

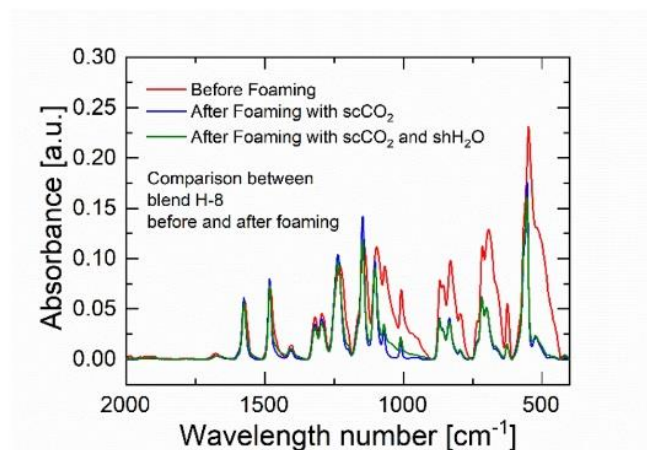


Figure S3. IR spectra of blend, non-foamed blend H-8 and after foaming with various foaming agents

Fourier transform infrared (FTIR) spectroscopy was carried out on some materials and their corresponding foams using a Bruker Alpha-P, platinum attenuated total reflection, equipped with diamond head (Bruker, Massachusetts, USA). Using FTIR spectroscopy, the chemical bonds in the material H-8, its foam using foaming agent CO₂ and its foam using foaming agent CO₂ and H₂O were analyzed. There is a significant difference between the material and the foams. The IR spectra of foams with both foaming agents show identical behavior. Due to foaming, a significant decrease in the sulfone (S=O) group, vinylene (C=C) group, and alkene (C=C) group can be seen. Exposure to loading temperature and sudden change in temperature after depressurization from loaded phase for foaming seem to cause the polymer system to undergo certain amount of degradation. Certain residual material was also observed on the inner lining of the reactor that could be wiped using organic solvents, indicating that they could be byproducts of these degradations.

4. DSC on unfoamed and foamed blend H-8

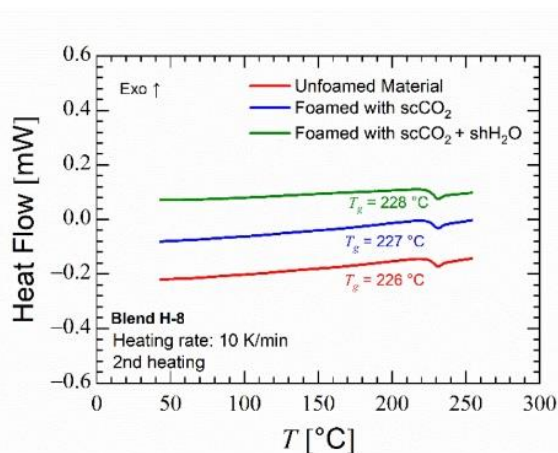


Figure S4. DSC 2nd heating curves of non-foamed blend H-8 and after foaming with various foaming agents

DSC measurements show minor and statistically insignificant differences between glass transition temperatures of material H-8 and its foams.

5. Rheological Analysis

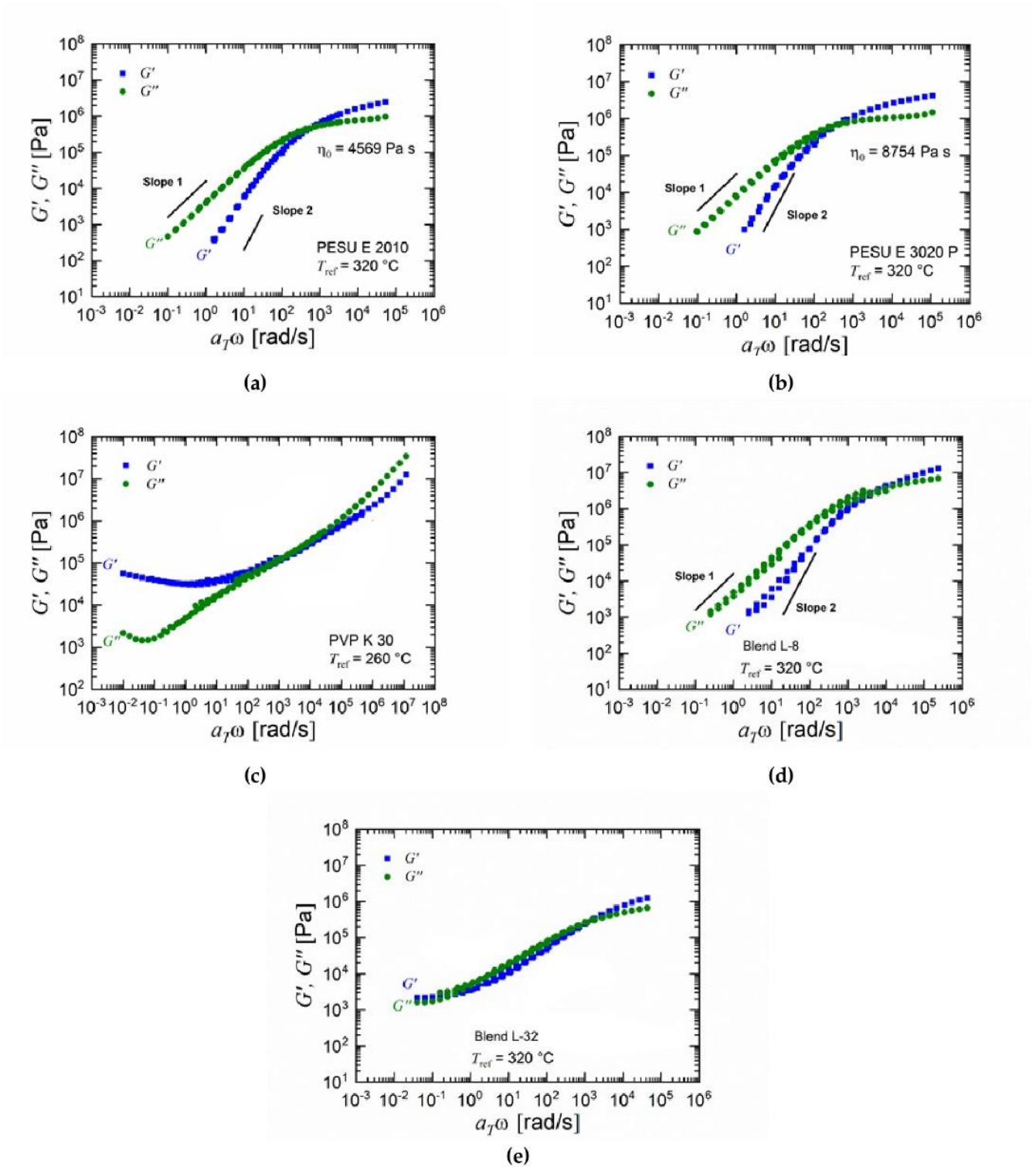


Figure S5. Master curves of selected materials from rheological analysis: (a) PESU E 2010; (b) PESU E 3020 P; (c) PVP K 30; (d) Blend L-8; (e) Blend L-32

6. Thermogravimetric analysis

Thermal gravimetric analysis (TGA) was carried out using a TGA 209 G1 220-11-0019-L Iris instrument (Netzsch, Selb, Germany). Measurements were carried out from 25 to 900 °C at a heating rate of 10 K min⁻¹ in an argon atmosphere.

TGA provided an overview of their stability and decomposition temperature. In Figure 5(a), in argon environment, it can be observed that PESU E 3020 P starts degrading only at 475 °C, confirming a high thermal stability. PVP begins to degrade at temperatures which are higher than its glass transition temperature of 172 °C up to 410 °C and then rapidly decomposes up to 475 °C to a final relative mass of 4%. In the blends with 32% PVP K 30, this effect is seen slightly as the mass degrades up to 376 °C. In the blends with 8% PVP K 30, the polymer degrades up to 400 °C. Since blends with 32% PVP K 30 content show only 20% of mass reduction of pure PVP K 30, some sort of shielding effect caused by PESU can be assumed in these blends.

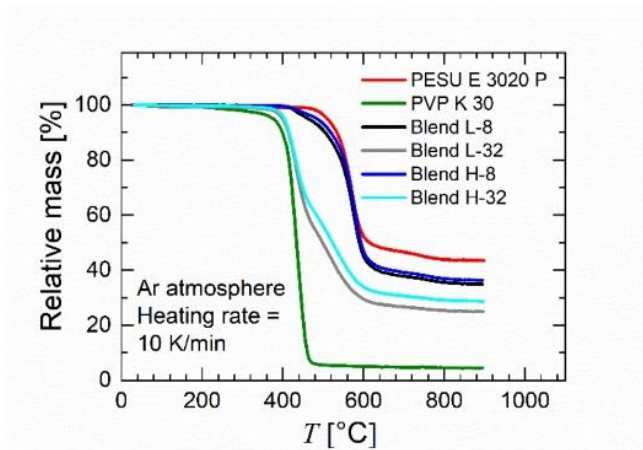
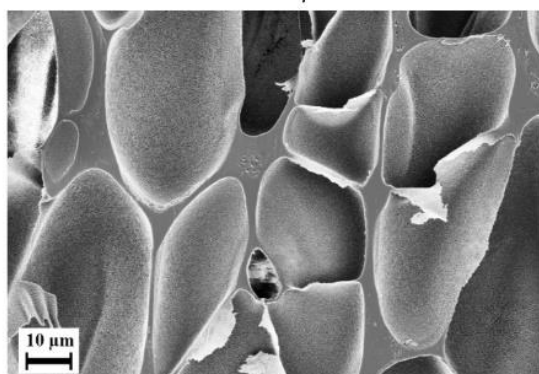


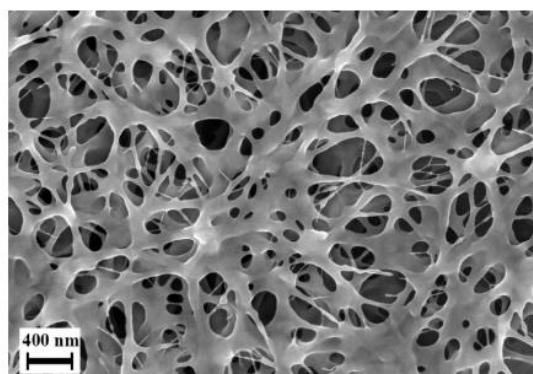
Figure S6. Results of thermogravimetric analysis for selected materials

B – Foams and membranes

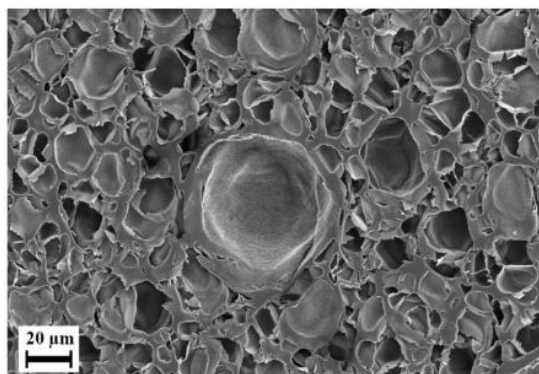
1. Scanning electron micrographs of foams of blends foamed using CO₂ and H₂O versus foaming temperature



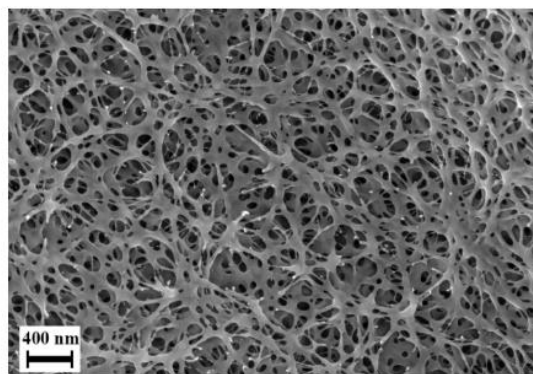
(a)



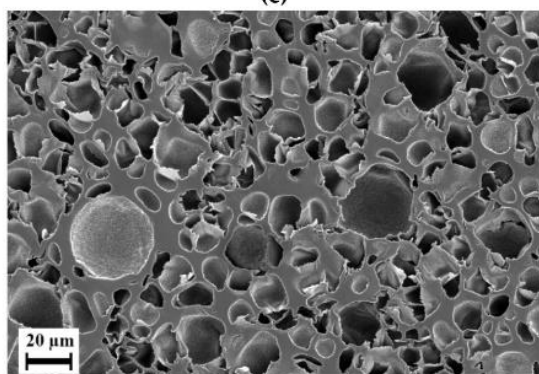
(b)



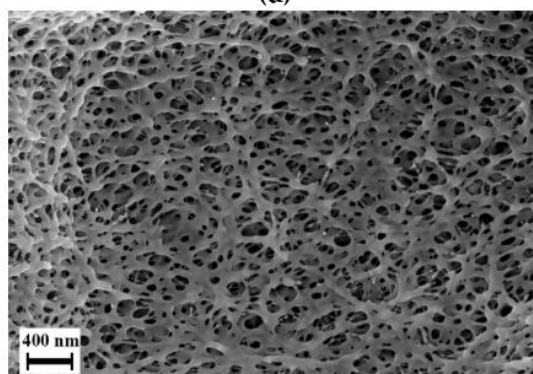
(c)



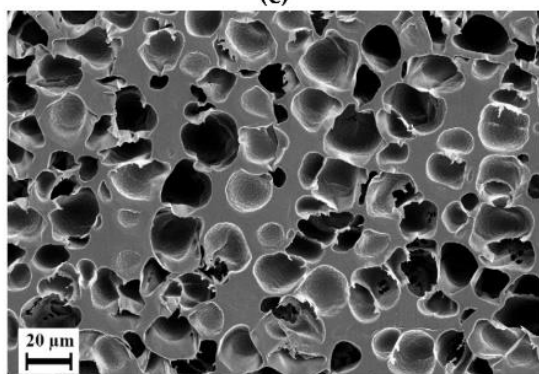
(d)



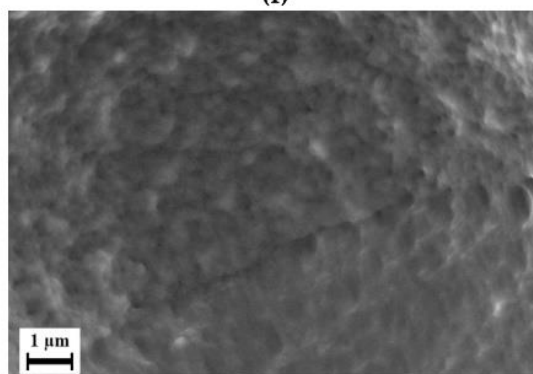
(e)



(f)

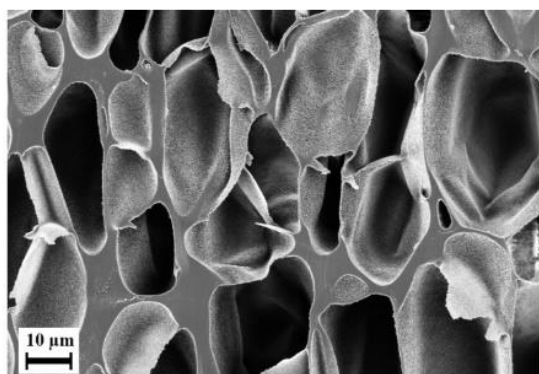


(g)

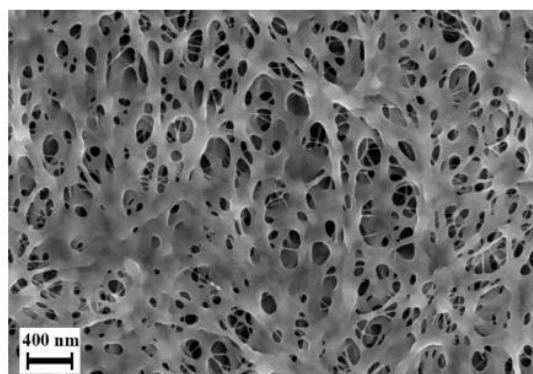


(h)

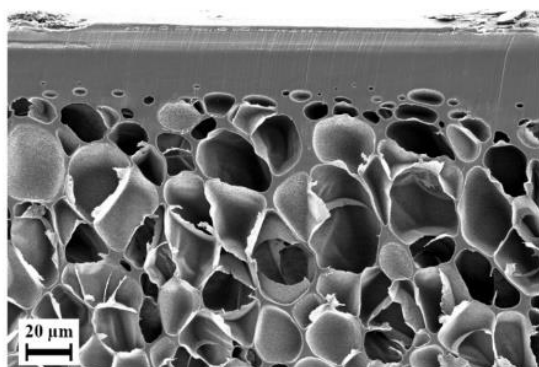
Figure S7. Scanning electron micrographs of blend I-8 foams manufactured using blowing agents CO₂ and H₂O at loading time 48 h, pressure 100 bar, loading temperature 150 °C, foaming time 100 s and various foaming temperatures: (a), (b) 210 °C; (c), (d) 230 °C; (e), (f) 250 °C; (g), (h) 270 °C



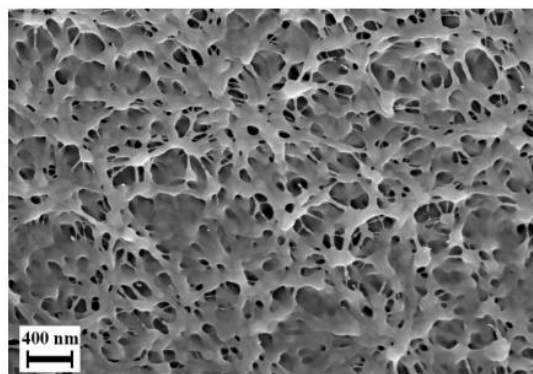
(a)



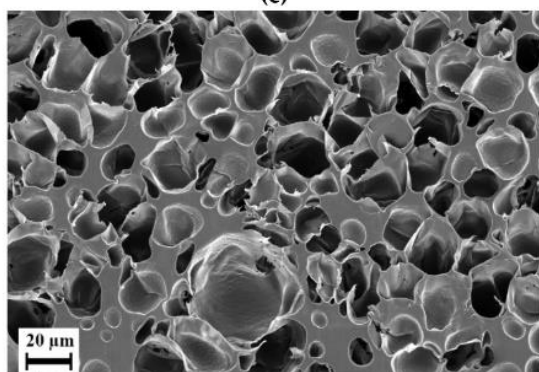
(b)



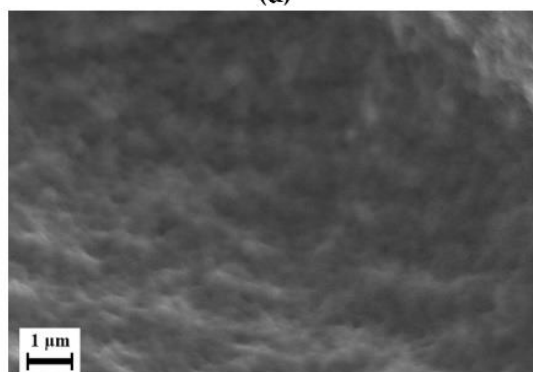
(c)



(d)

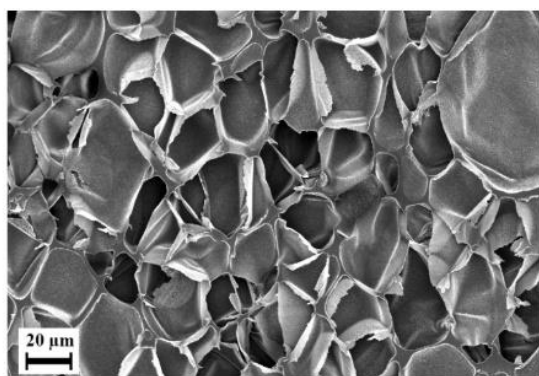


(e)

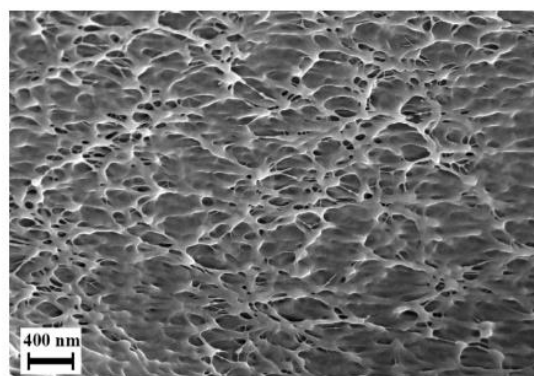


(f)

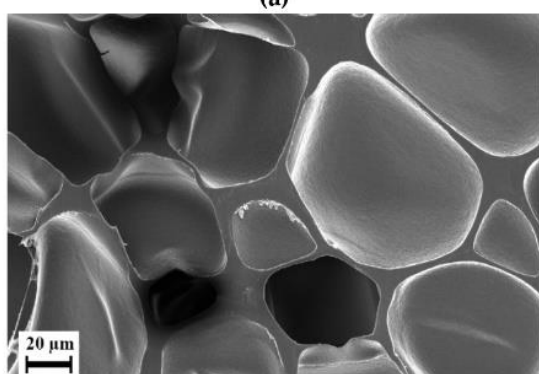
Figure S8. Scanning electron micrographs of blend H-8 foams manufactured using blowing agents CO₂ and H₂O at loading time 48 h, pressure 100 bar, loading temperature 150 °C, foaming time 100 s and various foaming temperatures: (a), (b) 210 °C; (c), (d) 250 °C; (e), (f) 270 °C



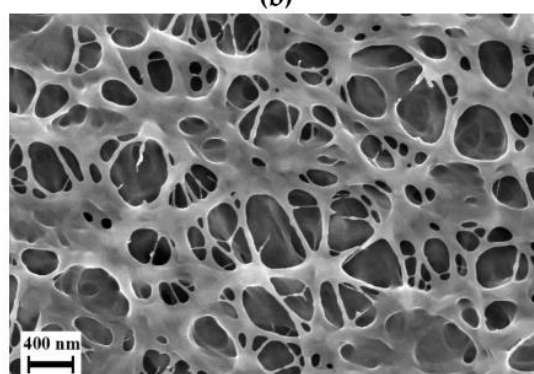
(a)



(b)



(c)



(d)

Figure S9. Scanning electron micrographs of foams of blend H-8 at the loading time 48 h, pressure 100 bar, foaming temperature 230 °C, foaming time 100 s, the blowing agent CO₂ and H₂O and various loading temperatures: (a), (b): 125 °C; (c), (d): 175 °C.

2. Miscellaneous scanning electron micrographs

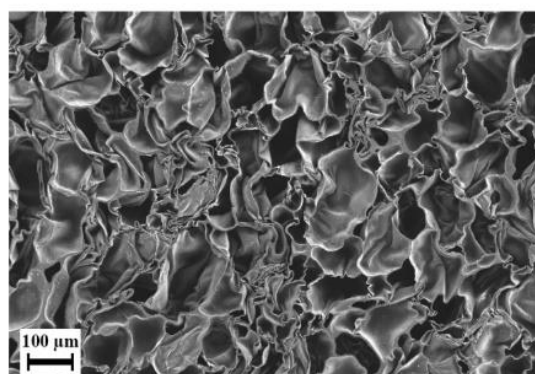
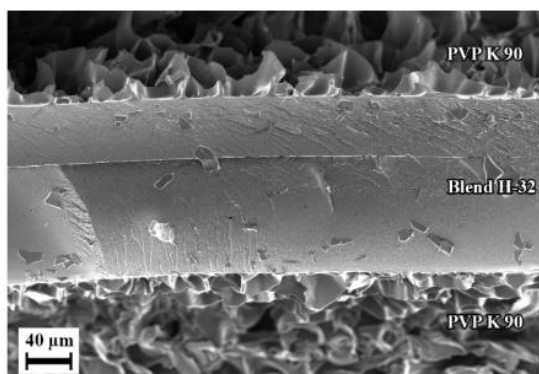
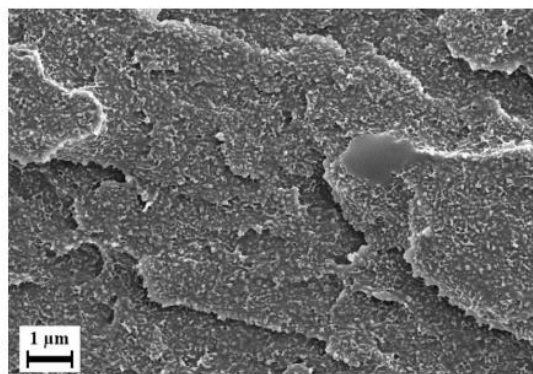


Figure S10. Scanning electron micrograph of collapsed PVP foam manufactured using blowing agent CO₂ at loading time 48 h, pressure 50 bar, loading temperature 150 °C, foaming time 100 s and foaming temperature 250 °C



(a)



(b)

Figure S11. Scanning electron micrographs of sandwich-type sample manufactured using method II with blend H-32: (a), (b) after loading phase without subjecting to foaming temperatures (Similar settings and method used as Figure 12)

References

35. Dibrov, G.; Kagramanov, G.; Sudin, V.; Grushevenko, E.; Yushkin, A.; Volkov, A. Influence of sodium hypochlorite treatment on pore size distribution of polysulfone/polyvinylpyrrolidone membranes. *Membranes* 2020, *10*, 356. <https://doi.org/10.3390/membranes10110356>.

9.2. Article 2: Open-Celled Foams from Polyethersulfone/Poly(Ethylene Glycol) Blends using Foam Extrusion

9.2.1. Graphical Abstract

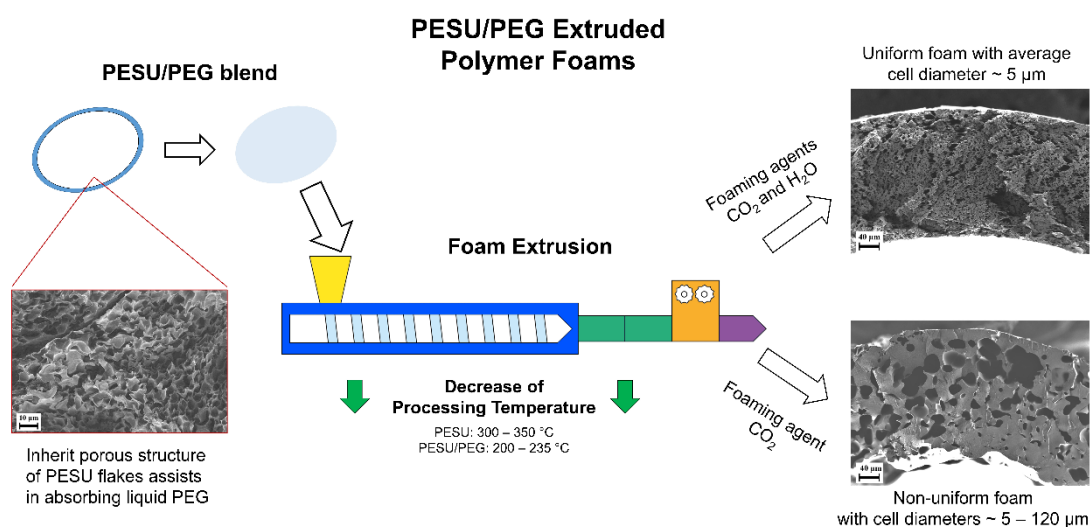


Figure 30: Graphical abstract of article 2.

9.2.2. Miscellaneous Information

Citation:

Raje, Aniket, Prokopios Georgopoulos, Joachim Koll, Jelena Lillepärq, Ulrich A. Handge, and Volker Abetz. 2023. "Open-Celled Foams from Polyethersulfone/Poly(Ethylene Glycol) Blends Using Foam Extrusion" *Polymers* 15, no. 1: 118. <https://doi.org/10.3390/polym15010118>

Journal impact factor at the time of publication:

4.967 (27-12-2022)

9.2.3. Supporting Information

(P.T.O.)

Supplementary Materials

Open-Celled Foams from Polyethersulfone/Poly(Ethylene Glycol) Blends Using Foam Extrusion

Aniket Rajе ¹, Prokopios Georgopoulos ^{1,*}, Joachim Koll ¹, Jelena Lillepärğ ¹, Ulrich A. Handge ^{1,2} and Volker Abetz ^{1,3}

¹ Helmholtz-Zentrum Hereon, Institute of Membrane Research, Max-Planck-Strasse 1, 21502 Geesthacht, Germany; aniket.raje@hereon.de (A.R.); joachim.koll@hereon.de (J.K.); jelena.lillepaerg@hereon.de (J.L.); ulrich.handge@tu-dortmund.de (U.A.H.); volker.abetz@hereon.de (V.A.)

² Chair of Plastics Technology, Faculty of Mechanical Engineering, TU Dortmund University, Leonhard-Euler-Straße 5, 44227 Dortmund, Germany

³ Institute of Physical Chemistry, Universität Hamburg, Grindelallee 117, 20146 Hamburg, Germany

* Correspondence: prokopios.georgopoulos@hereon.de; Tel.: +49-4152-87-2420

Supporting Information

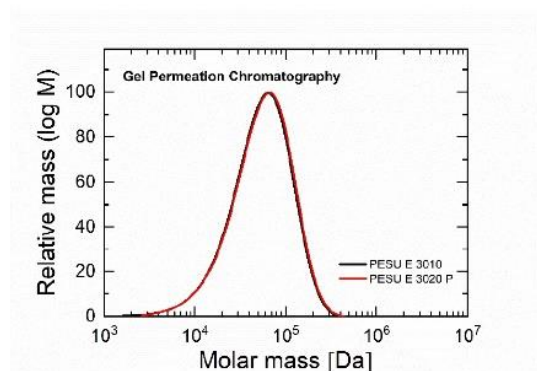
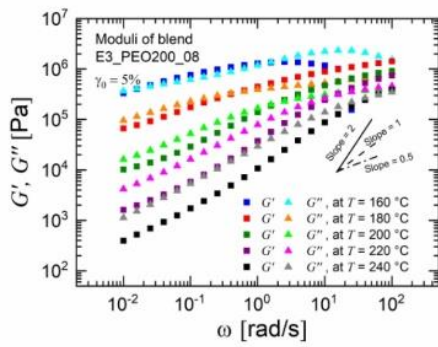
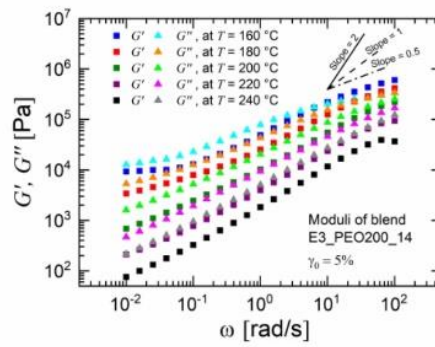


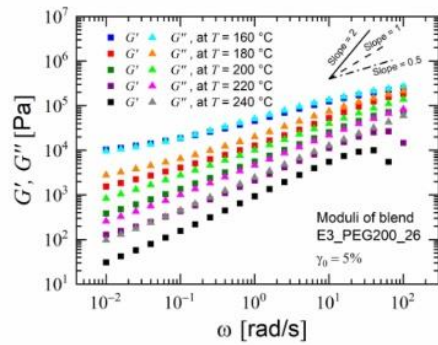
Figure S1. Gel permeation chromatography of PESU E 3010 and E 3020 P. The molecular weight estimation is based on calibration with polystyrene standards.



(a)



(b)



(c)

Figure S2. Rheological investigations on the PESU / PEG200 blends: Storage modulus G' and loss modulus G'' versus angular frequency ω at various temperatures of blend (a) E3_PEG200_08 (b) E3_PEG200_14; (c) E3_PEG200_26

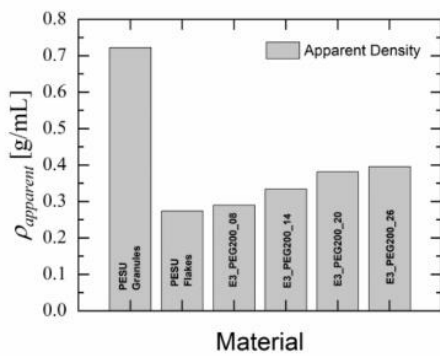


Figure S3. Apparent densities of PESU E 3010 granules, PESU E 3020 P flakes and PESU/PEO blend flakes.

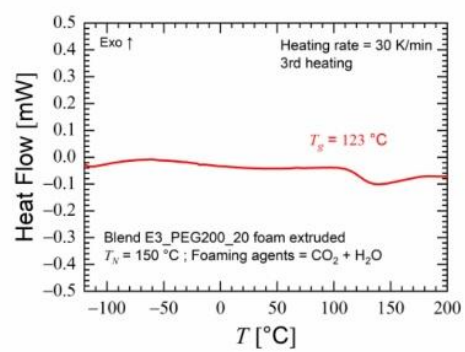


Figure S4. DSC third heating cycle of foam of blend E3_PEG200_20, extrusion foamed using CO_2 and water.

23

24

25

9.3. Article 3: A Novel Organic Solvent-Free Method of Manufacturing Polyethersulfone Hollow Fiber Membranes using Melt Extrusion

9.3.1. Graphical Abstract

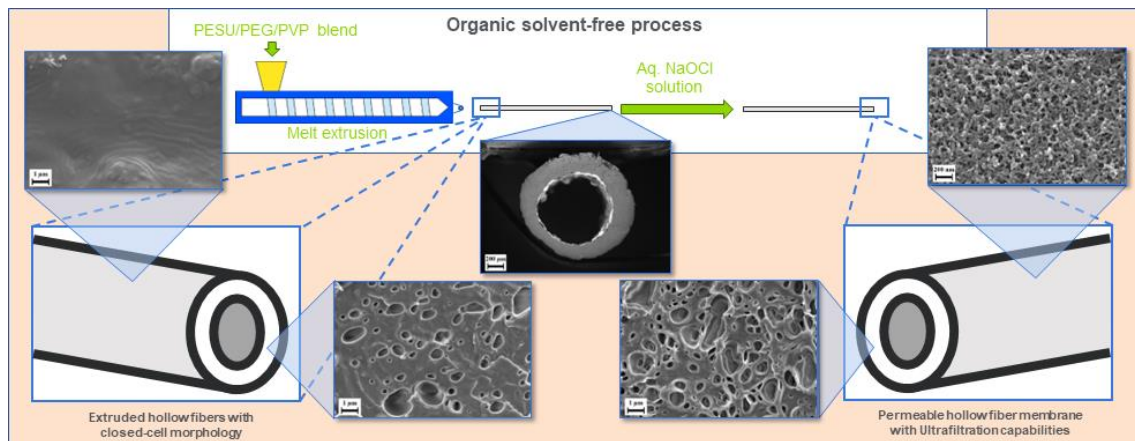


Figure 31: Graphical abstract of article 3.

9.3.2. Miscellaneous Information

Citation:

Raje, Aniket, Joachim Koll, Erik S. Sebastian and Prokopios Georgopoulos. 2023. " A Novel Organic Solvent-Free Method of Manufacturing Polyethersulfone Hollow Fiber Membranes using Melt Extrusion" *Journal of Membrane Science* V. 683, 121837. <https://doi.org/10.1016/j.memsci.2023.121837>

Journal impact factor at the time of publication:

10.53 (10-06-2023)

9.3.3. Supporting Information

(P.T.O.)

Supporting Information

A novel organic solvent-free method for manufacturing polyethersulfone hollow fiber membranes using melt extrusion

Aniket Raje^a, Joachim Koll^a, Erik S. Schneider^a, Prokopios Georgopoulos^{a,*}

^aHelmholtz-Zentrum Hereon, Institute of Membrane Research, Max-Planck Straße 1, 21502 Geesthacht, Germany

* Corresponding Author. E-Mail address: prokopios.georgopoulos@hereon.de

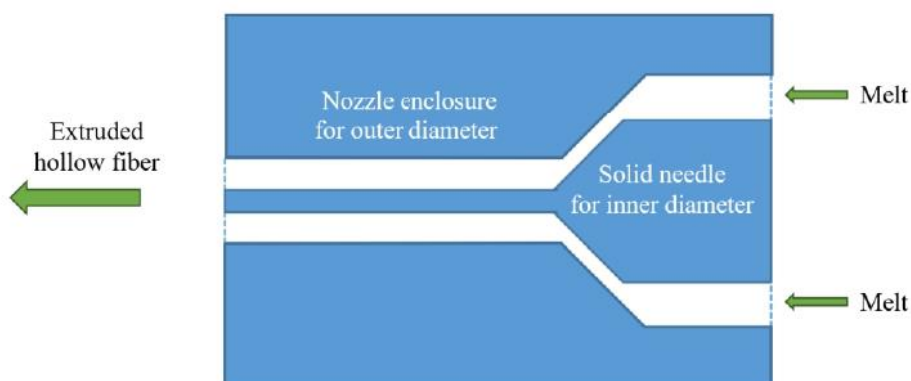


Figure S1: Basic schematic of the annular slit nozzle from a lateral view.

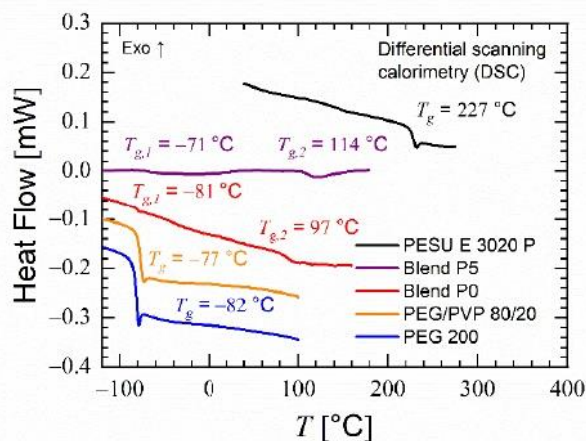


Figure S2: Glass transition temperatures observed in differential scanning calorimetry (DSC). Shown measurements are from the 2nd heating cycle for PESU E 3020 P, blend P5 and blend P0, whereas during 3rd heating cycle for PEG/PVP 80/20 solution and PEG 200. The latter being in a liquid state did not show a strong glass transition signal during 2nd heating at 10 K/min and faster heating was carried out at 30 K/min to detect it.

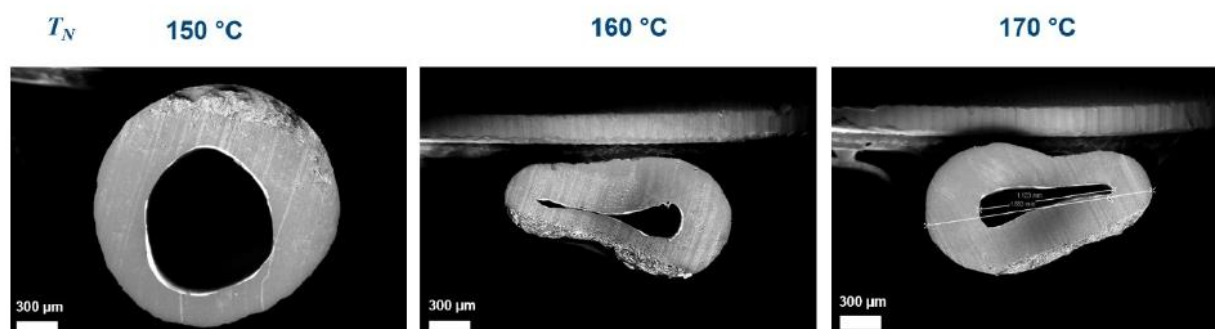


Figure S3: Cross-sectional scanning electron micrographs of extruded hollow fibers of blend P2.5 at various nozzle temperatures (T_N); Only $T_N = 150$ delivered hollow fiber shape.

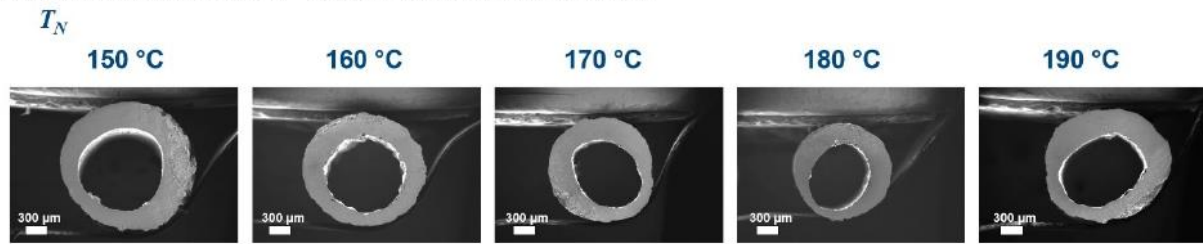


Figure S4: Cross-sectional scanning electron micrographs of extruded hollow fibers of blend P5 at various nozzle temperatures (T_N); All nozzle temperatures yielded hollow fiber shape.

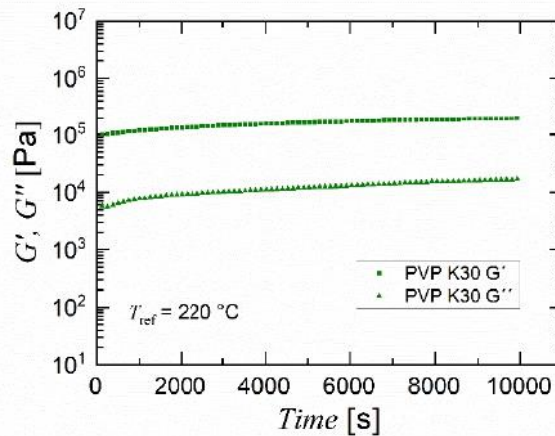


Figure S5: Rheological results of a time-sweep undertaken on an Anton Paar MCR502 Rheometer (Anton Paar, Graz, Austria) with a plate-plate geometry on compression molded samples of Poly(*N*-vinyl pyrrolidone) (PVP) K 30 at an angular frequency of $\omega = 0.1$ rad/s at $T_{ref} = 220$ °C. The compression molding protocol is followed as given elsewhere [1]. The higher storage modulus and the increase in the moduli over time when exposed to the given temperature indicate crosslinking taking place in the sample.

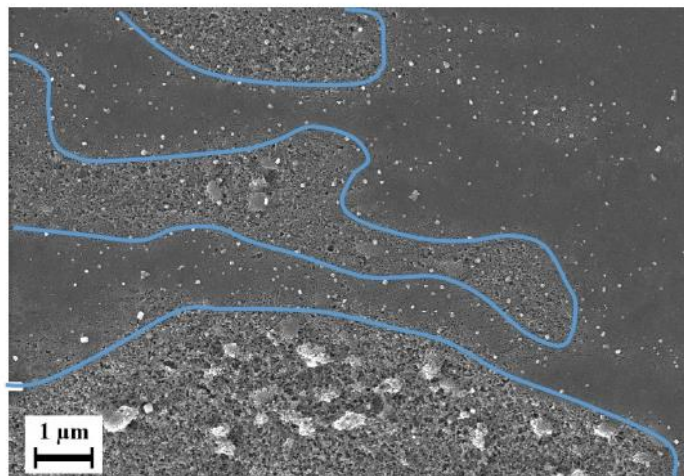


Figure S6: Scanning electron micrograph of the outer surface of a post-treated extruded hollow fiber of blend P5 extruded at $T_N = 160$ °C and post-treated with 0.1% NaOCl at 70 °C for 120 h; The post-treatment only partially creates pores on the outer surface thus leading to lower water flux. Porous regions are outlined in blue.

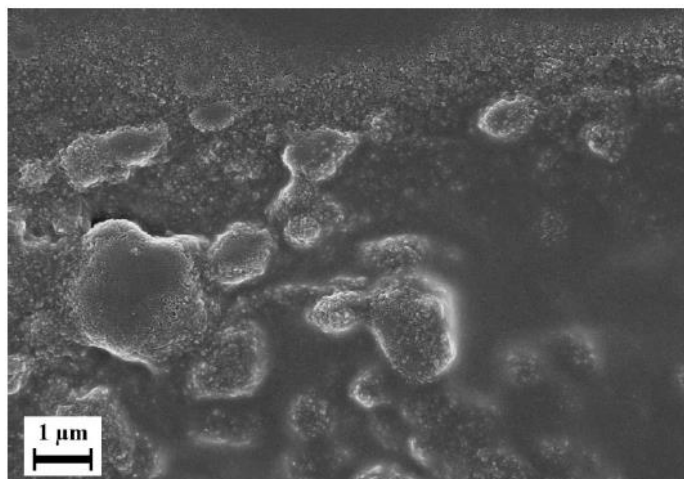


Figure S7: Scanning electron micrograph of the outer surface of a post-treated extruded hollow fiber of blend P5 extruded at $T_N = 160\text{ }^\circ\text{C}$ and post-treated with water at $70\text{ }^\circ\text{C}$ for 120 h; The rough surface is a sign of some amount of dissolution of PVP from the fiber's outer surface but failure to lead to pores.

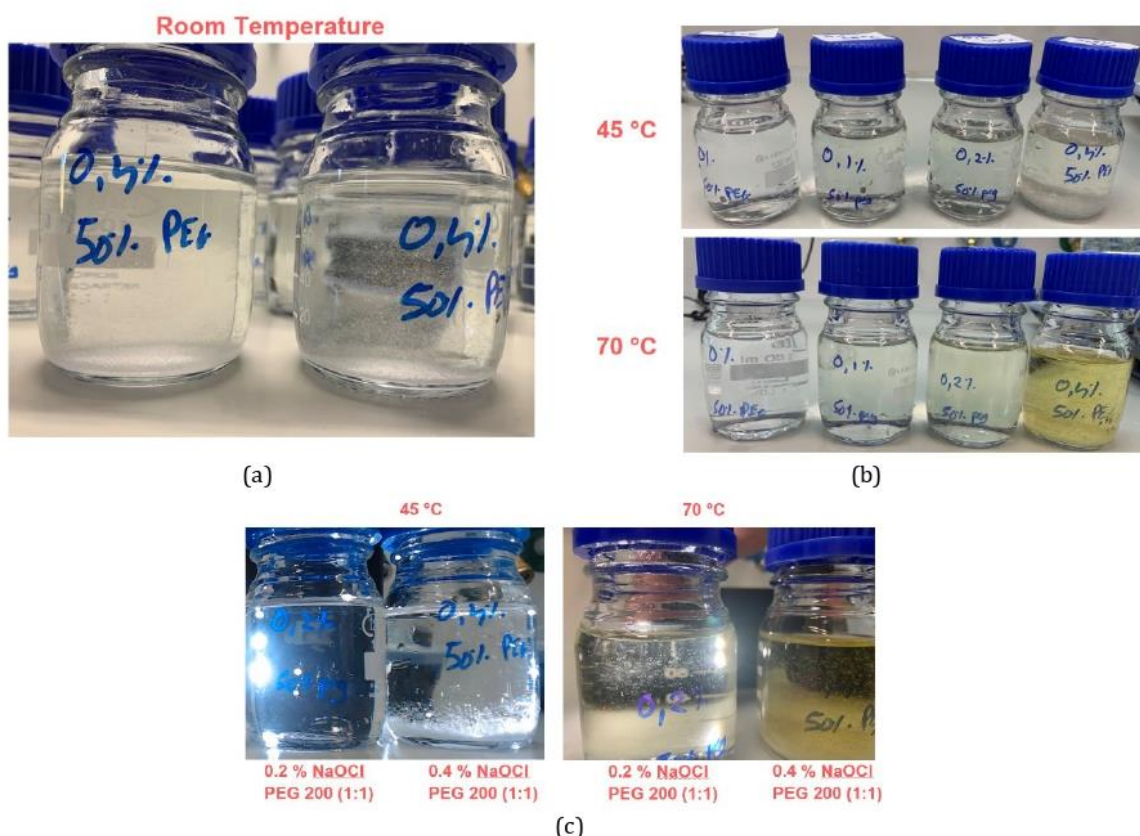


Figure S8: Results of turbidity test: (a) 0.4% aq. NaOCl in PEG (1:1) bottles showing turbidity at room temperature; (b) NaOCl in PEG (1:1) at various concentrations after exposure to $45\text{ }^\circ\text{C}$ (above) and $70\text{ }^\circ\text{C}$ (below) for 2 h; (c) Turbidity observed only in solution with 0.4% aq. NaOCl when exposed to $45\text{ }^\circ\text{C}$ for 2 h (left) and turbidity observed in 0.2% and 0.4% aq. NaOCl when exposed to $70\text{ }^\circ\text{C}$ for 2 h (right).

References:

1. Raje, A., K. Buhr, J. Koll, J. Lilleparg, V. Abetz, and U. A. Handge. "Open-Celled Foams of Polyethersulfone/Poly(N-Vinylpyrrolidone) Blends for Ultrafiltration Applications." *Polymers* 14, no. 6 (2022). ARTN 1177
10.3390/polym14061177





9.4. Software/Websites Used



Software used for writing this dissertation are provided in Table 10. The details of the software used in the published article are provided in them and not repeated here.

Software / Website	Vendor	Used for	URL
Acrobat Reader	Adobe. San Jose, CA, USA	PDF editing	https://get.adobe.com/reader/
Adobe Photoshop	Adobe. San Jose, CA, USA	Graphic design, Figures, Illustrations	https://www.adobe.com/products/photoshop.html
Bing Chat	Microsoft. Seattle, WA, USA	Literature research	https://www.bing.com
Endnote	Clarivate, London, UK	References and Citations	https://get.clarivate.com/endnote/
Excel	Microsoft. Seattle, WA, USA	Tables, Equations, Calculations	https://www.microsoft.com/de-de/microsoft-365?rtc=1
FreeCAD	Open source; Creators: Jürgen Riegel & Werner Mayer	Figures	https://www.freecad.org
Grammarly Premium	Grammarly. San Francisco, CA, USA	Grammar and Language improvement	https://get.grammarly.com/grammarly/
iLovePDF Desktop	iLovePDF. Barcelona, Spain	PDF editing	https://www.ilovepdfdesktop.com/
Notepad	Microsoft. Seattle, WA, USA	Data Clipboard	https://www.microsoft.com/de-de/microsoft-365?rtc=1
Origin	OriginLab. Northampton, MA, USA	Graphs, Data Processing	https://www.originlab.com/
Paint	Microsoft. Seattle, WA, USA	Figures, Illustrations	https://www.microsoft.com/de-de/microsoft-365?rtc=1
PowerPoint	Microsoft. Seattle, WA, USA	Figures, Illustrations	https://www.microsoft.com/de-de/microsoft-365?rtc=1
Scholar	Google. Mountain View, CA, USA	Literature research	https://get.google.com/scholar/
Science Direct	Elsevier. Amsterdam, The Netherlands	Literature research	https://www.sciencedirect.com/
Word	Microsoft. Seattle, WA, USA	Writing and formatting	https://www.microsoft.com/de-de/microsoft-365?rtc=1
Zotero	Corporation for Digital Scholarship. Vienna, VI, USA	References and Citations	https://get.corporation.com/zotero/

Table 10: Software/websites used for this work

9.5. Safety Hazards

Substance	GHS-Symbol	Hazard Statements	Precautionary Statements
Carbon dioxide	GHS04: Gas under Pressure 	H280 = contains gas under pressure; may explode if heated.	P410 + P403 store in accordance with regulations and store in a well-ventilated place
Ethanol	GHS02: Flammables self-reactive substances, self-heating, flammable gas, organic peroxides  GHS07: Acute toxic (harmful), irritant to skin, eyes or respiratory tract, skin sensitizer 	H225 = Highly flammable liquid and vapor, H319 = Causes serious eye irritation.	P210 = Keep away from heat, hot surfaces, sparks, open flames, and other ignition sources. No smoking, P233 = Keep container tightly closed, P305+P351+P338 = If in eyes: Rinse cautiously with water for several minutes. Remove contact lenses, if present and easy to do. Continue rinsing.
Hydrogen chloride	GHS05: Corrosive to metals, burns skin, damages eyes  GHS07: Acute toxic (harmful), irritant to skin, eyes or	H290 = May be corrosive to metals, H314 = Causes severe skin burns and eye damage, H335 = May cause respiratory irritation	P280 = Wear protective gloves/protective clothing/eye protection/face protection, P303+P361+P353 = If on skin (or hair): Take off immediately all contaminated clothing. Rinse skin with water [or shower],

	respiratory tract, skin sensitizer 		P304+P340 = If inhaled: Remove person to fresh air and keep comfortable for breathing, P305+P351+P338 = If in eyes: Rinse cautiously with water for several minutes. Remove contact lenses, if present and easy to do. Continue rinsing, P310 = Immediately call a poison center/doctor
Polyethersulfone	-	-	-
Poly(ethylene glycol)	-	-	-
Poly(<i>N</i> -vinylpyrrolidone)	-	-	-
Sodium hydroxide	GHS05: Corrosive to metals, burns skin, damages eyes 	H314 = Causes severe skin burns and eye damage	P280 = Wear protective gloves/protective clothing/eye protection/face protection, P305+P351+P338 = If in eyes: Rinse cautiously with water for several minutes. Remove contact lenses, if present and easy to do. Continue rinsing, P310 = Immediately call a poison center/doctor
Sodium hypochlorite	GHS05: Corrosive to metals, burns skin, damages eyes	H290 = May be corrosive to metals, H314 = Causes severe skin burns and eye damage, H410 = Very toxic to aquatic	P273 = Avoid release to the environment, P280 = Wear protective gloves/protective clothing/eye protection/face protection,




	 <p>GHS09: Toxic to aquatic Environment</p> 	<p>life with long lasting effects</p>	<p>P310+P330+P331 = If swallowed: rinse mouth. Do NOT induce vomiting, P303+P361+P353 = If on skin (or hair): Take off immediately all contaminated clothing. Rinse skin with water [or shower], P305+P351+P338 = If in eyes: Rinse cautiously with water for several minutes. Remove contact lenses, if present and easy to do. Continue rinsing, P310 = Immediately call a poison center/doctor</p>
--	--	---------------------------------------	--

Table 11: Safety instructions and hazardousness of used substances.

9.6. Copyright Permissions

9.6.1. Figure 4

Home Help ▾ Live Chat Sign in Create Account

Marangoni Flows during Nonsolvent Induced Phase Separation

Author: Douglas R. Tree, Tatsuhiko Iwama, Kris T. Delaney, et al

Publication: ACS Macro Letters

Publisher: American Chemical Society

Date: May 1, 2018

Copyright © 2018, American Chemical Society

PERMISSION/LICENSE IS GRANTED FOR YOUR ORDER AT NO CHARGE

This type of permission/license, instead of the standard Terms and Conditions, is sent to you because no fee is being charged for your order. Please note the following:

- Permission is granted for your request in both print and electronic formats, and translations.
- If figures and/or tables were requested, they may be adapted or used in part.
- Please print this page for your records and send a copy of it to your publisher/graduate school.
- Appropriate credit for the requested material should be given as follows: "Reprinted (adapted) with permission from {COMPLETE REFERENCE CITATION}. Copyright {YEAR} American Chemical Society." Insert appropriate information in place of the capitalized words.
- One-time permission is granted only for the use specified in your RightsLink request. No additional uses are granted (such as derivative works or other editions). For any uses, please submit a new request.

If credit is given to another source for the material you requested from RightsLink, permission must be obtained from that source.

[BACK](#) CLOSE WINDOW

© 2023 Copyright - All Rights Reserved | [Copyright Clearance Center, Inc.](#) | [Privacy statement](#) | [Data Security and Privacy](#)
| [For California Residents](#) | [Terms and Conditions](#) Comments? We would like to hear from you. E-mail us at customer@copyright.com

9.6.2. Figure 13

JOHN WILEY AND SONS LICENSE		
TERMS AND CONDITIONS		
Jul 30, 2023		
<hr/> <hr/>		
<p>This Agreement between Helmholtz-Zentrum Hereon -- Aniket Atul Rajee ("You") and John Wiley and Sons ("John Wiley and Sons") consists of your license details and the terms and conditions provided by John Wiley and Sons and Copyright Clearance Center.</p>		
License Number	5598681106343	
License date	Jul 30, 2023	
Licensed Content Publisher	John Wiley and Sons	
Licensed Content Publication	Wiley Books	
Licensed Content Title	Glass-Transition Phenomena in Polymer Blends	
Licensed Content Author	Ioannis M. Kalogeras	
Licensed Content Date	Jun 10, 2016	
Licensed Content Pages	134	
Type of use	Dissertation/Thesis	
Requestor type	University/Academic	
Format	Print and electronic	
Portion	Figure/table	
Number of figures/tables	1	
Will you be translating?	No	
Title	Organic-solvent-free fabrication of ultrafiltration membranes using foams	
Institution name	University of Hamburg	
Expected presentation date	Dec 2023	
Portions	Figure 1.15	
Requestor Location	Helmholtz-Zentrum Hereon Max-Planck-Straße 1 Geesthacht, 21502 Germany Attn: Helmholtz-Zentrum Hereon	
Publisher Tax ID	EU826007151	
Total	0.00 EUR	
Terms and Conditions		
TERMS AND CONDITIONS		

This copyrighted material is owned by or exclusively licensed to John Wiley & Sons, Inc. or one of its group companies (each a "Wiley Company") or handled on behalf of a society with which a Wiley Company has exclusive publishing rights in relation to a particular work (collectively "WILEY"). By clicking "accept" in connection with completing this licensing transaction, you agree that the following terms and conditions apply to this transaction (along with the billing and payment terms and conditions established by the Copyright Clearance Center Inc., ("CCC's Billing and Payment terms and conditions"), at the time that you opened your RightsLink account (these are available at any time at <http://myaccount.copyright.com>).

Terms and Conditions

- The materials you have requested permission to reproduce or reuse (the "Wiley Materials") are protected by copyright.
- You are hereby granted a personal, non-exclusive, non-sub licensable (on a stand-alone basis), non-transferable, worldwide, limited license to reproduce the Wiley Materials for the purpose specified in the licensing process. This license, **and any CONTENT (PDF or image file) purchased as part of your order**, is for a one-time use only and limited to any maximum distribution number specified in the license. The first instance of republication or reuse granted by this license must be completed within two years of the date of the grant of this license (although copies prepared before the end date may be distributed thereafter). The Wiley Materials shall not be used in any other manner or for any other purpose, beyond what is granted in the license. Permission is granted subject to an appropriate acknowledgement given to the author, title of the material/book/journal and the publisher. You shall also duplicate the copyright notice that appears in the Wiley publication in your use of the Wiley Material. Permission is also granted on the understanding that nowhere in the text is a previously published source acknowledged for all or part of this Wiley Material. Any third party content is expressly excluded from this permission.
- With respect to the Wiley Materials, all rights are reserved. Except as expressly granted by the terms of the license, no part of the Wiley Materials may be copied, modified, adapted (except for minor reformatting required by the new Publication), translated, reproduced, transferred or distributed, in any form or by any means,

and no derivative works may be made based on the Wiley Materials without the prior permission of the respective copyright owner. **For STM Signatory Publishers clearing permission under the terms of the [STM Permissions Guidelines](#) only, the terms of the license are extended to include subsequent editions and for editions in other languages, provided such editions are for the work as a whole in situ and does not involve the separate exploitation of the permitted figures or extracts,** You may not alter, remove or suppress in any manner any copyright, trademark or other notices displayed by the Wiley Materials. You may not license, rent, sell, loan, lease, pledge, offer as security, transfer or assign the Wiley Materials on a stand-alone basis, or any of the rights granted to you hereunder to any other person.

- The Wiley Materials and all of the intellectual property rights therein shall at all times remain the exclusive property of John Wiley & Sons Inc, the Wiley Companies, or their respective licensors, and your interest therein is only that of having possession of and the right to reproduce the Wiley Materials pursuant to Section 2 herein during the continuance of this Agreement. You agree that you own no right, title or interest in or to the Wiley Materials or any of the intellectual property rights therein. You shall have no rights hereunder other than the license as provided for above in Section 2. No right, license or interest to any trademark, trade name, service mark or other branding ("Marks") of WILEY or its licensors is granted hereunder, and you agree that you shall not assert any such right, license or interest with respect thereto
- NEITHER WILEY NOR ITS LICENSORS MAKES ANY WARRANTY OR REPRESENTATION OF ANY KIND TO YOU OR ANY THIRD PARTY, EXPRESS, IMPLIED OR STATUTORY, WITH RESPECT TO THE MATERIALS OR THE ACCURACY OF ANY INFORMATION CONTAINED IN THE MATERIALS, INCLUDING, WITHOUT LIMITATION, ANY IMPLIED WARRANTY OF MERCHANTABILITY, ACCURACY, SATISFACTORY QUALITY, FITNESS FOR A PARTICULAR PURPOSE, USABILITY, INTEGRATION OR NON-INFRINGEMENT AND ALL SUCH WARRANTIES ARE

HEREBY EXCLUDED BY WILEY AND ITS LICENSORS AND WAIVED BY YOU.

- WILEY shall have the right to terminate this Agreement immediately upon breach of this Agreement by you.
- You shall indemnify, defend and hold harmless WILEY, its Licensors and their respective directors, officers, agents and employees, from and against any actual or threatened claims, demands, causes of action or proceedings arising from any breach of this Agreement by you.
- IN NO EVENT SHALL WILEY OR ITS LICENSORS BE LIABLE TO YOU OR ANY OTHER PARTY OR ANY OTHER PERSON OR ENTITY FOR ANY SPECIAL, CONSEQUENTIAL, INCIDENTAL, INDIRECT, EXEMPLARY OR PUNITIVE DAMAGES, HOWEVER CAUSED, ARISING OUT OF OR IN CONNECTION WITH THE DOWNLOADING, PROVISIONING, VIEWING OR USE OF THE MATERIALS REGARDLESS OF THE FORM OF ACTION, WHETHER FOR BREACH OF CONTRACT, BREACH OF WARRANTY, TORT, NEGLIGENCE, INFRINGEMENT OR OTHERWISE (INCLUDING, WITHOUT LIMITATION, DAMAGES BASED ON LOSS OF PROFITS, DATA, FILES, USE, BUSINESS OPPORTUNITY OR CLAIMS OF THIRD PARTIES), AND WHETHER OR NOT THE PARTY HAS BEEN ADVISED OF THE POSSIBILITY OF SUCH DAMAGES. THIS LIMITATION SHALL APPLY NOTWITHSTANDING ANY FAILURE OF ESSENTIAL PURPOSE OF ANY LIMITED REMEDY PROVIDED HEREIN.
- Should any provision of this Agreement be held by a court of competent jurisdiction to be illegal, invalid, or unenforceable, that provision shall be deemed amended to achieve as nearly as possible the same economic effect as the original provision, and the legality, validity and enforceability of the remaining provisions of this Agreement shall not be affected or impaired thereby.
- The failure of either party to enforce any term or condition of this Agreement shall not constitute a waiver of either party's right to enforce each and every term and condition of this Agreement. No

breach under this agreement shall be deemed waived or excused by either party unless such waiver or consent is in writing signed by the party granting such waiver or consent. The waiver by or consent of a party to a breach of any provision of this Agreement shall not operate or be construed as a waiver of or consent to any other or subsequent breach by such other party.

- This Agreement may not be assigned (including by operation of law or otherwise) by you without WILEY's prior written consent.
- Any fee required for this permission shall be non-refundable after thirty (30) days from receipt by the CCC.
- These terms and conditions together with CCC's Billing and Payment terms and conditions (which are incorporated herein) form the entire agreement between you and WILEY concerning this licensing transaction and (in the absence of fraud) supersedes all prior agreements and representations of the parties, oral or written. This Agreement may not be amended except in writing signed by both parties. This Agreement shall be binding upon and inure to the benefit of the parties' successors, legal representatives, and authorized assigns.
- In the event of any conflict between your obligations established by these terms and conditions and those established by CCC's Billing and Payment terms and conditions, these terms and conditions shall prevail.
- WILEY expressly reserves all rights not specifically granted in the combination of (i) the license details provided by you and accepted in the course of this licensing transaction, (ii) these terms and conditions and (iii) CCC's Billing and Payment terms and conditions.
- This Agreement will be void if the Type of Use, Format, Circulation, or Requestor Type was misrepresented during the licensing process.
- This Agreement shall be governed by and construed in accordance with the laws of the State of New York, USA, without regards to such state's conflict of law rules. Any legal action, suit or

proceeding arising out of or relating to these Terms and Conditions or the breach thereof shall be instituted in a court of competent jurisdiction in New York County in the State of New York in the United States of America and each party hereby consents and submits to the personal jurisdiction of such court, waives any objection to venue in such court and consents to service of process by registered or certified mail, return receipt requested, at the last known address of such party.

WILEY OPEN ACCESS TERMS AND CONDITIONS

Wiley Publishes Open Access Articles in fully Open Access Journals and in Subscription journals offering Online Open. Although most of the fully Open Access journals publish open access articles under the terms of the Creative Commons Attribution (CC BY) License only, the subscription journals and a few of the Open Access Journals offer a choice of Creative Commons Licenses. The license type is clearly identified on the article.

The Creative Commons Attribution License

The [Creative Commons Attribution License \(CC-BY\)](#) allows users to copy, distribute and transmit an article, adapt the article and make commercial use of the article. The CC-BY license permits commercial and non-

Creative Commons Attribution Non-Commercial License

The [Creative Commons Attribution Non-Commercial \(CC-BY-NC\) License](#) permits use, distribution and reproduction in any medium, provided the original work is properly cited and is not used for commercial purposes.(see below)

Creative Commons Attribution-Non-Commercial-NoDerivs License

The [Creative Commons Attribution Non-Commercial-NoDerivs License](#) (CC-BY-NC-ND) permits use, distribution and reproduction in any medium, provided the original work is properly cited, is not used for commercial purposes and no modifications or adaptations are made. (see below)

Use by commercial "for-profit" organizations

Use of Wiley Open Access articles for commercial, promotional, or marketing purposes requires further explicit permission from Wiley and will be subject to a fee. Further details can be found on Wiley Online Library

<http://olabout.wiley.com/WileyCDA/Section/id-410895.html>

Other Terms and Conditions:

v1.10 Last updated September 2015

Questions? customercare@copyright.com.

9.6.3. Figure 17

ELSEVIER LICENSE TERMS AND CONDITIONS	
Jun 18, 2023	
<hr/> <hr/> <p>This Agreement between Helmholtz-Zentrum Hereon -- Aniket Atul Rajee ("You") and Elsevier ("Elsevier") consists of your license details and the terms and conditions provided by Elsevier and Copyright Clearance Center.</p>	
License Number	5571911238513
License date	Jun 18, 2023
Licensed Content Publisher	Elsevier
Licensed Content Publication	Polymer
Licensed Content Title	Evolution of polymer blend morphology during compounding in a twin-screw extruder
Licensed Content Author	Je Kyum Lee, Chang Dae Han
Licensed Content Date	Mar 1, 2000
Licensed Content Volume	41
Licensed Content Issue	5
Licensed Content Pages	17
Start Page	1799
End Page	1815
Type of Use	reuse in a thesis/dissertation
Portion	figures/tables/illustrations
Number of figures/tables/illustrations	1
Format	both print and electronic
Are you the author of this Elsevier article?	No
Will you be translating?	No
Title	Organic-solvent-free fabrication of ultrafiltration membranes using foams
Institution name	University of Hamburg
Expected presentation date	Dec 2023
Portions	1
Requestor Location	Helmholtz-Zentrum Hereon Max-Planck-Straße 1 Geesthacht, 21502

	Germany Attn: Helmholtz-Zentrum Hereon	
Publisher Tax ID	GB 494 6272 12	
Total	0.00 EUR	
Terms and Conditions		
<p style="text-align: center;">INTRODUCTION</p> <p>1. The publisher for this copyrighted material is Elsevier. By clicking "accept" in connection with completing this licensing transaction, you agree that the following terms and conditions apply to this transaction (along with the Billing and Payment terms and conditions established by Copyright Clearance Center, Inc. ("CCC"), at the time that you opened your RightsLink account and that are available at any time at https://myaccount.copyright.com).</p> <p style="text-align: center;">GENERAL TERMS</p> <p>2. Elsevier hereby grants you permission to reproduce the aforementioned material subject to the terms and conditions indicated.</p> <p>3. Acknowledgement: If any part of the material to be used (for example, figures) has appeared in our publication with credit or acknowledgement to another source, permission must also be sought from that source. If such permission is not obtained then that material may not be included in your publication/copies. Suitable acknowledgement to the source must be made, either as a footnote or in a reference list at the end of your publication, as follows: "Reprinted from Publication title, Vol /edition number, Author(s), Title of article / title of chapter, Pages No., Copyright (Year), with permission from Elsevier [OR APPLICABLE SOCIETY COPYRIGHT OWNER]." Also Lancet special credit - "Reprinted from The Lancet, Vol. number, Author(s), Title of article, Pages No., Copyright (Year), with permission from Elsevier."</p> <p>4. Reproduction of this material is confined to the purpose and/or media for which permission is hereby given. The material may not be reproduced or used in any other way, including use in combination with an artificial intelligence tool (including to train an algorithm, test, process, analyse, generate output and/or develop any form of artificial intelligence tool), or to create any derivative work and/or service (including resulting from the use of artificial intelligence tools).</p> <p>5. Altering/Modifying Material: Not Permitted. However figures and illustrations may be altered/adapted minimally to serve your work. Any other abbreviations, additions, deletions and/or any other alterations shall be made only with prior written authorization of Elsevier Ltd. (Please contact Elsevier's permissions helpdesk here). No modifications can be made to any Lancet figures/tables and they must be reproduced in full.</p> <p>6. If the permission fee for the requested use of our material is waived in this instance, please be advised that your future requests for Elsevier materials may attract a fee.</p> <p>7. Reservation of Rights: Publisher reserves all rights not specifically granted in the combination of (i) the license details provided by you and accepted in the course of this licensing transaction, (ii) these terms and conditions and (iii) CCC's Billing and Payment terms and conditions.</p>		

8. License Contingent Upon Payment: While you may exercise the rights licensed immediately upon issuance of the license at the end of the licensing process for the transaction, provided that you have disclosed complete and accurate details of your proposed use, no license is finally effective unless and until full payment is received from you (either by publisher or by CCC) as provided in CCC's Billing and Payment terms and conditions. If full payment is not received on a timely basis, then any license preliminarily granted shall be deemed automatically revoked and shall be void as if never granted. Further, in the event that you breach any of these terms and conditions or any of CCC's Billing and Payment terms and conditions, the license is automatically revoked and shall be void as if never granted. Use of materials as described in a revoked license, as well as any use of the materials beyond the scope of an unrevoked license, may constitute copyright infringement and publisher reserves the right to take any and all action to protect its copyright in the materials.

9. Warranties: Publisher makes no representations or warranties with respect to the licensed material.

10. Indemnity: You hereby indemnify and agree to hold harmless publisher and CCC, and their respective officers, directors, employees and agents, from and against any and all claims arising out of your use of the licensed material other than as specifically authorized pursuant to this license.

11. No Transfer of License: This license is personal to you and may not be sublicensed, assigned, or transferred by you to any other person without publisher's written permission.

12. No Amendment Except in Writing: This license may not be amended except in a writing signed by both parties (or, in the case of publisher, by CCC on publisher's behalf).

13. Objection to Contrary Terms: Publisher hereby objects to any terms contained in any purchase order, acknowledgment, check endorsement or other writing prepared by you, which terms are inconsistent with these terms and conditions or CCC's Billing and Payment terms and conditions. These terms and conditions, together with CCC's Billing and Payment terms and conditions (which are incorporated herein), comprise the entire agreement between you and publisher (and CCC) concerning this licensing transaction. In the event of any conflict between your obligations established by these terms and conditions and those established by CCC's Billing and Payment terms and conditions, these terms and conditions shall control.

14. Revocation: Elsevier or Copyright Clearance Center may deny the permissions described in this License at their sole discretion, for any reason or no reason, with a full refund payable to you. Notice of such denial will be made using the contact information provided by you. Failure to receive such notice will not alter or invalidate the denial. In no event will Elsevier or Copyright Clearance Center be responsible or liable for any costs, expenses or damage incurred by you as a result of a denial of your permission request, other than a refund of the amount(s) paid by you to Elsevier and/or Copyright Clearance Center for denied permissions.

LIMITED LICENSE

<p>The following terms and conditions apply only to specific license types:</p> <p>15. Translation: This permission is granted for non-exclusive world English rights only unless your license was granted for translation rights. If you licensed translation rights you may only translate this content into the languages you requested. A professional translator must perform all translations and reproduce the content word for word preserving the integrity of the article.</p> <p>16. Posting licensed content on any Website: The following terms and conditions apply as follows: Licensing material from an Elsevier journal: All content posted to the web site must maintain the copyright information line on the bottom of each image; A hyper-text must be included to the Homepage of the journal from which you are licensing at http://www.sciencedirect.com/science/journal/xxxxx or the Elsevier homepage for books at http://www.elsevier.com; Central Storage: This license does not include permission for a scanned version of the material to be stored in a central repository such as that provided by Heron/XanEdu.</p> <p>Licensing material from an Elsevier book: A hyper-text link must be included to the Elsevier homepage at http://www.elsevier.com . All content posted to the web site must maintain the copyright information line on the bottom of each image.</p> <p>Posting licensed content on Electronic reserve: In addition to the above the following clauses are applicable: The web site must be password-protected and made available only to bona fide students registered on a relevant course. This permission is granted for 1 year only. You may obtain a new license for future website posting.</p> <p>17. For journal authors: the following clauses are applicable in addition to the above:</p> <p>Preprints:</p> <p>A preprint is an author's own write-up of research results and analysis, it has not been peer-reviewed, nor has it had any other value added to it by a publisher (such as formatting, copyright, technical enhancement etc.).</p> <p>Authors can share their preprints anywhere at any time. Preprints should not be added to or enhanced in any way in order to appear more like, or to substitute for, the final versions of articles however authors can update their preprints on arXiv or RePEc with their Accepted Author Manuscript (see below).</p> <p>If accepted for publication, we encourage authors to link from the preprint to their formal publication via its DOI. Millions of researchers have access to the formal publications on ScienceDirect, and so links will help users to find, access, cite and use the best available version. Please note that Cell Press, The Lancet and some society-owned have different preprint policies. Information on these policies is available on the journal homepage.</p> <p>Accepted Author Manuscripts: An accepted author manuscript is the manuscript of an article that has been accepted for publication and which typically includes author-incorporated changes suggested during submission, peer review and editor-author communications.</p> <p>Authors can share their accepted author manuscript:</p>	
---	--

- immediately
 - via their non-commercial person homepage or blog
 - by updating a preprint in arXiv or RePEc with the accepted manuscript
 - via their research institute or institutional repository for internal institutional uses or as part of an invitation-only research collaboration work-group
 - directly by providing copies to their students or to research collaborators for their personal use
 - for private scholarly sharing as part of an invitation-only work group on commercial sites with which Elsevier has an agreement
- After the embargo period
 - via non-commercial hosting platforms such as their institutional repository
 - via commercial sites with which Elsevier has an agreement

In all cases accepted manuscripts should:

- link to the formal publication via its DOI
- bear a CC-BY-NC-ND license - this is easy to do
- if aggregated with other manuscripts, for example in a repository or other site, be shared in alignment with our hosting policy not be added to or enhanced in any way to appear more like, or to substitute for, the published journal article.

Published journal article (JPA): A published journal article (PJA) is the definitive final record of published research that appears or will appear in the journal and embodies all value-adding publishing activities including peer review co-ordination, copy-editing, formatting, (if relevant) pagination and online enrichment.

Policies for sharing publishing journal articles differ for subscription and gold open access articles:

Subscription Articles: If you are an author, please share a link to your article rather than the full-text. Millions of researchers have access to the formal publications on ScienceDirect, and so links will help your users to find, access, cite, and use the best available version.

Theses and dissertations which contain embedded PJAs as part of the formal submission can be posted publicly by the awarding institution with DOI links back to the formal publications on ScienceDirect.

If you are affiliated with a library that subscribes to ScienceDirect you have additional private sharing rights for others' research accessed under that agreement. This includes use for classroom teaching and internal training at the institution (including use in course packs and courseware programs), and inclusion of the article for grant funding purposes.

Gold Open Access Articles: May be shared according to the author-selected end-user license and should contain a [CrossMark logo](#), the end user license, and a DOI link to the formal publication on ScienceDirect.

Please refer to Elsevier's [posting policy](#) for further information.

18. **For book authors** the following clauses are applicable in addition to the above: Authors are permitted to place a brief summary of their work online only. You are not allowed to download and post the published electronic version of your chapter, nor may you scan the printed edition to create an electronic version. **Posting to a repository:** Authors are permitted to post a summary of their chapter only in their institution's repository.

19. **Thesis/Dissertation:** If your license is for use in a thesis/dissertation your thesis may be submitted to your institution in either print or electronic form. Should your thesis be published commercially, please reapply for permission. These requirements include permission for the Library and Archives of Canada to supply single copies, on demand, of the complete thesis and include permission for Proquest/UMI to supply single copies, on demand, of the complete thesis. Should your thesis be published commercially, please reapply for permission. Theses and dissertations which contain embedded PJAs as part of the formal submission can be posted publicly by the awarding institution with DOI links back to the formal publications on ScienceDirect.

Elsevier Open Access Terms and Conditions

You can publish open access with Elsevier in hundreds of open access journals or in nearly 2000 established subscription journals that support open access publishing. Permitted third party re-use of these open access articles is defined by the author's choice of Creative Commons user license. See our [open access license policy](#) for more information.

Terms & Conditions applicable to all Open Access articles published with Elsevier:

Any reuse of the article must not represent the author as endorsing the adaptation of the article nor should the article be modified in such a way as to damage the author's honour or reputation. If any changes have been made, such changes must be clearly indicated.

The author(s) must be appropriately credited and we ask that you include the end user license and a DOI link to the formal publication on ScienceDirect.

If any part of the material to be used (for example, figures) has appeared in our publication with credit or acknowledgement to another source it is the

<p>responsibility of the user to ensure their reuse complies with the terms and conditions determined by the rights holder.</p> <p>Additional Terms & Conditions applicable to each Creative Commons user license:</p> <p>CC BY: The CC-BY license allows users to copy, to create extracts, abstracts and new works from the Article, to alter and revise the Article and to make commercial use of the Article (including reuse and/or resale of the Article by commercial entities), provided the user gives appropriate credit (with a link to the formal publication through the relevant DOI), provides a link to the license, indicates if changes were made and the licensor is not represented as endorsing the use made of the work. The full details of the license are available at http://creativecommons.org/licenses/by/4.0.</p> <p>CC BY NC SA: The CC BY-NC-SA license allows users to copy, to create extracts, abstracts and new works from the Article, to alter and revise the Article, provided this is not done for commercial purposes, and that the user gives appropriate credit (with a link to the formal publication through the relevant DOI), provides a link to the license, indicates if changes were made and the licensor is not represented as endorsing the use made of the work. Further, any new works must be made available on the same conditions. The full details of the license are available at http://creativecommons.org/licenses/by-nc-sa/4.0.</p> <p>CC BY NC ND: The CC BY-NC-ND license allows users to copy and distribute the Article, provided this is not done for commercial purposes and further does not permit distribution of the Article if it is changed or edited in any way, and provided the user gives appropriate credit (with a link to the formal publication through the relevant DOI), provides a link to the license, and that the licensor is not represented as endorsing the use made of the work. The full details of the license are available at http://creativecommons.org/licenses/by-nc-nd/4.0. Any commercial reuse of Open Access articles published with a CC BY NC SA or CC BY NC ND license requires permission from Elsevier and will be subject to a fee.</p> <p>Commercial reuse includes:</p> <ul style="list-style-type: none"> • Associating advertising with the full text of the Article • Charging fees for document delivery or access • Article aggregation • Systematic distribution via e-mail lists or share buttons <p>Posting or linking by commercial companies for use by customers of those companies.</p> <p>20. Other Conditions:</p> <p>v1.10</p>	
<p>Questions? customercare@copyright.com.</p>	

10. Acknowledgements

I begin by thanking the universe for aligning the circumstances perfectly enough to allow me to fulfill the duties that led to completing this work. Next, I would like to thank every person, department, company, technology, equipment, material, book, academic literature, software, website, and conversation that supported me in achieving the milestones and goals of my doctoral dissertation.

I am eternally grateful to the supervisor of my doctoral thesis, Prof. Dr. Volker Abetz, Director of the Institute of Membrane Research at Helmholtz-Zentrum Hereon and Group Leader at the Institute of Physical Chemistry at the University of Hamburg. I thank him for not only for the opportunity to work on my doctoral thesis but also his constant support and faith in me toward pursuing an alternative membrane production method. Furthermore, his valuable scientific inputs in the entirety of this doctoral work and in each of the published articles allowed the realization of many previously-thought impossible tasks.

I want to extend my sincere thanks to Prof. Dr. Gerrit A. Luinstra for accepting the role as the second reviewer of this doctoral thesis.

The assistance, support, motivation, and understanding provided by Dr. Prokopios Georgopoulos, my direct supervisor and Head of the Department of Polymer Technology at Helmholtz-Zentrum Hereon, cannot be thanked enough. By working together as a partner, he saw my challenges as his own and supported me shoulder-to-shoulder in tackling them. The scientific, technical, administrative as well as personal conversations with him were very valuable. His scientific knowledge and years of hands-on experience assisted me in improving the quality of my work. Completing my experimental work in

less than three years was only possible by having a skilled scientist like Dr. Georgopoulos as a manager. Words cannot express my gratitude towards him.

Joachim Koll, a highly skilled engineer, supported me both physically and mentally as we worked on large machines together. Repair work, as well as experimental trials at extruder temperatures up to 380 °C and pressures reaching 400 bars, felt safe and assured when he was with me. I would like to express my deepest gratitude towards him for sharing his decades of experience in membranes as well as for making me feel comfortable and confident in laboratory and technical work. The adventures we had are always a treat to remember! Along with him, I am deeply indebted to the other former members of PMM: Ivonne Ternes for her non-stop assistance in material characterization as well as experimental support whenever I needed it; Kristian Buhr for his rheological support, batch foaming expertise, and friendly conversations that allowed my colloquial German to improve; Jelena Lillepärq for the immense scientific knowledge she carries and the support she provided with gas sorption experiments along with educating me about them.

My gratitude goes to the members of my department PMT, Dr. Felix Kandelhard, Emil Pashayev, and especially Juliane Schymura for providing laboratory support in the Polymer-Hydrogen Technology Center.

Many thanks to Petra Marten, Ivonne Ternes, Maren Brinkman, Silvio Neumann, and Barbara Bajer for not only providing the material characterization, laboratory, and equipment support but also their openness which comforted me during the most challenging times.

Special thanks to Dr. Sarah Glaß, who shared her office, passion and understanding of membranes with me. Our impromptu conversations enlightened me with knowledge, confidence, and motivation, and are unforgettable. Along with her, in no particular order,

I thank Bing-Ting Ho, Esra Çalışkan, Dr. Kirti Sankhala, Dr. Mahboubeh Kargar, Emil Paschayev, Drew Lawrence, Nicolas Cevallos-Cueva, Hluf Hailu Kinfu, Dr. Fynn Weigelt, Dr. Zhenzhen Zhang, Maria de los Angeles Ramirez Kantun, Dr. Michael Appold, and Charles Mbadike, for their friendship and support at the Institute of Membrane Research.

I had the pleasure of working with Dr. Martin Held, Dr. Erik S. Schneider, Dr. Evgeni Sperling, and Anke-Lisa Höhme of the microscopy department. I thank them for decorating my doctoral work with profound and professionally captured SEM images. Their regular support allowed me to smoothly proceed with my research. In addition, I acknowledge the technical support by Carsten Scholles, Sebastian Tödten, and Eugen Ebel, as well as the administrative support by Ilona Zillich and Dr. Karin Kirstein.

Hereby, I would also like to acknowledge Prof. Dr. Ulrich A. Handge, former supervisor, for the opportunity to start my doctoral thesis on this topic, along with project initiation and rheological expertise. I also thank BASF SE for the initial project funding, scientific discussions, and patent collaboration.

I am also grateful to Helmholtz-Zentrum Hereon for the opportunity to be elected as the Doctoral Representative of over 160 Doctoral researchers. In this voluntary role, I could serve for the greater good and am thankful for all the efforts and support from Prof. Dr. Mathias Rehahn, Dr. Iris Ulrich, Elina Valli, Prof. Dr. Markus Quante, the works council, Helmholtz-Juniors, and my fellow representative Claudia Schmidt.

I am thankful for the blessings and support provided by my parents, Atul Raje and Anuja Raje, grandparents, in-laws, relatives, and friends, who have always been there for me whenever I needed them.

Lastly, I would like to thank someone who deserves to be mentioned first: My wife Shreya, Researcher in Immunology, for being my constant support over these years and the years to come.

11. Declaration of Oath

Ich, Aniket Atul Raje, schwöre feierlich, dass die in dieser Dissertation mit dem Titel ‚*Organic-solvent-free production of ultrafiltration membranes using polymer foaming and extrusion*‘ vorgelegte Arbeit meine Originalarbeit ist und dass ich keinen einzigen Teil davon plagiiert habe. Ich bin dankbar für die Hilfe und Unterstützung aller Personen, Ressourcen und Hilfsmittel, die zu dieser Arbeit beigetragen haben. Des Weiteren versichere ich, dass diese Dissertation nicht zuvor bei einer anderen Institution für einen Abschluss oder eine Prüfung eingereicht wurde. Ich erkenne an, dass es sich bei dieser Dissertation um eine kumulative Arbeit handelt, die in Teilen bereits in wissenschaftlichen Zeitschriften und Patenten veröffentlicht wurde. Daher gibt es Ähnlichkeiten mit diesen Veröffentlichungen, die jedoch, wo immer nötig, in der Dissertation berücksichtigt wurden. Mir ist bekannt, dass ein Verstoß gegen diesen Eid disziplinarische Maßnahmen nach sich ziehen kann.



Kiel, 14.08.2023

(English translation on the next page)

I, Aniket Atul Raje, do solemnly swear that the work presented in this dissertation entitled '*Organic-solvent-free production of ultrafiltration membranes using polymer foaming and extrusion*' is my original work and that I have not plagiarized any part of it. I gratefully acknowledge the assistance and support of all persons, resources, and aids that contributed to this work. Furthermore, I swear that this dissertation has not been previously submitted for any degree or examination at any other institution. I acknowledge that this dissertation is a cumulative one, and parts of it have been published in scientific journals and patents. Therefore, similarities with those publications exist, but they have been acknowledged wherever necessary in the dissertation. I understand that any violation of this oath may result in disciplinary action.



Kiel, 14.08.2023
